

Functional Traits Affecting Photosynthesis, Growth, and Mortality of Trees Inferred from  
a Field Study and Simulation Experiments

by

Michael Fell

A Dissertation Presented in Partial Fulfillment  
of the Requirements for the Degree  
Doctor of Philosophy

Approved March 2016 by the  
Graduate Supervisory Committee:

Kiona Ogle, Chair  
Jarrett Barber  
Kevin Hultine  
Janet Franklin  
Thomas Day

ARIZONA STATE UNIVERSITY

May 2017

## ABSTRACT

Functional traits research has improved our understanding of how plants respond to their environments, identifying key trade-offs among traits. These studies primarily rely on correlative methods to infer trade-offs and often overlook traits that are difficult to measure (e.g., root traits, tissue senescence rates), limiting their predictive ability under novel conditions. I aimed to address these limitations and develop a better understanding of the trait space occupied by trees by integrating data and process models, spanning leaves to whole-trees, via modern statistical and computational methods. My first research chapter (Chapter 2) simultaneously fits a photosynthesis model to measurements of fluorescence and photosynthetic response curves, improving estimates of mesophyll conductance ( $g_m$ ) and other photosynthetic traits. I assessed how  $g_m$  varies across environmental gradients and relates to other photosynthetic traits for 4 woody species in Arizona. I found that  $g_m$  was lower at high aridity sites, varied little within a site, and is an important trait for obtaining accurate estimates of photosynthesis and related traits under dry conditions. Chapter 3 evaluates the importance of functional traits for whole-tree performance by fitting an individual-based model of tree growth and mortality to millions of measurements of tree heights and diameters to assess the theoretical trait space (TTS) of “healthy” North American trees. The TTS contained complicated, multi-variate structure indicative of potential trade-offs leading to successful growth. In Chapter 4, I applied an environmental filter (light stress) to the TTS, leading to simulated stand-level mortality rates up to 50%. Tree-level mortality was explained by 6 of the 32 traits explored, with the most important being radiation-use efficiency. The multidimensional space comprising these 6 traits differed in volume and

location between trees that survived and died, indicating that selective mortality alters the TTS.

## ACKNOWLEDGMENTS

I would like to acknowledge Kiona Ogle and my committee members: Jarrett Barber, Kevin Hultine, Janet Franklin, and Thomas Day for their feedback, access to equipment, assistance with experimental methods, and with writing this dissertation. I thank Clint Clarkson and Christina Bell for assistance with field and lab work. I thank Heather Kropp, Kimberly Samuels-Crow, Larissa Yocom Kent, Yao Liu, Jessica Guo, Abraham Cadmus, and Drew Peltier for their feedback on drafts of my chapters. Finally, I would like to thank my parents, David and Diane Fell for always supporting my academic efforts, and my wife Ashley for being patient with me as I worked on this over the years.

# TABLE OF CONTENTS

	Page
LIST OF TABLES .....	vii
LIST OF FIGURES .....	ix
CHAPTER	
1 INTRODUCTION .....	1
Background .....	1
References .....	8
2 INCORPORATING FLUORESCENCE DATA INTO A HIERARCHICAL BAYESIAN PHOTOSYNTHESIS MODELING FRAMEWORK TO BETTER ESTIMATE MESOPHYLL CONDUCTANCE ALONG REGIONAL AND LOCAL ARIDITY GRADIENTS .....	11
Abstract .....	11
Introduction .....	13
Methods .....	17
Results .....	30
Discussion .....	35
References .....	43
Tables .....	49
Figures .....	53
3 TRAIT SPECTRA PREDICTED BY A MECHANISTIC MODEL OF TREE GROWTH AND CARBON ALLOCATION .....	59
Abstract .....	59



APPENDIX	Page
B ADDITIONAL MODEL DETAILS AND CODE.....	185
C SUPPLEMENTAL TABLES AND FIGURES REGARDING THE ACGCA TRAIT SPACE.....	195
D SUPPLEMENTAL CODE USED TO GENERATE THE THEORETICAL TRAIT SPACE FOR NORTH AMERICAN TREES .....	202
E SUPPLEMENTAL TABLES AND FIGURES REGARDING FILTERING THE THEORETICAL TRAIT SPACE FOR NORTH AMERICN TREES	220
F STATEMENT OF CO-AUTHOR PERMISSION .....	234

## LIST OF TABLES

Table	Page
2.1 Site Mean Annual Precipitation, Minimum and Maximum Temperature .....	49
2.2 Symbols and Definitions of Quantities Used in the Photosynthesis Model .....	50
2.3 Farquhar <i>et al.</i> Equations .....	52
3.1 Description and units associated with the 32 parameters in the ACGCA model	105
3.2 Bivariate Correlations between Pairs of Parameters (traits) .....	107
3.3 The Number of Draws Required to Obtain a Parameter Vector Resulting in Realistic Tree Growth Under 11 Light Levels .....	110
3.4 Summary of Main Effects Included in Multiple-Regression Models Identified by a Stepwise Regression Routine .....	111
3.5 Summary of Main Effects and Two-way Interactions Included in Multiple- Regression Models Identified by a Stepwise Regression Routine.....	112
4.1 Descriptions of the 32 ACGCA Model Parameters Representative of Functional Traits .....	159
4.2 Methods of Calculating Mortality Relative to Simulation Design .....	161
S2.1 Prior Distributions for Photosynthesis Model Parameters.....	175
S2.2 Artificial Data Parameters .....	177
S2.3 CI widths for full and reduced models .....	178
S2.4 Posterior estimates for terminal nodes.....	179
S3.1 Prior Distributions for Semi-informative Priors Used for Fitting the ACGCA Model .....	196
S3.2 Posterior Estimates for all ACGCA Model Parameters .....	197

Table	Page
S3.3 Model Fits Obtained From Best Subsets and Stepwise Regressions for the 32 ACGCA Parameters.....	198
S4.1 Tree-Level Mortality Explained by Average Light Level Logistic Regression Results.....	221
S4.2 Tree-Level Mortality Explained by Functional Traits Stepwise Logistic Regression Results .....	222
S4.3 Tree-Level Mortality Explained by Functional Traits and Average Light Level Stepwise Logistic Regression Results .....	223
S4.4 Stand-Level Mortality as Explained by Time between Gaps .....	225
S4.5 Phenotype-Level Mortality versus 32 Functional Traits Results from a Stepwise Multiple Regression with Only Main Effects .....	226
S4.6 Phenotype-Level Mortality versus 32 Functional Traits Results from a Stepwise Multiple Regression with Main Effects and Two-Way Interactions .....	227
S4.7 Summary of Main Effects and Two-way Interactions Included in Multiple-Regression Models Identified by a Stepwise Regression Routine for Surviving Trees.....	230
S4.8 Summary of Main Effects and Two-way Interactions Included in Multiple-Regression Models Identified by a Stepwise Regression Routine for Dead Trees.....	231
S4.9 Summary of the Similarities and Differences between S4.7 and S4.8 .....	232

## LIST OF FIGURES

Figure	Page
2.1 Model Fit for artificial data.....	53
2.2 Artificial Data Model Parameter Estimates .....	54
2.3 Model Fit for Field Data .....	55
2.4 Parameter Estimates for Field Data .....	56
2.5 Stomatal Conductance and Plant Water Status vs posterior means for Mesophyll Conductance.....	57
2.6 Posterior Results for the Hierarchical Bayesian Model with or Without the Inclusion of the Quantum Yield of Photosystem II .....	58
3.1 Overlap Between ACGCA Model Output and the FIA Dataset Used.....	113
3.2 Marginal Posterior Probability Densities by Light Level for Three Parameters (traits).....	114
3.3 The Proportion of Values Accepted after Randomizing Parameter Order .....	115
3.4 Main Effects of Variables (traits) Included in Four Stepwise Multiple Regressions as Influenced by Interactions .....	116
3.5 Bivariate Posterior Plot Showing the Effect of Filtering on a Single Example Trait.....	117
4.1 Percent of Trees Correctly Classified as Surviving or Dead Based on Logistic Regressions Fit to Tree Level Mortality .....	162
4.2 Regression Results for Stand-level Mortality as Explained By Time between Gaps and Average Light Level .....	163
4.3 Stepwise Regression Results showing Relative Importance for Phenotype-level Mortality and Kernel Density Estimates for Traits of Interest .....	164

Figure	Page
4.4 Hypercube Centroid Distances and Volume Differences for Six Traits with High Relative Importance for Mortality .....	165
4.5 Hypercube Centroid Distances and Volume Differences for Six Traits Either from or Related to the Leaf and Wood Economics Spectra .....	166
S2.1 Log Transformed Means for Curve Level Mesophyll Conductance vs Stomatal Conductance from Gas Exchange Measurements.....	183
S3.1 The Marginal Posterior Densities of Senescence Rate of non-trunk Woody Tissue, $S_0$ for 11 Light Levels.....	199
S3.2 Posterior Means for Radiation-use Efficiency by Light Level.....	200
S3.3 Example of How Filtering the Posterior may Reveal Underlying Correlations between Traits .....	201
S4.1 Relationship between Gap Dynamics Simulation Variables and Average Light Level .....	233

## CHAPTER 1 – INTRODUCTION

### **Background**

Understanding the relationships of functional traits to tree growth and mortality, as well as processes underlying growth and mortality, such as photosynthesis, water dynamics, and carbon storage, can provide insights into the links between population and ecosystem processes useful to a range of fields. The links between tree traits and processes have important implications across topics and scales, from small-scale studies of plant competition, to large scale endeavors such as the development of global vegetation models (Scheiter et al. 2013, Fyllas et al. 2014, Van Bodegom et al. 2014). From a global perspective, having a better understanding of how tree traits relate to the environment, and to each other (via “tradeoffs”), may improve our ability to predict their responses to environmental perturbations. This is important because trees cover about 30% to 38% of the earth’s terrestrial surface (Dixon et al. 1994, Perry et al. 2008) and account for ~32% of the global carbon sink (Pan et al. 2011).

Research on functional traits has largely focused on analyzing relationships among traits and the environment using a number of correlative or phenomenological approaches, including regression analysis (e.g., multiple regression, standardized major axis regression) and dimension reduction (e.g. principle components analysis, multiple factor analysis). These approaches have led to the discovery of interesting relationships among groups of traits. For instance leaf lifespan is positively related to leaf mass per area (Wright et al. 2004), and wood density is negatively related to tree mortality rate (Chave et al. 2009). Such relationships have been summarized into a few economics spectra including the leaf, wood, and fast-slow economics spectra (Wright et al. 2004,

Chave et al. 2009, Reich 2014), and more recently, the global spectrum of plant form and function (Diaz et al. 2016). Each of these spectra encompasses one or several groups of traits and describes the relationships and tradeoffs between them. However, some of the relationships—those involving functional traits expressed on a per unit leaf area, such as area-specific maximum photosynthetic rate—in the leaf economics spectrum have been questioned in recent years, and may be an artifact of how the traits are quantified (Lloyd et al. 2013, Osnas et al. 2013).

Another branch of research on functional traits has examined the problem of coexistence, where many species occur in a given environment. Coexistence is not explained by classical theory, where exclusion would be expected, especially if there are only a limited number of tradeoffs (Tilman 1985). There are two possible explanations for why many species are often found in a given environment. One is environmental heterogeneity (Tilman 2004), which permits each species to outcompete others based on differences in resource availability across the environment. Another possible explanation is that there are many axes of variation leading to many potential tradeoffs permitting species to coexist through differential use of resources (Hutchinson 1957, Clark et al. 2010, McMahon et al. 2011). There also could be some combination of these explanations.

One way to better understand the relationships between traits is to utilize mechanistic models that represent important physiological processes underlying growth. For example, the Farquhar et al. (1980) leaf-level model of photosynthesis is often coupled to larger models such as dynamic global vegetation models and ultimately general circulation models to predict carbon uptake (Bonan et al. 2003, Shugart and

Woodward 2011). However, most models do not include mesophyll conductance ( $g_m$ , or internal conductance), a potentially important physiological trait that governs photosynthesis. Though, there is evidence  $g_m$  should be considered, because not including  $g_m$  can lead to incorrect estimates of other photosynthetic parameters and ultimately incorrect predictions of assimilation rates (Keenan et al. 2010, Flexas et al. 2012). By integrating models, such as the Farquhar et al. (1980) model, with tree growth models, a better understanding of how specific physiological (such as  $g_m$ ), morphological, and allometric traits influence overall carbon uptake can be gained. For example, by conducting a sensitivity analysis for a given physiological parameter like  $g_m$  it would be possible to assess its impact on overall tree growth. This could be taken a step further by integrating carbon-centric process models with other processes, such as plant hydraulics (Sperry et al. 1998, Tuzet et al. 2003).

While models of photosynthesis aim to model carbon uptake at the leaf scale, another common approach to understanding forest carbon dynamics is to model the growth, mortality, and competition of individual trees within forests. A variety of these models have been produced over the years, but they are often criticized for being either overly complex or not complex enough (Shugart and Woodward 2011). A few examples of forest patch models that consider individual-tree growth processes include JABOWA (Botkin et al. 1972, Bugmann 2001), SORTIE (Pacala et al. 1993, 1996), and ED (Moorcroft et al. 2001). By using patch models such as these, or truly individual-based models (Ogle and Pacala 2009), the trait space of trees can be analyzed theoretically and compared to empirically-derived trait relationships to explore the structure of the trait

space occupied by trees, including the potential factors that give rise to empirically observed tradeoffs.

## **Objectives**

The overall goal of my dissertation research was to better quantify tree functional traits and their interrelationships. Specific objectives included:

**O1:** Improve the quantification of mesophyll conductance ( $g_m$ ) by introducing fluorescence data into a biochemically based model of photosynthesis previously integrated in a Bayesian framework by Patrick et al. (2009).

**O2:** Quantify the trait space occupied by North American trees and gain a better understanding of the relationships between traits in the theoretical trait space that emerges from a process-based model of tree growth, allocation, and mortality.

**O3:** Assess the impact of filtering on the theoretical trait space of trees by imposing an environmental stress (light limitation) that would lead to mortality and a restriction of the trait space reminiscent of what happens in natural environments.

## **Approach and Insights**

My approach included a combination of field studies, statistical modeling, and computational approaches. I used these approaches to better understand how specific traits influence leaf-level photosynthesis and individual tree growth and mortality.

Chapter 2 addresses my first objective (**O1**). To better constrain a model of photosynthesis and improve estimates of commonly inferred photosynthetic traits, I conducted field work at three sites in Arizona, USA, including the McDowell Mountains and Sycamore Creek spanning the upper Sonoran Desert, and Chevelon Canyon on the lower Mogollon Rim (see Table 2.1). These sites varied in their temperature and

precipitation regimes. I collected simultaneous measurements of chlorophyll fluorescence and gas exchange to better estimate photosynthetic traits, including mesophyll conductance ( $g_m$ ). My focus on  $g_m$  was motivated by recent studies that point to the potentially overlooked importance of this trait for accurately predicting carbon assimilation. I then simultaneously fit the Farquhar et al. (1980) model of photosynthesis to light response curves, photosynthesis vs leaf-internal CO<sub>2</sub> curves, and fluorescence data. This also revealed interesting results with respect to intraspecific variation in  $g_m$  along the aridity gradient, such that estimated  $g_m$  and its variance decreased as aridity (water stress) increased in *Prosopis velutina*. I also found some evidence for differences between species and growth forms (angiosperms vs. gymnosperms). These findings could be important for correctly predicting productivity if the Farquhar et al. (1980) model is coupled to models at larger scales, as it often is.

Chapter 3 addresses my second objective (**O2**) of quantifying the trait space occupied by North American trees by using a Bayesian framework to fit the Allometrically Constrained Growth and Carbon Allocation (ACGCA) model (Ogle and Pacala 2009) to Forest Inventory and Analysis (FIA) data. ACGCA is an individual-based model of tree growth and mortality with inputs (parameters) that are directly interpreted as tree functional traits (32 traits). By using this modeling framework, I was able to assess the theoretical trait space (TTS) for North American trees in a way that complements work done in empirical studies. In particular, the TTS describes the multivariate trait space that is expected to produce realistic tree growth, as informed by FIA data. The trait space found ultimately had few strong bivariate interactions. However; there was evidence for trait-trait relationships found using stepwise regression that

indicated a more complicated multidimensional space. For example in a stepwise regression where radiation use efficiency was treated as dependent on the other 31 functional traits and light the resulting model had an  $R^2$  of 0.81 (Table S3.3, Figure 3.3). I also found that relationships between dependent traits and their predictors were in agreement with relationships seen in past work such as the leaf and wood economics spectra (Wright et al. 2004, Chave et al. 2009) when comparisons could be made.

Chapter 4 addresses my third objective (**O3**) of assessing the impact of filtering on the TTS of trees by applying a gap dynamics simulation to the TTS. This extended the results of my third chapter by allowing me to see how a more realistic environment can lead to both volume changes and shifts in the TTS. The simulations clearly demonstrated non-random mortality such that certain combinations of trait values were selected against (i.e., associated with trees that died under light stress); that is, the multivariate trait space of trees that died versus those that survived differed in their spread (volume) and nominal trait values (location). I also assessed the effects of filtering on relationships between traits (tradeoffs) as well as trait-mortality relationships. Interestingly, I found that six key traits (i.e., radiation use efficiency, maximum tree height, xylem conducting area to sapwood area ratio, senescence rate of coarse roots and branches, maintenance respiration rate of leaves, and maximum potential crown radius of a tree with diameter at breast height of 0m), out of 32 investigated, accounted for 93% of the variation in mortality rates among trees. Importantly, this study suggested that traits such as conducting area to sapwood area ratio and senescence rates of coarse roots and branches should be targeted in empirical, field studies, yet challenges associated with measuring such traits has led to

under-exploration of the importance of these traits for understanding whole-plant function and community dynamics.

## References

- Van Bodegom, P. M., J. C. Douma, and L. M. Verheijen. 2014. A fully traits-based approach to modeling global vegetation distribution. *Proceedings of the National Academy of Sciences* 111:13733–13738.
- Bonan, G. B., S. Levis, S. Sitch, M. Vertenstein, and K. W. Oleson. 2003. A dynamic global vegetation model for use with climate models: Concepts and description of simulated vegetation dynamics. *Global Change Biology* 9:1543–1566.
- Botkin, D. B., J. F. Janak, and J. R. Wallis. 1972. Some ecological consequences of a computer model of forest growth. *The Journal of Ecology* 60:849–872.
- Bugmann, H. 2001. A review of forest gap models. *Climatic Change* 51:259–305.
- Chave, J., D. Coomes, S. Jansen, S. L. Lewis, N. G. Swenson, and A. E. Zanne. 2009. Towards a worldwide wood economics spectrum. *Ecology Letters* 12:351–366.
- Clark, J. S., D. Bell, C. Chu, B. Courbaud, M. Dietze, M. Hersh, J. Hillerislambers, I. Ibáñez, S. Ladeau, S. McMahon, J. Metcalf, J. Mohan, E. Moran, L. Pangle, S. Pearson, C. Salk, Z. Shen, D. Valle, and P. Wyckoff. 2010. High-dimensional coexistence based on individual variation: A synthesis of evidence. *Ecological Monographs* 80:569–608.
- Diaz, S., J. Kattge, J. H. Cornelissen, I. J. Wright, S. Lavorel, S. Dray, B. Reu, M. Kleyer, C. Wirth, I. C. Prentice, E. Garnier, G. Bonisch, M. Westoby, H. Poorter, P. B. Reich, A. T. Moles, J. Dickie, A. N. Gillison, A. E. Zanne, J. Chave, S. J. Wright, S. N. Sheremet'ev, H. Jactel, C. Baraloto, B. Cerabolini, S. Pierce, B. Shipley, D. Kirkup, F. Casanoves, J. S. Joswig, A. Gunther, V. Falczuk, N. Ruger, M. D. Mahecha, and L. D. Gorne. 2016. The global spectrum of plant form and function. *Nature* 529:167–171.
- Dixon, R., A. Solomon, S. Brown, and R. Houghton. 1994. Carbon pools and flux of global forest ecosystems. *Science* 263:185–190.
- Farquhar, G. D., S. Caemmerer, and J. A. Berry. 1980. A biochemical model of photosynthetic CO<sub>2</sub> assimilation in leaves of C<sub>3</sub> species. *Planta* 149:78–90.
- Flexas, J., M. M. Barbour, O. Brendel, H. M. Cabrera, M. Carriquí, A. Díaz-Espejo, C. Douthe, E. Dreyer, J. P. Ferrio, J. Gago, A. Gallé, J. Galmés, N. Kodama, H. Medrano, Ü. Niinemets, J. J. Peguero-Pina, A. Pou, M. Ribas-Carbó, M. Tomás, T. Tosens, and C. R. Warren. 2012. Mesophyll diffusion conductance to CO<sub>2</sub>: an unappreciated central player in photosynthesis. *Plant Science* 193–194:70–84.
- Fyllas, N. M., E. Gloor, L. M. Mercado, S. Sitch, C. A. Quesada, T. F. Domingues, D. R. Galbraith, A. Torre-Lezama, E. Vilanova, H. Ramírez-Angulo, N. Higuchi, D. A.

- Neill, M. Silveira, L. Ferreira, G. a. Aymard C., Y. Malhi, O. L. Phillips, and J. Lloyd. 2014. Analysing Amazonian forest productivity using a new individual and trait-based model (TFS v.1). *Geoscientific Model Development* 7:1251–1269.
- Hutchinson, G. E. 1957. Concluding remarks. *Cold Spring Harbor Symposia on Quantitative Biology* 22:415–427.
- Keenan, T., S. Sabate, and C. Gracia. 2010. The importance of mesophyll conductance in regulating forest ecosystem productivity during drought periods. *Global Change Biology* 16:1019–1034.
- Lloyd, J., K. Bloomfield, T. F. Domingues, and G. D. Farquhar. 2013. Photosynthetically relevant foliar traits correlating better on a mass vs an area basis: Of ecophysiological relevance or just a case of mathematical imperatives and statistical quicksand? *New Phytologist* 199:311–321.
- McMahon, S. M., C. J. E. Metcalf, and C. W. Woodall. 2011. High-dimensional coexistence of temperate tree species: functional traits, demographic rates, life-history stages, and their physical context. *PloS One* 6:e16253.
- Moorcroft, P. R., G. C. Hurtt, and S. W. Pacala. 2001. A Method for Scaling Vegetation Dynamics : the Ecosystem Demography Model ( Ed ). *Ecological Monographs* 71:557–586.
- Ogle, K., and S. W. Pacala. 2009. A modeling framework for inferring tree growth and allocation from physiological, morphological and allometric traits. *Tree Physiology* 29:587–605.
- Osnas, J. L. D., J. W. Lichstein, P. B. Reich, and S. W. Pacala. 2013. Global Leaf Trait Relationships: Mass, Area, and the Leaf Economics Spectrum. *Science* 340:1–4.
- Pacala, S. W., C. D. Canham, J. Saponara, J. A. Silander Jr, R. K. Kobe, and E. Ribbens. 1996. Forest models defined by field measurements: estimation, error analysis and dynamics. *Ecological Monographs* 66:1–43.
- Pacala, S. W., C. D. Canham, and J. A. Silander Jr. 1993. Forest models defined by field measurements: I. The design of a northeastern forest simulator. *Canadian Journal of Forest Research* 23:1980–1988.
- Pan, Y., R. A. Birdsey, J. Fang, R. Houghton, P. E. Kauppi, W. a. Kurz, O. L. Phillips, A. Shvidenko, S. L. Lewis, J. G. Canadell, P. Ciais, R. B. Jackson, S. Pacala, A. D. McGuire, S. Piao, A. Rautiainen, S. Sitch, and D. Hayes. 2011. A Large and Persistent Carbon Sink in the World’s Forests. *Science* 333:988–993.
- Patrick, L. D., K. Ogle, and D. T. Tissue. 2009. A hierarchical Bayesian approach for estimation of photosynthetic parameters of C(3) plants. *Plant, Cell & Environment* 32:1695–1709.

- Perry, D. A., R. Oren, and S. C. Hart. 2008. *Forest Ecosystems*. Second Edi. The Johns Hopkins University Press, Baltimore, Maryland.
- Reich, P. B. 2014. The world-wide “fast-slow” plant economics spectrum: a traits manifesto. *Journal of Ecology* 102:275–301.
- Scheiter, S., L. Langan, and S. I. Higgins. 2013. Next-generation dynamic global vegetation models: Learning from community ecology. *New Phytologist* 198:957–969.
- Shugart, H. H., and F. I. Woodward. 2011. *Global Change and the Terrestrial Biosphere, Achievements and Challenges*. John Wiley & Sons.
- Sperry, J. S., F. R. Adler, G. S. Campbell, and J. P. Comstock. 1998. Limitation of plant water use by rhizosphere and xylem conductance: results from a model. *Plant, Cell & Environment* 21:347–359.
- Tilman, D. 1985. The resource-ratio hypothesis of plant succession. *American Naturalist* 125:827–852.
- Tilman, D. 2004. Niche tradeoffs, neutrality, and community structure: a stochastic theory of resource competition, invasion, and community assembly. *Proceedings of the National Academy of Sciences* 101:10854–10861.
- Tuzet, A., A. Perrier, and R. Leuning. 2003. A coupled model of stomatal conductance, photosynthesis and transpiration. *Plant, Cell and Environment* 26:1097–1116.
- Wright, I. J., P. B. Reich, M. Westoby, D. D. Ackerly, Z. Baruch, F. Bongers, J. Cavender-Bares, T. Chapin, J. H. C. Cornelissen, M. Diemer, J. Flexas, E. Garnier, P. K. Groom, J. Gulias, K. Hikosaka, B. B. Lamont, T. Lee, W. Lee, C. Lusk, J. J. Midgley, M.-L. Navas, U. Niinemets, J. Oleksyn, N. Osada, H. Poorter, P. Poot, L. Prior, V. I. Pyankov, C. Roumet, S. C. Thomas, M. G. Tjoelker, E. J. Veneklaas, and R. Villar. 2004. The worldwide leaf economics spectrum. *Nature* 428:821–827.

## 2. INCORPORATING FLUORESCENCE DATA INTO A HIERARCHICAL BAYESIAN PHOTOSYNTHESIS MODELING FRAMEWORK TO BETTER ESTIMATE MESOPHYLL CONDUCTANCE ALONG REGIONAL AND LOCAL ARIDITY GRADIENTS

### Abstract

Mesophyll conductance ( $g_m$ ) is important for understanding photosynthesis ( $A$ ), but current methods for estimating  $g_m$  do not simultaneously consider multiple relevant data sources, and they typically lack appropriate uncertainty quantification. Thus, we developed a hierarchical Bayesian (HB) approach for simultaneously fitting photosynthesis models to fluorescence and  $A-C_i$  and/or  $A-Q$  ( $C_i$  = leaf-internal  $[\text{CO}_2]$ ,  $Q$  = photon flux density) response curve data. We tested the HB model against artificial data, and explored the influence of including fluorescence data. We applied the HB model to estimate  $g_m$  in four woody species (*Prosopis velutina*, *Salix gooddingii*, *Quercus gambelii*, *Juniperus monosperma*) spanning regional and local gradients in water availability in Arizona. Estimates of  $g_m$  in *Prosopis velutina* (velvet mesquite) followed expected patterns, with higher  $g_m$  at low, vs intermediate, vs high aridity sites (12.56 vs 3.85, vs 0.75  $\mu\text{mol m}^{-2}\text{s}^{-1}\text{Pa}^{-1}$ ). *Juniperus monosperma* (one-seed juniper) had lower mean  $g_m$  values at the two sites where it was estimated (1.36 and 1.46  $\mu\text{mol m}^{-2}\text{s}^{-1}\text{Pa}^{-1}$ ) than mean  $g_m$  for angiosperm trees at four out of five sites (3.85, 4.30, 12.56, and 14.08  $\mu\text{mol m}^{-2}\text{s}^{-1}\text{Pa}^{-1}$ ). The exception for angiosperms was drought stressed *P. velutina* ( $\sim 0.75 \mu\text{mol m}^{-2}\text{s}^{-1}\text{Pa}^{-1}$ ). The values of  $g_m$  found for both *J. monosperma* and *P. velutina* were low enough to affect estimates of photosynthetic parameters if  $g_m$  was not included in the model. Thus,  $g_m$  should be considered when modeling photosynthesis in either arid

environments, or when gymnosperms are present. The HB approach applied to multiple datasets (fluorescence, response curves, and potentially isotopes) is likely to facilitate better estimates of  $g_m$ , which is important for estimating other biochemical parameters, especially in water stressed conditions where  $g_m$  is expected to have the greatest impact on photosynthesis.

**Keywords:**  $A-C_i$  curve;  $A-Q$  curve; CO<sub>2</sub>-response curve; fluorescence; Farquhar et al. model; hierarchical Bayesian; light-response curve; mesophyll conductance; photosynthesis

## Introduction

In many early papers on modeling photosynthesis (Caemmerer and Farquhar 1981, Farquhar and Sharkey 1982, Dubois et al. 2007), the only conductance term explicitly considered was stomatal conductance ( $g_s$ ), thus effectively assuming infinite leaf-internal (or mesophyll) conductance to CO<sub>2</sub> ( $g_m$ ). In recent years, this assumption of an infinite conductance has been shown to affect estimates of key photosynthetic parameters, including maximum rates of carboxylation ( $V_{cmax}$ ) and electron transport ( $J_{max}$ ). Specifically,  $V_{cmax}$  and  $J_{max}$  can be underestimated in water stressed conditions (e.g., arid environments, under drought) if  $g_m$  is not considered (Ethier and Livingston 2004, Flexas et al. 2007b, 2012, Niinemets et al. 2009a, Keenan et al. 2010a). As such, it has become evident that estimates of  $g_m$  should be included in mechanistic models of photosynthesis (Loreto et al. 1992, Warren and Adams 2006, Flexas et al. 2007a, 2007b, 2012), especially when considering variable environmental conditions.

Indeed, underestimating or ignoring  $g_m$  can have a large impact on predicted photosynthetic rates. When  $g_m$  is expected to be high, it can lead to an ~7% overestimation of photosynthesis (Niinemets et al. 2009a), while ignoring low values of  $g_m$  can lead to an underestimation of up to 70% (Niinemets et al. 2009b). Because it is common to scale leaf-level photosynthesis to the canopy using big-leaf models (De Pury and Farquhar 1997, Wang and Leuning 1998), underestimation of photosynthesis due to inadequate consideration of  $g_m$  could have large-scale repercussions. For example, in a study of Mediterranean systems, including  $g_m$  led to significantly lower modeled photosynthetic rates at high temperatures and vapor pressure deficits compared to when  $g_m$  was considered infinite (Keenan et al. 2010b).

Due to the importance of  $g_m$ , there have been advances in statistical and experimental methods for estimating  $g_m$  within the context of photosynthetic models (Harley et al. 1992, Loreto et al. 1992). Four common approaches of estimating  $g_m$  are the (1) variable  $J$  (electron transport) (Harley et al. 1992, Loreto et al. 1992), (2) constant  $J$  (Harley et al. 1992, Loreto et al. 1992), (3) carbon isotope (Evans et al. 1986, Loreto et al. 1992), and (4) curve fitting (Ethier and Livingston 2004) methods. The first three methods estimate  $g_m$  outside of the model fitting process using empirical measurements (Harley et al. 1992, Loreto et al. 1992, Pons et al. 2009). They then calculate the chloroplastic  $[\text{CO}_2]$  ( $C_c$ ) using the calculated  $g_m$ . The  $C_c$  estimates are subsequently treated as “data” and are used instead of intercellular  $[\text{CO}_2]$  ( $C_i$ ) when fitting the Farquhar *et al.* (1980) (FvCB) model to leaf-level gas exchange data. In the curve fitting approaches, generally no additional data (fluorescence or isotope data) are used, and estimates of  $g_m$  are obtained by treating it as one of the unknown parameters in the FvCB model (Sharkey et al. 2007). However, Bellasio *et al.* (2015) describe a step-by-step fitting procedure (in Excel) that assimilates data on four types of photosynthesis ( $A$ ) response curves— $A-Q$  (light) and  $A-C_i$  under ambient and low  $\text{CO}_2$ —to produce more accurate and precise estimates of  $g_m$ , but generating such response curves under low  $\text{CO}_2$  is challenging in field settings.

Alternative curve fitting approaches have been developed that also facilitate estimation of  $g_m$ . For example, Patrick *et al.* (2009) fit the FvCB model using a hierarchical Bayesian framework, allowing for (1) the incorporation of semi-informative priors for parameters that are not well-informed by the gas exchange data, and (2) the simultaneous estimation of model parameters, including  $g_m$  and its temperature

dependency. As an alternative, Gu *et al.* (2010) developed a model fitting procedure that minimizes a cost function based on three possible limitation states (Rubisco, RuBP regeneration, and Triose-phosphate utilization). The best fit is then chosen after fitting all possible limitation state distributions given the data (Gu *et al.* 2010). Both of these sophisticated model fitting approaches are still somewhat limited in the data that they use; Gu *et al.* (2010) only used  $A-C_i$  data, Patrick *et al.* (2009) used both  $A-Q$  and  $A-C_i$  data, and it appears that in both case, the curves were generated under ambient  $O_2$ . However, both of these approaches are potentially flexible enough to incorporate additional data types, and here we illustrate how the Bayesian model originally described by Patrick *et al.* (2009) can be extended to include fluorescence data.

Along with the realization that  $g_m$  should be included in models of photosynthesis, there have been advancements in measurement methods relevant to estimating  $g_m$ , some of which have led to the relatively easy collection of fluorescence data while simultaneously measuring photosynthesis. Fluorescence data can be used in conjunction with gas exchange measurements to derive values for  $g_m$  using the variable and constant  $J$  methods, both of which have limitations (Harley *et al.* 1992, Pons *et al.* 2009, Gilbert *et al.* 2012). For example, neither method directly incorporates fluorescence measurements into the FvCB model fitting procedure. As noted above, these approaches express  $g_m$  as a function of variables (e.g.,  $C_i$ ,  $J$ ,  $\Gamma^*$ ,  $R_d$ , and  $A$ ) that are subsequently treated as data (e.g.,  $C_c$ ,  $A$ ) or parameters (e.g.,  $\Gamma^*$ ,  $R_d$ ) in the process of fitting the FvCB model. Of these variables,  $A$  and  $C_i$  come from gas exchange measurements, and  $J$  and  $C_c$  are calculated from fluorescence data (Harley *et al.* 1992, Pons *et al.* 2009). It has recently been noted that using fluorescence data via the variable  $J$  approach can bias our understanding of the

response of  $g_m$  to CO<sub>2</sub> (Gu and Sun 2014). The Excel fitting methods developed by Bellasio *et al.* (2015), however, allows for estimation of photosynthesis parameters, including  $g_m$ , from combined gas exchange and fluorescence data. Their approach, however, may be described as a step-wise or piece-wise analysis that does not provide a full accounting of the uncertainty associated with measurement error or parameter uncertainty. Due to these considerations, a stochastic model incorporating fluorescence data while avoiding direct calculation of  $g_m$  from data used in fitting the FvCB model is desirable.

Our first objective was to improve photosynthetic parameter estimates by directly incorporating both response curve data and fluorescence data into a stochastic modeling framework. We chose to do this via a hierarchical Bayesian (HB) modeling approach that can easily accommodate multiple datasets (e.g.,  $A-C_i$  curves,  $A-Q$  curves, and accompanying fluorescence data) to simultaneously inform parameters in the FvCB model. We assessed our HB model by (1) using artificial data to recover known parameter values, and (2) evaluating the effect of including fluorescence data on model fit and estimation of  $g_m$  using gas exchange data collected in the field. Once establishing the validity of our HB model, our second objective was to utilize our model to determine the magnitude of  $g_m$  and its relative variation across an elevation gradient representing gradients in water availability (precipitation) and temperature in Arizona (Table 2.1). This was motivated by previous studies suggesting  $g_m$  is affected by temperature and plant water status (Bernacchi *et al.* 2002, Warren and Dreyer 2006, Warren 2008, Flexas *et al.* 2008). For instance, the sensitivity of  $g_m$  to water stress may be just as great as the sensitivity of stomatal conductance ( $g_s$ ), though, the exact nature of the relationship

between  $g_s$  and  $g_m$  (e.g., linear, non-linear, variable) is uncertain (Warren 2008). In particular, several studies (Warren 2008, Flexas et al. 2008) indicate that water stress may lead to reduced  $g_m$  over periods of time ranging from minutes to months, but it is not clear how  $g_m$  should be affected by different levels of water stress in plants native to a semi-arid climate. We hypothesized that plants growing along our elevation gradient would exhibit lower  $g_m$  and less variation in  $g_m$  when growing under more water stressed conditions compared to plants growing near a water source.

## **Methods**

### *Field sites and study species*

Field work was conducted along an aridity gradient that spans desert woodlands in the Sonoran Desert near Phoenix, AZ to forested high country around Payson, AZ (see Table 2.1 for sites and sample sizes). The sites along this gradient in elevation, temperature, and precipitation allowed us to investigate variation in photosynthetic parameters at two scales. Small scale (local) variation was assessed by sampling pronounced aridity gradients over short distances within a site created by the transitioning from lowland areas along creeks to dry uplands. Large scale (regional) variability was assessed by comparing parameter estimates across sites that occur at two elevations characterized by different climates (Table 2.1). The sites varied in temperature, precipitation (Table 2.1), and water availability, all of which have been found to directly or indirectly influence  $g_m$  (Bernacchi et al. 2002, Flexas et al. 2009, 2012, Tosens et al. 2012).

We focused on four perennial woody species, with varying leaf structure, common to each site, including *Prosopis velutina* (velvet mesquite), *Salix gooddingii* (Goodding's willow), *Juniperus monosperma* (one-seed juniper), and *Quercus gambelii* (Gambel oak). *P. velutina* is abundant at the McDowell Mountain and Sycamore Creek sites, and it was one of the few tree species found in both lowland and upland habitats at Sycamore Creek and has been shown to have a  $\Psi_{crit}$  (water potential at hydraulic failure) between -5 and -8 MPa (Pockman and Sperry 2000). *S. gooddingii* is a common riparian species in the southwestern United States and was also abundant along Sycamore Creek, but absent in upland areas. At Chevelon Canyon, *J. monosperma* and *Q. gambelii* were sampled; *J. monosperma* was found near the canyon bottom as well as in the upland areas and is known to be highly drought tolerant (Linton et al. 1998, Pockman and Sperry 2000, Plaut et al. 2012). *Q. gambelii* is also drought tolerant, but was only found in abundance along the creek, and is less tolerant of water stress compared to co-occurring *J. monosperma* (Neilson and Wullstein 1985, Williams and Ehleringer 2000). Sampling *P. velutina* and *J. monosperma* in upland and lowland areas, as well as *P. velutina* in the McDowell Mountains (only in the desert), allowed us to investigate the effects of differing levels of water stress.

#### *Leaf physiology measurements*

Leaf physiological measurements consisting of  $A-C_i$  (photosynthesis vs. leaf-internal  $[CO_2]$ ) and  $A-Q$  ( $A$  vs. light) responses curves were measured during a period from May to October 2012 using a LI-6400 equipped with a leaf chamber fluorometer (LI-COR Lincoln, Nebraska, 6400-40), which permits the simultaneous measurement of photosynthesis and chlorophyll fluorescence. Variable chlorophyll fluorescence is

primarily due to light emitted by photosystem II (PSII) and is related to the electron flow through PSII per quanta, or  $\phi_{PSII}$  (Murata et al. 1966, Schreiber et al. 1994, von Caemmerer 2000).

Fully expanded leaves exposed to full light were chosen from branches accessible with a tripod. Since the scaly leaves of *J. monosperma* often caused chamber leaks due to gaps between the leaves and gasket material, a viscoelastic liquid silicone putty was used to seal the chamber around these leaves. The leaf chamber fluorometer is different from the standard LI-6400 chamber in that the chamber area is one third that of the standard chamber (2 vs. 6 cm<sup>2</sup>), which can lead to increased measurement error. Since one of the main goals of this study was to simultaneously fit the FvCM model to fluorescence,  $A-C_i$ , and  $A-Q$  data, the limitations of the leaf chamber fluorometer were deemed acceptable in the absence of a more accurate method, and our statistical modeling approach explicitly quantifies observation error.

On each leaf, we measured  $A-C_i$  curves at a constant, saturating light level of 1500  $\mu\text{mol photons m}^{-2}\text{s}^{-1}$ .  $A-C_i$  measurements were made at chamber  $[\text{CO}_2]$  levels in order of 300, 200, 100, 50, 200, 400, 600, 800, 1200, 1500, and 2000  $\mu\text{mol mol}^{-1}$ . After measuring 11 curves and reviewing initial results, the  $[\text{CO}_2]$  of 100  $\mu\text{mol mol}^{-1}$  was added to better capture the initial part of the curve (at low  $[\text{CO}_2]$ ), and the 2000  $\mu\text{mol mol}^{-1}$  value was removed because it was found not to be necessary. Leaves were allowed to stabilize under initial chamber conditions (400 ppm  $\text{CO}_2$ ) for at least 5 min prior to starting  $A-C_i$  curves.

For  $A-Q$  curves, the chamber was maintained at near ambient  $[\text{CO}_2]$  of 400  $\mu\text{mol mol}^{-1}$ , and incident irradiance ( $Q$ ) was varied in order from 2000, 1800, 1500, 1000, 800,

500, 200, 100, 50, to 0  $\mu\text{mol m}^{-2} \text{s}^{-1}$ . The 2000 and 1800  $\mu\text{mol m}^{-2} \text{s}^{-1}$  levels were not included in the first nine of 46 curves; they were added later during the sampling season to ensure the entire curve was captured. Leaves were allowed 5 min at 1500  $\mu\text{mol m}^{-2} \text{s}^{-2}$  to stabilize prior to starting *A-Q* curves. Before each measurement, the light level was set and at least 2 min were allowed for stabilization.

While performing each curve, leaves were given at least 3 min to stabilize at each  $[\text{CO}_2]$  or light level prior to measurement. *A-C<sub>i</sub>* and *A-Q* curves (described below) were measured sequentially with each pair being considered one curve for analysis.

Temperatures were controlled near the ambient outside temperature for each curve and thus varied between curves. The change in temperature from start to completion of a single curve ranged from 0.12 to 6.56° C with a mean of 1.55° C. Oxygen ( $\text{O}_2$ ) levels were based on ambient conditions.

For both *A-C<sub>i</sub>* and *A-Q* curves, a leak correction was applied to all readings according to the LI-6400 manual, and it was necessary to correct the leaf area used in the calculation of *A*. For leaves not filling the chamber, the orientation was marked and they were scanned using a template representative of the shape and size of the LI-6400 chamber used. When leaves did not fill the chamber, their position in the chamber was marked on the leaf sample so area could be determined in the lab. For *P. velutina* and *J. monosperma*, there was some leaf overlap that occurred in the chamber. In the cases where this happened, the projected area was used such that the area was equal to the total area illuminated in the chamber. Leaf area was determined with ImageJ (Schneider et al. 2012) and corrections were made to the LI-6400 output, including *A* and stomatal conductance ( $g_s$ ) associated with each measurement.

Along with measuring leaf area, we also measured branch water potential ( $\psi_b$ , MPa) at the start and end of each  $A-C_i$  and  $A-Q$  curve pair to use as an indication of the plant's level of water stress. To do so, a small branch (twig) was cut near the leaf being used for  $A-C_i$  and  $A-Q$  measurements. The branch was inserted into a pressure chamber (PMS instruments Model 1505D) to determine  $\psi_b$ , which was subsequently used to calculate the relative difference in water potential given by

$\Delta\psi_b = (\psi_{b,crit} - \psi_{b,average})/\psi_{b,crit}$ , where the  $\psi_{b,crit}$  is the water potential expected at complete loss of water transport, based on literature-derived values (Pockman and Sperry 2000, Plaut et al. 2012). The  $\psi_{b,average}$  values represent the average  $\psi_b$  values for each plant.

#### *Data analysis and modeling approach*

First, we provide an overview of the photosynthesis model. Second, we detail the statistical approach used to fit the model to the data. Third, we outline the hierarchical structure of the parameter model. Finally, we describe how the Bayesian model was implemented and how convergence was assessed. A full listing of model parameters, descriptions, and units is given in Table 2.2.

#### *Photosynthesis model description*

The photosynthesis model is based on Farquhar *et al.* (1980), Farquhar and Wong (1984), Von Caemmerer (2000), Either and Livingston (2004), and Ethier *et al.* (2006), as described in Patrick *et al.* (2009). One of the important differences between our model

versus that of Patrick *et al.* (2009) is our treatment of the rate limiting photosynthesis.

We assume photosynthesis is given by a piecewise function:

$$A = \begin{cases} \min(A_c, A_j) & \text{if } \Gamma^* < C_c \\ A_c & \text{if } \Gamma^* > C_c \end{cases} \quad (1)$$

Where  $A_c$  (Rubisco-limited rate) and  $A_j$  (electron transport limited rate) are given by:

$$A_c = f(V_{cmax}, C_i, O, R_d, g_m, \Gamma^*, K_o, K_c) \quad (2)$$

$$A_j = f(J, C_i, R_d, g_m, \Gamma^*) \quad (3)$$

Finally,  $J$  (electron transport rate) is given by:

$$J = f(J_{max}, Q_2, \theta) \quad (4)$$

Where the functions on the right-hand sides of Eqns (2), (3), and (4) are given in (Table 2.3). The piecewise function in Eqn (1) is used to ensure that the correct limitation state will be chosen at low  $[\text{CO}_2]$  (i.e., when  $\Gamma^* > C_c$ ; Gu *et al.* (Gu et al. 2010)). This is necessary because photosynthesis is carboxylation limited ( $A_c$ ), not RuBP regeneration limited ( $A_j$ ) at low  $[\text{CO}_2]$  (Farquhar et al. 1980, von Caemmerer 2000, Gu et al. 2010). In theory, there may be conditions where RuBP regeneration limitation could be the correct limitation at low light such that Eqn (1) might lead to the wrong limitation state, but this was not an issue in our analysis given our data and parameter estimates. For simplicity, we do not include triose-phosphate utilization (TPU) limited rates following Patrick et al. (2009).

Equation (1) can also be viewed as a change-point model (Gu et al. 2010) in the sense that there is a critical  $C_c$  value ( $C_{crit} > \Gamma^*$ ) associated with the transition between  $A_c$  and  $A_j$ . Many past studies assume that  $C_{crit}$  is known by specifying a fixed value for this

change point (Dubois et al. 2007, Gu et al. 2010), thus avoiding the actual evaluation of  $\min(A_c, A_j)$  in Eqn (1) (Sharkey et al. 2007). Patrick *et al.* (2009) improved upon this by assuming that  $C_{crit}$  is unknown (as opposed to fixing it at pre-determined values), and they estimated it as part of the model fitting process. Alternatively, Gu *et al.* (2010) included checks to ensure points were not assigned to the wrong limitation state after fitting the model. In our approach, we do not explicitly estimate  $C_{crit}$ , and we take an approach similar to Gu *et al.* (2010) by computing both  $A_c$  and  $A_j$  for all observations, and the minimum function (value) is selected by the algorithm (when  $C_c < I^*$ ). Thus, this is no longer a true change-point model from a statistical perspective (e.g., Carlin et al. 1992, Perreault et al. 2000 Carlin et al. 1992; Perreault et al. 2000) given that we do not explicitly estimate  $C_{crit}$ .

We also extended the fitting approach by directly incorporating measured chlorophyll fluorescence data into the Bayesian routine (described below). We used the  $\phi PSII$  data obtained from the LI-6400, based on  $\phi PSII = f_{m_i} - f_{s_i} / f_{m_i}$ , where  $f_m$  is the maximum fluorescence during a saturating light pulse, and  $f_s$  is the steady state fluorescence.  $J$  is related to  $\phi PSII$  through the following equation (Genty et al. 1989):

$$J = \alpha \beta Q(\phi PSII) \quad (5)$$

where  $\alpha$  is the leaf absorptance, which we measured with a spectroradiometer and integrating sphere (Optronic Laboratories, 754) according to Day *et al.* (2015);  $\beta$  is the partitioning of electrons between photosystem I (PSI) and PSII;  $Q$  is the incident irradiance. We rearranged Eqn 5 to obtain an expression for  $\phi PSII$ :

$$\varphi_{PSII} = \begin{cases} \frac{J}{\alpha \beta Q} & \text{if } Q > 0 \\ \varphi_{max} & \text{if } Q = 0 \end{cases} \quad (6)$$

Eqn 6 was given as a piecewise function to accommodate situations when  $Q$  was set to 0  $\mu\text{mol m}^{-2} \text{s}^{-1}$ ; the use of  $\varphi_{max}$  was only relevant for <4% of the data, and only for  $A-Q$  curve data (i.e., for observations with  $Q = 0$ ). The remaining equations for the photosynthesis model are presented in Table 2.3.

### *Bayesian model fitting procedure*

We fit the FvCB model described above to the  $A-C_i$  and  $A-Q$  data using a modification of the HB approach presented in Patrick *et al.* (2009). The HB method allows for the simultaneous estimation of key parameters, including  $V_{cmax}$ ,  $J_{max}$ ,  $R_d$ ,  $g_m$ , etc. (Table 2.3), at the curve, plant, and species by site levels while also providing estimates of parameter uncertainty. Unique to the HB approach is the opportunity to integrate prior knowledge about parameters in the FvCB model that may not be directly informed by the field data; see Patrick *et al.* (2009) for a detailed discussion about this. We begin with describing the uncertainty in the observed data. For observation  $i$  ( $i = 1, \dots, 905$ ), the likelihood for the observed  $A$  data ( $A_{obs_i}$ ) obtained from both  $A-C_i$  and  $A-Q$  curves is given by a normal distribution:

$$A_{obs_i} \sim \text{Normal}(\overline{A}_i, \sigma_A^2) \quad (7)$$

where  $\overline{A}_i$  is the mean or predicated photosynthetic rate given by the FvCB model (based on Eqn 1 and associated equations in Table 2.3), and  $\sigma_A^2$  is the variance describing observation or measurement error.

The accompanying observed  $\varphi PSII$  data ( $\varphi PSII_{obs}$ ), which are defined on the interval (0,1), were logit transformed, and the transformed data were assumed to follow a normal distribution:

$$\text{logit}(\varphi PSII_{obs_i}) \sim \text{Normal}(\text{logit}(\overline{\varphi PSII_i}), \sigma_{PSII}^2) \quad (8)$$

where  $\overline{\varphi PSII_i}$  is the mean or predicted electron flow through PSII per quanta (given by Eqn 6), and  $\sigma_{PSII}^2$  is the variance describing the observation or measurement error.

Temperature dependencies of key photosynthesis parameters (see Table 2.2) were incorporated such that  $R_d$ ,  $g_m$ ,  $K_c$ ,  $K_o$ , and  $\Gamma^*$  were modeled using non-peaked Arrhenius functions, while  $V_{cmax}$  and  $J_{max}$  were modeled using peaked Arrhenius functions (Table 2.3), as described by Patrick *et al.* (2009).

#### *Prior specification*

Finally, as part of the HB framework, we specified priors for the photosynthesis parameters similar to Patrick *et al.*(2009). We summarize the priors that we used, and the full list of priors is given in Table S2.1 (supporting material). For those parameters that incorporated temperature dependencies, the temperature-corrected (relative to 25° C) parameters were assigned hierarchical priors depending on the level at which each parameter was expected to vary. Those defined at the curve level are denoted by  $Y_{25_c} = R_{d25}$ ,  $g_{m25}$ ,  $V_{cmax25}$ , or  $J_{max25}$ , where  $c$  indexes the curve ( $c = 1, \dots, 46$ ). These curve-level parameters were assumed to vary around plant-level parameters such that for plant  $p$  ( $p = 1, \dots, 23$ ) associated with curve  $c$ :

$$Y_{25_c} \sim \text{Normal}(\mu Y_{25_p}, \sigma_{Y_{25}}^2) \quad (9)$$

Likewise, each plant-level parameter ( $\mu Y_{25p}$ ) was assumed to vary around a species by site level parameter such that for species by site combination  $st$  ( $st = 1, \dots, 7$ ) associated with plant  $p$ :

$$\mu Y_{25p} \sim Normal(\mu^* Y_{25st}, \sigma_{Y_{25}}^{2*}) \quad (10)$$

One advantage of the HB approach is the ability to incorporate informative priors for parameters that are not expected to be well informed by the data while still allowing them to be stochastic quantities, thus acknowledging the fact that the values of such parameters are not known exactly. For example, the activation energies,  $E_r$ ,  $E_m$ ,  $E_v$ ,  $E_j$  (Table 2.2), in the temperature response functions for  $R_d$ ,  $g_m$ ,  $V_{cmax}$ , and  $J_{max}$ , respectively, were given non-hierarchical (i.e., independent) semi-informative priors at the species by site level (Table S2.1). The remaining activation energies ( $E_g$ ,  $E_{kc}$ , and  $E_{ko}$ , for  $\Gamma^*$ ,  $K_c$ , and  $K_o$ , respectively), entropy parameters ( $S_v$  and  $S_j$ ), deactivation parameters ( $H_v$  and  $H_j$ , for  $V_{cmax}$  and  $J_{max}$ , respectively), and  $\Gamma_{25}^*$  were given informative non-hierarchical priors at the species level (Table S2.1). Patrick *et al.* (2009) provide a detailed description and citations associated with the specification of these informative and semi-informative priors. It should be noted that many of these parameters (e.g.,  $E$ 's,  $S$ 's, and  $H$ 's) are typically held constant in most curve fitting approaches, but our HB approach acknowledges uncertainty in these parameters.

With the incorporation of fluorescence data, we introduced two additional parameters ( $\beta$  and  $\phi_{max}$ ) associated with the model for  $\phi_{PSII}$  (Eqn 6). We specified semi-informative beta distribution priors for both parameters given that they are constrained to the interval (0,1). A beta(10,10) prior was used for the species by site level

$\beta$  parameter, corresponding to a prior mean of 0.5, based on previous work (Laisk and Loreto 1996, von Caemmerer 2000) (Table S2.1). For convenience, a beta(16,4) prior, corresponding to a prior mean of 0.8, was specified for the scalar parameter  $\varphi_{max}$ ; this prior was based on the maximum observed  $\varphi_{PSII}$  in our dataset. All standard deviation parameters were assigned relatively non-informative folded-Cauchy priors as done in Patrick *et al.*(2009), following Gelman (2006). In practice, the utility of using semi-informative or informative priors is that uncertainty in the associated parameters is accounted for, and if the data do not provide additional information about these parameters, then the posterior estimates will reflect this prior uncertainty. In general, the majority of posteriors for parameters that were assigned semi-informative priors remained close to their priors or shifted slightly, indicating that either the data were insufficient to inform the parameter(s) or that the priors were consistent with the data. Use of informative priors and hierarchical priors also leads to a reduction in the effective number of model parameters relative to the actual or countable number of parameters in the model (Spiegelhalter *et al.* 2002).

Another benefit of the HB method is the ability to control feedback between different model components. In this study, we implemented feedback control as a way of indicating which data set should inform a given parameter or set of parameters. Feedback control or model modularization techniques have been found to be useful in a range of modeling applications such as meta-analyses, analysis of complex computer models, and in cases where some of the data in a model are not expected to influence all of the parameters (Liu *et al.* 2009, Ogle *et al.* 2013). In a full Bayesian model, the posteriors for all parameters would be affected by all of the data. Based on preliminary

analyses and Patrick *et al.* (2009), we used feedback control to ensure that the  $V_{cmax}$  and  $J_{max}$  models and their associated parameters are only informed by the  $A-C_i$  (not  $A-Q$ ) data. Similarly, the  $R_d$  model and its parameters were only informed by the  $A-Q$  data. All other parameters were informed by all data.

### *HB model implementation*

The goal of a Bayesian analysis is to obtain or estimate the posterior *distribution* of the model parameters. Algorithms for estimating the posterior, such as Markov chain Monte Carlo (MCMC), return parameter values that are sampled from the posterior. This is in contrast to optimization approaches that seek the maximum (or minimum) of an objective function, and which are more vulnerable to getting stuck in local optima. The stochastic nature of the MCMC algorithm, paired with running multiple chains started at diffuse parameter values, makes it much less susceptible to getting stuck in minor modes (Gamerman and Lopes 2006).

The HB model was implemented in OpenBUGS (see Appendix B for model code), a free, open source program for conducting Bayesian analysis (Lunn et al. 2009b). Feedback control was implemented using the built-in cut function in OpenBUGS (Lunn et al. 2009a, Molitor et al. 2009, Ogle et al. 2013). We ran three parallel Markov chain Monte Carlo (MCMC) chains, and the chains were allowed to burn in for 1000 iterations prior to convergence. Convergence was assessed using the BGR diagnostic tool provided in OpenBUGS. After burn in, the model was run for an additional ~60,000 iterations per chain, which were thinned by 50 to remove autocorrelation and reduce storage requirements. Thus, roughly 3600 independent samples were obtained from the (pseudo)-

posterior distribution, and the output was processed (e.g., to obtain posterior means and interval estimates) and graphed in R (R Core Team 2015).

### *Model assessment*

We employed the following methods for assessing the HB model: (1) challenging it with artificial data, (2) evaluating the effect of incorporating fluorescence data, and (3) evaluating model goodness of fit. Below, we describe each method in more detail.

First, artificial data were generated from a set of known parameter values. Realistic parameter values were derived from the literature based on three species (*Nicotiana tobacum*, *Acer rubrum*, and *Larrea tridentata*) representing different life forms (forb, tree, shrub) and characterized by different photosynthetic parameters (see Table S2.2). Data were generated for each species at a constant temperature (25 °C) and for variable temperatures (15, 20, 25, 30, 35 °C), with each scenario associated with 15 curves representing a single plant. Testing the model at constant versus varying temperature allowed us to assess if data collected across different temperatures (as in our field study) affected model fit.

We evaluated the FvCB model (Eqns 1-3 and Table 2.3) at the “true” parameter values (Table S2.2), over the range of  $C_i$  and  $Q$  values representative of our field data, producing “true” or predicted values for  $A$  and  $\phi PSII$ . Observation error was added to the predicted values to obtain pseudo observations of  $A_{obs}$  and  $\phi PSII_{obs}$ . Observation errors for  $A_{obs}$  were randomly generated from a normal distribution with a mean of zero and a standard deviation of 2.8, which was derived from the literature (Turnbull et al. 2002, Lefebvre et al. 2005). Observation errors for  $\phi PSII$  were generated from a normal with mean zero and a standard deviation of 0.05, with the constraint that  $\phi PSII \geq 0$ . The above

HB model was subsequently applied to the artificial data, and the estimated parameters were compared to the known values used to generate the data to assess the ability of the model to recover the true values of key parameters, including  $R_{d25}$ ,  $g_{m25}$ ,  $V_{cmax25}$ , and  $J_{max25}$ .

Second, to determine the effect of including  $\phi PSII$  data (calculated from fluorescence data) in the HB model, we removed the components that were added to accommodate  $\phi PSII$  data (“reduced” model). This included the likelihood given in Eqn 8 as well as the associated prior distributions for  $\sigma_{PSII}^2$ ,  $\beta$ , and  $\phi max$ . The remaining  $A-C_i$  and  $A-Q$  data were then used to fit the reduced model. The parameter estimates obtained from the reduced model were compared to those obtained from the above described “full” model.

Third, in all model scenarios (full and reduced models; real and artificial data), we evaluated model goodness of fit by plotting observed data ( $A_{obs}$  or  $\phi PSII_{obs}$ ) versus predicted values, and obtaining the coefficient of determination ( $R^2$ ). The predicted values were obtained by generating “replicated” data (Gelman et al. 2004) from the sampling distributions specified in Eqns (7) and (8), given the predicted means (e.g.,  $\bar{A}$  or  $\overline{\phi PSII}$ ).

## **Results**

### *Model assessment with artificial data*

The HB full model fit both the artificial  $A-C_i$  and  $A-Q$  data well. The observed versus predicted values for  $A$  fell around the 1:1 line with an  $R^2$  of 0.89 (Figure 2.1A).

The observed versus predicted values for  $\phi PSII$  also fell around the 1:1 line with an  $R^2$  of 0.95 (Figure 2.1B).

The effectiveness of the HB approach at recovering known parameter values varied by species and temperature scenario. The HB approach was successful at recovering the true  $g_{m25}$  values such that the central 95% Bayesian credible intervals (BCIs) contained the true value in two of three cases at constant temperature and one of three cases at variable temperature (Figure 2.2A). Posterior estimates of  $R_{d25}$  contained the true value of  $R_{d25}$  in both temperature scenarios for *N. tabacum* and *A. rubrum*, while the value was overestimated in both temperature cases for *L. tridentata* (Figure 2.2B). Values for  $V_{Cmax25}$  were overestimated for *N. tabacum* in both temperature scenarios, but the true value was contained in the 95% BCI for both cases for *L. tridentata*. The true  $V_{Cmax25}$  value was underestimated for *A. rubrum* at constant temperature and overestimated in the variable temperature scenario (Figure 2.2C). Finally for  $J_{max25}$ , the 95% BCIs contained the true value for *L. tridentata* and *A. rubrum* at constant temperature, and for *N. tabacum* and *L. tridentata* at variable temperature (Figure 2.2D).

## **Application of the HB model to field data**

### *Model fit*

The HB model fit the field-collected  $A-C_i$  and  $A-Q$  data well. The observed versus predicted values for  $A$  fell primarily around the 1:1 line with a slope of 0.97 and an  $R^2$  of 0.91 (Figure 2.3A). The model also fit the  $\phi PSII$  data fairly well (observed vs predicted: slope = 0.79,  $R^2 = 0.95$ ), but it tended to over predict high values ( $> 0.5$ ) of  $\phi PSII$  (Figure 2.3B). Given the relatively good fit of the model, we proceed to evaluate the parameter

estimates produced by the model. Posterior estimates for all parameters are given in Table S2.4.

#### *Photosynthesis parameter estimates*

The posterior estimates of  $g_{m25}$  generally did not vary among plants within each species by site combination. Thus, we report posterior results at the species by site level (see Figure 2.4 for plant and species by site level means). Site level estimates of  $g_{m25}$  for *P. velutina* increased from the Sycamore Creek upland, to the McDowell Mountains, to the Sycamore Creek lowland, with posterior means of 0.75, 3.85 and 12.56  $\mu\text{mol m}^{-2} \text{s}^{-1} \text{Pa}^{-1}$ , respectively. The width of the 95% BCIs increased in the same order as the means (Figure 2.4A). Site level estimates of  $g_{m25}$  for *J. monosperma* were similar between the upland and lowland sites at Chevelon Canyon, with posterior means of 1.35 and 1.46  $\mu\text{mol m}^{-2} \text{s}^{-1} \text{Pa}^{-1}$ , respectively (Figure 2.4A). No clear trends across sites emerged for *Q. gambelii* and *S. gooddingii* (Figure 2.4A), but their  $g_{m25}$  estimates differed from each other, with *S. gooddingii* having far higher values than *Q. gambelii* (14.08 vs. 4.30  $\mu\text{mol m}^{-2} \text{s}^{-1} \text{Pa}^{-1}$ ).

The posterior estimates of  $R_{d25}$  generally showed similar variation to  $g_{m25}$  but different patterns across species and sites.  $R_{d25}$  differed between species in the Sycamore Creek lowland and between upland and lowland *J. monosperma* at Chevelon canyon (posterior means of 8.43 and 4.88  $\mu\text{mol m}^{-2} \text{s}^{-1}$ , respectively; Figure 2.4B). Moreover, the lowest  $R_{d25}$  was estimated for *S. gooddingii* (0.74  $\mu\text{mol m}^{-2} \text{s}^{-1}$ ), which was significantly lower than the  $R_{d25}$  estimates for all other species and sites. On the other extreme, *J. monosperma* in the Chevelon upland site supported the highest  $R_{d25}$  (8.43  $\mu\text{mol m}^{-2} \text{s}^{-1}$ ),

which was significantly higher than the  $R_{d25}$  estimates for all other species and sites. In contrast to  $R_{d25}$  and  $g_{m25}$ , the estimates of  $V_{cmax25}$  and  $J_{max25}$  were not significantly different within or between any of the species or sites measured (Figure 2.4C-D). However,  $J_{max25}$  did exhibit significant variation among plants within a species at the Sycamore Creek lowland site (Figure 2.4D).

Most of the photosynthesis parameters that were given semi-informative priors (e.g.,  $K_{c25}$ ,  $K_{o25}$ ,  $E_r$ ,  $E_m$ ,  $E_v$ ,  $E_j$ ,  $E_g$ ,  $E_{kc}$ ,  $E_{ko}$ ,  $S_v$ ,  $S_j$ ,  $H_v$ ,  $H_j$ , and  $\Gamma_{25}^*$ ) generally were associated with posterior estimates (Table S2.4) that did not change much relative to the priors (Table S2.1); e.g., the posterior 95% BCI for each parameter often contained the prior mean. The exceptions included  $K_{o25}$  for *P. velutina*,  $S_v$  for *P. velutina* and *J. monosperma*,  $E_r$  for *P. velutina* growing in the McDowell Mountains, and  $\Gamma_{25}^*$ ; the posteriors for  $\Gamma_{25}^*$  were significantly updated by the data (differed from the priors) for all cases except *P. velutina*.

### *Plant water status*

We explored potential relationships between  $g_m$  and leaf water status at the curve level (n = 46), based on two indices of plant water stress:  $g_s$  and measures of plant water potential ( $\psi_b$  and  $\Delta\psi_b$ ). Curve-level estimates of  $\log(g_m)$  and  $\log(g_s)$  were weakly and positively correlated ( $r = 0.57$ ; Figure S2.1). Mean plant-level  $\psi_b$  for *P. velutina* was between -2.3 and -6.3 MPa and followed the same pattern as the plant-level  $g_{m25}$  estimates and  $\Delta\psi_b$ , going from highest (less negative, least water stressed), to intermediate, to lowest (most negative, most water stressed) values for plants in the Sycamore lowland, McDowell Mountain, and Sycamore upland sites, respectively

(Figure 2.5B). This trend, though weaker, also occurred for  $g_m$  versus  $g_s$  at the curve level (Figure 2.5A). Plant-level mean  $\psi_b$  for *J. monosperma* spanned a narrow range from -1.9 to -2.6 MPa as did  $\Delta\psi_b$  across both sites (Figure 2.5B). A similarly narrow range is seen for  $g_m$  versus  $g_s$  (Figure 2.5A). *Q. gambelii* and *S. gooddingii*, both in lowland areas, had mean  $\psi_b$  of -1.3 and -2.7 MPa, respectively, but had generally overlapping  $\Delta\psi_b$  (Figure 2.5B), but significantly different  $g_m$ . *S. gooddingii* in all cases had higher curve-level  $g_m$  and  $g_s$  than *Q. gambelii*. These two species also followed opposite patterns, with *Q. gambelii* having a narrow range of  $g_s$  but variable  $g_m$ , and *S. gooddingii* having a narrow range of  $g_m$  but variable  $g_s$ .

#### *Effect of including fluorescence data*

A comparison of the full (including  $\phi PSII$  data) and reduced (excluding  $\phi PSII$  data) models revealed the effect of including fluorescence data. The primary effect of including  $\phi PSII$  data was on  $g_{m25}$ ,  $R_{d25}$ , and  $J_{max25}$ , all of which are related to the electron transport limited rate of CO<sub>2</sub> assimilation; inclusion of  $\phi PSII$  data did not affect  $V_{cmax25}$ , which is related to the Rubisco limited rate of CO<sub>2</sub> assimilation (Figure 2.6A-D). In most cases, the posterior means for the primary photosynthesis parameters were not significantly different between the full and reduced models. For example, of the seven species by site combinations, the full and reduced models produced different parameter estimates for two ( $g_{m25}$ , Figure 2.6A;  $R_{d25}$ , Figure 2.6B), three ( $J_{max25}$ , Figure 2.6D), and none ( $V_{cmax25}$ , Figure 2.6C) of the combinations. However, even when the parameter estimates were not statistically different between the two models, including the  $\phi PSII$  data often reduced parameter uncertainty (narrower BCIs). For example, in the case of

$g_{m25}$ , the BCIs were 1.5 (for mean widths) to 3.8 (for median widths) times wider when the  $\phi PSII$  data were excluded (see Table S2.3 for all BCI widths).

## **Discussion**

### *Improved modeling framework*

A primary objective of our study was to develop and demonstrate an alternative method for fitting photosynthesis models to gas exchange data that allows for integration of different types of data, which also addresses some of the concerns identified by Gu and Sun (2014). In particular, our method does not compute  $g_m$  as a function of  $C_i$ ,  $J$ ,  $\Gamma^*$ ,  $R_d$ , and  $A$ , but estimates  $g_m$  as part of the non-linear model fitting routine, as done by Sharkey *et al.* (2007), Patrick *et al.* (2009), Gu *et al.* (2010), and Bellasio *et al.* (2015). All of these methods, including our approach, essentially involve the same photosynthesis equations (Farquhar *et al.* 1980, von Caemmerer 2000, Ethier and Livingston 2004, Ethier *et al.* 2006) and include temperature corrections for most of the parameters (e.g.,  $V_{cmax}$ ,  $J_{max}$ ,  $R_d$ ,  $g_m$ ). However, Sharkey *et al.* (2007), Gu *et al.* (2010), and Bellasio *et al.* (2015) include TPU limited rates, which are not considered by Patrick *et al.* (2009) or in this study. However, the Bayesian modeling framework can easily accommodate TPU limitation, but the increased model complexity would likely increase the computational demands.

Importantly, the four aforementioned methods and our HB approach treat  $g_m$  similarly in that it is included as a variable in the equations being fit (Table 2.3), but the methods used to estimate  $g_m$  and fit the FvCB model to the data differ between the approaches. Sharkey *et al.* (2007) and Bellasio *et al.* (2015) use a non-linear curve fitting routine where the user must *a priori* assign points in the  $A-C_i$  curve to a limitation state

before the model is fit. Each limitation state of the model is fit independently using only the points assigned to that state. The Excel fitting tool developed by Bellasio *et al.* (2015) expands on the type of methodology used for the Sharkey *et al.* (2007) tool by making use of additional information including  $A-Q$  and fluorescence data (Bellasio *et al.* 2015). Gu *et al.* (2010) took a different approach to improve upon Sharkey *et al.* (2007) by removing the necessity for defining a limitation state *a priori* by modeling all possible limitation state distributions (they assign all the points to the three possible limitation states in all possible combinations), fitting all possible models, and then picking the best one based on a cost function. They check for inadmissible fits (where the predicted coefficients lead to a point being in the wrong limitation state) and employ measures to correct the inconsistency. Finally, Patrick *et al.* (2009) and our method both employ an HB approach, which has several advantages, but there are potential drawbacks, both of which we describe below.

A notable difference among these approaches is that Sharkey *et al.* (2007) and Gu *et al.* (2010) only utilize  $A-C_i$  data, while Patrick *et al.* (2009) added the ability to assimilate  $A-Q$  data into the model. Like our approach, Bellasio *et al.* (2015) extend existing approaches by accommodating the addition of fluorescence data. Importantly, our work naturally extends the Patrick *et al.* (2009) approach by also incorporating chlorophyll fluorescence data directly into the fitting process, while also accounting for uncertainty in photosynthesis parameters. Our model incorporated fluorescence measurements by explicitly accommodating likelihoods for both  $A$  (e.g., from  $A-C_i$  and  $A-Q$  response curves) and  $\phi PSII$  data, which are conditional on their associated predicted values defined by components of the non-linear FvCB photosynthesis model. Since the predicted

values (e.g.,  $\bar{A}$  and  $\overline{\phi PSII}$ , Eqns 7 and 8) are linked to many of the same underlying photosynthesis quantities (e.g.,  $g_m$ ,  $J_{max}$ ,  $V_{cmax}$ ,  $R_d$ ), simultaneous incorporation of  $A$  and  $\phi PSII$  data is expected to result in more realistic and more precise parameter estimates. In fact, including fluorescence data resulted in improved estimates of  $g_m$  and its associated parameters such as  $g_{m25}$ , as demonstrated by reduced uncertainty (narrower BCIs).

Future model fitting exercises could improve upon our work by resolving some remaining issues such as improving the fit to the  $\phi PSII$  data, which were overestimated for high values. This overestimation could be due to a potential underestimation of  $\phi PSII$  in the measurement of fluorescence. For example, Loriaux *et al.* (2013) show that the maximum yield of chlorophyll fluorescence ( $Fm'$ ) is prone to underestimation of up to ~10% using a single saturation pulse as was done by the LI-6400 fluorometer. If the  $\phi PSII$  data were underestimated, then the predicted values could be closer to the true values. Another issue is that it is possible to obtain values of  $R_{d25}$  that are not physiologically realistic. For instance, in the case of *J. monosperma*, the  $R_{d25}$  values obtained in this study imply a negative  $C^*$ , which is the intercellular CO<sub>2</sub> partial pressure where  $C_c = I^*$ . However, within the HB framework, it would be possible to modify the prior for  $R_{d25}$  such that it obeys the constraint  $C^* = I^* - R_d/g_m > 0$ . Even if the Bayesian fitting approach described herein is improved upon to address these issues, there are potential computational hurdles associated with applying this approach. For example, in our study, it took over a week for the MCMC simulations to finish, even for the smaller, artificial dataset. Moreover, although we provide the annotated OpenBUGS code for other potential users, application of the model requires familiarity with Bayesian methods and MCMC procedures.

Future work could also include carbon isotope data into the HB model either alone or in conjunction with fluorescence and photosynthesis response curve data. This could be accomplished by incorporating known relationships between the discrimination of  $^{13}\text{CO}_2$  versus  $^{12}\text{CO}_2$  ( $\Delta^{13}$ ) during photosynthesis (Evans et al. 1986, Gu and Sun 2014). The difference between the observed  $\Delta^{13}$  and the expected  $\Delta^{13}$  under the assumption of infinite  $g_m$  can be used to obtain estimates of  $g_m$  (Evans et al. 1986, Warren 2006). Incorporating isotope information would involve adding a third likelihood for the  $\Delta^{13}$  data, and the mean or predicted  $\Delta^{13}$  would share quantities with the mean models for  $A$  and/or  $\phi PSII$ , including  $C_a$ ,  $C_i$ ,  $R_d$  and  $\Gamma^*$ , which would likely help to refine the estimates of their shared parameters. Though, addition of  $\Delta^{13}$  data would also increase model complexity and introduce new parameters related to multiple fractionation processes (Gu and Sun 2014), and could exacerbate computational demands.

#### *Estimates of $g_m$ from application of HB model to field data*

A secondary objective of our study was to apply our HB method to evaluate variation in  $g_m$  across naturally occurring local and regional aridity gradients. The results for *P. velutina* provided support for the hypothesis that  $g_m$  should decrease with increasing water stress when considering  $\Delta\psi_b$  and to some extent  $g_s$ ; for this species, temperature-corrected  $g_m$  (i.e.,  $g_{m25}$ ) was lower in magnitude and less variable under lower  $\Delta\psi_b$  (Figure 2.5B). In fact,  $g_{m25}$  was generally more variable in three of the four species growing near a water source (lowland sites) compared to upland areas, with the exception of *J. monosperma*. When comparing variation in  $g_m$  to  $g_s$  at saturating light and ambient  $\text{CO}_2$ , no increase in variation (width of BCI) was observed; however, point estimates of  $g_m$  (but not variation in  $g_m$ ) tended to increase with  $g_s$  (Figure 2.5A, Figure

S2.1), indicating covariation in these physiological traits, which has also been observed in other studies (Flexas et al. 2012). The  $g_{m25}$  estimates for *J. monosperma* growing in lowland (low  $g_{m25}$ ) versus upland (high  $g_{m25}$ ) sites appeared to contradict our hypothesis because the lowland areas are expected to be characterized by greater water availability. However, these results could be explained by  $\psi_b$  observed for *J. monosperma*, which varied little among plants and sites (range: -2.6 to -1.8 MPa) and was much higher than the expected critical water potential of  $\psi_{crit} = -13$  MPa (Pockman and Sperry 2000). In fact, Pockman and Sperry (2000) did not measure significant cavitation in *J. monosperma* until  $\psi_b$  dropped below -10 MPa. This suggests that *J. monosperma* plants at both sites were experiencing similar and relatively low water stress, which could help to explain why  $g_{m25}$  did not vary between the sites.

Within the lowland environments,  $g_{m25}$  differed significantly among species, with *Q. gambelii* having the lowest and least variable  $g_{m25}$  values and experiencing lower water potentials. However, some of the differences among species could be attributed to leaf anatomy, which is expected to influence  $g_m$  (Evans et al. 2009, Terashima et al. 2011, Flexas et al. 2012, Tomás et al. 2013). For example,  $g_m$  has been shown to differ among functional groups (e.g., grasses, herbs, semi-deciduous, deciduous, evergreen, conifers, liverworts/hornworts) such that  $g_m$  may be highest in the most phylogenetically evolved groups (Flexas et al. 2012). Moreover,  $g_m$  also varies with specific leaf area and other morphological features affecting components of the diffusion pathway (Tomás et al. 2013). In the case of the species studied here, the expected trends seen in the literature were followed. The most drought stressed *P. velutina* had the lowest  $g_m$ , while *P. velutina* under low stress (Sycamore lowland) had the second highest  $g_m$ , following the

expected trend with water stress (Warren and Adams 2006, Flexas et al. 2012). *J. monosperma* had low  $g_m$  under low water stress, which could reflect its unique leaf morphology (Tomás et al. 2013).

The magnitude and variability in the estimated  $g_m$  could also have implications at larger scales. In both locations that *J. monosperma* was sampled, and in the Sycamore Creek upland for *P. velutina*, mean  $g_{m25}$  values were similar in magnitude to values found to influence canopy-level net assimilation by Keenan *et al.* (2010b). In fact, Keenan *et al.* (2010b) found that their photosynthesis model could only explain seasonal fluxes in CO<sub>2</sub> and water if  $g_m$  was included. Over- or under-estimation of leaf-level  $A$  will become even more important when scaling to canopy-level assimilation since small errors can be greatly compounded over time. This is especially relevant here given that the effect of  $g_m$  on predicted  $A$  is expected to be most pronounced under high temperatures, radiation, and vapor pressure deficits (Keenan et al. 2010b), all of which are common in the arid and semi-arid environments that we sampled in this study.

### *Conclusions*

We developed a hierarchical Bayesian (HB) model that simultaneously fit a mechanistic model of photosynthesis to fluorescence data and photosynthesis response (versus light and leaf-internal [CO<sub>2</sub>]) curves. Photosynthetic parameters that are generally weakly informed by such data were constrained with semi-informative priors based on the literature. This Bayesian approach provided estimates of biochemical-based photosynthesis parameters and their uncertainties. Incorporation of these multiple types of data reduced parameter uncertainty for the majority of the photosynthesis parameters

of interest. Incorporation of such multiple data sources is expected to yield improved estimates of key parameters, such as mesophyll conductance ( $g_m$ ), which is becoming increasingly recognized as an important component underlying photosynthesis predictions at the leaf and canopy levels. We demonstrate our modeling approach with data collected for species growing in arid and semi-arid sites, which produced  $g_m$  estimates that varied among species and sites, and the relatively low values for  $g_m$  indicate this is an important factor affecting plant photosynthesis.

## **Acknowledgements**

We thank Clint Clarkson for help processing samples. Members of the Ogle Lab, including Heather Kropp, Edmund Ryan, Jessica Guo and Drew Peltier, provided feedback on earlier drafts. We thank Thomas Day for access to his spectroradiometer. We thank the staff at McDowell Mountain Regional Park for their support and assistance with site access. We also thank Ashley Fell for her help assuring the grammatical accuracy of earlier drafts of this manuscript. Finally, we thank Michael Fell's committee members for their support and feedback including Janet Franklin, Thomas Day, Kevin Hultine, and Jarrett Barber.

## References

- Bellasio, C., D. J. Beerling, and H. Griffiths. 2015. An Excel tool for deriving key photosynthetic parameters from combined gas exchange and chlorophyll fluorescence: theory and practice. *Plant, Cell & Environment* 39:1180–1197.
- Bernacchi, C. J., A. R. Portis, H. Nakano, S. Von Caemmerer, and S. P. Long. 2002. Temperature Response of Mesophyll Conductance . Implications for the Determination of Rubisco Enzyme Kinetics and for Limitations to Photosynthesis in Vivo. *Plant Physiology* 130:1992–1998.
- von Caemmerer, S. 2000. *Biochemical Models of Leaf Photosynthesis*. Brown Prior Anderson, Collingwood.
- von Caemmerer, S., and G. Farquhar. 1981. Some relationships between the biochemistry of photosynthesis and the gas exchange of leaves. *Planta* 153:376–387.
- Carlin, B. P., A. E. Gelfand, and A. F. M. Smith. 1992. Hierarchical Bayesian Analysis of Change-point Problems. *Journal of the Royal Statistical Society. Series C* 41:389–405.
- Day, T., R. Guenon, and C. Ruhland. 2015. Photodegradation of plant litter in the Sonoran Desert varies by litter type and age. *Soil Biology & Biochemistry* 89:109–122.
- Dubois, J.-J. B., E. L. Fiscus, F. L. Booker, M. D. Flowers, and C. D. Reid. 2007. Optimizing the statistical estimation of the parameters of the Farquhar-von Caemmerer-Berry model of photosynthesis. *The New Phytologist* 176:402–14.
- Ethier, G. J., and N. J. Livingston. 2004. On the need to incorporate sensitivity to CO<sub>2</sub> transfer conductance into the Farquhar-von Caemmerer-Berry leaf photosynthesis model. *Plant, Cell & Environment* 27:137–153.
- Ethier, G. J., N. J. Livingston, D. L. Harrison, T. a Black, and J. a Moran. 2006. Low stomatal and internal conductance to CO<sub>2</sub> versus Rubisco deactivation as determinants of the photosynthetic decline of ageing evergreen leaves. *Plant, Cell & Environment* 29:2168–2184.
- Evans, J. R., R. Kaldenhoff, B. Genty, and I. Terashima. 2009. Resistances along the CO<sub>2</sub> diffusion pathway inside leaves. *Journal of Experimental Botany* 60:2235–2248.
- Evans, J., T. Sharkey, J. Berry, and G. Farquhar. 1986. Carbon isotope discrimination measured concurrently with gas exchange to investigate CO<sub>2</sub> diffusion in leaves of higher plants. *Functional Plant Biology* 13:281–292.

- Farquhar, G. D., S. Caemmerer, and J. A. Berry. 1980. A biochemical model of photosynthetic CO<sub>2</sub> assimilation in leaves of C<sub>3</sub> species. *Planta* 149:78–90.
- Farquhar, G. D., and T. D. Sharkey. 1982. Stomatal conductance and photosynthesis. *Annual Review of Plant Physiology* 33:317–345.
- Farquhar, G., and S. Wong. 1984. An Empirical Model of Stomatal Conductance. *Australian Journal of Plant Physiology* 11:191–210.
- Flexas, J., M. M. Barbour, O. Brendel, H. M. Cabrera, M. Carriquí, A. Díaz-Espejo, C. Douthe, E. Dreyer, J. P. Ferrio, J. Gago, A. Gallé, J. Galmés, N. Kodama, H. Medrano, Ü. Niinemets, J. J. Peguero-Pina, A. Pou, M. Ribas-Carbó, M. Tomás, T. Tosens, and C. R. Warren. 2012. Mesophyll diffusion conductance to CO<sub>2</sub>: an unappreciated central player in photosynthesis. *Plant Science* 193–194:70–84.
- Flexas, J., M. Barón, J. Bota, J.-M. Ducruet, A. Gallé, J. Galmés, M. Jiménez, A. Pou, M. Ribas-Carbó, C. Sajnani, M. Tomàs, and H. Medrano. 2009. Photosynthesis limitations during water stress acclimation and recovery in the drought-adapted *Vitis* hybrid Richter-110 (*V. berlandierixV. rupestris*). *Journal of Experimental Botany* 60:2361–2377.
- Flexas, J., A. Díaz-Espejo, J. A. Berry, J. Cifre, J. Galmés, R. Kaldenhoff, H. Medrano, and M. Ribas-Carbó. 2007a. Analysis of leakage in IRGA's leaf chambers of open gas exchange systems: quantification and its effects in photosynthesis parameterization. *Journal of Experimental Botany* 58:1533–1543.
- Flexas, J., A. Diaz-Espejo, J. Galmés, R. Kaldenhoff, H. Medrano, and M. Ribas-Carbo. 2007b. Rapid variations of mesophyll conductance in response to changes in CO<sub>2</sub> concentration around leaves. *Plant, Cell & Environment* 30:1284–98.
- Flexas, J., M. Ribas-Carbó, A. Diaz-Espejo, J. Galmés, and H. Medrano. 2008. Mesophyll conductance to CO<sub>2</sub>: current knowledge and future prospects. *Plant, Cell & Environment* 31:602–621.
- Gamerman, D., and H. F. Lopes. 2006. Markov Chain Monte Carlo: Stochastic Simulation for Bayesian Inference. 2nd edition. Chapman & Hall/CRC Press, Boca Raton.
- Gelman, A. 2006. Prior distributions for variance parameters in hierarchical models (Comment on Article by Browne and Draper). *Bayesian Analysis* 1:515–534.
- Gelman, A., J. B. Carlin, H. S. Stern, and D. B. Rubin. 2004. Bayesian Data Analysis. Second. Chapman & Hall/CRC Press.

- Genty, B., J.-M. Briantais, and N. R. Baker. 1989. The relationship between the quantum yield of photosynthetic electron transport and quenching of chlorophyll fluorescence. *Biochimica et Biophysica Acta* 990:87–92.
- Gilbert, M. E., A. Pou, M. A. Zwieniecki, and N. M. Holbrook. 2012. On measuring the response of mesophyll conductance to carbon dioxide with the variable J method. *Journal of Experimental Botany* 63:413–425.
- Gu, L., S. G. Pallardy, K. Tu, B. E. Law, and S. D. Wullschleger. 2010. Reliable estimation of biochemical parameters from C leaf photosynthesis-intercellular carbon dioxide response curves. *Plant, Cell & Environment* 33:1852–1874.
- Gu, L., and Y. Sun. 2014. Artefactual responses of mesophyll conductance to CO<sub>2</sub> and irradiance estimated with the variable J and online isotope discrimination methods. *Plant, Cell & Environment* 37:1231–1249.
- Harley, P. C., F. Loreto, G. Di Marco, and T. D. Sharkey. 1992. Theoretical Considerations when Estimating the Mesophyll Conductance to CO<sub>2</sub> Flux by Analysis of the Response of Photosynthesis to CO<sub>2</sub>. *Plant Physiology* 98:1429–1436.
- Keenan, T., S. Sabate, and C. Gracia. 2010a. The importance of mesophyll conductance in regulating forest ecosystem productivity during drought periods. *Global Change Biology* 16:1019–1034.
- Keenan, T., S. Sabate, and C. Gracia. 2010b. Soil water stress and coupled photosynthesis–conductance models: Bridging the gap between conflicting reports on the relative roles of stomatal, mesophyll conductance and biochemical limitations to photosynthesis. *Agricultural and Forest Meteorology* 150:443–453.
- Laisk, A., and F. Loreto. 1996. Determining Photosynthetic Parameters from Leaf CO<sub>2</sub>, Exchange and Chlorophyll Fluorescence'. *Plant Physiology* 110:903–912.
- Lefebvre, S., T. Lawson, M. Fryer, O. V Zakhleniuk, J. C. Lloyd, and C. A. Raines. 2005. Increased Sedoheptulose-1,7-Bisphosphatase Activity in Transgenic Tobacco Plants Stimulates Photosynthesis and Growth from an Early Stage in Development. *Plant Physiology* 138:451–460.
- Linton, M. J., J. S. Sperry, and D. G. Williams. 1998. Limits to water transport in *Juniperus osteosperma* and *Pinus edulis*: implications for drought tolerance and regulation of transpiration. *Functional Ecology* 12:906–911.
- Liu, F., M. J. Bayarri, and J. O. Berger. 2009. Modularization in Bayesian analysis, with emphasis on analysis of computer models. *Bayesian Analysis* 4:119–150.

- Loreto, F., P. C. Harley, G. Di Marco, and T. D. Sharkey. 1992. Estimation of Mesophyll Conductance to CO<sub>2</sub> Flux by Three Different Methods. *Plant Physiology* 98:1437–1443.
- Loriaux, S. D., T. J. Avenson, J. M. Welles, D. K. McDermitt, R. D. Eckles, B. Riensche, and B. Genty. 2013. Closing in on maximum yield of chlorophyll fluorescence using a single multiphase flash of sub-saturating intensity. *Plant, Cell & Environment* 36:1755–1770.
- Lunn, D., N. Best, D. Spiegelhalter, G. Graham, and B. Neuenschwander. 2009a. Combining MCMC with “sequential” PKPD modelling. *Journal of Pharmacokinetics and Pharmacodynamics* 36:19–38.
- Lunn, D., D. Spiegelhalter, A. Thomas, and N. Best. 2009b. The BUGS project : Evolution , critique and future directions. *Statistics in Medicine* 28:3049–3067.
- Molitor, N.-T., N. Best, C. Jackson, and S. Richardson. 2009. Using Bayesian graphical models to model biases in observational studies and to combine multiple sources of data: application to low birth weight and water disinfection by-products. *Journal of the Royal Statistical Society, A* 172:615–637.
- Murata, N., M. Nishimura, and A. Takamiya. 1966. Fluorescence of chlorophyll in photosynthetic systems. II. Induction of fluorescence in isolated spinach chloroplasts. *Biochimica et Biophysica Acta* 120:23–33.
- Neilson, R. P., and L. H. Wullstein. 1985. Comparative Drought Physiology and Biogeography of *Quercus gambelii* and *Quercus turbinella*. *American Midland Naturalist* 114:259–271.
- Niinemets, U., A. Díaz-Espejo, J. Flexas, J. Galmés, and C. R. Warren. 2009a. Role of mesophyll diffusion conductance in constraining potential photosynthetic productivity in the field. *Journal of Experimental Botany* 60:2249–2270.
- Niinemets, U., A. Díaz-Espejo, J. Flexas, J. Galmés, and C. R. Warren. 2009b. Importance of mesophyll diffusion conductance in estimation of plant photosynthesis in the field. *Journal of Experimental Botany* 60:2271–2282.
- Ogle, K., J. Barber, and K. Sartor. 2013. Feedback and Modularization in a Bayesian Meta-analysis of Tree Traits Affecting Forest Dynamics. *Bayesian Analysis* 8:133–168.
- Patrick, L. D., K. Ogle, and D. T. Tissue. 2009. A hierarchical Bayesian approach for estimation of photosynthetic parameters of C<sub>3</sub> plants. *Plant, Cell & Environment* 32:1695–1709.

- Perreault, L., J. Bernier, B. Bobée, and E. Parent. 2000. Bayesian change-point analysis in hydrometeorological time series. Part 1. The normal model revisited. *Journal of Hydrology* 235:221–241.
- Plaut, J. a, E. a Yepez, J. Hill, R. Pangle, J. S. Sperry, W. T. Pockman, and N. G. McDowell. 2012. Hydraulic limits preceding mortality in a piñon-juniper woodland under experimental drought. *Plant, Cell & Environment* 35:1601–1617.
- Pockman, W., and J. Sperry. 2000. Vulnerability to xylem cavitation and the distribution of Sonoran desert vegetation. *American Journal of Botany* 87:1287–1299.
- Pons, T. L., J. Flexas, S. von Caemmerer, J. R. Evans, B. Genty, M. Ribas-Carbo, and E. Bruognoli. 2009. Estimating mesophyll conductance to CO<sub>2</sub>: methodology, potential errors, and recommendations. *Journal of Experimental Botany* 60:2217–2234.
- De Pury, D. G. G., and G. D. Farquhar. 1997. Simple scaling of photosynthesis from leaves to canopies without the errors of big-leaf models. *Plant, Cell & Environment* 20:537–557.
- R Core Team. 2015. R: A language and environment for statistical computing. R Foundation for Statistical Computing, Vienna, Austria.
- Schneider, C. a, W. S. Rasband, and K. W. Eliceiri. 2012. NIH Image to ImageJ: 25 years of image analysis. *Nature Methods* 9:671–675.
- Schreiber, U., W. Bilger, and C. Neubauer. 1995. Chlorophyll Fluorescence as a Nonintrusive Indicator for Rapid Assessment of In Vivo Photosynthesis. Pages 49–70 in E. D. Schulze and M. M. Caldwell, editors. *Ecophysiology of Photosynthesis*. Springer-Verlag, Berlin Heidelberg.
- Sharkey, T. D., C. J. Bernacchi, G. D. Farquhar, and E. L. Singsaas. 2007. Fitting photosynthetic carbon dioxide response curves for C(3) leaves. *Plant, Cell & Environment* 30:1035–1040.
- Spiegelhalter, D. J., N. G. Best, B. P. Carlin, and A. Van Der Linde. 2002. Bayesian measures of model complexity and fit. *J. R. Statist. Soc. B* 64:583–616.
- Terashima, I., Y. T. Hanba, D. Tholen, and Ü. Niinemets. 2011. Leaf functional anatomy in relation to photosynthesis. *Plant Physiology* 155:108–116.
- Tomás, M., J. Flexas, L. Copolovici, J. Galmés, L. Hallik, H. Medrano, M. Ribas-Carbó, T. Tosens, V. Vislap, and U. Niinemets. 2013. Importance of leaf anatomy in determining mesophyll diffusion conductance to CO<sub>2</sub> across species: quantitative limitations and scaling up by models. *Journal of Experimental Botany* 64:2269–2281.

- Tosens, T., U. Niinemets, V. Vislap, H. Eichelmann, and P. Castro Díez. 2012. Developmental changes in mesophyll diffusion conductance and photosynthetic capacity under different light and water availabilities in *Populus tremula*: how structure constrains function. *Plant, Cell & Environment* 35:839–856.
- Turnbull, M. H., D. Whitehead, D. T. Tissue, W. S. F. Schuster, K. J. Brown, V. C. Engel, and K. L. Griffin. 2002. Photosynthetic characteristics in canopies of *Quercus rubra*, *Quercus prinus* and *Acer rubrum* differ in response to soil water availability. *Oecologia* 130:515–524.
- Wang, Y.-P., and R. Leuning. 1998. A two-leaf model for canopy conductance, photosynthesis and partitioning of available energy I: Model description and comparison with a multi-layered model. *Agricultural and Forest Meteorology* 91:89–111.
- Warren, C. 2006. Estimating the internal conductance to CO<sub>2</sub> movement. *Functional Plant Biology* 33:431–442.
- Warren, C. R. 2008. Stand aside stomata, another actor deserves centre stage: the forgotten role of the internal conductance to CO<sub>2</sub> transfer. *Journal of Experimental Botany* 59:1475–1487.
- Warren, C. R., and M. a Adams. 2006. Internal conductance does not scale with photosynthetic capacity: implications for carbon isotope discrimination and the economics of water and nitrogen use in photosynthesis. *Plant, Cell & Environment* 29:192–201.
- Warren, C. R., and E. Dreyer. 2006. Temperature response of photosynthesis and internal conductance to CO<sub>2</sub>: results from two independent approaches. *Journal of Experimental Botany* 57:3057–3067.
- Williams, D., and J. Ehleringer. 2000. Intra-and interspecific variation for summer precipitation use in pinyon-juniper woodlands. *Ecological Monographs* 70:517–537.

## Tables

**Table 2.1** Mean annual precipitation (MAP) and minimum (Tmin) and maximum (Tmax) temperature are based on the nearest weather stations, which occur within 13.7 to 35.4 km of each site. Elev = elevation. *Prosopis velutina* and *Juniperus monosperma* were sampled in both upland and lowland areas at Sycamore Creek (33°43'53.49" N, 111°30'53.07" W) and Chevelon Canyon (34°35'27.59" N, 110°47'15.82" W), respectively. *Salix gooddingii* and *Quercus gambelii* were only sampled in lowland areas at Sycamore Creek and Chevelon Canyon, respectively. The McDowell Mountain site (33°43'32.38" N, 111°41'50.45" W) was relatively flat, and it did not have a lowland area, so we consider it an upland area given the lack of nearby surface water. The site codes correspond to the McDowell Mountains (MD), Sycamore Creek upland (Syc.) and lowland (Syc. L.), and Chevelon Canyon upland (Che.) and lowland (Che. L.).

Site	Species (# trees, # curves)	Elev (m)	MAP (mm)	Tmin, Tmax (°C)
1.MD	<i>P. velutina</i> (5, 20)	533	325	13.9, 30.6
2. Sycamore Creek				
Syc.	<i>P. velutina</i> (3, 3)	625	408	13.6, 29.0
Syc. L.	<i>P. velutina</i> (3, 3), <i>S. gooddingii</i> (3, 3)			
3. Chevelon Canyon				
Che.	<i>J. monosperma</i> (3, 6)	1830	508	2.0, 16.4
Che. L.	<i>J. monosperma</i> (3, 6), <i>Q. gambelii</i> (3, 5)			

**Table 2.2.** Symbols and definitions of quantities used in the photosynthesis (FvCB) model.

Symbol*	Description	Node type	Unit
$A$	Rate of CO <sub>2</sub> assimilation (photosynthesis)	SD	$\mu\text{mol m}^{-2} \text{s}^{-1}$
$C_i$	Intercellular CO <sub>2</sub> partial pressure	D	Pa
$Q$	Photon flux density	D	$\mu\text{mol m}^{-2} \text{s}^{-1}$
$T$	Leaf temperature	D	°C
$P$	Pressure	D	Pa
$\alpha$	Absorptance	D	
$\Phi_{PSII}$	Electron flow through photosystem II (PSII) per unit quantum absorbed	SD	
$A_c$	Rubisco-limited rate of CO <sub>2</sub> assimilation	SQ	$\mu\text{mol m}^{-2} \text{s}^{-1}$
$A_j$	Electron transport limited rate of CO <sub>2</sub> assimilation	SQ	$\mu\text{mol m}^{-2} \text{s}^{-1}$
$E \begin{pmatrix} E_g, E_m, E_r, E_{kc}, \\ E_{ko}, E_v, E_j \end{pmatrix}$	Activation energies used in Arrhenius temperature functions	SQ	$\text{kJ mol}^{-1}$
$f$	Spectral light quality factor	C	
$g_m$	Mesophyll conductance to CO <sub>2</sub>	SQ	$\mu\text{mol m}^{-2} \text{s}^{-1} \text{Pa}^{-1}$
$H(H_v, H_j)$	Deactivation factors used in Arrhenius temperature functions	SQ	$\text{kJ mol}^{-1}$
$J$	Rate of electron transport	SQ	$\mu\text{mol m}^{-2} \text{s}^{-1}$
$J_{\text{max}}(J_{\text{max}25})$	Maximum electron transport rate (standardized to 25 °C)	SQ	$\mu\text{mol m}^{-2} \text{s}^{-1}$
$K_c(K_{c25})$	Michaelis-Menten constant for Rubisco for CO <sub>2</sub> (standardized to 25 °C)	SQ	Pa
$K_o(K_{o25})$	Michaelis-Menten constant for Rubisco for O <sub>2</sub> (standardized to 25 °C)	SQ	kPa
$O$	Partial pressure of O <sub>2</sub>	C	Pa
$Q_2$	Photosynthetically active radiation absorbed by PSII	D	$\mu\text{mol m}^{-2} \text{s}^{-1}$
$R$	Universal gas constant ( $8.314 \text{ J K}^{-1} \text{ mol}^{-1}$ )	C	$\text{J K}^{-1} \text{ mol}^{-1}$
$R_d(R_{d25})$	Mitochondrial respiration in the light (standardized to 25 °C)	SQ	$\mu\text{mol m}^{-2} \text{s}^{-1}$
$\Delta S(\Delta S_v, \Delta S_j)$	Entropy factors used in Arrhenius temperature functions	SQ	$\text{J K}^{-1} \text{ mol}^{-1}$
$T$	Leaf temperature	D	°C
$V_{\text{cmax}}(V_{\text{cmax}25})$	Maximum rate of Rubisco carboxylation (standardized to 25 °C)	SQ	$\mu\text{mol m}^{-2} \text{s}^{-1}$
$\beta$	Proportion of irradiance absorbed by PSII relative to PSI	SQ	
$\Gamma^*(\Gamma_{25}^*)$	Chloroplastic CO <sub>2</sub> compensation point (standardized to 25 °C)	SQ	Pa
$\theta$	Empirical curvature factor	C	
$Y_{25}$	Plant-level mean of parameter $Y$ standardized to 25 °C	SQ	
$\mu Y_{25}$	Species-level mean of parameter $Y$ standardized to 25 °C	SQ	
$\mu * Y_{25}$	Population-level mean of parameter $Y$ standardized to 25 °C	SQ	

$\sigma^2$	Variance parameter describing observation and measurement error	SQ
$\sigma^2_{Y_{plant}}$	Precision (1/variance) parameter describing plant-to-plant variation within species	SQ
$\sigma^2_{Y_{spp}}$	Precision (1/variance) parameter describing species-to-species variability	SQ

---

Note Type: D = data (fixed), SQ = stochastic quantity (unknown), SD = stochastic data, C = constant

Symbols based on Patrick *et al.* (2009) and von Caemmerer (2000).

\*When data are available for a particular quantity, we often write the quantity as *Xobs* to indicated “observed *X*” (such as *Aobs*, *Qobs*, etc.)

**Table 2.3:** Farquhar *et al.* equations

Eqn no.	Equation
1	$A_{C_i} = \frac{-b + \sqrt{b^2 - 4ac}}{2a}$ $a = -\frac{1}{g_m}$ $b = \frac{(V_{cmax} - R_d)}{g_m} + C_i + K_c \left( \frac{1 + O}{K_o} \right)$ $c = R_d \left[ C_i + K_c \left( \frac{1 + O}{K_o} \right) \right] - V_{cmax}(C_i - \Gamma^*)$
2	$A_{j_i} = \frac{-b + \sqrt{b^2 - 4ac}}{2a}$ $a = -\frac{1}{g_m}$ $b = \frac{\frac{J}{4} - R_d}{g_m} + C_i + 2\Gamma^*$ $c = R_d(C_i + 2\Gamma^*) - \frac{J}{4}(C_i - \Gamma^*)$
3	$J_i = \frac{Q_2 + J_{max} - \sqrt{(Q_2 + J_{max})^2 - 4\theta Q_2 J_{max}}}{2\theta}$ <p>where <math>\theta=0.7</math> (Evans 1987) and</p> $Q_{2i} = Q \cdot \alpha\beta(1 - f)$ <p>where <math>f=0.15</math> (Evans 1987)</p>
4	$Y = f_1(Y_{25}, E_Y, T) = Y_{25} \exp_Y(T - 298) / ((298 \cdot R \cdot T))$ $Y = f_2(Y_{25}, E_Y, T, \Delta S_Y, H_Y)$
5	$= Y_{25} \exp \left[ \frac{E_Y(T - 298)}{298 \cdot R \cdot T} \right] \left[ \frac{1 + \exp \left( \frac{298\Delta S_Y - H_Y}{298R} \right)}{1 + \exp \left( \frac{T\Delta S_Y - H_Y}{R \cdot T} \right)} \right]$

---

Farquhar *et al.* (1980) (FvCB model) equations used, modified from Patrick *et al.* (2009)

## Figures

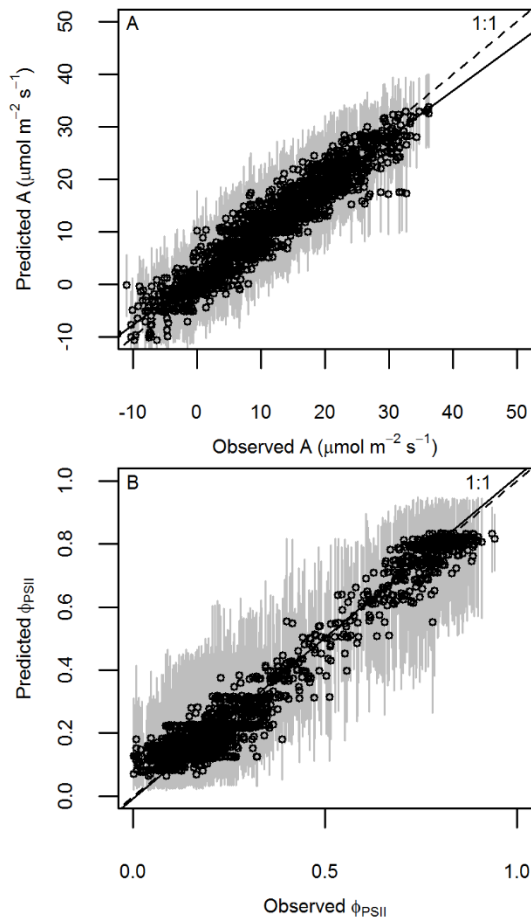


**Figure 2.1.** Model fit for artificial data. (A) Predicted versus observed photosynthetic rate ( $A$ ). (B) Predicted versus observed values  $\phi_{PSII}$ . The predicted values are the posterior means and the error bars represent the 95% Bayesian credible intervals (CIs) for replicated data. The dashed diagonal lines represent the 1:1 lines. The solid lines show the regression of predicted versus observed, which had an  $R^2$  of 0.89 and 0.95 for  $A$  and  $\phi_{PSII}$ , respectively.

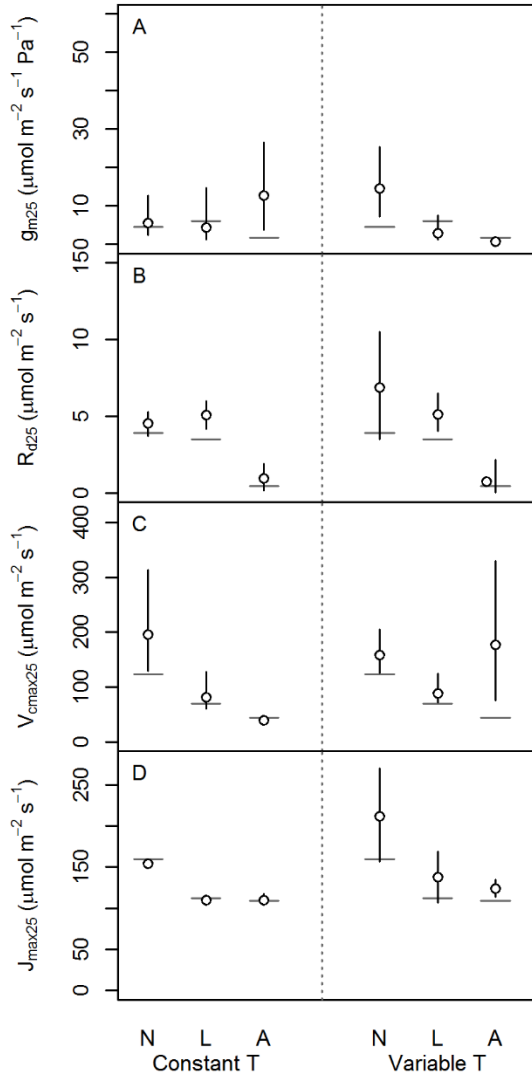


**Figure 2.2.** Artificial data model parameter estimates. Results from the Bayesian model with 95% Bayesian credible intervals (BCIs) based on fitting the FvCB model to data for  $n = 15$  curves per species for both constant ( $25^\circ \text{C}$ ) and variable temperature ( $15, 20, 25, 30, 35^\circ \text{C}$ ;  $n = 3$  for each temperature) scenarios. The short horizontal lines indicate the true parameter value. Results are shown for four key photosynthesis parameters at  $25^\circ \text{C}$ : (A) mesophyll conductance ( $g_{m25}$ ), (B) mitochondrial respiration in the light ( $R_{d25}$ ), (C) maximum rate of Rubisco carboxylation ( $V_{cmax25}$ ), and (D) maximum electron transport rate ( $J_{max25}$ ). Species are indicated by: N = *N. tabacum*, L = *L. tridentata*, and A = *A. rubrum*.

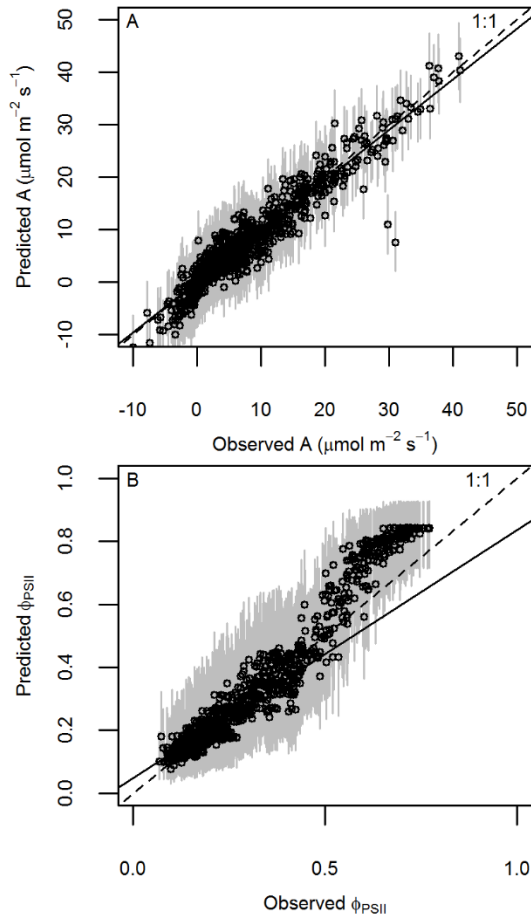


**Figure 2.3.** Model fit for the field data. (A) Predicted versus observed photosynthetic rate (A). (B) Predicted versus observed values  $\phi_{PSII}$ . The predicted values are the posterior means and the error bars represent the 95% Bayesian credible intervals (BCIs) for replicated data. The dashed diagonal lines represent the 1:1 lines. The solid lines show the regression of predicted versus observed, which had an  $R^2$  of 0.91 and 0.95 for A and  $\phi_{PSII}$ , respectively.

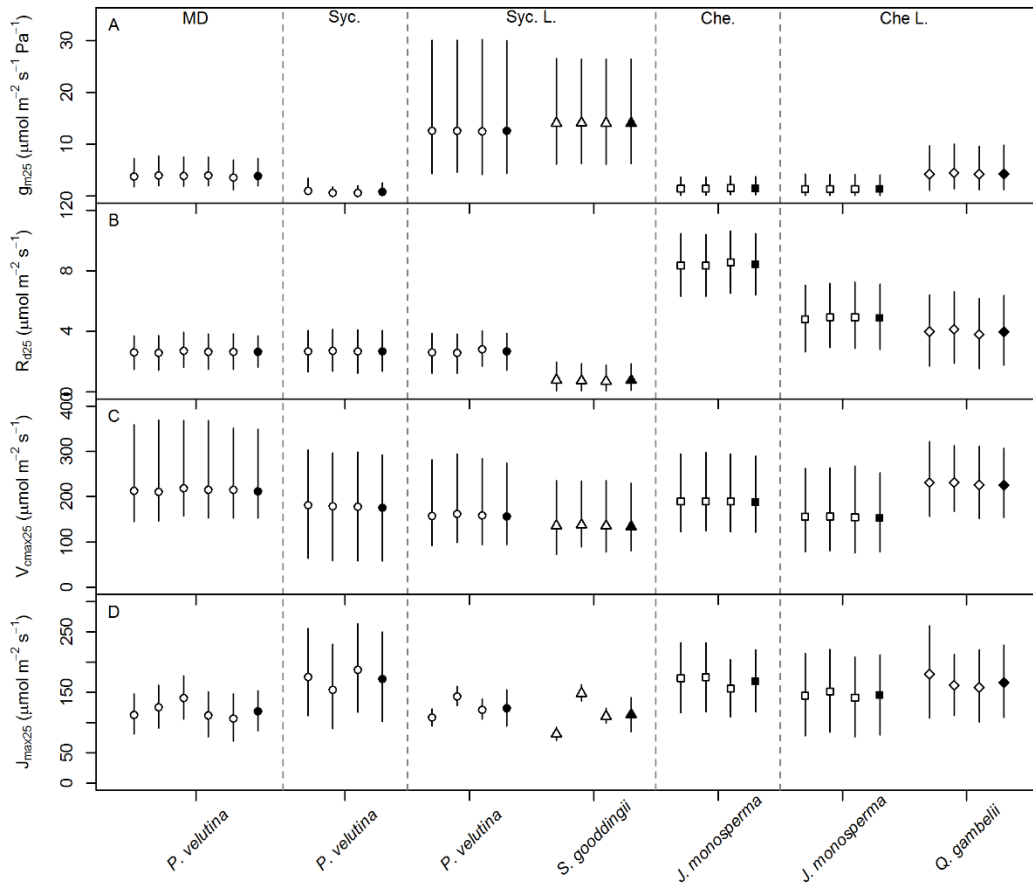


**Figure 2.4.** Parameter estimates for field data. Plant (open symbols) and species by site level (filled symbols) posterior means and 95% BCIs across all seven sampling locations for four key photosynthesis parameters at 25°C: (A) mesophyll conductance ( $g_{m25}$ ), (B) mitochondrial respiration in the light ( $R_{d25}$ ), (C) maximum rate of Rubisco carboxylation ( $V_{cmax25}$ ), and (D) maximum electron transport rate ( $J_{max25}$ ). Descriptions of site codes are in Table 2.1.

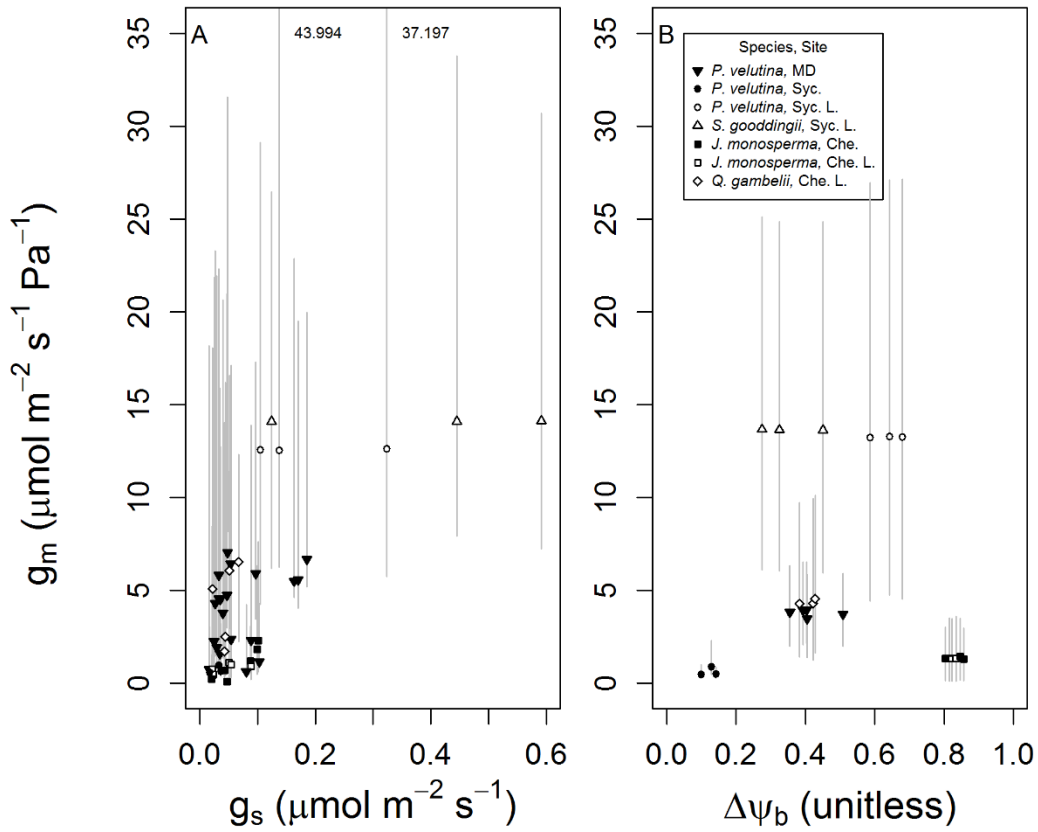


**Figure 2.5.** Plant water status vs  $g_{m2}$ . Posterior means and 95% BCIs for (A) predicted  $g_{m25}$  vs  $g_s$  (measured by the licor) at the curve level and (B) temperature corrected  $g_m$  at 25 °C ( $g_{m25}$ ) versus plant water status at the plant level, which is represented as the relative difference in plant water potentials, where  $\Delta\psi_b = (\psi_{b,crit} - \psi_{b,average})/\psi_{b,crit}$ . In panel B, the further a plant is to the left (nearer  $\Delta\psi_b = 0$ ), the closer it is to its critical value where complete hydraulic failure is expected (i.e., smaller values of  $\Delta\psi_b$  indicate greater plant water stress). Each  $\psi_{b,average}$  value is the average measured branch water potential of a plant across all measurements taken. The  $\psi_{b,crit}$  values were obtained from the literature and are: -4.1 (Sperry et al. 1991), -13.5, -2, and -7 (Pockman and Sperry 2000) MPa for *Q. gambelii*, *J. monosperma*, *S. gooddingii*, and *P. velutina*, respectively. Open symbols represent lowland plants; solid symbols represent upland plants. Numbers by error bars indicate values outside of the figure's range. Descriptions of site codes are in Table 2.1.

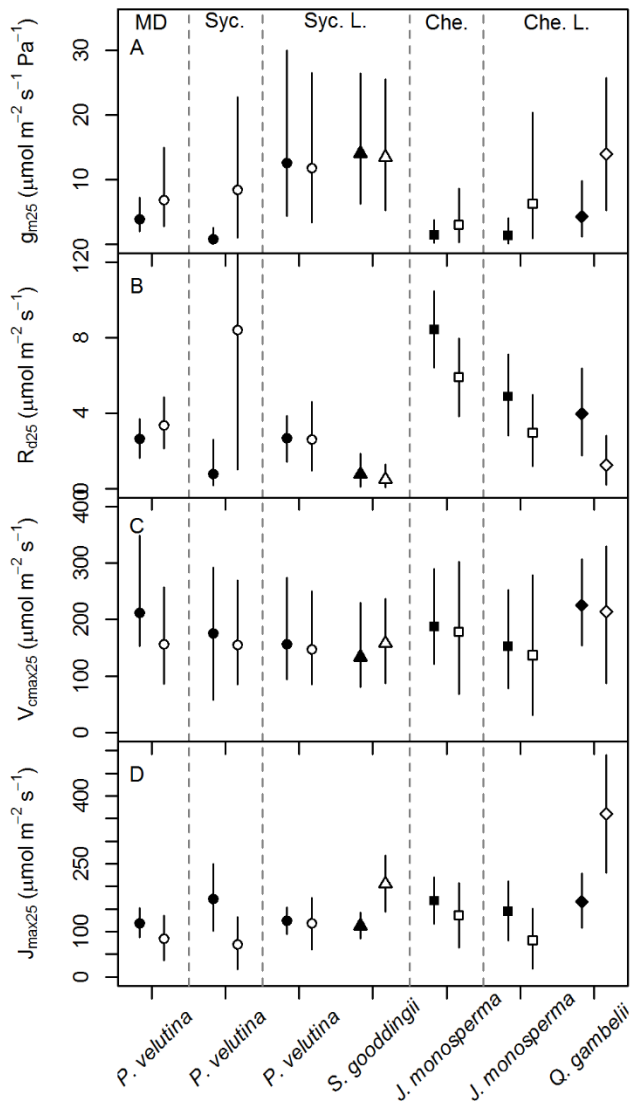


**Figure 2.6:** Posterior results obtained from applying HB model to field data with the  $\phi PSII$  data (solid symbols, full model) or without the  $\phi PSII$  data (open symbols, reduced model). The parameter estimates were significantly different between the full and reduces models in two cases for  $g_{m25}$ , in three cases for  $J_{max25}$ , and in zero cases for  $V_{cmax25}$ . Inclusion of the  $\phi PSII$  data generally resulted in narrower 95% BCIs in most cases. Descriptions of site codes are in Table 2.1.

### 3. TRAIT SPECTRA PREDICTED BY A MECHANISTIC MODEL OF TREE GROWTH AND CARBON ALLOCATION

#### **Abstract**

Research on plant functional traits has revealed many interesting and potentially important patterns among morphological, physiological, and life history traits and the environment. These are exemplified in studies finding trade-offs between groups of traits in the leaf and wood economics spectra. Most empirical studies, however, suffer from at least three limitations: 1) the correlative nature of the analysis limits the ability to make predictions under novel conditions; 2) due to incomplete trait data, they often work with means at various levels without accounting for variation; 3) they tend to focus on traits that are easy to measure, and thus may overlook other traits important for understanding plant or tree growth. Here, we take a different approach and use an individual-based model of tree growth and mortality (ACGCA) to investigate the theoretical trait space (TTS) of North American trees. The model includes 32 parameters representing allometric, physiological, and anatomical traits, some of which overlap with the leaf and wood economics spectra. Using a Bayesian approach, we fit the ACGCA model to individual tree heights and diameters from the USFS Forest Inventory and Analysis (FIA) dataset, with further constraints by literature-based priors. This is accomplished by fitting the model to 1.6 million FIA records that are aggregated across individuals, species, and sites, producing a “global” (posterior) distribution of traits (parameters) that lead to realistic growth. We explored this multidimensional (joint) distribution (the TTS) to evaluate trait-trait relationships that emerge from the ACGCA model, and to compare these against empirical patterns. Only three notable bivariate correlations ( $r > 0.2$ ),

among 496 possible pairs of traits, were contained in the TTS, but stepwise and best subsets regressions uncovered a complicated multivariate structure. For example, a subset of traits—related to photosynthesis (e.g., radiation-use efficiency) and maintenance respiration traits—exhibited strong multivariate trade-offs with each other, while half of the traits—mostly related to allometries and construction costs—varied independent of other traits. Interestingly, SLA (specific leaf area) was related to several root traits that are rarely measured in empirical studies. The trade-offs that emerged in the TTS tend to reflect mass-balance (related to carbon allocation) and engineering (mostly related to allometries) tradeoffs that are represented in the ACGCA model, and point to potentially important traits that are under-explored in field studies (e.g., root traits, branch senescence rates, xylem conducting area).

**Keywords:** FIA, Forest Inventory and Analysis, Individual-based model, Markov chain Monte Carlo, North American trees, plant functional traits, trait space, trait trade-offs, tree growth model

## **Introduction**

Functional trait research has led to the recent discovery of important patterns among plant morphological, physiological, and life history traits and between such traits and the environment. Functional traits are well-defined properties of organisms, often measured at the level of an individual, that strongly influence organismal performance or fitness (McGill et al. 2006). For trees, key traits include properties of leaves/needles, wood/stems, and roots that are important determinants of plant function, such as those related to water transport, carbon gain, mechanical limitations, and nutrient uptake (Wright et al. 2004, Chave et al. 2009, Reich 2014). Empirical studies—those based primarily on trait measurements without a significant theoretical or modeling component—of hundreds (Reich et al. 1997, Baraloto et al. 2010) to thousands (Wright et al. 2004, Shipley et al. 2006, Chave et al. 2009) of species have discovered important trait tradeoffs or correlations (e.g., leaf lifespan increases with leaf mass per area; relative growth rate decreases with wood density).

It is often the case, however, that easily measured traits are favored over those that are more difficult to measure, but that may be more directly related to mechanisms (Weiher et al. 1999, Lavorel and Garnier 2002, Lavorel et al. 2007). This “measurement bias” can potentially limit inferences about traits that may be key predictors of whole-plant performance. Mechanistic models have the potential to overcome such bias by incorporating traits—regardless of how easy or difficult they are to measure—that underlie mechanisms or processes (e.g., photosynthesis, allocation, structural constraints) that govern performance. Thus, simulation experiments with mechanistic models may

allow us to explore tradeoffs between multitudes of traits that cannot be easily accomplished by field studies.

A major development in trait-based ecology are trait spectra, which place organisms along one or more continuous axes (e.g., tradeoffs or life-history dimensions). For instance, the leaf economics spectrum (LES) quantifies tradeoffs among leaf mass per area (LMA), leaf lifespan (LL), and mass-normalized values of photosynthetic capacity ( $A_{\text{mass}}$ ), leaf nitrogen ( $N_{\text{mass}}$ ), leaf phosphorus ( $P_{\text{mass}}$ ), and leaf dark respiration ( $R_{\text{mass}}$ ) (Wright et al. 2004). Trait-environment relationships are also often evaluated; for instance, LES traits are often correlated with annual rainfall and temperature (Wright et al. 2004). Another spectra relevant to trees is the wood economics spectrum (WES), which links wood traits to major ecological functions, including competitive ability, resistance to stress, and disturbance responses (Chave et al. 2009). An important tradeoff revealed by the WES is that growth and mortality rates are both negatively correlated with wood density (Chave et al. 2008, 2009). A third spectra, the worldwide ‘fast-slow’ economics spectrum, integrates key leaf, wood, and fine root traits, including those in the LES and WES, into a single spectrum by demonstrating consistent tradeoffs between traits leading to fast versus slow growth (Reich 2014). Although the validity and interpretation of some trait spectra have been questioned (Lloyd et al. 2013, Osnas et al. 2013), there is still broad interest in quantifying empirical trait spectra (Diaz et al. 2016) and using these patterns to more realistically represent plant functional diversity in global carbon-climate models (Scheiter et al. 2013, Van Bodegom et al. 2014, Fisher et al. 2015). Yet, the underlying factors giving rise to empirical patterns are not always clear and likely emerge from different types of tradeoffs, such as those related to resource

allocation or physical constraints (Scheiter et al. 2013). It is possible that more complex multivariate patterns are contained within such trait spectra that could underlie species coexistence mechanisms (Clark et al. 2010).

The majority of studies exploring functional traits and associated trait spectra focus on assessing trait-trait and/or trait-environment relationships. Standard approaches include regression analyses such as bivariate, multiple, and stepwise multiple regression (Reich et al. 1999, Atkin et al. 2015), standardized major axis regression (Wright et al. 2004), and Dirichlet regression (Adler et al. 2014). The general goal of such analyses is to discover how functional traits are related to other traits, to an emergent process (e.g., rates of survival, growth, reproduction), or to the environment. Ordination methods such as principle components analysis (Reich et al. 1999, Diaz et al. 2004, Cavender-Bares et al. 2004), principle coordinate analysis (Stahl et al. 2013), and multiple factor analysis (MFA) (Baraloto et al. 2010) reduce the dimensionality of the problem and produce low dimensional axes that can be evaluated to identify tradeoffs. For instance, Diaz et al. (2004) found that the first principle component axis (PCA1) was primarily driving by SLA and leaf thickness, but in opposite directions such that as SLA increases, leaf thickness decreases, as would be expected. While standard multivariate approaches such as ordination are useful, they typically do not account for conditional relationships among traits; i.e., the relationship between a pair of traits may depend on the values of other traits. We refer to these common approaches (i.e., regression and ordination methods) as describing “empirical trait spectra” because they are revealed by analyses of trait data collected on living plants, often growing in field conditions. Though these studies provide vital insights, they are often limited by the traits they can assess (due to the practicality of

measurement) and by the phenomenological or correlational nature of the analyses. This results in the inability to explicitly consider mechanisms that give rise to empirically observed tradeoffs. These limitations may render empirical spectra inappropriate for predicting plant function under novel conditions (Webb et al. 2010, Evans 2012, Scheiter et al. 2013).

To move beyond phenomenological models of trait relationships, and to develop the capacity to predict plant function under future novel environments, tradeoffs should be related to plant function and underlying processes and mechanisms. Scheiter et al. (2013) envisaged that trait tradeoffs fall into one of three categories describing mechanisms that give rise to the tradeoffs, and they suggested that this would facilitate incorporating a trait perspective into dynamic global vegetation model (DGVM). These include: (1) mass conservation tradeoffs related to resource use and allocation, (2) engineering tradeoffs that prevent structures or architectures of plants that are not feasible, and (3) empirical tradeoffs that are more difficult to derive mathematically and that are not explicitly considered in a given modeling framework (Scheiter et al. 2013). We propose a complimentary approach to understanding trait spectra that takes these considerations into account by using theoretical or process-based models of whole-plant function to determine how functional traits interact with each other to influence whole-plant function (e.g., growth and survival).

To produce realistic behavior of whole-plant performance, theoretical models should consider important plant physiological processes (e.g., photosynthesis, respiration, etc.), carbon allocation (mass conservation tradeoffs), structural characteristics (e.g., anatomical features), and allometric relationships (engineering tradeoffs). Examples

include the many existing individual-based models (IBMs) of plant growth (Bugmann 2001, Ogle and Pacala 2009, Fyllas et al. 2014). These models are useful in relating key traits—which usually take the form of model parameters—to processes such as carbon acquisition, allocation, and metabolism, and provide a novel way of investigating the influence of key functional traits (model parameters) on growth and/or survival (model outputs). By fitting IBMs to empirical data on plant performance and functional traits, it may be possible to investigate the “theoretical” trait space that emerges from the mass conservation and engineering tradeoffs (Scheiter et al. 2013) that are built into the IBM. Evaluation of the theoretical trait space (or spectra) should provide insight into the factors giving rise to observed, empirical trait spectra, and possibly reveal potentially important trait relationships or tradeoffs that have not been previously identified.

The main objectives of this study are to quantify the theoretical trait space (TTS) of North American tree species, and to use this TTS to understand empirical trait spectra (e.g., LES and WES). To accomplish these objectives, we fit an IBM of tree growth and survival, the ACGCA model (Ogle and Pacala 2009), to 1.6 million observations of “healthy” trees from the USFS Forest Inventory and Analysis (FIA) database that were pooled across sites, species, and individuals, complemented by literature information (TreeTraits database; Kattge et al. 2011; Ogle et al. 2013; Ogle et al. 2014) to help constrain parameter values (traits) to realistic ranges. To achieve this, we employed a Bayesian framework that utilized a fast, custom stochastic algorithm for fitting the ACGCA model to the aggregated FIA data and literature information. This produced a 32-dimensional (joint) posterior distribution of parameters (traits) that lead to realistic tree growth, which we refer to as the TTS. We evaluated this TTS to address the

following questions: (1) Are notable bivariate correlations or trait-trait tradeoffs contained in the TTS? (2) Do higher dimensional relationships exist between traits in the TTS, and if so, which traits contribute to these relationships? (3) How does the TTS compare to empirical spectra such as the LES and WES?

## **Methods**

### *Overview*

We fit the Allometrically Constrained Growth and Carbon Allocation (ACGCA) model (Ogle and Pacala 2009) to USFS Forest Inventory and Analysis (FIA) data on individual tree heights and stem diameters within a Bayesian framework to investigate the theoretical trait space (TTS) of North American trees. Computational challenges involved with fitting the ACGCA model to the large FIA dataset and the limitations of precompiled software necessitated development of a customized Metropolis-Hastings (MH) algorithm. In addition to fitting the ACGCA model to the FIA data, model parameters (Table 3.1) were partially constrained by priors derived from the TreeTraits database (Kattge et al. 2011b, Ogle et al. 2013, 2014). Below, we first summarize the ACGCA model, then we provide an overview of the data sources used to inform the ACGCA model, followed by a description of the Bayesian approach used to fit the ACGCA model to the data, including a description of the custom MH algorithm and how the Bayesian results were analyzed.

### *Tree growth and carbon allocation model*

The ACGCA model is an individual-based model (IBM) of tree growth and mortality (Ogle and Pacala 2009). The ACGCA model recognizes the importance of

including both allometric relationships (related to engineering tradeoffs) and physiological (mass balance) processes underlying labile and structural carbon dynamics, including allocation and growth (Ogle and Pacala 2009); these processes are governed by 32 functional traits (i.e., model parameters, see Table 3.1). Tree growth is simulated by dynamically allocating labile carbon to storage and structural biomass pools in a way that obeys observed allometric relationships among leaf, stem, branch, and root compartments (Ogle and Pacala 2009). Structural (biomass) pools of different tissue compartments (leaves; fine roots; and root, branch, and trunk sapwood and heartwood) are predicted at each time step.

Labile carbon dynamics are essential to the ACGCA model. There are two main types of labile carbon storage pools. One is associated with storage in leaf and fine root tissue, and labile carbon in this pool is retranslocated when structural tissue is lost (e.g., via senescence of leaves or fine roots). The other storage pool is associated with storage in sapwood and can be drawn upon during times of stress (high labile carbon demand). The ACGCA model also includes a transient carbon pool (e.g., recent photosynthesis and retranslocated carbon) that is not associated with storage in any specific tissue and is immediately redistributed within the plant to accommodate structural biomass production, growth respiration, and allocation to storage pools (Ogle and Pacala 2009).

Labile carbon allocation and storage aligns with six physiological states: healthy, static, shrinking, recovering, recovered, or dead. Each physiological state is described by a set of difference equations that satisfy mass-balance relationships among the structural and labile carbon pools (Eqn. 4-8, below). Negative carbon balance (demand > supply) results in a “reduced” allometry, an unhealthy state, and eventual tree death. For reasons

discussed below in the MH algorithm section, only the healthy state is relevant to this study, which we summarize here. In the healthy state, labile carbon is allocated so that the sizes of the structural and storage pools are kept in allometric proportion by solving a set of difference equations that tie the size of each pool to trunk radius. Below, we highlight key aspects of the model relevant to this study, and note specific functional traits relevant to these processes; a full description of the model is given in Ogle & Pacala (2009).

Light is the only environmental driving variable in the current version of the ACGCA model. A simple radiation-use function is applied to determine the amount of labile carbon fixed by a tree (gross photosynthesis,  $P_G$ ) per year:

$$P_G(t) = \varepsilon \cdot APAR(t) \quad (11)$$

Where  $\varepsilon$  is radiation-use efficiency (a functional trait),  $APAR$  is the absorbed photosynthetically active radiation ( $PAR$ ), and  $t$  is time (years).  $APAR$  is based on the maximum annual  $PAR$  above the tree's crown ( $PAR_{max}$ ), modified by the light extinction coefficient of the tree's crown ( $k$ , a trait), its leaf area ( $LA$ ), and its leaf area index ( $LAI$ ) using the Beer-Lambert equation (Ogle and Pacala 2009):

$$APAR(t) = PAR_{max} \left\{ 1 - \exp(-k \cdot LAI(t - \Delta t)) \right\} \cdot \left( \frac{LA(t - \Delta t)}{LAI(t - \Delta t)} \right) \quad (12)$$

The numerical time step,  $\Delta t$ , is set to 1/16 of a year to achieve numerical convergence, and the model outputs individual tree states at an annual time-scale (Ogle and Pacala 2009). The effect of light was tested by running simulations that varied  $PAR_{max}$  from 10% (e.g., representing an overtopped tree in a dense canopy) to 100% (an open-grown tree) of the maximum incident radiation expected above the forest canopy, following a

logarithmic progression (206, 259, 326, 411, 517, 651, 820, 1032, 1300, 1636, 2060 MJ m<sup>-2</sup> year<sup>-1</sup>), yielding 11 light levels.  $LA$  is assumed to be related to xylem conducting area ( $XA$ , a trait) via an allometric function.  $LAI$  is equal to  $LA$  divided by the tree's projected crown area (Ogle and Pacala 2009).

The amount of “excess” labile carbon determines the size of the transient pool available for biomass production at time  $t$ ,  $E(t)$ .  $E(t)$  is computed as a simple mass-balance that first scales up area-specific photosynthesis to tree-level carbon assimilation (input variable) as  $P_G(t) \cdot LA(t - \Delta t)$ . Other inputs to  $E(t)$  are associated with retranslocation of labile carbon from senescing leaf and root tissues and sapwood to heartwood conversion (incorporated through  $\delta$  terms explained below). Losses from  $E(t)$  are attributed to maintenance respiration ( $R_M$ ) of all living tissues (tissue-specific trait). Thus,  $E(t)$  is given by:

$$E(t) = P_G(t) \cdot LA(t - \Delta t) + \delta_S(t) \cdot S_O \cdot B_{OS}(t - \Delta t) + \sum_{i=L,R} \delta_i \cdot S_i \cdot B_i(t - \Delta t) - R_M(t) \quad (13)$$

Key traits here include  $\delta_S$ ,  $\delta_L$ , and  $\delta_R$  (g gluc g dw<sup>-1</sup>), which are the labile carbon storage capacities of the bulk sapwood, leaves, and fine roots, respectively (see Ogle and Pacala 2009 for full derivation of  $\delta$  terms).  $B_{OS}$ ,  $B_L$ , and  $B_R$  (g dw) represent the structural biomass of other (e.g., branches and coarse roots) sapwood, leaves, and fine roots, and  $S_O$ ,  $S_L$ , and  $S_R$  are their corresponding senescence rates (traits) (Ogle and Pacala 2009).

Excess labile carbon (when  $E > 0$ ) is subsequently allocated to the different tissue compartments to produce structural biomass,  $B_i$ , where  $i = L$  (leaves),  $R$  (fine roots),  $TS$  (trunk softwood),  $TH$  (trunk heartwood),  $T$  (bulk trunk,  $B_{TS+B_{TH}}$ ),  $OS$  (other sapwood),

*OH* (other heartwood), *O* (bulk otherwood). For each time step in the model, the excess carbon allocated to each compartment is simultaneously converted to biomass and allocated to storage according to each tissue's labile carbon storage capacity ( $\delta$ 's, traits as defined above). The allocation of labile carbon and production of structural carbon must satisfy constraints set by the tree's allometric relationships, which are tied the radius ( $r$ ) of the tree's trunk. For a tree growing according to the healthy allometry (Ogle & Pacala 2009):

$$\Delta B_{OS} = \lambda \cdot \Delta B_{TS} \quad (14)$$

$$\Delta B_{OH} = \lambda \cdot \Delta B_{TH} \quad (15)$$

$$\frac{\Delta LA(r(t))}{SLA} = \Delta B_L \quad (16)$$

$$\rho_R \cdot \frac{r_R}{2} \cdot \Delta RA(r(t)) = \Delta B_R \quad (17)$$

$$\rho_W(t) \cdot \Delta V_T(r(t)) = \Delta B_T \quad (18)$$

The  $\Delta B_i$ 's denote the change in structural biomass in a given time step. Allometric relationships are incorporated via the changes in  $LA$  ( $\Delta LA$ ), fine root area ( $\Delta RA$ ), and trunk volume ( $\Delta V_T$ ), which are expressed as functions of trunk radius ( $r$ ) under the healthy allometry. The parameters  $\lambda$ ,  $SLA$ ,  $r_R$ ,  $\rho_R$  and  $\rho_W$  are functional traits (see Table 3.1) that link allometric and mass-balance constraints.

The above equations (4-8) are solved numerically using a root-finding routine (Ogle and Pacala 2009), yielding solutions for  $r$  and all other state variables (e.g.,  $LA$ ,  $RA$ ,  $B$ 's, etc.), including tree height ( $H$ ), which is linked to  $r$  by a simple allometric equation:

$$H(t) = H_{max} \cdot \left\{ 1 - \exp\left(-\frac{\varphi_H}{H_{max}} \cdot r(t)\right) \right\} \quad (19)$$

Two key allometric traits are the maximum tree height,  $H_{max}$ , and the initial (at  $r = 0$ ) slope of the  $H$  versus  $r$  allometric curve,  $\varphi_H$ .

For the purpose of fitting the ACGCA model to FIA data, the model can be viewed as a non-linear function of the vector of parameters (traits) and inputs (Table 3.1) that yields outputs such as  $H$  and  $r$  for each year of the simulation.

#### *Data sources*

The ACGCA model parameters are informed by two primary data sources: the Forest Inventory and Analysis (FIA) data compiled by the US Forest Service (<http://www.fia.fs.fed.us/>) and the TreeTraits database compiled from published literature (Kattge et al. 2011b, Ogle et al. 2013, 2014) (see details below). The FIA database provided radius and height data for 965,003 individual trees occurring in approximately 100,779 plots that are an unbiased sample of forested areas in the U.S. (Bechtold and Patterson 2005).

*Forest inventory data.*—The FIA data were filtered such that only individuals with at least two height and diameter measurements were included in the study to facilitate calculating change in radius ( $\Delta r$ ) and height ( $\Delta H$ ). The data were further filtered to select for “healthy,” growing trees such that an individual was discarded if: (1) it was missing  $r$  and/or  $H$  values, (2)  $\Delta r \leq 0$  or  $\Delta H \leq 0$ , (3)  $r < 0.05$  m (the starting radius for the ACGCA simulations), or (4) the annualized  $\Delta r$  or  $\Delta H$  values were larger than the 99.9% quantile of all data (i.e., remove outliers). The resulting, filtered FIA dataset (1,270,510 remeasurements) had minimum and maximum (min, max)  $r$ ,  $H$ ,  $\Delta r$ , and  $\Delta H$  values of

(0.050 m, 0.923 m), (0.051 m, 78.030 m), ( $3.24 \times 10^{-5}$  m yr<sup>-1</sup>, 0.012 m yr<sup>-1</sup>), and ( $1.23 \times 10^{-2}$  m yr<sup>-1</sup>, 3.360 m yr<sup>-1</sup>), respectively.

The sheer size of the FIA data precludes fitting the ACGCA model to individual- or tree-level data as this would greatly exceed available computational resources. Thus, to quantify the distribution of observed tree growth based on the FIA data, the  $r$ ,  $H$ ,  $\Delta r$ , and  $\Delta H$  data were log-transformed and used to construct a four-dimensional histogram describing the distribution of “realistic” values corresponding the healthy, growing trees. The histogram had nine evenly spaced bins in each dimension ( $9^4 = 6,516$  total bins). The number of bins was chosen based on trial and error to provide sufficient resolution for analysis, but avoiding excessive computational issues associated with using more bins. Limits in each dimension were based on the minimum and maximum values in the filtered FIA data, with the exception of the minimum value for  $r$  which was set to 0.05. Each point ( $r_i$ ,  $H_i$ ,  $\Delta r_i$ ,  $\Delta H_i$ ) representing an individual tree with multiple measurements was assigned to a bin, for  $i = 1, 2, \dots, 1,270,510$  remeasurment points. The proportion of trees falling in each of the 6,561 bins was computed, yielding a histogram in four dimensions representing an empirical, 4-dimensional probability distribution of the FIA data (henceforth referred to as *Hist*), aggregated across individuals, species, and sites.

*Tree functional traits database.*—Data from the TreeTraits database (Kattge et al. 2011b, Ogle et al. 2013, 2014) were used to derive semi-informative priors to constrain the parameters (traits) to realistic ranges. TreeTraits contains summary statistics (e.g., sample means or parameter estimates) for functional traits extracted from the literature; it provided over 7400 records for 27 functional traits with sample sizes ranging from 6 ( $r_r$  and  $\rho_r$ ) to >1700 (SLA and  $\rho$ ) (see Table 3.1 for parameter/trait descriptions). The

Bayesian model (described below) requires priors for log- or logit-scale parameters, and means and standard deviations of the transformed values (log or logit, Table S3.1) were derived from the TreeTraits database and used to construct semi-informative priors. The TreeTraits database lacked data for  $\lambda_s$ ,  $\lambda_h$ ,  $f_I$ ,  $\eta_B$ , and  $m$  (see Table 3.1 for definitions); in these cases, the prior means were set to the values used for *Pinus taeda* and *Acer rubrum* in Ogle and Pacala (2009), and the prior standard deviations were set to constrain parameters to reasonable ranges. See Table S3.1 for the prior distributions.

### *Bayesian model*

The ACGCA model was fit to the FIA data (histogram) in a Bayesian framework to yield posterior distributions of parameters (traits) leading to “realistic tree” growth based on the FIA data and partially constrained by the TreeTraits priors. The basic Bayesian formulation defines the posterior distribution of the parameters, conditional on the data (FIA), as proportional to the likelihood of the data (based on *Hist*) multiplied by the prior(s):

$$p(\boldsymbol{\theta}|FIA) \propto p(FIA|r(\boldsymbol{\theta}), H(\boldsymbol{\theta}), \Delta r(\boldsymbol{\theta}), \Delta H(\boldsymbol{\theta})) \cdot p(\boldsymbol{\theta}) \quad (20)$$

Note that  $\boldsymbol{\theta}$  represents the vector of 32 ACGCA model parameters (we use bold font to explicitly refer to the *vector* of parameters). The term  $p(\boldsymbol{\theta}|FIA)$  is the posterior distribution of  $\boldsymbol{\theta}$  conditional on the FIA data;  $p(FIA/r(\boldsymbol{\theta}), H(\boldsymbol{\theta}), \Delta r(\boldsymbol{\theta}), \Delta H(\boldsymbol{\theta}))$  is the likelihood of the FIA data given the ACGCA outputs for  $r$ ,  $H$ ,  $\Delta r$ , and  $\Delta H$ , which are deterministic function of  $\boldsymbol{\theta}$ ; and,  $p(\boldsymbol{\theta})$  is the joint prior for  $\boldsymbol{\theta}$ .

The likelihood of the FIA data given the ACGCA output was computed by evaluating *Hist* at the ACGCA output ( $r$ ,  $h$ ,  $\Delta r$ ,  $\Delta h$ ). In particular, for each annual time

step ( $t = 1, 2, \dots, T$ ) for which ACGCA output are produced, the likelihood is computed as:

$$\begin{aligned}
 & p(FIA|r(\boldsymbol{\theta}), H(\boldsymbol{\theta}), \Delta r(\boldsymbol{\theta}), \Delta H(\boldsymbol{\theta})) \\
 & = \prod_{t=1}^T \text{Hist}(r_t(\boldsymbol{\theta}), H_t(\boldsymbol{\theta}), \Delta r_t(\boldsymbol{\theta}), \Delta H_t(\boldsymbol{\theta})) \quad (21)
 \end{aligned}$$

That is, for a vector of outputs for  $r$ ,  $H$ ,  $\Delta r$ , and  $\Delta H$  (where  $\Delta r_t = r_t - r_{t-\Delta t}$ , and likewise for  $\Delta H$ ), at each time,  $t$ , we find the 4-dimensional bin in *Hist* that contains these values, and we return the probability of observing this vector based on the relative frequencies of the FIA data that are looked up in *Hist*. Equation (11) thus obtains the (histogram) probability of each simulated  $(r, H, \Delta r, \Delta H)$  over the simulation period from initial year  $t = 1$  to final year  $t = T$ , and the product of these probabilities is the likelihood of the data given the particular outputs produced by the ACGCA model for a given vector of parameters  $(\boldsymbol{\theta})$ . If the ACGCA simulation associated with a particular vector of trait values  $(\boldsymbol{\theta})$  resulted in a tree that was in the healthy state for the entire 50-year simulation, then  $T = 50$  (approximately the average age of a tree in the FIA data). But, if the tree died during the simulation period (not in the healthy state), or had values outside of the minimum and maximum values set by *Hist*, the parameters were rejected in the MH algorithm (see below), because the likelihood is defined as 0 in these cases.

The prior,  $p(\boldsymbol{\theta})$ , in Eqn 10 is computed as the product of 32 independent univariate priors for each trait  $k$  in the parameter vector  $\boldsymbol{\theta}$ ; i.e.,  $p(\boldsymbol{\theta}) = \prod_{k=1}^{32} p(\theta_k)$ , where the priors for each  $\theta_k$  are given in Table S3.1. As noted previously, all parameters were log- or logit-transformed, and each is assigned a normal or truncated normal prior (see Eqn 13). For the normal priors:

$$\log(\theta_k) \text{ or } \text{logit}(\theta_k) \sim \text{Normal}(\bar{\theta}_k, \sigma_k) \quad (22)$$

Eqn 12 applies to a subset of parameters in  $k = 1, \dots, 32$ ;  $\bar{\theta}_k$  and  $\sigma_k$  represent the prior mean and standard deviation, respectively, derived from the corresponding log- or logit-transformed TreeTraits data (see Table S3.1 for the transformations applied to each parameter).

Truncated normal priors were used for  $\eta$ ,  $\eta_B$ ,  $H_{max}$ , and  $\rho_{max}$  (see Table 3.1 for definitions, and Table S3.1 for transformations) to exclude unrealistic or extreme values:

$$\log(\theta_k) \text{ or } \text{logit}(\theta_k) \sim \text{TruncNormal}(\bar{\theta}_k, \sigma_k, a_k, b_k) \quad (23)$$

where  $\bar{\theta}_k$  and  $\sigma_k$  are the prior mean and standard deviation, and  $a_k$  and  $b_k$  are the lower and upper bounds, respectively. Both trunk-tapering parameters,  $\eta$  and  $\eta_B$ , were given bounds relative to each other such that  $\eta > \eta_B$ . This was accomplished by setting  $a = \log(\eta_B)$  and  $b = \infty$  for  $\eta$ , and  $a = -\infty$  and  $b = \log(\eta)$  for  $\eta_B$ . The maximum potential tree height,  $H_{max}$ , was given a lower bound of  $a = -\infty$  and an upper bound of  $b = \log(127 \text{ m})$  based on physical limitations of water transport (Domec et al. 2008). Finally, wood density,  $\rho$ , was given bounds based on physical (or engineering) constraints imposed by  $\gamma_x$ ,  $\gamma_w$ , and  $VwVc$ , where  $VwVc$  represents the volume ratio of structural tissue to internal cell volume for living sapwood cells such that:

$$a = \frac{VwVc - \gamma_x(VwVc - \beta)}{\gamma_w(1 + VwVc)} \quad (24)$$

$$b = \frac{1 - \gamma_x}{\gamma_w} \quad (25)$$

Eqn 14 is based on the assumption that there is a lower limit to the ratio of xylem cell wall area (mostly cellulose with density  $1/\gamma_w$ ; see Table 3.1) to xylem conduit lumen area

(set by  $\beta$ ). Eqn 15 is based on the assumption that the conduit lumens do not contain structural tissues, and thus do not contribute mass to the bulk wood density. Here, we assume  $V_w V_c = 0.5$  and  $\beta \cong 0.05$ , and we treat  $\gamma_x$  and  $\gamma_w$  as unknown parameters (traits).

The above Bayesian model is relatively simple and does not involve any hierarchical structures. No attempt was made to estimate individual-, site-, or species-specific parameters. Instead, the goal of the Bayesian model is to yield distributions of the “global”  $\theta$  vectors that are consistent with the “aggregated” FIA data—pooled across all individuals, sites, and species—and the semi-informative priors, which also pooled across all studies (publications) and species. This greatly simplifies the model formulation and computational requirements (i.e., the ACGCA model is only run once for every  $\theta$  vector, and the likelihood only needs to be evaluated once for a given ACGCA output vector at a each simulation year). Hence, the posterior distribution of  $\theta$  can be viewed as the probability distribution of trait values leading to realistic tree growth of healthy trees, across all species and environments combined; i.e., the posterior marginalizes over individuals, sites and species, such that posterior distributions for any individual, site, or species are expected to be contained within the aggregated distribution.

As described above, the 4-dimensional histogram (*Hist*) was used for the likelihood rather than an alternative distribution such as a multivariate normal or a kernel density estimate of the 4-dimensional distribution. Both of these alternative approaches were explored, but they led to greater computational expense and/or undesirable behavior of the MH algorithm (below). Use of *Hist* greatly reduced the computational demands because it only needed to be computed once and then referenced via a “look-up” function

when running the MH algorithm. The resulting simple, global analysis allowed us to run the MH algorithm on a desktop computer in a reasonable amount of time (~2 days).

### *Metropolis-Hastings (MH) algorithm*

We used an MH algorithm custom coded to allow simultaneous evaluation of the ACGCA model and to compare the ACGCA output against *Hist*. The actual MH algorithm for sampling from the posterior distribution is standard and follows Gelman et al. (2014). In summary, the algorithm proposes a vector of potential parameter values at each MH iteration  $z$  and accepts or rejects the proposed parameters. In particular, let  $\theta^*$  denote the proposed vector of parameter values, and let  $r_t^*$ ,  $H_t^*$ ,  $\Delta r_t^*$ , and  $\Delta H_t^*$  denote the corresponding ACGCA outputs at simulation year  $t$ , given  $\theta^*$  proposed at iteration  $z$ . We obtain  $\theta^*$  by independently generating individual  $\theta_k^*$  (again, for  $k = 1, 2, \dots, 32$  components) from a jumping distribution,  $J_z(\theta_k^* | \theta^{z-1})$ . Truncated normal jumping distributions were employed for parameters with truncated priors (i.e.,  $\eta$ ,  $\eta_B$ ,  $H_{max}$ , and  $\rho_{max}$ ), using the same upper and/or lower limits as the priors. Normal jumping distributions were used all other  $\theta_k^*$ .

As each component ( $\theta_k^*$ ) is proposed, it is either accepted or rejected based on the following acceptance ratio ( $ar_k$ ) that involves evaluation of the posterior distribution (density), up to some normalizing constant (see Eqn 10), and the jumping distribution:

$$\begin{aligned}
 ar_k &= \frac{p(\theta_k^* | FIA) / J_z(\theta_k^* | \theta^{z-1})}{p(\theta_k^{z-1} | FIA) / J_z(\theta_k^{z-1} | \theta^*)} & (26) \\
 &= \frac{p(\theta_k^* | FIA) J_z(\theta_k^{z-1} | \theta^*)}{p(\theta_k^{z-1} | FIA) J_z(\theta_k^* | \theta^{z-1})}
 \end{aligned}$$

If  $ar_k > 1$ , the posterior density evaluated at  $\theta_k^*$  is greater than the posterior density evaluated at  $\theta_k^{z-1}$ , and  $\theta_k^*$  is accepted such that  $\theta_k^z = \theta_k^*$ . If the proposed value decreases the posterior density ( $ar_k < 1$ ), it is accepted with probability  $ar_k$ ; otherwise,  $\theta_k^z = \theta_k^{z-1}$  (Gelman et al. 2014). To prevent numerical overflow Eqn 16 was transformed to the log-scale, yielding:

$$\begin{aligned} \log(ar_k) = & \log p(\theta_k^*|FIA) - \log p(\theta_k^{z-1}|FIA) \\ & + \log J_z(\theta_k^{z-1}|\theta^*) - \log J_z(\theta_k^*|\theta^{z-1}) \end{aligned} \quad (27)$$

Acceptance is determined by comparing  $\log(ar_k)$  to a random variable ( $r_{exp}$ ) generated from an exponential distribution such that if  $-\log(ar_k) < r_{exp}$ , the proposed value is accepted (again,  $\theta_k^z = \theta_k^*$ ); otherwise,  $\theta_k^z = \theta_k^{z-1}$ .

*MH implementation*—Five parallel MH chains were simulated for each of the 11 light levels ( $PAR_{max}$ ) described in the ACGCA model section above, with  $PAR_{max}$  fixed at a single light level for the duration of a given simulation. Starting values (at  $z = 0$ ) for each parameter component,  $\theta_k^0$ , were generated for each chain by randomly sampling from the prior distributions. Starting values were rejected if they resulted in a zero likelihood according to *Hist* (Eqn 11); i.e., we continued to randomly draw starting values for each  $\theta_k$  until we obtained starting values that produced realistic growth curves.

Once acceptable starting values were obtained, jumping distributions for each MH chain were tuned for 30,000 iterations to achieve near optimal acceptance rates of ~44% (Gelman et al. 1996). The simulations were executed for an additional 50,000 iterations after tuning, the first 20,000 of which were discarded as burn-in, yielding a sample of 30,000 iterations per chain. Thus, we obtained a total of 1,650,000 (5 chains  $\times$  11 light levels  $\times$  30,000 iterations) parameter sets overall, which we thinned by 50 to reduce both

within-chain autocorrelation and storage requirements ( $n = 33,000$  samples). All results refer to the thinned output unless otherwise noted.

All MH code for the analysis was written in the R programming language (R Core Team 2015), and the ACGCA model was coded in C based on code developed by Ogle and Pacala (2009) and Gemoets et al. (2013). A wrapper function in C was written to pass inputs from R to the ACGCA C code (Gemoets et al. 2013), and return outputs to R. This code was then implemented via a custom parallelization algorithm allowing multiple R sessions to run simultaneously, each running a single chain. The R code is provided in Appendix D.

### *Output Analysis*

*Posterior parameter space*— Again, we only used FIA data for trees that are assumed to be healthy and growing, we do not explicitly account for various filtering processes (e.g., environmental stress or competition), and we impose mass-balance and engineering constraints contained with the ACGCA model. Thus, we interpret the joint posterior distribution of the parameters,  $\theta$ , as the theoretical trait space. To evaluate the structure of this trait space, we graphically explored if the theoretical trait space is refined compared to the independent prior distributions used for each trait. To initially address this, we overlaid the marginal posterior distributions for each  $\theta_k$  (each trait) with the corresponding prior distribution for that trait. Next, we analyzed the posterior samples of  $\theta$  to explore trait correlations (or trade-offs) associated with the theoretical trait space. In particular, bivariate correlations between all unique pairs of the 32  $\theta_k$  were assessed, yielding  $(32 \times 31) / 2 = 496$  bivariate plots and associated Pearson correlation coefficients.

To further explore the correlation structure of the  $\theta$  space, as contained in the posterior samples, we evaluated how perturbations to this structure affect tree growth. For these simulations, the posterior samples of the individual  $\theta_k$ , for all 11 light levels, were stored in a 33,000 (MH iterations)  $\times$  32 (parameters) matrix that maintained the correlation structure produced by the MH simulations. This correlation structure was subsequently perturbed such that, for a given column ( $k$  denotes a column corresponding to a trait), all of the sampled values (rows) were randomized without replacement, producing a new matrix of parameter values. This was repeated for each column (parameter), while maintaining the original row (iteration) order of the other 31 columns (parameters). Thus, we produced 33 matrices of posterior samples; one maintained the original correlation structure, and the others (32) maintained the correlation structure of all but one of the parameters (or traits). For each of these 32 randomized parameter matrices, the ACGCA model was run for each of the 33,000 rows (each containing a randomized parameter vector), resulting in associated output vectors ( $r$ ,  $H$ ,  $\Delta r$ , and  $\Delta H$ ). The likelihood of each output vector was evaluated with Eqn 11 (*Hist*) to determine evaluate if the corresponding, randomized parameter vector produced realistic tree growth (i.e., a likelihood greater than 0), indicating that the simulated tree survived for 50 years, remained in a healthy state, and was not associated with unrealistic values for  $r$ ,  $H$ ,  $\Delta r$ , and/or  $\Delta H$ . From these simulations, we calculated, across all light levels, the proportion of the “new” (randomized) 33,000 parameter vectors that produced realistic tree growth, for each of the 32 matrices for which one trait was randomized.

*Multivariate trait correlation structure*—The above randomization of individual trait values suggested a more complicated correlation structure among the 32 traits that

was not revealed by the bivariate analyses (see Results). Thus, we applied two multiple regression approaches (see below) to further assess the correlation structure of the theoretical trait space defined by the joint posterior for  $\theta$ . The rationale for the regressions was to consider the MH posterior samples as a dataset, and then to treat each of the 32 traits ( $\theta_k$ ) in turn as the dependent variable with the remaining 31 traits and light level serving as 32 independent (explanatory) variables. Each trait, whether treated as the independent or dependent variable, was log- or logit-transformed according to the transformation used in the Bayesian model (see Table S3.1). The transformed values were standardized by subtracting their posterior mean and dividing by their posterior standard deviation. We refer to each transformed and standardized parameter as  $\delta_k$ , all of which are unitless, with mean 0 and variance 1. For consistency, light level was rescaled from -3 (lowest light level) to +3 (highest level), roughly the same range as the standardized traits ( $\delta_k$ ).

The first regression approach used best subsets regression, which was implemented in R using the leaps package (Lumley and Miller 2009). Two best subsets regressions were conducted; one only considered main effects (i.e., the 32 possible independent variables), and the second considered main effects and all possible two-way interactions. For each of the best subsets regressions, the best model was identified with exactly 10 independent variables.

In the leaps package, a variable may be included in the final (best) model through a two-way interaction, even if it is not included as a main effect. However, it is often difficult to interpret the importance of a variable that is included in an interaction, but that is not included as a main effect. Thus, we also conducted stepwise regressions that

ensured that variables were included as main effects (whether or not the main effect is significant), if they are included in an interaction. As above for the best subsets regression, we fit two models for each trait: a one with only main effects, and one with main effects and all possible two-way interactions. All stepwise regressions used forward and backward selection. BIC (Bayesian Information Criterion) was used for model selection because it tends to select more parsimonious models compared to AIC given that BIC's penalty term is larger per variable added for large data sets (Gelman et al. 2014).

Results from stepwise regression allowed exploration of the importance of trait-trait interactions for understanding the “direct” effect of one trait on another trait. For example, consider the following generic regression model for dependent variable trait  $\delta_k$ , which is significantly correlated with independent variable traits  $\delta_i$  and  $\delta_j$  and their interaction ( $k \neq i$  or  $j$ ):

$$\delta_k = \beta_0 + \beta_i \delta_i + \beta_j \delta_j + \beta_{ij} \delta_i \delta_j \quad (28)$$

The overall effect of  $\delta_i$  is given by combining all terms on the right-hand side involving  $\delta_i$ , and factoring out  $\delta_i$ , Eqn 18 can be rewritten as:

$$\delta_k = \beta_0 + (\beta_i + \beta_{ij} \delta_j) \delta_i + \beta_j \delta_j \quad (29)$$

Thus, the overall effect of  $\delta_i$  (i.e.,  $\beta_i + \beta_{ij} \delta_j$ ) depends on the partial regression coefficients for its main effect ( $\beta_i$ ) and interaction term ( $\beta_{ij}$ ) and the value of  $\delta_j$ . Because the regression variables ( $\delta$ ) are linear transformations of the trait parameters ( $\theta$ ), Eqn 19 allowed us to quantify how correlations between pairs of traits depend on the values of other traits. Thus, interactions with other traits could potentially result in a wide range of

possible bivariate correlations (negative, uncorrelated, or positive) and strengths of correlations (strong to weak) between two traits (e.g.,  $\theta_k$  and  $\theta_i$ ), conditional on the values of other traits (e.g.,  $\theta_j$ ).

We used Eqn 19 to approximate the posterior distributions for the overall effects for each dependent trait. That is, for each of the 32 dependent trait models, Eqn 19 was evaluated at the point estimates of the regression coefficients ( $\beta$ 's), for every posterior parameter vector ( $n = 33,000$  MH iterations) of the associated dependent traits (e.g.,  $\theta_i$  and  $\theta_j$  in Eqn 19). This approach ignores uncertainty in the regression coefficients ( $\beta$ ), but it does account for uncertainty in and covariation among the traits, as quantified by the joint posterior for  $\theta$ .

## Results

### *ACGCA model versus FIA comparison*

The posterior region of the ACGCA simulations for tree radius versus height generally had good overlap with the FIA data (Figure 3.1 A). Since the ACGCA model was only run for 50 years in each simulation, it did not reach the large radii and heights reported for tree from older stands. The ACGCA model also did not sufficiently capture the FIA region characterized by short trees with small radii, perhaps because these trees may not align with the ACGCA model's "healthy" condition.

### *Posterior parameter samples*

Posterior estimates for  $\theta$  are given in Table S3.2. For 30 of the 32  $\theta_k$  (traits), the 95% posterior credible intervals (CIs) included the prior mean, for each of the 11 light-

level specific marginal distributions. Based on visual inspection, the posteriors closely resembled the priors for 19 of the  $\theta_k$  (as in Figure 3.2c); for 11  $\theta_k$ , the posteriors were not notably different from the prior, but were slightly shifted (as in Figure 3.2b); for only two  $\theta_k$  ( $\epsilon$  and  $S_o$ ), the posterior and prior distributions were notably different (as in Figure 3.2a). For  $S_o$ , the posteriors did not differ by light level, but the overall posterior mean and 95% CI were 0.13 [0.01, 0.47] year<sup>-1</sup>, resulting in a slower senescence rate (longer life-span) for other, non-trunk woody tissue compared to what would be predicted from the literature (prior mean = 1.85 year<sup>-1</sup>; Figure S3.1). Only one parameter ( $\epsilon$ , radiation use efficiency) had posterior distributions that noticeably differed across light-levels (Figure 3.2a). The four highest light levels ( $PAR_{max}$  = 1032, 1300, 1636, and 2060 units) resulted in posterior means and 95% CIs for  $\epsilon$  that varied from 15.0 [4.8, 35.0], 13.6 [3.7, 31.4], 9.9 [3.0, 24.4], to 11.3 [2.9, 28.8] g gluc MJ<sup>-1</sup>, respectively. These posterior estimates were significantly different from the prior mean (37.81 g gluc MJ<sup>-1</sup>) and showed a trend of decreasing  $\epsilon$  as  $PAR_{max}$  increased (Figure S3.2).

### *Bivariate relationships*

Bivariate correlations among all possible pairs of the  $\theta_k$  (496 total pairs) were generally weak (Table 3.2); for example, 178 pairs were associated with significant ( $p \leq 0.05$ ) correlations, ranging from  $r = -0.25$  to 0.42. The three strongest bivariate correlations occurred between the proportion of xylem conducting area ( $\gamma_X$ ) versus sapwood maintenance respiration rate ( $R_{mS}$ ) ( $r = 0.42$ ,  $p < 0.01$ ), fine root area to leaf area ratio ( $f_1$ ) versus root maintenance respiration rate ( $R_{mR}$ ) ( $r = -0.25$ ,  $p < 0.01$ ), and  $\gamma_X$  versus wood density ( $\rho$ ) ( $r = -0.23$ ,  $p < 0.01$ ). The remaining 175 correlations may be

deemed biologically insignificant given that  $|r| < 0.2$ , but many of these were still statistically significant (Table 3.2) due to the large number of posterior samples used to compute  $r$ .

### *Starting values and resampling*

Generation of starting values required an average ( $n = 10$  repetition of generating starting values for each light level) of 7,004 (32% light) to 52,353 (100% light) draws from the priors to obtain a single vector of starting values for  $\theta$ , with an overall mean (across all 11 light levels) of 24,996 draws ( $n = 110$ , Table 3.3). There was large variation in the number of iterations required to find a viable set of starting values at each light level, with standard deviations ranging from 4,834 (25% light) to 56,124 (100% light). The high number of draws required to generate starting values indicates that many parameter sets lead to “unrealistic” tree growth, such that the simulated tree heights and diameters fell outside the empirical distribution estimated from FIA data (as determined by *Hist*).

The resampling procedure for evaluating the importance of the parameter correlation structure, as quantified by the MH posterior samples, resulted in acceptance rates from 13.4% (when radiation-use efficiency,  $\varepsilon$ , was randomized relative to the other traits) to ~100% (when labile carbon storage capacity of leaves,  $\delta_L$ , or roots,  $\delta_R$ , was randomized) (Figure 3.3). Randomization of four other parameters (traits) lead to acceptance rates lower than 50%: maximum potential crown radius of a tree with diameter at breast height (1.37 m) of 40 cm ( $R_{40}$ ), root and leaf maintenance respiration rates ( $R_{mR}$  and  $R_{mL}$ ), and the fine root to leaf area ratio ( $fi$ ) (Figure 3.3).

### *Multiple regression results*

Best subsets and stepwise regressions, with and without two-way interactions, produced statistically significant models ( $p < 0.05$ ), with  $R^2$  values as high as 0.81 (stepwise with interactions) when  $\varepsilon$  was treated as the dependent variable (Table S3.3, Figure 3.3). Many models with low  $R^2$  (e.g.,  $H_{max}$ ,  $R^2 = 0.009$ ) were still statistically significant (e.g.,  $p \ll 0.01$ ) due to large the sample size ( $n = 33,000$ ). The stepwise regression procedure that only considered main effects produced models only containing intercept terms when  $\gamma_c$ ,  $C_{gL}$ ,  $C_{gR}$ ,  $C_{gW}$ , and  $\delta_L$  were treated as the dependent variable. When the procedure included 2-way interactions, it produced models only containing intercepts for the aforementioned variables, in addition to  $\phi_H$ , and  $m$  (see Table 3.1 for trait definitions). In these cases, no relationship was identified between the aforementioned “dependent variable” traits and other “independent variable” traits. As expected, models for these traits yielded the smallest  $R^2$  values, and when these traits were randomized, they had high acceptance rates in the resampling procedure (Figure 3.3), and they were associated with many low, non-significant bivariate correlations (Table 3.2).

Across the 32 different  $\theta_k$ , the  $R^2$  values from the different regression models increased as the acceptance rate from the resampling procedure decreased (Figure 3.3, Table S3.3). When adding two-way interactions to the best subsets regressions that were limited to finding the best model with only 10 variables, there was at most a small increase (a maximum of 0.04 for  $R_{ms}$ ) in  $R^2$  relative to the best subsets model that only considered main effects of other traits. In contrast to the best subsets regressions, adding two-way interactions in the stepwise regressions greatly increased the  $R^2$  for some

models; e.g. when two-way interactions were included, the  $R^2$  for the model of  $R_{40}$  increased from 0.32 (main effects only) to 0.53, but was accompanied by a large increase in the number of model parameters, from 21 to 114 (Table S3.3). The increase in parameters when including two-way interactions was driven by the inclusion of a large numbers of interaction terms, and occasionally an additional main effect (Tables 3.4 and 3.5). The direction (positive or negative) of the main effects was generally not changed by adding interactions.

The trait models with the highest  $R^2$  values were the same for the stepwise regressions both with and without two-way interactions. The top five models with the highest  $R^2$  values corresponded to the models for  $\varepsilon$ ,  $R_{mR}$ ,  $f_1$ ,  $R_{mL}$ , and  $R_{40}$ , with  $R^2$  values of 0.74, 0.42, 0.38, 0.33, and 0.32 (main effects only), respectively, and 0.82, 0.53, 0.51, 0.48, and 0.53 (main effects and interactions), respectively. It is worth noting that of these traits,  $R_{mL}$  is part of the LES (Wright et al. 2004) and  $\varepsilon$  is related to the LES via its relationship to leaf N (Sinclair and Horie 1989, Wang et al. 1991, Martin and Jokela 2004). The model for SLA—an important LES trait—had  $R^2$  values of 0.28 (with interactions) and 0.14 (without interactions). With respect to the WES,  $\rho$  is the only ACGCA parameter that is explicitly included in the WES; the models for  $\rho$  had low  $R^2$  values (e.g.,  $R^2 = 0.07$  with interactions). However,  $\gamma_X$  is indirectly related to the WES, and it had the sixth highest  $R^2$  (0.31 with interactions). In general,  $\theta_k$  that were associated with models with relatively high  $R^2$  values, were also typically included as predictors in models for other  $\theta_k$  and were included in more interactions (Tables 3.4 and 3.5). Further,  $\theta_k$  that are directly or indirectly related to the LES or WES were often included as predictors in regression models for other LES or WES related traits. For instance, the leaf

traits  $SLA$  and  $R_{mL}$  were included as predictors of  $\varepsilon$ , and the wood traits  $R_{mS}$  and  $\rho$  were included as predictors of  $\gamma_X$  (Tables 3.4 and 3.5).

With respect to the stepwise multiple regressions with two way interactions, the coefficients for the main effects indicate the partial effect of a given variable (trait) when all other variables (traits) are held constant. The overall effect of each independent variable (e.g.,  $\delta_i$ , see Eqns 18 and 19) shows that the effect (or correlation between the dependent and independent variable) can change when considering interactions with other traits (e.g.,  $\delta_j$  in Eqns 18 and 19; Figure 3.4). In some cases, the overall effect can switch signs relative to the main effect—for example, see the overall effect of  $R_{mS}$  (along x axes) on  $\varepsilon$  (Figure 3.4a),  $R_{mL}$  (Figure 3.4b), and  $R_{mR}$  (Figure 3.4c), depending on the values of the interacting traits. In most cases, the overall effect is primarily negative or positive, with the magnitude of the effect being influenced by interacting traits. For example, the main effect of  $\varepsilon$  on  $R_{mL}$  is 1.29 (Figure 3.4b), but the approximated 95% central credible interval representing the overall effect is (0.06, 2.71).

## **Discussion**

### *Structure of the theoretical trait space*

The theoretical trait space produced by the individual-based tree growth model (ACGCA), constrained by forest inventory (FIA) and literature (TreeTraits) data, suggests complex multivariate relationships among key traits related to tree growth and carbon allocation. Bivariate, trait-trait correlations were generally weak within the theoretical trait space (Figure 3.5, Table 3.2). Yet, it is clear from evaluation of the data-constrained ACGCA output (posterior for  $\theta$ ) that the 32 functional traits ( $\theta_k$ 's) cannot be

randomly combined; specific combinations of traits are necessary to achieve predictions of realistic tree growth. This is further emphasized by independently drawing values of each  $\theta_k$  (trait) from the literature-based marginal priors that do not capture interdependence among traits; the majority of parameter sets are rejected because they lead to growth patterns that do not agree with the FIA data (Table 3.3). For example, most cases of randomly drawn  $\theta$  vectors resulted in trees that died during the simulation, and the majority died during the first simulation time step. Similarly, the results from independently randomizing each  $\theta_k$  (Figure 3.3) within the joint posterior for  $\theta$  clearly show that the joint distribution of  $\theta$  contains important correlation structure that is necessary to produce realistic predictions of tree growth. Taken together with the multiple regressions, our findings provide evidence for complex, multi-dimensional relationships between functional traits that govern tree growth and carbon allocation, utilization, and starvation.

The theoretical space represents a multi-dimensional hypervolume of traits that does not explicitly account for biotic constraints such as competition. However, competitive effects are implicitly contained in the FIA data and the priors estimated from the TreeTraits database, which is mostly based on observations of trees growing in field settings (Ogle et al. 2013, 2014). To the extent that competition was not explicitly considered in our analysis, the resulting theoretical trait space parallels the fundamental niche concept (Hutchinson 1957). If environmental factors (e.g., moisture, disturbances) or biotic interactions (e.g., competition) had been explicitly accounted for in our analysis, the resulting trait space (posterior distribution of  $\theta$ ) associated with different scenarios would likely have been refined relative to the theoretical trait space described herein.

This refinement or filtering of the theoretical trait space to reflect additional constraints on tree growth may have resulted in stronger bivariate relationships among traits, representing more pronounced trade-offs under specific conditions. For instance, filtering the theoretical trait space by limiting the range of values associated with four traits ( $f_1$ ,  $SLA$ ,  $R_{mL}$ , and  $R_{40}$ ; see Table 3.1) and light level ( $PAR_{max}$ ) revealed a potential trade-off (strong correlation) between root maintenance respiration ( $R_{mR}$ ) and radiation-use efficiency ( $\epsilon$ ) (see Figures 3.5 and S3.3). Filtering by light represents a particular environmental constraint, while filtering by the other four traits represents potential environmental or biotic selection pressures.

Moreover, our approach to quantifying the theoretical trait space is agnostic to site conditions or species identity. Binning the FIA data by both site and species would have produced an insufficient number of data points to develop representative 4-dimensional histogram (*Hist*) of observed heights, radii, and associated growth rates for each bin. However, we would expect that binning by species, for abundant species, may have produced trait spaces that differed among species, with each being contained in the overall theoretical trait space describe here for a “generic” North American tree in a healthy, growing state.

### *Relationships between traits*

Multiple regression analysis of the theoretical trait space provided insight into relationships among traits and between traits and light level. First, we focus on traits that are frequently measured in field or lab settings and that are related to empirical trait spectra (e.g., LES, WES). For instance, when  $SLA$  was treated as the dependent variable trait, it was positively related to leaf maintenance respiration ( $R_{mL}$ ), as expected (Wright

et al. 2004), and negatively related to light level ( $PAR_{max}$ ), in agreement with previous work showing that  $SLA$  is up to two times higher for leaves produced in shade compared to high light (Evans and Poorter 2001, Ogle et al. 2013). Unanticipated relationships also emerged. For example,  $SLA$  was correlated with a number of root traits ( $R_{mR}, f_1, r_R, \rho_r$ ), many of which are often challenging to measure and could possibly define a root economic spectrum (Reich 2014). Other infrequently-measured traits (e.g.,  $R_0, R_{40}, S_o$ ) were often included as predictors of more frequently-measured traits (e.g.,  $SLA, R_{mL}, R_{mR}, \rho$ ) (Table 3.5; see Table 3.1 for trait definitions). While it is often impractical, due to logistics or expense, to measure traits such as  $S_o$  (branch and coarse root senescence rate) and various root traits (Weiher et al. 1999, Lavorel et al. 2007), we demonstrate that modeling can help reveal potential relationships among traits that might otherwise be impractical to investigate. Although the trait relationships that emerge from our analysis are not directly equivalent to those measured in the field that explicitly evaluate inter- and/or intraspecific relationships, the model-based theoretical trait space suggests that future observational or experimental studies should consider potentially important traits (e.g.,  $R_0, R_{40}, S_o, SW_{max}, f_1, R_{mR}, R_{mS}$ ; see Table 3.1) that are not included in most measurement campaigns.

The regression analyses of the theoretical trait space suggests that a notable number of traits (~50% of the 32 explored here) are independent of all other traits. However, for a subset of traits, their relations (tradeoff) with another traits appear somewhat complex. For example, while the bivariate correlation between light-use efficiency ( $\varepsilon$ ) and root maintenance respiration ( $R_{mR}$ ) is weak (Table 3.2),  $R_{mR}$  is a significant predictor of  $\varepsilon$  when other traits are considered (e.g.,  $f_1, SLA, R_{mL}, R_{40}$ ), partly

because of interactions between  $R_{mR}$ , these other traits, and light level (Table 3.5, Figure S3.3). Existing empirical trait spectra—including the LES (Wright et al. 2004), WES (Chave et al. 2009), and the world-wide fast-slow spectrum (Reich 2014)—typically do not evaluate trait-trait relationships beyond at most three traits (e.g., 3D plots). Studies using ordination methods provide an indication that interactions exist, in that multiple traits are often found to be correlated with a particular axis in the ordination (Diaz et al. 2004, Cavender-Bares et al. 2004, Baraloto et al. 2010, Stahl et al. 2013). The results from this study, however, indicate that explicit consideration of multiple trait-trait or trait-environment interactions is potentially important (Table 3.5). Considering the variety of relationships proposed in plant physiological models—such as photosynthetic models (Farquhar et al. 1980), water transport models (Sperry et al. 1998, Tuzet et al. 2003), stomatal conductance models (Ball et al. 1987, Damour et al. 2010, Medlyn et al. 2011)—it is perhaps unsurprising that multiple plant functional traits interact to govern lower dimensional trait spaces (e.g., bivariate trait relationships), especially when they are known to be correlated with the same underlying physiological processes.

We highlight potential mechanisms that may give rise to some of the trait-trait relationships that emerged through our multivariate analyses. These tradeoffs result from a combination of constraints inherent to the structure of the ACGCA model as well as the constraints placed on tree growth by fitting the model to FIA and TreeTraits data. Consider one of the tradeoffs that emerged for *SLA* that may be representative of a hidden mass conservation tradeoff. To achieve a particular growth rate or size, as *SLA* increases, this implies that for a fixed amount of leaf biomass, leaf area (*LA*) increases, which is expected to lead to increased photosynthesis ( $P_G$ ). If more carbon is fixed, then this

“excess” carbon must be incorporated into tissues, respired, or lost. Again, to achieve a particular (fixed) growth rate as  $SLA$  increase, this would require that the excess carbon be lost, which is reflected in the positive correlation between  $SLA$  versus respiration ( $R_{mR}$  and  $R_{mL}$ ) and/or tissue senescence ( $S_R$  and  $S_L$ ) (Table 3.4). The negative correlation between  $\gamma_X$  and  $\rho$  may be interpreted as an engineering tradeoff. For a fixed trunk radius, as the conducting area in the sapwood increases (increase in  $\gamma_X$ ), this leads to less structural tissue, and lower overall wood density ( $\rho$ ).

In the absence of fitting the ACGCA model to the FIA data, randomly chosen combinations of parameters can result in trees that grow unrealistically fast, tall, or wide, trees that do not grow, or trees that immediately die, even under high light conditions. For example, combining high values of  $SLA$  and  $\epsilon$  with low values of respiration, construction costs, and senescence rates will lead to a tree that unrealistically reaches its maximum height within one annual time step. Thus, the tradeoffs that emerge by fitting the ACGCA model to the FIA and TreeTraits data represent a combination of the mass balance and engineering mechanisms that are built into the model, combined with empirical relationships contained in the FIA data.

#### *Tradeoffs from economics spectra*

Our analysis did not reveal strong correlations or tradeoffs between pairs of traits (Table 3.2), in contrast to previously described trait spectra such as the LES and WES (Wright et al. 2004, Chave et al. 2009, Reich 2014). Though, this apparent discrepancy between the (lack of) bivariate tradeoffs in our theoretical trait space versus the fairly strong (e.g.,  $R^2 = 0.16$  to  $0.72$ ) correlations in, for example, the LES could arise from at least two explanations. First, as noted previously, our theoretical trait space is

representative of a “generic” tree and essentially aggregates over all individuals (millions), species (ca. 300), and sites (thousands) represented in the FIA. In contrast, the LES evaluates interspecific trait tradeoffs by summarizing species-specific traits (for over 2000 species) and evaluating tradeoffs across these species; although it aggregates across sites ( $n = 175$ ), it does explore how the interspecific trait tradeoffs potentially vary along climatic gradients (Wright et al. 2004). Second, normalization of leaf traits—such as maximum photosynthetic rate, respiration rate, and nitrogen and phosphorous contents—by leaf mass, instead of leaf area has been shown to change the correlation strength between pairs of traits related to the LES (Lloyd et al. 2013, Osnas et al. 2013). However, LES leaf traits and related traits in the ACGCA model (e.g.,  $R_{mL}$ ) are both normalized by leaf mass, but a key ACGCA photosynthesis parameter demonstrating the strongest multivariate trait relationships (i.e.,  $\epsilon$ , radiation-use efficiency) is independent of the leaf size unit (mass or area) (Table 3.1).

However, the multiple regression results, in general, provide evidence for the existence of trait tradeoffs in the theoretical trait spectra, many of which agree with the empirical economics spectra. One example, mentioned above, is the relationship between  $SLA$  and  $R_{mL}$  (equivalent to  $R_{mass}$  in the LES). When  $SLA$  is treated as the dependent trait, the partial regression coefficient for  $R_{mL}$  is positive, which agrees with the relationship in the LES (Wright et al. 2004). The LES correlation between leaf lifespan ( $LL = S_L^{-1}$ ) and  $LMA$  ( $LMA = SLA^{-1}$ ) is positive (Wright et al. 2004), which agrees with the partial regression coefficient for  $S_L$  in the model for  $SLA$ . Likewise,  $R_{mL}$  and leaf life span ( $LL$ ) are positively correlated in the LES (Wright et al. 2004), which agrees with the negative

partial regression coefficient for  $S_L$  (since  $S_L = LL^{-1}$ ) in the regression model that treats  $R_{mL}$  as the dependent variable (Table 3.5).

There is considerably less overlap between the WES (Chave et al. 2009) and the functional traits in the ACGCA model, with only wood density ( $\rho$ ) being explicitly included in both. However, the proportion of xylem conducting area ( $\gamma_X$ ) is an important wood trait in ACGCA, and it can be derived from traits in the WES, including mean conduit diameter and conduit density (i.e., number of conduits per cross-sectional area), given assumptions about conduit shape (e.g., circular cross-section). In the WES, conduit density is often found to be negatively correlated with  $\rho$  (Chave et al. 2009). This is in agreement with our theoretical trait spectra; the bivariate correlation between  $\rho$  and  $\gamma_X$  and associated partial regression coefficients were both negative and significant. Our study suggests that the WES could be expanded upon by considering other wood traits (e.g.,  $R_{mS}$ ,  $S_o$ ,  $SW_{max}$ ) that emerged here as important predictors of traits included in the WES ( $\gamma_X$  and  $\rho$ ) (Table 3.5).

The general agreement between patterns contained in our theoretical trait space and analogous aspects of common, empirical trait spectra (LES and WES) suggests that quantifying the theoretical trait space provides another approach to understanding tradeoffs among functional traits. The ACGCA model directly incorporates mass conservation (via carbon allocation, utilization, and storage mechanisms) and engineering tradeoffs (via structural and allometric relationships) (Scheiter et al. 2013). The theoretical trait spectra produced by the ACGCA model produced trait tradeoffs similar to those seen in the LES and WES, at least in direction (positive versus negative), suggesting that mass conservation and engineering tradeoffs likely govern much of the

variation in these empirical spectra. It is notable that prominent empirical trait relationships were contained in the theoretical trait spectra given that the ACGCA model, as implemented here, did not include important factors like water, nutrients, disturbances, or biotic interactions that act on actual trees. If such factors are included in theoretical (modeling) analyses of functional trait spectra, they could possibly generate a more refined description of how specific physiological and environmental processes influence the functional trait space.

#### *Future directions*

Other theoretical trait spectra could be constructed with different process-based models of tree or plant function, or by including species-specific traits and fitting to data on individual trees or species. The parameters in such models should be directly interpreted as plant traits, and for comparison against field-based empirical spectra, at least a subset of parameters should overlap with traits in such empirical spectra. We could further refine the theoretical trait spectra emergent from the ACGCA model by including additional environmental limitations. For instance, the modular structure of the ACGCA model could accommodate a more mechanistic model of carbon acquisition, but incorporating, for example, the Farquhar et al. (1980) model of photosynthesis and a stomatal conductance model (Ball et al. 1987, Leuning 1995, Ogle and Reynolds 2002, Medlyn et al. 2011). Incorporation of a more mechanistic photosynthesis model, along with a water transport model, could allow for the possible incorporation of a full representation of the soil-plant atmosphere continuum (Sperry et al. 1998, Tuzet et al. 2003), and thus, evaluate the effects of water availability on the theoretical trait spectra.

The type of model-based analysis conducted herein could provide unique opportunities to

investigate how specific processes—such as those related to physiology, mass conservation, and engineering constraints—interact with each other to govern functional trait distributions and tradeoffs.

### *Conclusions*

Though strong bivariate patterns among traits did not directly emerge from the theoretical trait space described by the posterior distribution of parameters ( $\theta$ ) in the ACGCA model, complex multidimensional relationships are contained in this trait space, for at least a subset of traits. Thus, the theoretical space implies that realistic tree growth can only be predicted if the multivariate structure of  $\theta$  is maintained; if individual traits within  $\theta$  are randomly combined, this leads to immediate tree death in the vast majority of simulations. The theoretical trait space also suggested a number of root traits and other less commonly quantified traits may be important for understanding trait spectra, whole-plant performance, and life-history tradeoffs, and such traits should be considered in future observational and experimental studies. Finally, the directions (positive or negative) of the trait-trait relationships in the theoretical trait space generally agreed with existing empirical spectra (e.g., LES and WES), pointing to the validity of quantifying theoretical traits spaces, while also suggesting mechanisms giving rise to the observed variation in empirical trait spectra.

## **Acknowledgements**

We thank Jessica Guo, Drew Peltier, and Heather Kropp for valuable input on the manuscript. We thank Michael Fell's committee members for their support and feedback, including Janet Franklin, Thomas Day, Kevin Hultine, and Jarrett Barber.

## References

- Adler, P. B., R. Salguero-Gómez, A. Compagnoni, J. S. Hsu, J. Ray-Mukherjee, C. Mbeau-Ache, and M. Franco. 2014. Functional traits explain variation in plant life history strategies. *Proceedings of the National Academy of Sciences* 111:740–745.
- Atkin, O. K., K. J. Bloomfield, P. B. Reich, M. G. Tjoelker, G. P. Asner, D. Bonal, G. Bönisch, M. G. Bradford, L. A. Cernusak, E. G. Cosio, D. Creek, K. Y. Crous, T. F. Domingues, J. S. Dukes, J. J. G. Egerton, J. R. Evans, G. D. Farquhar, N. M. Fyllas, P. P. G. Gauthier, E. Gloor, T. E. Gimeno, K. L. Griffin, R. Guerrieri, M. A. Heskell, C. Huntingford, F. Y. Ishida, J. Kattge, H. Lambers, M. J. Liddell, J. Lloyd, C. H. Lusk, R. E. Martin, A. P. Maksimov, T. C. Maximov, Y. Malhi, B. E. Medlyn, P. Meir, L. M. Mercado, N. Mirotchnick, D. Ng, Ü. Niinemets, O. S. O’Sullivan, O. L. Phillips, L. Poorter, P. Poot, I. C. Prentice, N. Salinas, L. M. Rowland, M. G. Ryan, S. Sitch, M. Slot, N. G. Smith, M. H. Turnbull, M. C. VanderWel, F. Valladares, E. J. Veneklaas, L. K. Weerasinghe, C. Wirth, I. J. Wright, K. R. Wythers, J. Xiang, S. Xiang, and J. Zaragoza-Castells. 2015. Global variability in leaf respiration in relation to climate, plant functional types and leaf traits. *New Phytologist* 206:614–636.
- Ball, J., I. Woodrow, and J. Berry. 1987. A model predicting stomatal conductance and its contribution to the control of photosynthesis under different environmental conditions. *Progress in Photosynthesis Research*:221–224.
- Baraloto, C., C. E. T. Paine, L. Poorter, J. Beauchene, D. Bonal, A. M. Domenach, B. Hérault, S. Patiño, J. C. Roggy, and J. Chave. 2010. Decoupled leaf and stem economics in rain forest trees. *Ecology Letters* 13:1338–1347.
- Bechtold, W. A., and P. L. Patterson. 2005. The Enhanced Forest Inventory and Analysis Program — National Sampling Design and Estimation Procedures. USDA General Technical Report SRS-80:85.
- Van Bodegom, P. M., J. C. Douma, and L. M. Verheijen. 2014. A fully traits-based approach to modeling global vegetation distribution. *Proceedings of the National Academy of Sciences* 111:13733–13738.
- Bugmann, H. 2001. A review of forest gap models. *Climatic Change* 51:259–305.
- Cavender-Bares, J., K. Kitajima, and F. a. Bazzaz. 2004. Multiple Trait Associations in Relation To Habitat Differentiation Among 17 Floridian Oak Species. *Ecological Monographs* 74:635–662.
- Chave, J., R. Condit, H. C. Muller-Landau, S. C. Thomas, P. S. Ashton, S. Bunyavejchewin, L. L. Co, H. S. Dattaraja, S. J. Davies, S. Esufali, C. E. N. Ewango, K. J. Feeley, R. B. Foster, N. Gunatilleke, S. Gunatilleke, P. Hall, T. B.

- Hart, C. Hernández, S. P. Hubbell, A. Itoh, S. Kiratiprayoon, J. V. LaFrankie, S. Loo de Lao, J.-R. Makana, M. N. S. Noor, A. R. Kassim, C. Samper, R. Sukumar, H. S. Suresh, S. Tan, J. Thompson, M. D. C. Tongco, R. Valencia, M. Vallejo, G. Villa, T. Yamakura, J. K. Zimmerman, and E. C. Losos. 2008. Assessing Evidence for a Pervasive Alteration in Tropical Tree Communities. *PLoS Biology* 6:455–462.
- Chave, J., D. Coomes, S. Jansen, S. L. Lewis, N. G. Swenson, and A. E. Zanne. 2009. Towards a worldwide wood economics spectrum. *Ecology Letters* 12:351–366.
- Clark, J. S., D. Bell, C. Chu, B. Courbaud, M. Dietze, M. Hersh, J. Hillerislambers, I. Ibáñez, S. Ladeau, S. McMahon, J. Metcalf, J. Mohan, E. Moran, L. Pangle, S. Pearson, C. Salk, Z. Shen, D. Valle, and P. Wyckoff. 2010. High-dimensional coexistence based on individual variation: A synthesis of evidence. *Ecological Monographs* 80:569–608.
- Damour, G., T. Simonneau, H. Cochard, and L. Urban. 2010. An overview of models of stomatal conductance at the leaf level. *Plant, Cell & Environment*:1419–1438.
- Diaz, S., J. G. Hodgson, K. Thompson, M. Cabido, J. H. C. Cornelissen, a. Jalili, G. Montserrat-Martí, J. P. Grime, F. Zarrinkamar, Y. Asri, S. R. Band, S. Basconcelo, P. Castro-Díez, G. Funes, B. Hamzehee, M. Khoshnevi, N. Pérez-Harguindeguy, M. C. Pérez-Rontomé, F. a. Shirvany, F. Vendramini, S. Yazdani, R. Abbas-Azimi, a. Bogaard, S. Boustani, M. Charles, M. Dehghan, L. Torres-Espuny, V. Falczuk, J. Guerrero-Campo, a. Hynd, G. Jones, E. Kowsary, F. Kazemi-Saeed, M. Maestro-Martínez, a. Romo-Díez, S. Shaw, B. Siavash, P. Villar-Salvador, and M. R. Zak. 2004. The plant traits that drive ecosystems: Evidence from three continents. *Journal of Vegetation Science* 15:295–304.
- Diaz, S., J. Kattge, J. H. Cornelissen, I. J. Wright, S. Lavorel, S. Dray, B. Reu, M. Kleyer, C. Wirth, I. C. Prentice, E. Garnier, G. Bonisch, M. Westoby, H. Poorter, P. B. Reich, A. T. Moles, J. Dickie, A. N. Gillison, A. E. Zanne, J. Chave, S. J. Wright, S. N. Sheremet'ev, H. Jactel, C. Baraloto, B. Cerabolini, S. Pierce, B. Shipley, D. Kirkup, F. Casanoves, J. S. Joswig, A. Gunther, V. Falczuk, N. Ruger, M. D. Mahecha, and L. D. Gorne. 2016. The global spectrum of plant form and function. *Nature* 529:167–171.
- Domec, J.-C., B. Lachenbruch, F. C. Meinzer, D. R. Woodruff, J. M. Warren, and K. a McCulloh. 2008. Maximum height in a conifer is associated with conflicting requirements for xylem design. *Proceedings of the National Academy of Sciences* 105:12069–12074.
- Evans, J. R., and H. Poorter. 2001. Photosynthetic acclimation of plants to growth irradiance: the relative importance of specific leaf area and nitrogen partitioning in maximizing carbon gain. *Plant, Cell & Environment* 24:755–767.

- Evans, M. R. 2012. Modelling ecological systems in a changing world. *Philosophical transactions of the Royal Society of London. Series B, Biological sciences* 367:181–190.
- Farquhar, G. D., S. Caemmerer, and J. A. Berry. 1980. A biochemical model of photosynthetic CO<sub>2</sub> assimilation in leaves of C<sub>3</sub> species. *Planta* 149:78–90.
- Fisher, R. A., S. Muszala, M. Verstein, P. Lawrence, C. Xu, N. G. McDowell, R. G. Knox, C. Koven, J. Holm, B. M. Rogers, A. Spessa, D. Lawrence, and G. Bonan. 2015. Taking off the training wheels: The properties of a dynamic vegetation model without climate envelopes, CLM4.5(ED). *Geoscientific Model Development* 8:3593–3619.
- Fyllas, N. M., E. Gloor, L. M. Mercado, S. Sitch, C. A. Quesada, T. F. Domingues, D. R. Galbraith, A. Torre-Lezama, E. Vilanova, H. Ramírez-Angulo, N. Higuchi, D. A. Neill, M. Silveira, L. Ferreira, G. a. Aymard C., Y. Malhi, O. L. Phillips, and J. Lloyd. 2014. Analysing Amazonian forest productivity using a new individual and trait-based model (TFS v.1). *Geoscientific Model Development* 7:1251–1269.
- Gelman, A., J. B. Carlin, H. S. Stern, D. B. Dunson, A. Vehtari, and D. B. Rubin. 2014. *Bayesian Data Analysis Third Edition*. Third. CRC Press, New York.
- Gelman, A., G. Roberts, and W. Gilks. 1996. Efficient metropolis jumping rules. *Bayesian Statistics* 5:599–607.
- Gemoets, D., J. Barber, and K. Ogle. 2013. Reversible jump MCMC for inference in a deterministic individual-based model of tree growth for studying forest dynamics. *Environmetrics* 24:433–448.
- Hutchinson, G. E. 1957. Concluding remarks. *Cold Spring Harbor Symposia on Quantitative Biology* 22:415–427.
- Kattge, J., K. Ogle, G. Bönisch, S. Díaz, S. Lavorel, J. Madin, K. Nadrowski, S. Nöllert, K. Sartor, and C. Wirth. 2011. A generic structure for plant trait databases. *Methods in Ecology and Evolution* 2:202–213.
- Lavorel, S., S. Díaz, J. H. C. Cornelissen, E. Garnier, S. P. Harrison, S. McIntyre, J. G. Pausas, N. P. Catherine, and R. Carlos. 2007. Chapter 13 Plant Functional Types : Are We Getting Any Closer to the Holy Grail ? Pages 149–164 *in* J. G. Canadell, D. E. Pataki, and L. F. Pitelka, editors. *Terrestrial Ecosystems in a Changing World*. First edition. Springer, New York.
- Lavorel, S., and E. Garnier. 2002. Predicting changes in community composition and ecosystem functioning from plant traits : *Functional Ecology*:545–556.

- Leuning, R. 1995. A critical appraisal of a combined stomatal-photosynthesis model for C<sub>3</sub> plants. *Plant Cell & Environment* 18:339–355.
- Lloyd, J., K. Bloomfield, T. F. Domingues, and G. D. Farquhar. 2013. Photosynthetically relevant foliar traits correlating better on a mass vs an area basis: Of ecophysiological relevance or just a case of mathematical imperatives and statistical quicksand? *New Phytologist* 199:311–321.
- Lumley, T., and A. Miller. 2009. leaps: regression subset selection.
- Martin, T. a, and E. J. Jokela. 2004. Developmental patterns and nutrition impact radiation use efficiency components in southern pine stands. *Ecological Applications* 14:1839–1854.
- McGill, B. J., B. J. Enquist, E. Weiher, and M. Westoby. 2006. Rebuilding community ecology from functional traits. *Trends in Ecology and Evolution* 21:178–85.
- Medlyn, B. E., R. a. Duursma, D. Eamus, D. S. Ellsworth, I. C. Prentice, C. V. M. Barton, K. Y. Crous, P. De Angelis, M. Freeman, and L. Wingate. 2011. Reconciling the optimal and empirical approaches to modelling stomatal conductance. *Global Change Biology* 17:2134–2144.
- Ogle, K., J. Barber, and K. Sartor. 2013. Feedback and Modularization in a Bayesian Meta-analysis of Tree Traits Affecting Forest Dynamics. *Bayesian Analysis* 8:133–168.
- Ogle, K., and S. W. Pacala. 2009. A modeling framework for inferring tree growth and allocation from physiological, morphological and allometric traits. *Tree Physiology* 29:587–605.
- Ogle, K., S. Pathikonda, K. Sartor, J. W. Lichstein, J. L. D. Osnas, and S. W. Pacala. 2014. A model-based meta-analysis for estimating species-specific wood density and identifying potential sources of variation. *Journal of Ecology* 102:194–208.
- Ogle, K., and J. F. Reynolds. 2002. Desert dogma revisited: coupling of stomatal conductance and photosynthesis in the desert shrub, *Larrea tridentata*. *Plant, Cell & Environment* 25:909–921.
- Osnas, J. L. D., J. W. Lichstein, P. B. Reich, and S. W. Pacala. 2013. Global Leaf Trait Relationships: Mass, Area, and the Leaf Economics Spectrum. *Science* 340:1–4.
- R Core Team. 2015. R: A language and environment for statistical computing. R Foundation for Statistical Computing, Vienna, Austria.
- Reich, P. B. 2014. The world-wide “fast-slow” plant economics spectrum: a traits manifesto. *Journal of Ecology* 102:275–301.

- Reich, P. B., D. S. Ellsworth, M. B. Walters, J. M. Vose, C. Gresham, J. C. Volin, and W. D. Bowman. 1999. Generality of Leaf Trait Relationships: A Test Across Six Biomes. *Ecology* 80:1955–1969.
- Reich, P. B., M. B. Walters, and D. S. Ellsworth. 1997. From Tropics to Tundra: Global Convergence in Plant Functioning. *Proceedings of the National Academy of Science* 94:13730–13734.
- Scheiter, S., L. Langan, and S. I. Higgins. 2013. Next-generation dynamic global vegetation models: Learning from community ecology. *New Phytologist* 198:957–969.
- Shipley, B., M. J. Lechowicz, I. Wright, and P. B. Reich. 2006. Fundamental trade-offs generating the worldwide leaf economics spectrum. *Ecology* 87:535–541.
- Sinclair, T. R., and T. Horie. 1989. Leaf Nitrogen, Photosynthesis, and Crop Radiation Use Efficiency: A Review. *Crop Science* 29:90.
- Sperry, J. S., F. R. Adler, G. S. Campbell, and J. P. Comstock. 1998. Limitation of plant water use by rhizosphere and xylem conductance: results from a model. *Plant, Cell & Environment* 21:347–359.
- Stahl, U., J. Kattge, B. Reu, W. Voigt, and K. Ogle. 2013. Whole-plant trait spectra of North American woody plant species reflect fundamental ecological strategies. *Ecosphere* 4:128.
- Tuzet, A., A. Perrier, and R. Leuning. 2003. A coupled model of stomatal conductance, photosynthesis and transpiration. *Plant, Cell & Environment* 26:1097–1116.
- Wang, A. Y. P., P. G. Jarvis, and C. M. a Taylor. 1991. PAR Absorption and Its Relation to Above-Ground Dry Matter Production of Sitka Spruce. *Journal of Applied Ecology* 28:547–560.
- Webb, C. T., J. a. Hoeting, G. M. Ames, M. I. Pyne, and N. LeRoy Poff. 2010. A structured and dynamic framework to advance traits-based theory and prediction in ecology. *Ecology Letters* 13:267–283.
- Weihner, E., A. van der Werf, K. Thompson, M. Roderick, E. Garnier, and O. Eriksson. 1999. Challenging Theophrastus: a common core list of plant traits for functional ecology. *Journal of Vegetation Science* 10:609–620.
- Wright, I. J., P. B. Reich, M. Westoby, D. D. Ackerly, Z. Baruch, F. Bongers, J. Cavender-Bares, T. Chapin, J. H. C. Cornelissen, M. Diemer, J. Flexas, E. Garnier, P. K. Groom, J. Gulias, K. Hikosaka, B. B. Lamont, T. Lee, W. Lee, C. Lusk, J. J. Midgley, M.-L. Navas, U. Niinemets, J. Oleksyn, N. Osada, H. Poorter, P. Poot, L. Prior, V. I. Pyankov, C. Roumet, S. C. Thomas, M. G. Tjoelker, E. J.

Veneklaas, and R. Villar. 2004. The worldwide leaf economics spectrum. *Nature* 428:821–827.

## Tables

**Table 3.1:** Descriptions and units associated with the 32 parameters ( $\theta_k$ ) in the ACGCA model that are representative of potentially important functional traits.

Symbol	Unit	Description
$H_{max}$	m	Maximum tree height
$\varphi_H$	-	Slope at $H$ versus $r$ curve at $r = 0$ m
$\eta$	-	Relative height at which trunk transitions from paraboloid to cone
$SW_{max}$	m	Maximum sapwood width
$\lambda_S$	-	Proportionality between $B_T$ and $B_O$ for sapwood
$\lambda_H$	-	Proportionality between $B_T$ and $B_O$ for heartwood
$\rho$	g dw m <sup>-3</sup>	Wood density
$f_1$	-	Fine root area to leaf area ratio
$f_2$	-	Leaf area to xylem conducting area ratio
$\gamma_C$	g gluc m <sup>-3</sup>	Maximum storage capacity of living sapwood cells
$\gamma_X$	-	Xylem conducting area to sapwood area ratio
$C_{GL}$	g gluc g dw <sup>-1</sup>	Construction costs of producing leaves
$C_{GR}$	g gluc g dw <sup>-1</sup>	Construction costs of producing fine roots
$C_{Gw}$	g gluc g dw <sup>-1</sup>	Construction costs of producing sapwood
$\delta_L$	g gluc g dw <sup>-1</sup>	Labile carbon storage capacity of leaves
$\delta_R$	g gluc g dw <sup>-1</sup>	Labile carbon storage capacity of fine roots
$S_L$	year <sup>-1</sup>	Senescence rate of leaves
$SLA$	m <sup>2</sup> g dw <sup>-1</sup>	Specific leaf area
$S_R$	year <sup>-1</sup>	Senescence rate of fine roots
$S_O$	year <sup>-1</sup>	Senescence rate of coarse roots and branches
$r_R$	m	Average fine root radius
$\rho_R$	g dw m <sup>-3</sup>	Tissue density of fine roots
$R_{mL}$	g gluc g dw <sup>-1</sup> year <sup>-1</sup>	Maintenance respiration rate of leaves
$R_{mS}$	g gluc g dw <sup>-1</sup> year <sup>-1</sup>	Maintenance respiration rate of sapwood
$R_{mR}$	g gluc g dw <sup>-1</sup> year <sup>-1</sup>	Maintenance respiration rate of fine roots
$\eta_B$	-	Relative height at which trunk transitions from neiloid to paraboloid
$k$	-	Crown light extinction coefficient
$\varepsilon$	g gluc MJ <sup>-1</sup>	Radiation-use efficiency
$m$	-	Maximum relative crown depth
$\alpha$	-	Crown curvature parameter
$R_0$	m	Maximum potential crown radius of a tree with diameter at breast height of 0 m (i.e., for a tree that is exactly 1.37 m tall)

$R_{40}$  m

---

Maximum potential crown radius of a tree with diameter at breast height of 0.4 m (40 cm).

**Table 3.2:** Bivariate correlations between pairs of parameters (traits) are shown in the upper triangle (blue for +, red for – correlations). The lower triangle contains p-values for the Pearson correlations (shading indicates the level of significance). There were relatively few strong correlations ( $|r|>0.2$ ). Many weak correlations were significant, possibly due to sample size ( $n = 33,000$ ).

$\theta$	$\epsilon$	$R_{40}$	$R_{mR}$	$R_{mL}$	$f_1$	SLA	$R_{mS}$	$r_R$	$\rho_R$	$S_o$	$f_2$	k	$SW_{max}$	$\gamma_X$
$\epsilon$		-0.03	0.15	0.16	0.14	-0.08	0.04	0.04	0.04	0.08	-0.01	-0.05	-0.07	-0.04
$R_{40}$	0.00		0.15	0.17	0.09	-0.07	-0.01	0.03	0.04	0.18	0.12	0.01	0.15	-0.11
$R_{mR}$	0.00	0.00		0.03	-0.25	0.00	0.03	-0.09	-0.10	0.06	-0.07	0.00	-0.09	-0.02
$R_{mL}$	0.00	0.00	0.00		0.02	0.13	0.04	0.00	0.00	0.09	-0.06	-0.01	-0.08	-0.01
$f_1$	0.00	0.00	0.00	0.00		-0.02	0.03	-0.06	-0.02	0.09	-0.02	0.02	-0.06	0.00
SLA	0.00	0.00	0.79	0.00	0.00		-0.04	-0.01	0.00	-0.05	0.01	0.00	0.04	-0.01
$R_{mS}$	0.00	0.16	0.00	0.00	0.00	0.00		0.00	0.01	0.07	0.06	0.03	-0.06	0.42
$r_R$	0.00	0.00	0.00	0.47	0.00	0.04	0.93		-0.02	0.00	-0.02	0.00	-0.01	-0.01
$\rho_R$	0.00	0.00	0.00	0.69	0.00	0.80	0.20	0.01		0.02	-0.02	0.00	0.00	-0.01
$S_o$	0.00	0.00	0.00	0.00	0.00	0.00	0.00	0.38	0.00		0.12	0.05	0.07	0.12
$f_2$	0.16	0.00	0.00	0.00	0.00	0.24	0.00	0.00	0.00	0.00		0.01	-0.08	-0.01
k	0.00	0.07	0.49	0.29	0.00	0.48	0.00	0.55	0.87	0.00	0.03		-0.03	0.01
$SW_{max}$	0.00	0.00	0.00	0.00	0.00	0.00	0.00	0.09	0.45	0.00	0.00	0.00		0.04
$\gamma_X$	0.00	0.00	0.00	0.01	0.90	0.28	0.00	0.04	0.03	0.00	0.34	0.29	0.00	
$R_0$	0.00	0.00	0.75	0.41	0.00	0.11	0.00	0.01	0.05	0.00	0.00	0.00	0.00	0.00
$\alpha$	0.00	0.55	0.00	0.00	0.15	0.04	0.47	0.96	0.65	0.00	0.02	0.00	0.07	0.37
$\eta$	0.00	0.40	0.03	0.00	0.12	0.93	0.00	0.13	0.59	0.00	0.00	0.01	0.01	0.00
$S_L$	0.00	0.00	0.14	0.06	0.02	0.00	0.12	0.55	0.32	0.00	0.12	0.00	0.01	0.96
$\rho$	0.00	0.02	0.48	0.25	0.66	0.23	0.00	0.04	0.52	0.00	0.48	0.89	0.01	0.00
$S_R$	0.01	0.01	0.06	0.04	0.00	0.00	0.62	0.73	0.21	0.99	0.00	0.88	0.00	0.34
m	0.79	0.21	0.12	0.00	0.21	0.63	0.57	0.01	0.12	0.11	0.93	0.99	0.32	0.06
$\lambda_s$	0.00	0.02	0.24	0.62	0.70	0.61	0.00	0.83	0.49	0.00	0.53	0.15	0.00	0.18
$H_{max}$	0.00	0.00	0.80	0.96	0.33	0.85	0.00	0.06	0.25	0.00	0.04	0.08	0.00	0.23
$\eta_B$	0.01	0.00	0.04	0.92	0.90	0.12	0.56	0.45	0.61	0.00	0.94	0.01	0.00	0.70
$\phi_H$	0.51	0.01	0.75	0.76	0.14	0.20	0.65	0.61	0.89	0.40	0.71	0.29	0.03	0.34
$\lambda_h$	0.18	0.03	0.12	0.39	0.57	0.28	0.13	0.06	0.90	0.00	0.42	0.32	0.00	0.38
$C_{Gw}$	0.10	0.55	0.15	0.76	0.23	0.84	0.24	0.71	0.53	0.00	0.95	0.22	0.04	0.06
$C_{GR}$	0.60	0.04	0.17	0.28	0.89	0.81	0.77	0.06	0.28	0.01	0.50	0.55	0.64	0.39
$C_{GL}$	0.43	0.33	0.74	0.59	0.86	0.93	0.98	0.80	0.92	0.68	0.12	0.32	0.56	0.02
$\delta_R$	0.28	0.56	0.93	0.16	0.33	0.88	0.39	0.56	0.98	0.07	0.59	0.02	0.58	0.37
$\delta_L$	0.60	0.04	0.27	0.33	0.48	0.74	0.37	0.44	0.26	0.44	0.22	0.24	0.01	0.80
$\gamma_C$	0.86	0.10	0.98	0.25	0.35	0.68	0.11	0.53	0.20	0.00	0.12	0.12	0.05	0.00
$PAR_{max}$	0.00	0.01	0.00	0.00	0.00	0.00	0.05	0.00	0.00	0.00	0.01	0.00	0.00	0.00

Table 3.2 continued:

$\theta$	$R_0$	$\alpha$	$\eta$	$S_L$	$\rho$	$S_R$	$m$	$\lambda_s$	$H_{\max}$	$\eta_B$	$\Phi_H$	$\lambda_h$
$\varepsilon$	-0.14	0.04	0.05	0.04	0.05	0.01	0.00	0.03	0.02	-0.01	0.00	0.01
$R_{40}$	0.19	0.00	0.00	0.05	-0.01	0.01	0.01	-0.01	-0.02	0.02	-0.02	-0.01
$R_{mR}$	0.00	-0.02	-0.01	0.01	0.00	0.01	-0.01	0.01	0.00	-0.01	0.00	0.01
$R_{mL}$	0.00	-0.02	-0.02	0.01	0.01	0.01	-0.02	0.00	0.00	0.00	0.00	0.00
$f_1$	-0.02	-0.01	-0.01	0.01	0.00	-0.02	-0.01	0.00	-0.01	0.00	-0.01	0.00
$SLA$	-0.01	0.01	0.00	0.02	0.01	0.02	0.00	0.00	0.00	-0.01	0.01	-0.01
$R_{ms}$	-0.04	0.00	0.02	0.01	-0.05	0.00	0.00	-0.02	-0.02	0.00	0.00	0.01
$r_R$	0.01	0.00	-0.01	0.00	0.01	0.00	-0.01	0.00	-0.01	0.00	0.00	0.01
$\rho_R$	-0.01	0.00	0.00	-0.01	0.00	-0.01	-0.01	0.00	0.01	0.00	0.00	0.00
$S_0$	-0.19	0.02	0.02	0.02	-0.07	0.00	0.01	-0.02	-0.03	0.04	0.00	-0.09
$f_2$	-0.09	0.01	0.02	-0.01	0.00	-0.02	0.00	0.00	-0.01	0.00	0.00	0.00
$k$	-0.06	0.02	0.01	-0.02	0.00	0.00	0.00	0.01	-0.01	-0.02	-0.01	0.01
$SW_{\max}$	-0.02	-0.01	-0.02	-0.01	0.01	-0.03	-0.01	0.02	0.02	-0.03	0.01	-0.02
$\gamma_X$	0.04	0.00	0.02	0.00	-0.23	-0.01	0.01	0.01	0.01	0.00	0.01	0.00
$R_0$		-0.02	-0.01	0.00	0.02	0.01	0.01	0.01	0.02	-0.01	0.02	-0.01
$\alpha$	0.00		0.01	0.00	0.00	-0.01	0.00	0.00	-0.01	-0.01	-0.01	0.00
$\eta$	0.01	0.09		-0.01	-0.01	0.00	0.00	-0.01	-0.02	0.02	0.00	0.01
$S_L$	0.71	0.97	0.21		0.01	0.00	-0.01	0.00	0.00	0.00	0.00	0.00
$\rho$	0.00	0.65	0.01	0.01		0.00	0.00	0.00	0.01	0.00	0.01	0.00
$S_R$	0.23	0.05	0.37	0.93	0.78		-0.01	-0.01	0.00	0.00	0.00	0.00
$m$	0.26	0.43	0.54	0.28	0.82	0.03		0.00	-0.01	0.01	-0.01	-0.01
$\lambda_s$	0.02	0.66	0.26	0.59	0.64	0.01	0.62		0.00	0.00	-0.01	0.01
$H_{\max}$	0.00	0.01	0.00	0.92	0.08	0.79	0.07	0.66		0.01	-0.01	0.00
$\eta_B$	0.02	0.14	0.00	0.71	0.95	0.73	0.35	0.97	0.01		-0.01	-0.01
$\Phi_H$	0.00	0.26	0.50	0.70	0.13	0.98	0.22	0.22	0.17	0.01		-0.01
$\lambda_h$	0.16	0.54	0.13	0.72	0.66	0.83	0.25	0.11	0.56	0.01	0.13	
$C_{g_w}$	0.01	0.01	0.21	0.82	0.02	0.24	0.05	0.83	0.02	0.92	0.19	0.50
$C_{g_R}$	0.85	0.49	0.44	0.02	0.57	0.19	0.20	0.49	0.43	0.17	0.36	0.85
$C_{g_L}$	0.10	0.90	0.45	0.48	0.01	0.06	0.51	0.69	0.40	0.47	0.76	0.08
$\delta_R$	0.29	0.57	0.61	0.25	0.61	0.71	0.07	0.58	0.00	0.21	0.12	0.89
$\delta_L$	0.25	0.51	0.46	0.62	0.93	0.91	0.57	0.21	0.04	0.91	0.83	0.22
$\gamma_C$	0.86	0.66	0.65	0.62	0.81	0.76	0.82	0.23	0.28	0.89	0.15	0.01
$PAR_{\max}$	0.00	0.02	0.07	0.00	0.03	0.00	0.01	0.14	0.22	0.17	0.00	0.01

**Table 3.2 continued:**

$\theta$	$C_{g_w}$	$C_{g_R}$	$C_{g_L}$	$\delta_R$	$\delta_L$	$\gamma_c$	$PAR_{max}$
$\epsilon$	0.01	0.00	0.00	-0.01	0.00	0.00	-0.63
$R_{d0}$	0.00	0.01	0.01	0.00	0.01	-0.01	-0.01
$R_{mR}$	-0.01	0.01	0.00	0.00	0.01	0.00	0.11
$R_{mL}$	0.00	-0.01	0.00	0.01	0.01	-0.01	0.14
$f_1$	0.01	0.00	0.00	0.01	0.00	-0.01	0.12
$SLA$	0.00	0.00	0.00	0.00	0.00	0.00	-0.06
$R_{ms}$	0.01	0.00	0.00	0.00	0.00	-0.01	0.01
$r_R$	0.00	-0.01	0.00	0.00	0.00	0.00	0.03
$\rho_R$	0.00	0.01	0.00	0.00	0.01	0.01	0.03
$S_o$	-0.02	-0.01	0.00	-0.01	0.00	-0.02	0.06
$f_z$	0.00	0.00	0.01	0.00	0.01	-0.01	-0.01
$k$	-0.01	0.00	0.01	0.01	-0.01	0.01	-0.04
$SW_{max}$	0.01	0.00	0.00	0.00	-0.02	0.01	-0.06
$\gamma_x$	0.01	0.00	-0.01	0.00	0.00	-0.02	-0.05
$R_0$	0.01	0.00	0.01	0.01	0.01	0.00	-0.10
$\alpha$	0.01	0.00	0.00	0.00	0.00	0.00	0.01
$\eta$	-0.01	0.00	0.00	0.00	0.00	0.00	0.01
$S_L$	0.00	0.01	0.00	0.01	0.00	0.00	0.03
$\rho$	0.01	0.00	0.01	0.00	0.00	0.00	0.01
$S_R$	0.01	0.01	-0.01	0.00	0.00	0.00	0.02
$m$	-0.01	0.01	0.00	-0.01	0.00	0.00	0.01
$\lambda_s$	0.00	0.00	0.00	0.00	-0.01	-0.01	0.01
$H_{max}$	-0.01	0.00	0.00	-0.02	-0.01	0.01	0.01
$\eta_B$	0.00	0.01	0.00	0.01	0.00	0.00	-0.01
$\phi_H$	0.01	-0.01	0.00	0.01	0.00	0.01	0.02
$\lambda_h$	0.00	0.00	0.01	0.00	-0.01	0.01	0.01
$C_{g_w}$		0.01	0.00	0.00	0.00	0.01	-0.01
$C_{g_R}$	0.27		-0.01	-0.02	0.01	-0.01	-0.01
$C_{g_L}$	0.83	0.32		0.00	0.00	0.00	0.00
$\delta_R$	0.37	0.00	0.84		0.00	-0.01	0.01
$\delta_L$	0.98	0.24	0.83	0.62		0.00	0.01
$\gamma_c$	0.21	0.34	0.98	0.14	0.54		0.01
$PAR_{max}$	0.17	0.08	0.72	0.12	0.32	0.22	

**Table 3.3:** The mean number of draws from the priors required to obtain a parameter vector,  $\theta$ , that resulted in realistic tree growth under each light level depicted by the  $PAR_{max}$  values (mean and standard deviation [SD] based on  $n = 10$  simulations). For example, when  $PAR_{max} = 206 \text{ MJ m}^{-2} \text{ yr}^{-1}$ , over 43,000 random draws from the priors are generally required to find a single set of parameter values that lead to predicted  $r$ ,  $H$ ,  $\Delta r$ , and  $\Delta H$  associated with a probability greater than 0 given the FIA histogram (*Hist*).

Mean # draws	SD	$PAR_{max}$
43235.9	38392.1	206
13806.3	10946.8	259
21053.3	24366.2	326
14530.5	9413.5	411
7041.2	4834.6	517
7004.3	7448.3	651
13958.7	7711.6	820
29815.2	31777.0	1032
26828.7	16398.4	1300
45324.5	37804.6	1636
52352.8	56124.9	2060

**Table 3.4:** Main effects included in the multiple-regression models identified by a stepwise regression routine that only considered main effects. Each column represents a model (i.e., columns are associated with the trait that was treated as the dependent variable), and each row represents a potential covariate in the model. When appropriate, +/- in a cell indicates the direction of the regression coefficient for a given variable; gray shaded cells denote statistically significant effects ( $p < 0.05$ , most  $p \ll 0.05$ ). White boxes indicate a variable was not included in the model.

	$\varepsilon$	$R_{mR}$	$f_1$	$R_{mL}$	$R_{40}$	$\gamma_X$	$R_0$	$R_{mS}$	$S_0$	SLA	$SW_{max}$	$f_2$	$r_R$	$\rho_R$	$\rho$	$k$	$S_L$	$\eta$	$\alpha$	$\lambda_H$	$H_{max}$	SR	$\eta_B$	$\lambda_S$	$m$	$\phi_H$	$\delta_R$	$\gamma_C$	CgL	CgR	CgW	$\delta_L$
$\varepsilon$	+	+	+	-	-	-	+	+	-	-	+	+	+	+	+	-	+	+	+	+	+	+	-	+	+	+						
$R_{mR}$	+	-	-	+	+	+		+	+	-	-	-	-	-	-	-	+	+	+	+	+	-	-	-	-	-						
$f_1$	+	-	-	+	+	+		+	+	-	-	-	-	-	-	-	+	+	+	+	+	-	-	-	-	-						
$R_{mL}$	+	-	-	+	+	+		+	+	-	-	-	-	-	-	-	+	+	+	+	+	-	-	-	-	-						
$R_{40}$	-	+	+	+	-	+	+	+	+	+	+	+	+	+	+	-	+	+	+	+	+	+	+	+	+	+						
$\gamma_X$	-	+	+	+	-	+	+	+	+	-	+	+	+	+	+	-	+	+	+	+	+	+	+	+	+	+						
$R_0$	-	+	+	+	+	-	+	+	+	-	+	+	+	+	+	-	+	+	+	+	+	+	+	+	+	+						
$R_{mS}$	+			+	+	+	-	+	+	-	+	+	+	+	+	+	+	+	+	+	+	+	+	+	+	+						
$S_0$	+		+	+	+	+	-	-	+	+	+	+	+	+	+	+	+	+	+	+	+	+	+	+	+	+						
SLA	-	+	+	+	-	-	-	+	+	+	+	+	+	+	+	+	+	+	+	+	+	+	+	+	+	+						
$SW_{max}$	-	+	+	+	+	+	-	+	+	+	+	+	+	+	+	+	+	+	+	+	+	+	+	+	+	+						
$f_2$	+	-	-	+	+	+	-	+	+	+	+	+	+	+	+	+	+	+	+	+	+	+	+	+	+	+						
$r_R$	+	-	-	+	+	+	-	+	+	+	+	+	+	+	+	+	+	+	+	+	+	+	+	+	+	+						
$\rho_R$	+	-	-	+	+	+	-	+	+	+	+	+	+	+	+	+	+	+	+	+	+	+	+	+	+	+						
$\rho$	+	-	-	+	+	+	-	+	+	+	+	+	+	+	+	+	+	+	+	+	+	+	+	+	+	+						
$k$	-	+	+	+	-	-	+	+	+	-	+	+	+	+	+	+	+	+	+	+	+	+	+	+	+	+						
$S_L$	+	-	-	+	+	+	-	+	+	+	+	+	+	+	+	+	+	+	+	+	+	+	+	+	+	+						
$\eta$	+	-	-	+	+	+	-	+	+	+	+	+	+	+	+	+	+	+	+	+	+	+	+	+	+	+						
$\alpha$	+	-	-	+	+	+	-	+	+	+	+	+	+	+	+	+	+	+	+	+	+	+	+	+	+	+						
$\lambda_H$	+			+	+	+	-	+	+	+	+	+	+	+	+	+	+	+	+	+	+	+	+	+	+	+						
$H_{max}$	+	-	-	+	+	+	-	+	+	+	+	+	+	+	+	+	+	+	+	+	+	+	+	+	+	+						
SR	+	-	-	+	+	+	-	+	+	+	+	+	+	+	+	+	+	+	+	+	+	+	+	+	+	+						
$\eta_B$	-							+	+	+	+	+	+	+	+	+	+	+	+	+	+	+	+	+	+	+						
$\lambda_S$	+	-	-	+	+	+	-	+	+	+	+	+	+	+	+	+	+	+	+	+	+	+	+	+	+	+						
$m$	+	-	-	+	+	+	-	+	+	+	+	+	+	+	+	+	+	+	+	+	+	+	+	+	+	+						
$\phi_H$	+	-	-	+	+	+	-	+	+	+	+	+	+	+	+	+	+	+	+	+	+	+	+	+	+	+						
$\delta_R$																																
$\gamma_C$																																
CgL	+																															
CgR																																
CgW																																
$\delta_L$																																
PAR <sub>max</sub>	-	+	+	+	-	-	-	+	+	-		+	+	+	+	-	+	+	+	+	+	+	+	+	+	+	+	+	+	+	+	+

**Table 3.5:** Summary of effects included in multiple-regression models found with a stepwise regression routine including main effects and all two-way interactions. Each column represents a model (i.e., columns are associated with the trait that is treated as the dependent variable), and each row represents a potential covariate in the model. When appropriate, +/- in a cell indicates the direction of the main effect for a given variable. The number under each diagonal line in a cell represents the number of interaction terms that the corresponding covariate trait was included in; if left blank, then it only occurred as a main effect. Gray shaded cells denote statistically significant main effects ( $p < 0.05$ , most  $p \ll 0.05$ ); all interaction effects were statistically significant, all but 3 main effects were statistically significant, and the three non-significant main effects were included in at least one significant interaction within the corresponding model.

	$\varepsilon$	$R_{mR}$	$R_{40}$	$f_1$	$R_{mL}$	$\gamma_X$	$R_{mS}$	$S_0$	$R_0$	SLA	$r_R$	$p_R$	$SW_{max}$	$f_2$	$k$	$p$	$\alpha$	$S_L$	$\eta$	$S_R$	$\lambda_H$	$H_{max}$	$\eta_B$	$\lambda_S$	$\delta_R$	$\phi_H$	$\gamma_C$	CgL	CgR	CgW	$\delta_L$	m			
$\varepsilon$																																			
$R_{mR}$																																			
$R_{40}$																																			
$f_1$																																			
$R_{mL}$																																			
$\gamma_X$																																			
$R_{mS}$																																			
$S_0$																																			
$R_0$																																			
SLA																																			
$r_R$																																			
$p_R$																																			
$SW_{max}$																																			
$f_2$																																			
$k$																																			
$p$																																			
$\alpha$																																			
$S_L$																																			
$\eta$																																			
$S_R$																																			
$\lambda_H$																																			
$H_{max}$																																			
$\eta_B$																																			
$\lambda_S$																																			
$\delta_R$																																			
$\phi_H$																																			
$\gamma_C$																																			
CgL																																			
CgR																																			
CgW																																			
$\delta_L$																																			
m																																			
PAR <sub>max</sub>																																			

## Figures

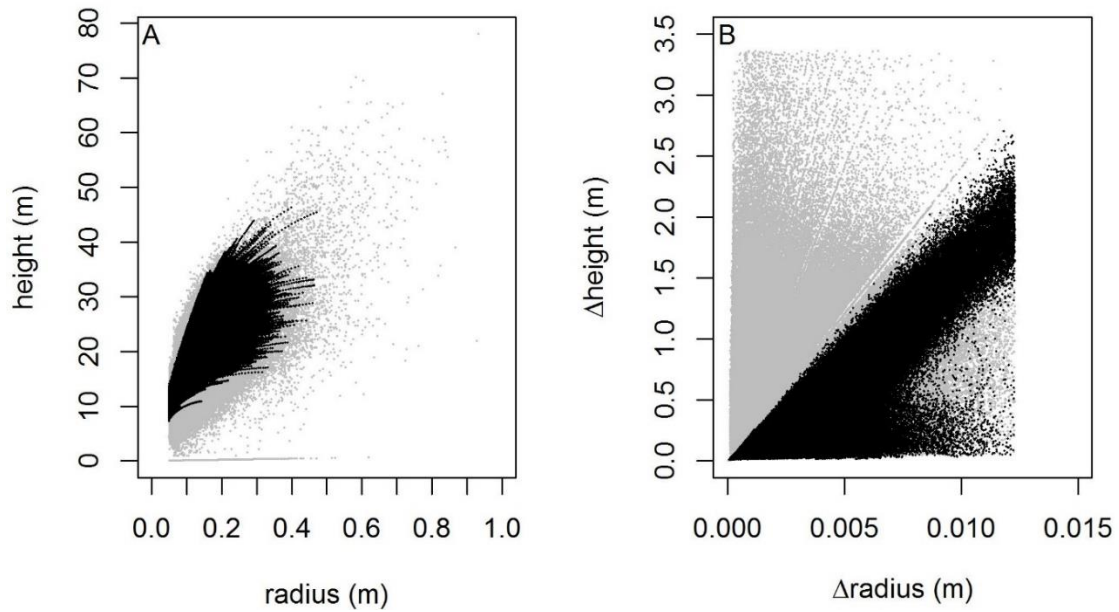


**Figure 3.1:** Panel A: Tree height ( $H$ ) versus trunk radius ( $r$ ) space covered by the ACGCA model output for “realistic tree growth” (black;  $n = 1,650,000$  simulation points) overlaid on top of the FIA data (gray;  $n = 1,270,510$  data points). Panel B: Tree  $\Delta$  height and  $\Delta$  radius from the FIA data (grey), covered by ACGCA (black simulation points).

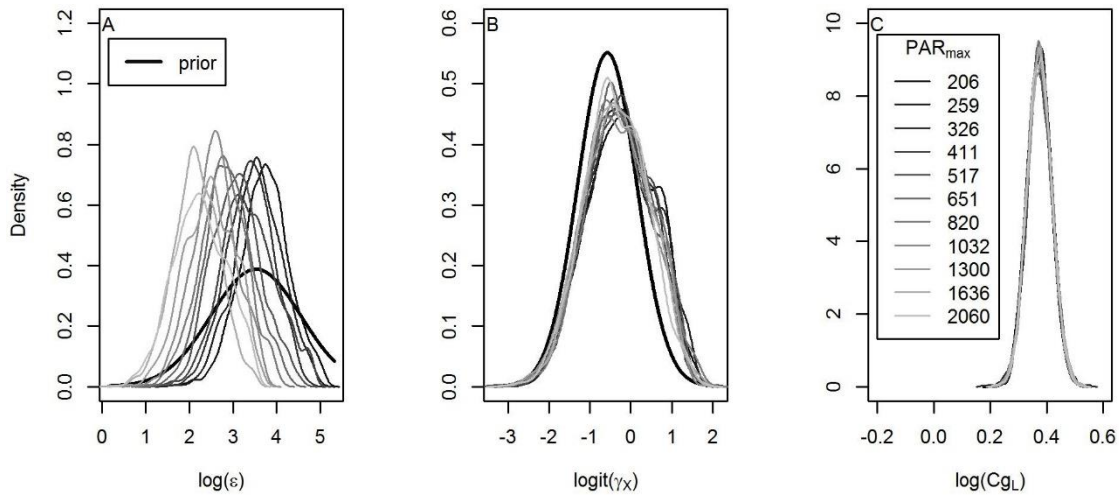


**Figure 3.2:** Marginal posterior probability densities by light level (11 thin lines) for a select set of parameters (traits), overlaid with their prior probability distributions (thick black lines) for transformed values of: **(A)** radiation-use efficiency ( $\epsilon$ , g gluc MJ<sup>-1</sup>), **(B)** proportion of xylem conducting area ( $\gamma_x$ , unitless), and **(C)** construction cost of producing leaves ( $C_{gL}$ , g gluc g dw<sup>-1</sup>). Three main patterns emerged across the 32 traits: **(A)** shows the only case of notable differentiation of the posterior by light level, and it also illustrates differences between the prior and posteriors;  $S_o$  was the only other parameter (trait) where the posterior visually differed from the prior; **(B)** shows that the posterior distributions obtained under the 11 light levels were nearly identical, and the prior and posteriors were only slightly differentiated, but effectively very similar; and, **(C)** shows one of ~18 traits described by a high degree of overlap between the prior and posterior distributions.

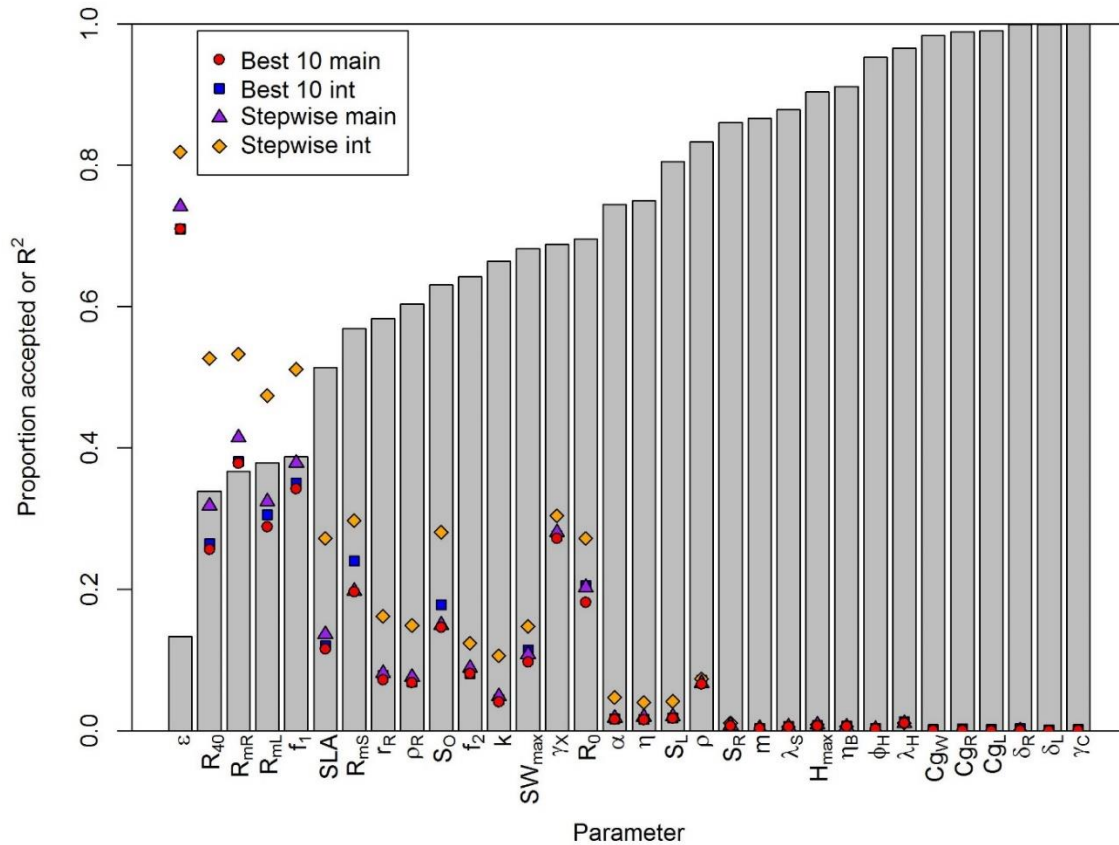


**Figure 3.3:** The proportion of values accepted after randomizing the order each parameter with respect to MH iteration number (gray bars) overlaid with the  $R^2$  values associated with four different multiple regression procedures (points) that treated each parameter as the dependent variable. The  $R^2$  values are shown for: best subsets regressions with a maximum of 10 effects main effects only (circle) or with 10 main effects and/or two-way interactions (square); or for stepwise regressions with main effects only (triangle) or main effects and two-way interactions (diamond). In general,  $R^2$  values increased as the proportion accepted increased. In some cases (for parameters such as  $R_{40}$ ,  $R_{mR}$ ,  $R_{mL}$ ,  $f_1$ ,  $SLA$ , and  $S_O$ ), it is clear from the stepwise regressions that including interactions drastically improved model fit. However, there were often many more variables in these models (for  $SLA$ , 23 terms in the main effects-only model versus 116 in the model with main effects and interactions). See Table 3.1 for definitions of the parameters.

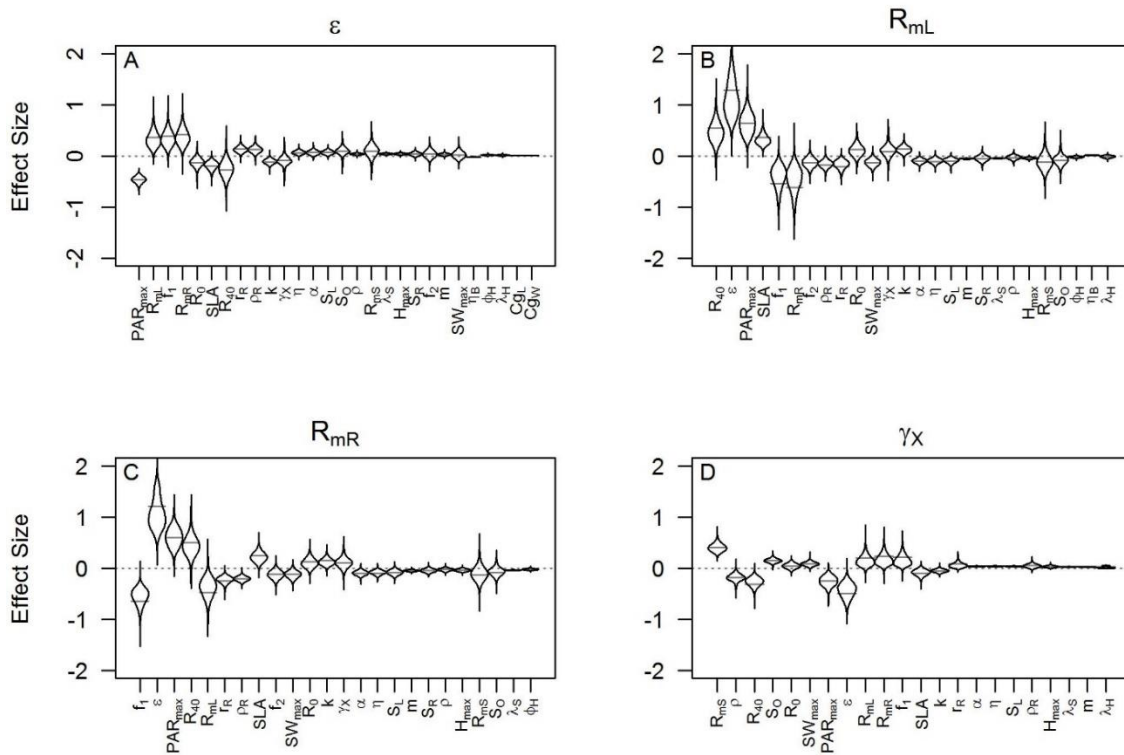


**Figure 3.4:** Main effects of variables (traits) included in the stepwise multiple regressions that treated the following four traits as dependent variables: **(A)** radiation-use efficiency ( $\epsilon$ ), **(B)** leaf maintenance respiration ( $R_{mL}$ ), **(C)** fine root maintenance respiration ( $R_{mR}$ ), and **(D)** proportion xylem conducting area ( $\gamma_X$ ). In these regressions, the dependent trait and the independent traits (x axes) were normalized such that the normalized variable are unitless. The violin plots show the overall main effect of each variable (on x-axes) when taking into account interactions (e.g., Eqns 18 and 19), which contain the corresponding partial regression coefficient for the actual main effect (light gray horizontal lines). Three primary cases are illustrated: (1) the interactions lead to a variable overall main effect such that the violin plot is comparatively wide, but the direction of the overall effect is consistent with the partial main effect (negative or positive); (2) the overall main effect can shift from negative to positive, or vice versa, given the values of interacting variables (e.g., violin plots to overlap the dashed, horizontal zero line); and (3) the interactions have little influence such that the overall main effect is nearly indistinguishable from the partial main effect (e.g., very narrow violin plots).

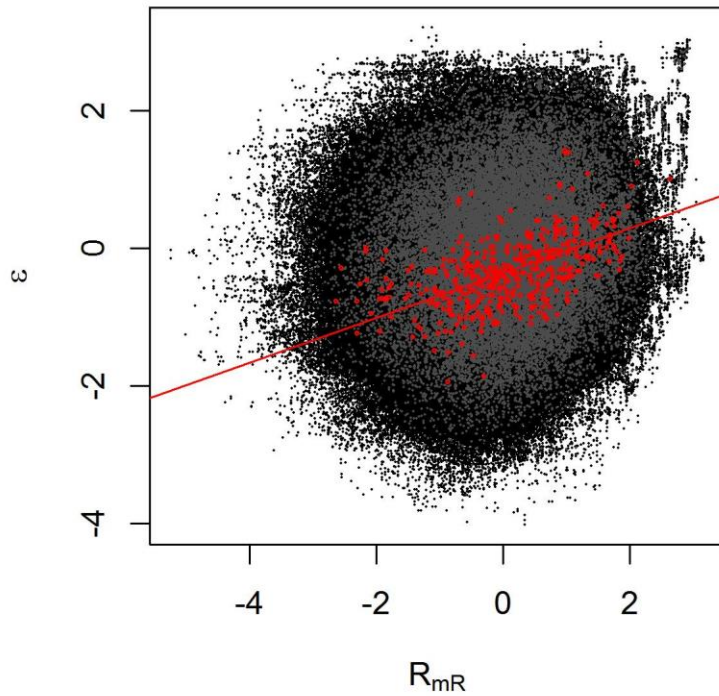


**Figure 3.5:** Bivariate posterior plots for an example parameter (trait) pair (see Table 3.1 for parameter definitions). The black points are the 1.65 million parameter pairs generated by the MH routine before thinning by 50, and the grey points represent the subset of 33,000 points used to calculate posterior statistics. The red points represent a subset of the posterior space obtained by filtering the MH output such that the middle 20% quantile for  $PAR_{max}$ ,  $f_1$ ,  $R_{mL}$ ,  $R_{40}$ , and  $SLA$  were retained (all other samples ignored), resulting in 733 parameter sets out of 1.65 million that met these criteria (red points); this filtering by other traits lead to a significant correlation ( $r = 0.57$ ,  $p < 0.05$ ) between the focal pair of traits ( $\varepsilon$  and  $R_{mR}$ ).

#### 4. REFINEMENT OF A THEORETICAL TRAIT SPACE FOR NORTH AMERICAN TREES VIA ENVIRONMENTAL FILTERING

##### **Abstract**

The theoretical trait space (TTS) for North American trees represents an n-dimensional hypervolume (“hypercube”) characterizing the range of values and covariations among multiple functional traits, in the absence of explicit filtering mechanisms. A 32-dimensional TTS was previously generated by fitting the Allometrically Constrained Growth and Carbon Allocation (ACGCA) model to USFS Forest Inventory and Analysis (FIA) data. We sampled traits from this TTS, representing different individual “trees,” and subjected these trees to a series of gap dynamics simulations resulting in different annual light (photosynthetically active radiation) levels. Variation in light limitation led to non-random mortality and a refinement of the TTS. A set of six key “mortality” traits and six traits related to the leaf and wood economics spectrums (LES and WES) were used to construct hypercubes of the traits represented by both dead and living trees. For trees capable of surviving a given gap scenario, the volume of their refined trait space decreased linearly with increasing stand-level mortality rates (to ~50% mortality). The location of the hypercubes also shifted, as indicated by non-zero distances between the hypercube centroids of surviving trees compared to dead trees and the original TTS. We investigated potential mechanisms underlying such filtering processes by exploring how traits and the environment relate to mortality rates at the tree, phenotype (a specific set of traits representing a tree), and stand (a specific gap scenario) levels. The average light level at the forest floor explained 42% of the stand-level mortality, while phenotype- and tree-level mortality were best explained by functional traits, especially radiation use efficiency, maximum tree height,

and xylem conducting area to sapwood area ratio. Overall, the patterns were consistent with empirical studies of functional traits, in terms of which traits predict mortality and the direction of the relationships. This work also identified potentially important functional traits that are not commonly measured in empirical studies. For example, the ratio of xylem conducting area to sapwood area and senescence rates of relatively long-lived tissues were both found to be important predictors of tree- and phenotype-level mortality..

**Keywords:** environmental filtering, functional traits, gap dynamics, hypercube, hypervolume, IBM, North American trees, simulation experiment, trait space, trait spectra

## Introduction

Quantifying how plant functional traits can determine individual success, and how traits interact with the environment to affect individual performance is a challenging problem. Longstanding and recent interest in functional traits encompasses many research areas, including plant competition, community assembly, species coexistence, demographics (Weiher et al. 1999, McGill et al. 2006, Westoby and Wright 2006, Clark et al. 2010, McMahon et al. 2011), biogeography (Violle et al. 2014), global vegetation models (Scheiter et al. 2013, Fyllas et al. 2014, Van Bodegom et al. 2014), and conservation (Devictor et al. 2010). An exciting aspect of functional traits research has been the discovery of correlations among traits representing tradeoffs at the global scale. Examples of these include the leaf, wood, and fast-slow economics spectra (Wright et al. 2004, Chave et al. 2009, Reich 2014), and more recently, a global spectrum of plant form and function (Diaz et al. 2016). These spectra are based on correlations found through statistical curve fitting (e.g., regression), dimension reduction methods (e.g., PCA), or other multivariate approaches such as the estimation of convex hulls combined with PCA (Diaz et al. 2016). These approaches have advanced our understanding of the interrelatedness of functional traits, but because they use empirical or statistical models, it is challenging to extend the observed patterns to novel conditions (Pearl and Reed 1920, Webb et al. 2010, Evans et al. 2011).

More robust predictions of plant performance (e.g., growth, survival) in novel environments may be gained by linking novel trait data to mechanisms (Savage et al. 2007, Webb et al. 2010, Evans et al. 2011, Scheiter et al. 2013). Functional trait distributions are influenced by both environmental and biotic filters that lead to non-

random mortality, selecting only individuals that can survive in a given environment (Van der Valk 1981, Woodward and Diament 1991, Weiher and Keddy 1999, Webb et al. 2010). The ways in which species respond to these filters are limited by inherent mass balance and engineering constraints (Scheiter et al. 2013). Environmental filters tend to limit the range of trait distributions in a given environment; these filters relate to limiting factors such as resources, temperature, or soil characteristics (Van der Valk 1981, Woodward and Diament 1991, Weiher and Keddy 1999, Webb et al. 2010), and variation in these factors tends to select for plants (trees) that remain above their zero-net-growth isoclines (Tilman 1985). Interspecific competition can limit the similarity of the remaining species traits in a community (Macarthur and Levins 1967, Stubbs and Wilson 2004, Cornwell and Ackerly 2009). Thus, both environmental and biotic filters can lead to non-random mortality. Thus, one way to investigate how filtering influences the trait space is to investigate how traits influence mortality. Another way to assess filtering's influence on the trait space is to determine how filtering affects correlations indicative of tradeoffs. In this case, the range of possible trait relationships/tradeoffs will depend on the dimensionality of the trait space (Clark et al. 2010). Such trait tradeoffs are beginning to be incorporated into predictive models, such as dynamic global vegetation models. By allowing plants in a community to adapt to their environment over the course of the simulation (via fairly simple reproduction and inheritance sub-models), traits possessed by the community changed over time in response to environmental change (Scheiter et al. 2013). Importantly, realistic tradeoffs were found to emerge from this framework without being too computationally intensive for use in larger, more complex models (Scheiter et al. 2013).

The multidimensional nature of the niche (Hutchinson 1957, Clark et al. 2010), and large variation in tree traits, seen in several studies (Wright et al. 2005, Kattge et al. 2011a), suggests that trees possess many ways of responding to a given environment. However, even if there is a great degree of variation within the traits of a species or community, this does not imply that any or all combinations of trait values are possible. The traits expressed by a tree are governed by mass-balance and engineering tradeoffs (Scheiter et al. 2013). Common tradeoffs are seen in groups of related traits in the leaf (Wright et al. 2004), wood (Chave et al. 2009), and “fast-slow” (Reich 2014) economics spectra, as well as the global spectrum of plant form and function (Diaz et al. 2016). These tradeoffs are often based on sample means computed at various levels of organization (e.g., site, species, genus), partly to ameliorate problems due to incomplete data (Reich et al. 1999, Wright et al. 2004, Diaz et al. 2004, Chave et al. 2009, Stahl et al. 2013). However, by focusing analyses on means the variability in the data is not well represented, potentially leading to erroneous results due to the problem of aggregation (Clark et al. 2011). One potential solution to exploring such trait tradeoffs is to use mechanistic models to simulate ecological processes, and subsequently assess the tradeoffs that emerge under varying environmental conditions via simulation experiments.

For many boreal and temperate forests, forest canopy gap dynamics can produce widely varying environmental conditions, potentially acting as an important filtering process leading to non-random mortality and trait tradeoffs (McCarthy 2001). For example, forest gap formation and closure are important in determining community dynamics (Runkle 1985, Runkle and Yetter 1987). Tree success can depend on gap

dynamics, including how often gaps form, how long the gap remains open, and how long it takes for the forest canopy to close (Runkle 1985, Valverde and Silvertown 1997, McCarthy 2001, Ogle and Pacala 2009), due to impacts on light availability, and subsequently carbon uptake.

The Allometrically Constrained Growth and Carbon Allocation (ACGCA) model developed by Ogle and Pacala (2009) predicts tree growth, carbon allocation, and survival status at annual time-steps, given average, annual light levels above the forest canopy. In particular, ACGCA uses known tree allometries along with physiological and morphological traits to control carbon allocation from a transient (fast) pool to structural compartments and a storage (slow) pool within an individual tree, and tree death occurs if the non-structural carbohydrate (slow and fast) pools are depleted (Ogle and Pacala 2009). We integrated the ACGCA model with a simple gap dynamics simulator to investigate if an individual tree, defined by a specific set of functional trait values, is capable of surviving a particular gap dynamics scenario. We imposed a wide range of realistic gap scenarios to create varying levels of environmental stress (Ogle and Pacala 2009), allowing the investigation of the relationship between selective mortality due to environmental filtering (light stress) and tree traits (ACGCA parameters). Through repeated simulation, we used the gap dynamics simulations to explore how the multi-dimensional trait space changes with increasing stress (filtering), and to learn which traits experience the greatest filtering and/or are the best predictors of mortality.

In previous work, we used the ACGCA model to estimate the theoretical trait space (TTS) for North American trees (see Table 1 for a full list of traits). This was done by fitting the ACGCA model to FIA data while restricting parameter values to realistic

ranges through the use of semi-informative priors. The TTS represents the trait space that is consistent with *living* trees in the FIA data. In this study, our objective was to use this framework to assess how this TTS may be refined when applying the ACGCA model to a range of gap dynamics simulations that lead to some level of mortality (i.e., not all simulated trees survive). In doing so, we address the following questions: 1) How well do environmental factors versus functional traits explain tree-level mortality? 2) How do environmental factors, such as time between gaps, relate to stand-level mortality? 3) Which functional traits in the TTS, if any, predict the mortality rate of a given phenotype defined by a specific combination of trait values? 4) Does environmental filtering associated with the gap scenarios lead to a refinement of the trait space relative to the original TTS? That is, does the trait space differ between trees that survived versus those that died, or between surviving and dead trees versus the original TTS? How are such differences (e.g., in terms of centroid distances or volume) affected by the level of environmental (light) stress? 5) In what ways are trait tradeoffs affected by subjecting the TTS to environmental filtering (non-random mortality) via gap dynamics?

## **Methods**

### *Theoretical Trait Space*

The ACGCA model involves 32 parameters (inputs) representing physiological, morphological, and allometric traits (see Table 1 for ACGCA parameter definitions). We used parameter (trait) values representative of the theoretical trait space (TTS) of North American trees (Fell et al. *in review*). Based on previous work to quantify the TTS, 33000 parameter sets were obtained, each set representing a vector of 32 parameters.

These parameter sets were found by fitting the ACGCA model to US Forest Service (<http://www.fia.fs.fed.us/>) Forest Inventory and Analysis (FIA) data, including tree heights, diameters, and their estimated rates of change per year. The model was fit to the FIA data via a simple Bayesian framework that employed a custom Metropolis-Hastings (MH) algorithm to sample from the posterior of the parameters, allowing estimation of parameter spaces for each trait in the ACGCA model. The likelihood of the modeled (ACGCA) outputs—annual heights, diameters, and annual rates of change in each—was evaluated against a four-dimensional histogram representing realistic tree growth based on 1.27 million FIA re-measurements of height, radius, change in height, and change in radius for living, healthy trees (i.e., data for dead trees or trees associated with no growth or negative growth were eliminated). The ACGCA model parameters were further constrained by informative prior distributions based on the TreeTraits literature database (Kattge et al. 2011b, Ogle et al. 2013, 2014), which contains reported values for 27 of the 32 traits (parameters) used in the ACGCA model. In cases where no trait data were available (i.e., for parameters  $\lambda_s$ ,  $\lambda_h$ ,  $f_I$ ,  $\eta_B$ , and  $m$ , see Table 1), semi-informative priors were based on values derived for *Pinus taeda* and *Acer rubrum* in Ogle and Pacala (2009). The final output from this analysis (posterior samples of the traits [or parameters]) can be thought of as representing an unfiltered trait space, or the TTS, that simultaneously agrees with FIA data, the semi-informative priors, and the ACGCA model structure.

### *Gap Dynamics Simulations*

The overarching goal of the gap dynamics simulations was to impose environmental stress on the aforementioned unfiltered trait space (TTS). Though it could

be argued that gap dynamics simulations really impose a biotic stress due to competition for light by surrounding trees, as opposed to a strictly abiotic (i.e., environmental) stress (Kraft et al. 2015), the sole effect of the gap formation and closure process in our simulations is to reduce light availability, an important abiotic factor determining carbon uptake. Regardless of which perspective is employed (abiotic versus biotic stress), the gap dynamics scenarios are constructed to explore how varying stress conditions may refine the TTS by potentially eliminating sub-regions of the trait space, associated with trees (or sets of trait values) that die during the simulation. Our gap scenarios are based on those described in Ogle and Pacala (2009); only details relevant to our objectives and questions are provided here.

Gap simulations were conducted with three repeated phases: open gap, gap closure, and closed canopy. Following Ogle and Pacala (2009), three levels were used for the open gap phase ( $gt = 4, 6, \text{ and } 8$  years), five for the closure phase ( $ct = 5, 10, 15, 25, \text{ and } 45$  years), and five for the time between gaps ( $tbg = 20, 35, 50, 100, \text{ and } 200$  years). Some combinations were removed due to inconsistencies (e.g., a time between gaps of 20 years and a closure phase of 45 years are inconsistent), resulting in 62 unique simulation scenarios. Each scenario was run for a 200 year period, and the average light at the forest floor was calculated for the 200 year period based on supplemental material in Ogle and Pacala (2009), using a standard Beer-Lambert light-extinction model, combined with modeled variation in forest canopy leaf area index ( $LAI_F$ ) as gaps form and close. Average light level at the forest floor ( $PAR_{avg}$ ) was found to be closely related to  $tbg$  and stand/scenario-level mortality (see results), and thus was used as a continuous variable

representative of the level of environmental stress in a subset of regression analyses described below.

The gap scenario simulations were kept simple by employing an empirical model that described the  $LAI_F$  of the surrounding forest canopy, rather than modeling individual trees in the surrounding forest. The ACGCA model, however, was used to model growth and survival of the target tree defined by a particular set of parameters (traits), under each gap scenario. The forest was prescribed a canopy height ( $H_F$ ) and  $LAI_F$ , both of which were zero during the gap phase and both increase linearly during the closure phase, until reaching their maximum values ( $H_{F,max}$  and  $LAI_{F,max}$ ) during the closed phase (Ogle and Pacala 2009). The forest canopy affects the modeled (target) tree through its effect on annual photosynthetically active radiation (APAR) according to the Beer-Lambert equation (Ogle and Pacala 2009). The light environment experienced by the target tree is determined by its crown height ( $H$ ) relative to  $H_F$ , yielding three scenarios: (1) the tree is not limited by light ( $H > H_F$ ), (2) its crown is partially exposed to full sunlight ( $H\eta < H_F < H$ , where  $H\eta$  is the height to the base of the target tree's crown), or (3) the tree can be completely overtopped by the surrounding forest ( $H_F > H$ ) (Ogle and Pacala 2009).

Output from the gap dynamics simulations was used to determine if a given parameter set led to a target tree that survived or died over the 200 year period, for each of the 62 gap scenarios. This yielded 2,046,000 (33,000 parameter sets  $\times$  62 gap scenarios) binary values, where 0 indicated a tree that survived the 200 year simulation, and 1 indicated death during the simulation. These binary outputs were summarized to quantify three types of mortality (Table 2). For the first type of mortality, the individual binary values are representative of tree-level mortality ( $m_{g,p}$ ) for gap scenario  $g$  ( $g = 1, 2,$

..., 62) and parameter (trait) set  $p$  ( $p = 1, 2, \dots, 33000$ ), which were used in addressing how environmental factors versus functional traits explain  $m_{g,p}$  (Q1). Two additional indices of mortality—stand-level (denoted by  $m_g^S$ ) and phenotype-level (denoted by  $m_p^\theta$ )—summarize mortality rates for each gap scenario ( $m_g^S$ , for  $g = 1, 2, \dots, 62$ ) or for an individual set of parameters ( $m_p^\theta$ , for  $p = 1, 2, \dots, 33,000$ ), respectively. (Table 2).

Mortality associated with each gap scenario ( $m_g^S$ ) can be thought of as similar to stand-level mortality since each set of traits was subjected to a fixed environment. In particular, for each gap scenario:

$$m_g^S = \frac{\sum_{p=1}^{33,000} m_{g,p}}{33,000} \quad (30)$$

Thus, there are 62  $m_g^S$  values of stand-level mortality, one for each gap scenario; these mortality values were analyzed to evaluate how environmental factors (e.g., time between gaps,  $PAR_{avg}$ ) relate to stand-level mortality (Q2).

Phenotype-level mortality ( $m_p^\theta$ ) was calculated for each parameter set drawn from the original (unfiltered) TTS (Fell et al. *in review*). Each parameter set can be thought of as a phenotype since it represents a specific combination of functional traits within the TTS. Phenotype-level mortality was calculated as:

$$m_p^\theta = \frac{\sum_{g=1}^{62} m_{g,p}}{62} \quad (31)$$

These mortality values were analyzed to evaluate if, and which, functional traits can explain  $m_p^\theta$  (Q3). Both  $m^S$  and  $m^\theta$  describe the proportion of trees that died for each gap scenario and phenotype (parameter set), respectively.

### *Statistical Analyses*

*Mortality regressions*—We conducted stepwise regression analyses to evaluate the factors underlying tree-, stand-, and phenotype-level mortality. In all cases, the Bayesian Information Criterion (BIC) was used for the model selection criterion because it has a greater penalty term for each added variable and it tends to select more parsimonious models (Gelman et al. 2014). All stepwise regressions used forward and backward selection.

We evaluated how well the environment and functional traits explain tree-level mortality (Q1),  $m_{g,p}$  (given by 0 [survived] or 1 [died]), by conducting three logistic, stepwise regression analyses: (1) light + trait model, (2) trait only model, and (3) light only model. Each of these models was fit to half of the  $m_{g,p}$  values ( $n = 1,023,000$ ), chosen randomly from the full dataset. The remaining 50% of the  $m_{g,p}$  values were used as a test dataset to assess the extent to which  $m_{g,p}$  could be correctly predicted by each model. The light + trait model included each of the 32 TTS functional traits associated with each  $p$  and the average light for each gap scenario  $g$  as potential predictors of  $m_{g,p}$ . Interactions between  $PAR_{avg}$  and each of the 32 traits were included in the full model to account for differing effects of the traits depending on light level. The trait only model included only the functional trait values associated with each  $p$ , and the light only model included  $PAR_{avg}$  associated with each  $g$  as the sole explanatory variable.

The relationship of stand-level mortality ( $m_g^S$ ) to environmental factors (Q2) was addressed by regressing the 62  $m_g^S$  values on each of the gap dynamics variables ( $gt$ ,  $ct$ , and  $tbg$ ) associated with each scenario  $g$ . We treated  $gt$ ,  $ct$ , and  $tbg$  as categorical factors in the regressions. Another simple linear regression was carried out by regressing  $m_g^S$  on

the  $PAR_{avg}$  of each scenario. These regression models allowed an assessment which aspect of the gap dynamics process (environment) best explained mortality at the stand level. We were also able to confirm that  $PAR_{avg}$  was an effective composite variable representing the environment in each simulation.

To evaluate the factors affecting phenotype-level mortality ( $m_p^\theta$ ; Q3), we conducted a stepwise regression where each of the 33,000  $m_p^\theta$  values were regressed on the 32 trait values associated with parameter set  $p$ . Two regressions were conducted; one with only main effects (main effects only model) and another including main effects and all two-way interactions among each of the 32 traits (interaction model). The relative importance of each parameter in the main effects only model was determined using the “relaimpo” package in R (Grömping 2006), which computes the proportion of variation explained by each trait (independent variable) relative to the total variation explained ( $R^2$ ) by the model. This was only done for the main effects only model; the complexity of the interaction model and the sample size used led to computational challenges when trying to calculate the relative importance (the computer’s memory was exceeded).

*Hypercube trait space analysis* —We evaluated how the trait space changed with the filtering introduced by the gap scenarios (Q4). As a simple qualitative analysis, plots of kernel density estimates for each trait were constructed for each gap scenario, for surviving and dead trees (32 traits  $\times$  62 scenarios  $\times$  2 types [dead or living]), to visualize the separation in trait space between surviving and dead trees. A more rigorous evaluation of the emergent trait spaces was achieved by using the “hypercube” package in R (Blonder et al. 2014), which allowed us to quantitatively assess how the multi-dimensional trait space (i.e., hypervolume) shifts as a result of environmental stress. The

hypercube package characterizes high-dimensional spaces, and was used to estimate hypercube volumes and centroid distances between two hypercubes. We constructed hypercubes for the trees that survived and for those that died during each of the 62 gap scenarios. The number of parameter sets (trees) differed among the surviving and dead groups due to differing mortality rates in each gap scenario. For instance, while 33,000 trees were simulated in each scenario, half the trees may have died in one scenario, while only a little over 3000 died in another, leading to different sample sizes for surviving and dead trees. Thus, to construct hypercubes for each stand (gap scenario) and each group of trees, 3000 parameter sets were randomly sampled from each group, without replacement, to avoid potential problems due to differences in sample sizes.

To ensure that the above subsampling did not bias our results, the analysis was repeated 100 times to assess the effect of subsampling. Furthermore, we also randomly sampled from the TTS to construct a data structure similar to each gap scenario; for example, if  $N_g^D$  trees died and  $N_g^S$  trees survived gap scenario  $g$ , we randomly drew two groups of parameters sets from the TTS of size  $N_g^D$  and  $N_g^S$ . These samples were then further subsampled by randomly selecting 3000 parameter sets, which were subsequently used to construct hypercubes representative of the TTS, and to evaluate the potential effect of differential sample size on the hypercube results.

One limitation of the hypercube method is that the number of dimensions cannot exceed the natural log of the sample size (Blonder et al. 2014). In the case of our model output, this allowed a maximum of 8 dimensions (i.e.,  $\log_e(3000) = 8.01$ ), though we only used six. For these analyses, a bandwidth of 0.4 (the lowest value that did not cause errors) and a quantile of 0.05 (95% included) were used. With this in mind, the six traits

with the greatest relative importance (accounting for over 90% of the  $R^2$ ) in explaining  $m_p^\theta$  were included (i.e.,  $H_{max}$ ,  $\varepsilon$ ,  $\gamma_X$ ,  $S_O$ ,  $R_{mL}$ , and  $R_O$ ; see Figure 3 and Table 1 for a description of the traits; hereafter referred to as the “mortality traits”). We also constructed hypercubes based on six traits that are related to the LES and WES (i.e.,  $SLA$ ,  $\varepsilon$ ,  $R_{mL}$ ,  $S_L$ ,  $\gamma_X$ , and  $\rho$ ; hereafter referred to as the “leaf/wood traits”). For each group of traits (mortality traits and leaf/wood traits), we used the aforementioned subsampling procedure to construct hypercubes for the surviving and dead trees for each gap scenario, as well as for the TTS, which is independent of gap scenario. Using the three constructed hypercubes, the traits of surviving and dead trees were compared to each other as well as to the TTS, allowing us to assess if stress results in a refinement of the trait space.

Comparisons of the trait spaces represented by the hypercubes were made by calculating the difference in volumes between two hypercubes and the centroid distances. Centroid distances and volume differences were found between the TTS hypercube and the surviving and dead hypercubes (TS = TTS vs. surviving hypercube, TD = TTS vs. dead hypercube), and between the surviving and dead hypercubes (SD = surviving vs. dead hypercube) for each of the 62 gap dynamics scenarios. When calculating volume differences, surviving and dead hypercubes were subtracted from the TTS hypercubes (TTS served as the reference). When comparing the surviving and dead hypercubes, the dead hypercubes were subtracted from the surviving hypercubes (surviving served as the reference). Linear regressions were used to determine the relationship between centroid distances and volume differences, and how these relate to stand-level mortality ( $m_g^S$ ), for hypercubes representing both mortality traits and leaf/wood traits. This resulted in 12

regressions ( $3 \times 2 \times 2$ ); three (TS, TD, SD) for centroid differences, three (TS, TD, SD) for volume differences, with each repeated for the two set of traits (mortality and leaf/wood).

*Tradeoffs analysis*—Finally, we investigated how trait tradeoffs are affected by environmental filtering (Q5). This was accomplished by conducting a sequence of stepwise regressions that treated each of the functional traits (1 of the 32 traits) as the dependent variable, and regressed the dependent trait on all the other (31 traits) traits and stand-level mortality ( $m_g^S$ ). These regressions included both main effects of the other traits and mortality, and all two-way interactions. The regressions were conducted separately for trees that died and for trees that survived a particular gap scenario, with 3000 randomly selected parameter sets representative of each population of trees (dead, surviving). The aforementioned hypercube analyses led us to focus our regression analysis on the gap dynamics scenario with the lowest mortality ( $gt=8$  years,  $ct=25$  year,  $tbg=35$  years) since low mortality was associated with the greatest shift in the parameter or trait space (see results below). Thus, 64 ( $32 \text{ traits} \times 2 \text{ types [dead or surviving]}$ ) stepwise regressions were completed. Significant effects of one trait on another suggest potential tradeoffs, and these effects were evaluated for both surviving and dead trees.

## **Results**

### *Mortality Regressions*

*Tree-level mortality*—The logistic regressions for tree-level mortality ( $m_{g,p}$ ) show that the light + trait model was the best at correctly predicting a tree's live/dead status, such that it correctly predicted 82% of the validation cases. The trait only model

was comparable (80% correct), but the light only model was notably inferior (42% correct) (Figure 1). The light only model performed poorly because it tended to predict that nearly all trees died such that it correctly classified 95% of the dead trees, but misclassified 90% of the surviving trees (Figure 1). By comparison, the traits only and traits + light models predicted dead trees correctly in 67% and 72% of the test sample, respectively, and classified surviving trees correctly in 87% and 88% of the test sample, respectively.

Based on the stepwise regression models involving traits, the specific traits from the TTS that had the greatest effect sizes (all significant at  $p < 0.01$ ) on  $m_{g,p}$  were, in order of decreasing importance,  $\varepsilon$  (- effect),  $H_{max}$  (-),  $\gamma_X$  (-),  $S_O$  (+),  $R_{mL}$  (+), and  $R_0$  (-) for the traits only model (see Table S2). For the light + traits model, the traits or predictors with the largest effect sizes were  $\varepsilon$  (-),  $H_{max}$  (-),  $\gamma_X$  (-),  $PAR_{avg}$  (-),  $S_O$  (+), and  $R_{mL}$  (+) (see Table S3); some of these traits overlap with the traits only model, but clearly light level is also an important predictor of tree-level mortality. See Tables S1, S2 and S3 for a more detailed summary of the results (effects) from the three logistic regression models.

*Stand-level mortality*—Of the three gap phase variables, time between gaps ( $tbg$ ) was the best predictor ( $p < 0.05$ ) of stand-level mortality ( $m_g^S$ ), and the model that only included this categorical factor (4 levels) yielded  $R^2 = 0.74$  (Table S4, Figure 2 A). Mortality increased with increasing  $tbg$  in a non-linear fashion such that  $m_g^S$  was less sensitive to  $tbg$  at higher values. The regressions where  $m_g^S$  was modeled as a function of either gap period ( $gt$ ) or gap closure time ( $ct$ ) yielded worse fits ( $R^2 = 0.002$  and  $0.052$ , respectively). Finally, when  $m_g^S$  was regressed on the average light level ( $PAR_{avg}$ ) over

the 200-year simulation,  $PAR_{avg}$  was a significant predictor of  $m_g^S$  ( $p < 0.05$ ,  $R^2=0.85$ , Figure 2 B).

*Phenotype-level mortality*—The step-wise regression for phenotype-level mortality ( $m_p^\theta$ ) that only involved main effects of tree traits converged to a model involving 20 of the original 32 traits ( $R^2 = 0.48$ ; Table S5). The model that included main effects and two-way interactions included 72 effects involving 22 main effects and 50 interaction terms ( $R^2 = 0.62$ ; Table S6). Based on the main effects only model, the six traits with the greatest effect sizes were  $\varepsilon$  (-),  $H_{max}$  (-),  $\gamma_X$  (-),  $S_O$  (-),  $R_{mL}$  (+), and  $R_0$  (-) (Table S5), and these traits accounted for over 93% the overall  $R^2$  for (Figure 3 A). Though the relative importance ( $R^2$  contribution) of each term could not be calculated for the model including interactions, of the main effects, these same six traits emerged among the top nine with the greatest effect sizes, and they maintained the same relationships to mortality (negative or positive) (see Table S6).

### *The Multi-dimensional Trait Space*

A general shift was seen in the kernel density estimates for parameters (traits) with larger effect sizes in the mortality regressions, as seen by a separation between the distributions of traits associated with trees that survived a simulation versus those that died (Figure 3 B-D). Such a separation is not apparent for traits, however, that were non-significant predictors of mortality.

*Centroid differences*—The hypercube analysis for the top six traits ( $\varepsilon$ ,  $H_{max}$ ,  $\gamma_X$ ,  $S_O$ ,  $R_{mL}$ , and  $R_0$ ) identified as the most significant predictors of tree- and phenotype-level mortality clearly indicated shifts in the trait spaces for the surviving and dead trees

associated with the gap dynamics simulations. Centroid differences between surviving trees versus the TTS (TS) had a significant positive relationship with stand-level mortality ( $m_g^S$ ;  $R^2 = 0.96$ ,  $p < 0.01$ ), with distances ranging from 0.18 to 0.65 across the 62 gap scenarios (distances are unitless because trait values were normalized relative to their posterior standard deviations, Figure 4A). This range exceeds the mean and maximum centroid distances of 0.14 and 0.18, respectively, found by randomly sampling the TTS (Figure 4 A). Distances between centroids for trees that died versus the TTS (TD) had a significant negative relationship with  $m_g^S$  ( $R^2 = 0.95$ ,  $p < 0.01$ ), with minimum and maximum distances of 0.54 and 1.02, respectively (Figure 4 B). Finally, distances between centroids for surviving versus dead (SD) trees had a significant negative relationship with  $m_g^S$  ( $R^2 = 0.99$ ,  $p < 0.01$ ), with a range from 0.15 to 0.79 (Figure 4C). That is, as  $m_g^S$  increases, the centroids of the surviving and dead trees converge to similar values (Figure 4C). These results were essentially the same when the analysis was repeated for six leaf/wood traits related to the LES and WES (Figure 5 A-C), with comparable  $R^2$  values of 0.95, 0.94 and 0.99 for TS, TD, and SD, respectively.

*Volume differences*—Differences between hypercube volumes for both groups of traits (mortality and leaf/wood traits) followed the same patterns as the centroid distances, with all models being statistically significant ( $p < 0.01$ ). Volume differences spanned a minimum and maximum of ~0 to 51.06, 24.01 to 98.20, and -14.65 to 81.64 for the TS, TD, and SD comparisons of mortality traits, respectively; these differences demonstrate a restriction (shrinking) of the trait space of both surviving and dead trees as  $m_g^S$  increases. The volume differences between the three hypercubes (TS, TD, and SD) exceeded the null model found by randomly sampling the TTS, which yielded mean and

maximum volume differences of 0.006 and 0.021, respectively. Though the trends in volume differences were in the same direction as those for centroid distances, mortality ( $m_g^S$ ) explained less of the variation in the volume differences;  $R^2 = 0.47, 0.78, \text{ and } 0.84$  for TS, TD, and SD, respectively (Figure 4 D-F). Volume differences between surviving and dead trees are greatest under lower stand-level mortality ( $m_g^S$ ), with dead trees associated with more restricted trait spaces, but these differences disappear as  $m_g^S$  approaches 50% (Figure 4F). These results for the hypercube volumes are essentially the same when repeated for the leaf/wood traits; regressions of the volume differences versus  $m_g^S$  gave  $R^2 = 0.59, 0.82, \text{ and } 0.90$  for TS, TD, and SD, respectively (Figure 5 D-F).

#### *Trait Relationships and Tradeoffs*

Regressions assessing multivariate relationships between each trait in the TTS and the other 31 traits and  $m_p^\theta$  resulted in significant models for each dependent trait. Most main effects and interactions were statistically significant ( $p < 0.05$ , Tables S7 and S8), but  $R^2$  values were generally low. For surviving trees, seven traits resulted in models with adjusted  $R^2 \geq 0.2$  (from highest to lowest  $R^2$ :  $\varepsilon, \gamma_X, S_O, H_{max}, R_{40}, R_{mR}, R_{mS}$ ), with the maximum ( $R^2 = 0.38, 0.35$ ) occurring for  $\varepsilon$  and  $\gamma_X$ , (Table S7). For trees that died, nine traits had  $R^2 \geq 0.2$  (from highest to lowest  $R^2$ :  $\varepsilon, R_{40}, S_O, R_{mL}, R_{mS}, R_{mR}, R_0, f_1, H_{max}$ ), with the maximum ( $R^2 = 0.63$ ) occurring for  $\varepsilon$  (Table S8). For the five “top” traits shared among surviving and dead trees (i.e.,  $\varepsilon, R_{40}, S_O, R_{mS}, H_{max}$ ), their models tended to include many of the same predictor traits (covariates) (e.g., compare Tables S7 and S8). Overall, compared to dead trees, the trait models for surviving trees included less covariates (i.e., fewer trait main effects and/or interactions), generally had lower adjusted  $R^2$  values, and

were less likely to include  $m_p^\theta$  as a main effect (Table S9). There were also some differences between surviving and dead trees models with respect to which predictor trait main effects and interactions were included and the strength of the effect of a predictor trait (Table S9). However, most predictor traits included in the dependent trait models for both surviving and dead trees had coefficients with the same sign (Table S9).

## Discussion

### *Mortality and Functional Traits*

Stand-level mortality was analyzed in relation to environmental factors (light), and we discuss these results in the context of our second research question that focuses on how stand-level mortality is related to environmental factors (average light at the forest floor and gap simulation variables). Both tree- and phenotype-level mortality were related to TTS traits, and subsets of traits emerged as being important predictors of both types of mortality. Thus, we discuss results for both tree- and phenotype-level mortality simultaneously, in the context of our first and third questions, addressing how environment versus functional traits explain mortality, and identifying which functional traits (parameters) predict phenotype-level mortality, respectively. We follow this with an evaluation of how our results compare to trait patterns reported in the literature.

*Stand-level mortality*—Towards addressing how environmental factors relate to stand-level mortality (our second question), we found that the average light level at the forest floor ( $PAR_{avg}$ ) was an excellent predictor of stand-level mortality ( $m_g^S$ ) (Figure 2B). While time between gaps ( $tbg$ ) was also a good predictor of stand-level mortality (Figure

2A), with longer times leading to higher mortality rates, other indices of the gap phase—such as the length of the forest gap ( $gt$ ) during which a tree could experience high light or the time it takes for the forest canopy to close after a gap has formed ( $ct$ )—offered little insight into stand-level mortality.  $PAR_{avg}$  is ultimately a function of the three gap phase variables ( $tbg$ ,  $gt$ , and  $ct$ ), and thus, it is not surprising that  $PAR_{avg}$  was the best predictor of stand-level mortality. For example, of the three gap phase variables,  $tbg$  most strongly influenced  $PAR_{avg}$  (Figure S1 C), especially when  $tbg$  was long, in which case the gap length ( $gt$ ) and closure time ( $ct$ ) were less important. In the most extreme case, where  $tbg$  was equal to the simulation length (200 years), a gap was created at the beginning of the simulation, followed by canopy closure and an extended closed canopy phase, leading to the lowest  $PAR_{avg}$  and highest mortality.

We note that in our simulation study, functional traits were irrelevant for understanding stand-level mortality since we did not simulate communities of trees, but simply evaluated the proportion of individually simulated trees that died during each gap scenario (a “stand”). For approaches that consider an entire community of trees competing explicitly for resources—such as the JABOWA (Botkin et al. 1972, Bugmann 2001), SORTIE (Pacala et al. 1993, 1996), or Ecosystem Demography (Moorcroft et al. 2001) models—one could compute community-weighted functional traits to determine the importance of traits for predicting stand-level mortality.

*Tree- and phenotype-level mortality*—Towards answering how environment versus functional traits explain mortality, our first question, we found that simulated tree-level mortality ( $m_{g,p}$ ) was better explained by traits in the theoretical trait space (TTS) rather than by  $PAR_{avg}$  (environment). This may not be surprising given that  $PAR_{avg}$  served

as the only environmental predictor, while a total of 32 functional traits were considered.  $PAR_{avg}$  alone successfully predicted death for trees that actually died, but it also predicted that most surviving trees would have died during the 200-year simulation. In cases where simulated trees died, death was ultimately due to carbon starvation resulting from low light. However, the actual light level experienced by the tree—which was not tracked as such data would be difficult to obtain for real trees—over the simulation period is mediated by the tree’s crown height relative to the forest canopy. Due to this,  $PAR_{avg}$ —the quantity considered here—alone cannot discriminate between trees that could succeed when overtopped (shade tolerators) versus trees that can grow above the forest canopy (shade avoiders) (e.g., Givnish 1988, Falster and Westoby 2005). Thus, average light ( $PAR_{avg}$ ) was insufficient to explain tree-level mortality, but the combination of  $PAR_{avg}$  and functional traits improved the ability to successfully predict tree-level mortality (Figure 1). Hence,  $PAR_{avg}$  appears only informative for predicting mortality if key functional traits are also considered.

Towards addressing our third question focused on understanding which trait combinations predicts mortality of a specific phenotype, we found that functional traits in the TTS reasonably explained variation in phenotype-level mortality ( $m_p^\theta$ ). In particular, 48% of the variation was explained by the independent effects of 20 traits, and 62% explained by the independent and interacting effects of a subset of traits from the TTS (Table S5). The most important traits for predicting phenotype-level mortality were also the most important for predicting tree-level mortality. For example, mortality rates were lower for trees and phenotypes with greater potential to grow above the forest canopy (high  $H_{max}$ ), with higher radiation-use efficiency (high  $\epsilon$ ), and/or with stems supporting

more conducting area (high  $\gamma_x$ ), which would allow for greater investment in height growth.

The tree- and phenotype-level mortality regressions are generally consistent with empirical studies. For example, maximum potential height of a mature tree ( $H_{max}$ ) often emerges as a predictor of population- or species-level mortality (e.g, Poorter et al. 2008, Wright et al. 2010, Ruger et al. 2012); trees or phenotypes associated with high  $H_{max}$  are less likely to die during closed canopy phases. This relationship may be expected if a tree with the potential for high  $H_{max}$  can also grow quickly, allowing it to position its crown above the forest canopy. However, some studies show that  $H_{max}$  is only a weak predictor of mortality for species associated with  $H_{max} > 25$  m (Ruger et al. 2012), or for seedlings as seedling growth rates do not necessarily correlate with  $H_{max}$  (Wright et al. 2010). Thus, it appears that the degree to which  $H_{max}$  can serve as a predictor of mortality may depend on species identity and the growth stage of the tree.

In addition to  $H_{max}$ , we also found that radiation-use efficiency ( $\epsilon$ ) was just as, or more, important for predicting mortality. This trait is related to how efficiently light is used to acquire carbon, with higher values being especially beneficial in low light. Empirical studies indicate that  $\epsilon$  is related to leaf nitrogen content (Sinclair and Horie 1989, Wang et al. 1991, Martin and Jokela 2004), which in-turn is related to a number of other leaf traits, including specific leaf area (SLA), leaf lifespan, and mass-based photosynthetic rate (Wright et al. 2004). Thus, it is also possible that the importance of  $\epsilon$  could reflect the contribution of these other, related traits for predicting tree-, phenotype-, population-, and/or species-level mortality.

While we also found that the conducting area to sapwood area ratio ( $\gamma_X$ ) was an important predictor of mortality under light stress, this trait is rarely measured in field studies that attempt to link mortality to functional traits. While  $\gamma_X$  can be measured (e.g., Hacke et al. 2001, Kaakinen et al. 2004, Lens et al. 2005, 2011), such measurements are time-consuming and potentially challenging, which likely explains the reporting of limited data related to this trait. However, our simulation experiments indicate that this may be an important trait to target in mortality studies. In contrast, many empirical studies have reported relationships between wood density ( $\rho$ ) and tree mortality, where lower  $\rho$  is typically related to higher mortality rates (Poorter et al. 2008, Chave et al. 2009, Wright et al. 2010). But,  $\rho$  did not emerge as a top predictor of mortality in our analyses. However,  $\rho$  in the ACGCA model describes the density of wood formed under “optimal” conditions. In reality, bulk  $\rho$  varies from year-to-year (Bouriaud et al. 2005, Skomarkova et al. 2006), and field-based measurements of  $\rho$  represent a composite trait that reflects anatomical features, such as  $\gamma_X$  and cell wall thickness. Thus, our finding that conducting area  $\gamma_X$  is a key predictor of mortality is consistent with the observation that field-based  $\rho$  is often predictive of mortality.

### *The Multi-dimensional Trait Space*

*Centroids and volumes*—Towards addressing our fourth question related to how environmental filtering can modify the trait space, we found that the trait spaces (hypercubes) were altered by selective mortality. This agrees with the concept that environmental filtering restricts the functional trait space (Van der Valk 1981, Webb et al. 2010). When comparing surviving trees to the potential population of trees, as captured by the TTS, both centroid distances and volume differences became greater as

mortality increased (e.g., Figures 4A and 4D), implying a restriction of the multidimensional trait under light limitation. This is in agreement with a recent empirical study—using data from over ten thousand species—that found plants have a highly restricted trait space relative to what is theoretically possible given the overall range of observed trait values (Diaz et al. 2016); these findings are based on six traits, including mass-based leaf nitrogen content, leaf area, SLA, diaspore mass, adult plant height, and stem specific density (similar to  $\rho$ ). Most of the variation in these traits could be attributed to two axes in a PCA (principle components analysis), but the correlative nature of the analysis precluded mechanistic explanations for why so many potential trait combinations are not realized (Diaz et al. 2016). A few potential explanations include mass conservation or engineering tradeoffs (Scheiter et al. 2013), competition, or natural selection (Levine 2015). Our study suggests mass conservation and engineering tradeoffs are important in that a restricted trait space emerged from an individual-based model (ACGCA) subjected to only one environmental limitation (light); however, this finding does not exclude competition or natural selection as potentially important since they were not explicitly assessed in this study.

*Trait variation*—For those traits that were the strongest predictors of tree- and/or phenotype-level mortality, their distributions differed among the surviving and dead groups of trees (for  $H_{max}$ ,  $\varepsilon$ , and  $\gamma_X$ , see Figure 3 B-D). The location of each distribution clearly differed between the two groups (e.g., the mean or mode of  $H_{max}$  was lower for dead compared to surviving trees, Figure 3B), but the spread or variance did not notably differ. The location differences agree with the hypercube results in that the centroids (an index of location in multi-variate space) significantly differed between the two groups of

trees, with distances being highest under gap scenarios leading to low stand-level mortality, but approaching zero as mortality approached 50% (Figures 4C, 5C). The similarity in spread among the univariate distributions (Figure 3B-D) seemingly conflicts with the hypercube volumes (i.e., indices of “spread” in six dimensions). For example, as for the centroid distances, volume differences were greatest under low stand-level mortality, but disappeared as mortality rates approached 50% (Figs. 4F, 5F). Overall, the trait space of dead trees was much narrower (smaller volume) under low mortality conditions compared to the surviving trees, indicating that very specific combinations or ranges of traits were “selected” against under comparatively low light stress. As light stress increased, a larger proportion of trees died, thus expanding the trait space associated with the dead group of trees, while simultaneously shrinking the trait space associated with surviving trees.

The apparent inconsistency between the marginal distributions for individual traits and the hypercube characteristics can likely be explained by tradeoffs in the multidimensional trait space, reflecting the possibility that a tree can respond to a given stressor in different ways. In support of this, a simulation that employed a genetic algorithm to identify the trait values—for 34 functional traits—that optimize seedling growth, survival, and fitness produced multiple, essentially infinite, combinations of “optimal” trait values that spanned up to two orders of magnitude (Marks and Lechowicz 2006). This was attributed to the concept that even in a heterogeneous environment, it is possible to have many optimal solutions, provided there are many tradeoffs that can occur (Marks and Lechowicz 2006). Similar results were also found in a laboratory study of evolution in bacteria where uniform environments were found to lead to similar levels of

fitness even though genetic divergence and changes in individual traits occurred over 1000 generations (Korona 1996). Unfortunately, it would be impractical to conduct an observational experiment of this type for long-lived trees, pointing to the utility of simulation experiments.

Though we do not explicitly model competition between individuals, a recent study found that trait-dissimilarity is not critical for determining local competitive effects on growth. A tradeoff in performance could permit the coexistence of species with diverse traits, when competition is present versus when competition is absent, provided disturbance (such as gap formation) creates an environment with multiple successional stages (Kunstler et al. 2016). Our results support this in that they generally show wide ranges of traits can be present in surviving individuals, even as stand-level mortality approaches 50%. This implies multiple strategies exist, allowing individuals to tolerate relatively inhospitable environments (here, low light). However, the trait space would likely become highly restricted if stand-level mortality were to continue increasing, and as it approaches 100%, we would predict that the trait space describing trees capable of tolerating increasingly lower light would become much less variable (narrower [univariate] or smaller volume [multi-variate]).

### *Trait Relationships and Tradeoffs*

The trait-trait stepwise regressions provide insight into our fifth question, which asks how does non-random mortality induced via gap dynamics affect trait tradeoffs? Recall that for each of the 32 functional traits, we regressed the values associated with one trait (dependent trait) on the values of the other traits (predictor traits or covariates) representative of each tree, with separate regressions for trees that died and survived a

particular gap scenario. Here, we focus on the gap scenario that produced the lowest stand-level mortality (~19%) since this scenario lead to the largest separation in the trait hypercubes of the surviving and dead trees (see Figures 4 and 5). Overall, many relationships among traits were comparable within the dead and surviving groups of trees. For example, whether a trait was positively or negatively correlated with another trait was generally consistent between the two groups of trees, suggesting similar trait tradeoffs for both populations.

However, the trait space associated trees that died appeared to contain more structure and tighter or stronger tradeoffs compared to the surviving trees (as indicated by higher  $R^2$  values for all traits; Tables S7 and S8). We highlight three traits ( $\varepsilon$ ,  $R_{mL}$ , and  $\gamma_X$ ) that are significant predictors of mortality and that are related to the leaf ( $\varepsilon$ ,  $R_{mL}$ ) and wood ( $\gamma_X$ ) economics spectrums. In the ACGCA model,  $\gamma_X$  is fundamental to computing the maximum potential amount of non-structural carbohydrates (NSCs) that can be stored in sapwood, and it also trades-off with height growth (Ogle and Pacala 2009). As  $\gamma_X$  increases, the amount of NSCs that can be stored generally decreases, and this reduced investment in storage, accompanied by production of lighter bulk wood, tends to facilitate rapid height growth. In the regression for  $\gamma_X$  in surviving trees (Table S7), a number of tradeoffs are indicated;  $\gamma_X$  is negatively correlated with  $\varepsilon$  and  $\rho$  and positively correlated with  $H_{max}$ . The relationship between  $\gamma_X$  and  $H_{max}$  in surviving trees is most likely related to growth rate via mass balance constraints (lower  $\gamma_X$  implies higher  $\rho$  and construction costs), while its relationship to mortality is likely related to the ability to store NSCs. The model for  $\varepsilon$  revealed tradeoffs with  $H_{max}$  (negative relationship) and  $R_{mL}$  (positive relationship). If a tree has a large  $H_{max}$ , it could avoid investing in highly efficient

photosynthetic machinery (high  $\epsilon$ ) because it would presumably have access to high light if its crown extends above the forest canopy. On the other hand, if a tree is overtopped and has leaves or needles associated with high maintenance costs (high  $R_{mL}$ ), one way to meet these demands, and avoid carbon starvation, is to increase light-use efficiency (higher  $\epsilon$ ), thus allowing for greater production of photosynthates under low light.

### *Limitations and Future Directions*

The creation of the TTS (Fell et al. in review) and the evaluation of filtering processes affecting the functional trait space of trees was based on simulation experiments conducted with an individual-based model of tree growth and mortality (ACGCA, Ogle and Pacala (2009)). The current version of ACGCA is only driven by one environmental variable: light. Given our overarching goal to assess the TTS for North American trees and the effect of environmental stress (gap dynamics) on refining this trait space, limiting the environmental drivers to only light eased interpretation of the results. However, the simplicity of the gap dynamics simulations and the coarse physiology sub-model limit extension of our results to other filtering processes and environmental stressors. In reality, trees can experience a multitude of limitations, leading to a wide variety of tradeoffs (Wright et al. 2004, Chave et al. 2009, Scheiter et al. 2013, Diaz et al. 2016, Kunstler et al. 2016). Even with the significant limitations implied by only considering one environmental variable, meaningful changes in the trait space were identified, and the presence of realistic, multidimensional relationships between traits emerged. Including more physiological processes and drivers in the ACGCA model would allow us to explore the impacts of other stressors (e.g., drought) or interacting stressors (e.g., drought and shading) on the trait space. It is likely that the key

traits predicting mortality under different stressors (e.g., drought, nutrient limitation) would likely differ from the important traits identified here that relate to mortality under light limitation.

One of our goals is to integrate the ACGCA model with more detailed physiological sub-models (e.g., photosynthesis (Farquhar et al. 1980), stomatal conductance (Ball et al. 1987, Medlyn et al. 2011), hydraulics (Sperry et al. 1998, Tuzet et al. 2003)), allowing the investigation of additional stressors and associated physiological limitations. For instance, incorporation of a sub-model for water uptake, transport, and transpiration would permit the integration of soil moisture availability, plant water relations, and photosynthesis (Sperry et al. 1998, Tuzet et al. 2003). A second goal is to integrate the ACGCA model with a forest stand model that would enable explicit representation of competition and community dynamics—such as the Perfect Plasticity Approximation (Purves et al. 2008, Strigul et al. 2008), SORTIE (Pacala et al. 1993, 1996), or the Ecosystem Demography (Moorcroft et al. 2001) models—thus allowing for the evaluation of both biotic and environmental filters. There is the potential to simultaneously implement these modifications, provided the computational challenges can be overcome. This may be possible if the sub-models are chosen carefully. Some guidance could come from work on dynamic global vegetation models (DGVMs) that integrate functional traits and individual-level processes in a computationally tractable way (Scheiter et al. 2013, Fyllas et al. 2014).

### *Conclusions*

Through a series of simulation experiments with a semi-mechanistic model of tree growth and carbon allocation, we found that non-random mortality induced by light

limitation led to a refinement of the functional trait space occupied by trees. This was demonstrated through changes in the hypercube characteristics that define the multidimensional trait spaces occupied by surviving trees and dead trees compared to the theoretical trait space (TTS). The trait space occupied by trees that died due to light stress notably differed from that of living trees and the TTS, especially under conditions leading to relatively low mortality. Mortality at the stand-level was best explained by light level, while tree- and phenotype-level mortality were best explained by a subset of the 32 traits in the TTS. For example, maximum height ( $H_{max}$ ), radiation use efficiency ( $\epsilon$ ), and the conducting area to sapwood area ratio ( $\gamma_X$ ) were consistently identified as important predictors of mortality, and  $\epsilon$  and  $\gamma_X$  exhibited fairly strong tradeoffs with other traits. Given that only a few traits were strong predictors of mortality, this supports assertions that there is an upper limit to the number of traits needed to explain processes such as community assembly (Laughlin 2014). Many of the trait-mortality and trait-trait relationships that emerged from the relatively simple gap dynamics simulations were generally in agreement with empirical studies, suggesting that model-based approaches, as described here, may be helpful in understanding how traits are related, as well as identifying relationships that may not be evident or practical to investigate through empirical approaches. Model-based approaches may also be useful for understanding how trees respond to novel environmental conditions, especially if the models include additional environmental constraints such as temperature and precipitation and their impacts on carbon balance and mortality.

## **Acknowledgments**

This work was partially supported by an NSF-Division of Biological Infrastructure grant to K. Ogle (#0850361). We thank Abraham Cadmus, Jessica Guo, Yao Liu, Drew Peltier, Kimberly Samuels-Crow, and Larissa Yocom-Kent for valuable input on the manuscript. Finally we thank Michael Fell's committee members for their support and feedback including Janet Franklin, Thomas Day, Kevin Hultine, and Jarrett Barber.

## References

- Ball, J., I. Woodrow, and J. Berry. 1987. A model predicting stomatal conductance and its contribution to the control of photosynthesis under different environmental conditions. *Progress in Photosynthesis Research*:221–224.
- Blonder, B., C. Lamanna, C. Violle, and B. J. Enquist. 2014. The n-dimensional hypervolume. *Global Ecology and Biogeography* 23:595–609.
- Van Bodegom, P. M., J. C. Douma, and L. M. Verheijen. 2014. A fully traits-based approach to modeling global vegetation distribution. *Proceedings of the National Academy of Sciences* 111:13733–13738.
- Botkin, D. B., J. F. Janak, and J. R. Wallis. 1972. Some ecological consequences of a computer model of forest growth. *The Journal of Ecology* 60:849–872.
- Bouriaud, O., J.-M. Leban, D. Bert, and C. Deleuze. 2005. Intra-annual variations in climate influence growth and wood density of Norway spruce. *Tree Physiology* 25:651–60.
- Bugmann, H. 2001. A review of forest gap models. *Climatic Change* 51:259–305.
- Chave, J., D. Coomes, S. Jansen, S. L. Lewis, N. G. Swenson, and A. E. Zanne. 2009. Towards a worldwide wood economics spectrum. *Ecology Letters* 12:351–366.
- Clark, J. S., D. Bell, C. Chu, B. Courbaud, M. Dietze, M. Hersh, J. Hillerislambers, I. Ibáñez, S. Ladeau, S. McMahon, J. Metcalf, J. Mohan, E. Moran, L. Pangle, S. Pearson, C. Salk, Z. Shen, D. Valle, and P. Wyckoff. 2010. High-dimensional coexistence based on individual variation: A synthesis of evidence. *Ecological Monographs* 80:569–608.
- Clark, J. S., D. M. Bell, M. H. Hersh, M. C. Kwit, E. Moran, C. Salk, A. Stine, D. Valle, and K. Zhu. 2011. Individual-scale variation, species-scale differences: Inference needed to understand diversity. *Ecology Letters* 14:1273–1287.
- Cornwell, W. K., and D. D. Ackerly. 2009. Community assembly and shifts in plant trait distributions across an environmental gradient in coastal California. *Ecological Monographs* 79:109–126.
- Devictor, V., D. Mouillot, C. Meynard, F. Jiguet, W. Thuiller, and N. Mouquet. 2010. Spatial mismatch and congruence between taxonomic, phylogenetic and functional diversity: The need for integrative conservation strategies in a changing world. *Ecology Letters* 13:1030–1040.
- Diaz, S., J. G. Hodgson, K. Thompson, M. Cabido, J. H. C. Cornelissen, a. Jalili, G. Montserrat-Martí, J. P. Grime, F. Zarrinkamar, Y. Asri, S. R. Band, S.

- Basconcelo, P. Castro-Díez, G. Funes, B. Hamzehee, M. Khoshnevi, N. Pérez-Harguindeguy, M. C. Pérez-Rantomé, F. a. Shirvany, F. Vendramini, S. Yazdani, R. Abbas-Azimi, a. Bogaard, S. Boustani, M. Charles, M. Dehghan, L. Torres-Espuny, V. Falczuk, J. Guerrero-Campo, a. Hynd, G. Jones, E. Kowsary, F. Kazemi-Saeed, M. Maestro-Martínez, a. Romo-Díez, S. Shaw, B. Siavash, P. Villar-Salvador, and M. R. Zak. 2004. The plant traits that drive ecosystems: Evidence from three continents. *Journal of Vegetation Science* 15:295–304.
- Diaz, S., J. Kattge, J. H. Cornelissen, I. J. Wright, S. Lavorel, S. Dray, B. Reu, M. Kleyer, C. Wirth, I. C. Prentice, E. Garnier, G. Bonisch, M. Westoby, H. Poorter, P. B. Reich, A. T. Moles, J. Dickie, A. N. Gillison, A. E. Zanne, J. Chave, S. J. Wright, S. N. Sheremet'ev, H. Jactel, C. Baraloto, B. Cerabolini, S. Pierce, B. Shipley, D. Kirkup, F. Casanoves, J. S. Joswig, A. Gunther, V. Falczuk, N. Ruger, M. D. Mahecha, and L. D. Gorne. 2016. The global spectrum of plant form and function. *Nature* 529:167–171.
- Evans, M. R., K. J. Norris, and T. G. Benton. 2011. Predictive ecology: systems approaches. *Philosophical Transactions of the Royal Society B: Biological Sciences* 367:163–169.
- Falster, D. S., and M. Westoby. 2005. Alternative height strategies among 45 dicot rain forest species from tropical Queensland, Australia. *Journal of Ecology* 93:521–535.
- Farquhar, G. D., S. Caemmerer, and J. A. Berry. 1980. A biochemical model of photosynthetic CO<sub>2</sub> assimilation in leaves of C<sub>3</sub> species. *Planta* 149:78–90.
- Fyllas, N. M., E. Gloor, L. M. Mercado, S. Sitch, C. A. Quesada, T. F. Domingues, D. R. Galbraith, A. Torre-Lezama, E. Vilanova, H. Ramírez-Angulo, N. Higuchi, D. A. Neill, M. Silveira, L. Ferreira, G. a. Aymard C., Y. Malhi, O. L. Phillips, and J. Lloyd. 2014. Analysing Amazonian forest productivity using a new individual and trait-based model (TFS v.1). *Geoscientific Model Development* 7:1251–1269.
- Gelman, A., J. B. Carlin, H. S. Stern, D. B. Dunson, A. Vehtari, and D. B. Rubin. 2014. *Baysian Data Analysis Third Edition*. Third. CRC Press, New York.
- Givnish, T. J. 1988. Adaptation to Sun and Shade : *Australian Journal of Plant Physiology* 15:63–92.
- Grömping, U. 2006. Relative importance for linear regression in R: the package relaimpo. *Journal Of Statistical Software* 17:139–147.
- Hacke, U. G., J. S. Sperry, W. T. Pockman, S. D. Davis, and K. A. McCulloh. 2001. Trends in wood density and structure are linked to prevention of xylem implosion by negative pressure. *Oecologia* 126:457–461.

- Hutchinson, G. E. 1957. Concluding remarks. *Cold Spring Harbor Symposia on Quantitative Biology* 22:415–427.
- Kaakinen, S., K. Kostianen, F. Ek, P. Saranpää, M. E. Kubiske, J. Sober, D. F. Karnosky, and E. Vapaavuori. 2004. Stem wood properties of *Populus tremuloides*, *Betula papyrifera* and *Acer saccharum* saplings after 3 years of treatments to elevated carbon dioxide and ozone. *Global Change Biology* 10:1513–1525.
- Kattge, J., S. Díaz, S. Lavorel, I. C. Prentice, P. Leadley, G. Bönisch, E. Garnier, M. Westoby, P. B. Reich, I. J. Wright, J. H. C. Cornelissen, C. Violle, S. P. Harrison, P. M. van Bodegom, M. Reichstein, B. J. Enquist, N. a. Soudzilovskaia, D. D. Ackerly, M. Anand, O. Atkin, M. Bahn, T. R. Baker, D. Baldocchi, R. Bekker, C. C. Blanco, B. Blonder, W. J. Bond, R. Bradstock, D. E. Bunker, F. Casanoves, J. Cavender-Bares, J. Q. Chambers, F. S. Chapin, J. Chave, D. Coomes, W. K. Cornwell, J. M. Craine, B. H. Dobrin, L. Duarte, W. Durka, J. Elser, G. Esser, M. Estiarte, W. F. Fagan, J. Fang, F. Fernández-Méndez, A. Fidelis, B. Finegan, O. Flores, H. Ford, D. Frank, G. T. Freschet, N. M. Fyllas, R. V. Gallagher, W. a. Green, A. G. Gutierrez, T. Hickler, S. Higgins, J. G. Hodgson, A. Jalili, S. Jansen, C. Joly, A. J. Kerkhoff, D. Kirkup, K. Kitajima, M. Kleyer, S. Klotz, J. M. H. Knops, K. Kramer, I. Kühn, H. Kurokawa, D. Laughlin, T. D. Lee, M. Leishman, F. Lens, T. Lenz, S. L. Lewis, J. Lloyd, J. Llusià, F. Louault, S. Ma, M. D. Mahecha, P. Manning, T. Massad, B. Medlyn, J. Messier, A. T. Moles, S. C. Müller, K. Nadrowski, S. Naeem, Ü. Niinemets, S. Nöllert, A. Nüske, R. Ogaya, J. Oleksyn, V. G. Onipchenko, Y. Onoda, J. Ordoñez, G. Overbeck, W. a. Ozinga, S. Patiño, S. Paula, J. G. Pausas, J. Peñuelas, O. L. Phillips, V. Pillar, H. Poorter, L. Poorter, P. Poschlod, A. Prinzing, R. Proulx, A. Rammig, S. Reinsch, B. Reu, L. Sack, B. Salgado-Negret, J. Sardans, S. Shiodera, B. Shipley, A. Siefert, E. Sosinski, J.-F. Soussana, E. Swaine, N. Swenson, K. Thompson, P. Thornton, M. Waldram, E. Weiher, M. White, S. White, S. J. Wright, B. Yguel, S. Zaehle, A. E. Zanne, and C. Wirth. 2011a. TRY - a global database of plant traits. *Global Change Biology*:2905–2935.
- Kattge, J., K. Ogle, G. Bönisch, S. Díaz, S. Lavorel, J. Madin, K. Nadrowski, S. Nöllert, K. Sartor, and C. Wirth. 2011b. A generic structure for plant trait databases. *Methods in Ecology and Evolution* 2:202–213.
- Korona, R. 1996. Genetic Divergence and Fitness Convergence Under Uniform Selection in Experimental Populations of Bacteria. *Genetics* 143:637–64.
- Kraft, N. J. B., P. B. Adler, O. Godoy, E. C. James, S. Fuller, and J. M. Levine. 2015. Community assembly, coexistence and the environmental filtering metaphor. *Functional Ecology* 29:592–599.
- Kunstler, G., D. Falster, D. A. Coomes, F. Hui, M. Kooyman, Robert, D. C. Laughlin, L. Poorter, M. Vanderwel, G. Vieilledent, S. J. Wright, M. Aiba, C. Baraloto, J.

- Caspersen, J. H. C. Cornelissen, S. Gourlet-Fleury, M. Hanewinkel, B. Herault, J. Kattge, H. Kurokawa, Y. Onoda, J. Penuelas, H. Poorter, M. Uriarte, S. Richardson, and P. Ruiz-Benito. 2016. Plant functional traits have globally consistent effects on competition. *Nature* 529:1–15.
- Laughlin, D. C. 2014. The intrinsic dimensionality of plant traits and its relevance to community assembly. *Journal of Ecology* 102:186–193.
- Lens, F., S. Dressler, S. Jansen, L. van Evelghem, and E. Smets. 2005. Relationships Within Balsaminoid Ericales: A Wood Anatomical Approach. *American Journal of Botany* 92:941–953.
- Lens, F., J. S. Sperry, M. A. Christman, B. Choat, D. Rabaey, and S. Jansen. 2011. Testing hypotheses that link wood anatomy to cavitation resistance and hydraulic conductivity in the genus *Acer*. *New Phytologist* 190:709–723.
- Levine, J. M. 2015. A trail map for trait-based studies. *Nature* 529:163–164.
- MacArthur, R., and R. Levins. 1967. The Limiting Similarity, Convergence, and Divergence of Coexisting Species. *The American Naturalist* 101:377–385.
- Marks, C. O., and M. J. Lechowicz. 2006. Alternative designs and the evolution of functional diversity. *The American Naturalist* 167:55–66.
- Martin, T. a, and E. J. Jokela. 2004. Developmental patterns and nutrition impact radiation use efficiency components in southern pine stands. *Ecological Applications* 14:1839–1854.
- McCarthy, J. 2001. Gap dynamics of forest trees : A review with particular attention to boreal forests. *Environmental Reviews* 59:1–59.
- McGill, B. J., B. J. Enquist, E. Weiher, and M. Westoby. 2006. Rebuilding community ecology from functional traits. *Trends in Ecology and Evolution* 21:178–85.
- McMahon, S. M., C. J. E. Metcalf, and C. W. Woodall. 2011. High-dimensional coexistence of temperate tree species: functional traits, demographic rates, life-history stages, and their physical context. *PloS One* 6:e16253.
- Medlyn, B. E., R. a. Duursma, D. Eamus, D. S. Ellsworth, I. C. Prentice, C. V. M. Barton, K. Y. Crous, P. De Angelis, M. Freeman, and L. Wingate. 2011. Reconciling the optimal and empirical approaches to modelling stomatal conductance. *Global Change Biology* 17:2134–2144.
- Moorcroft, P. R., G. C. Hurtt, and S. W. Pacala. 2001. A Method for Scaling Vegetation Dynamics : the Ecosystem Demography Model (Ed). *Ecological Monographs* 71:557–586.

- Ogle, K., J. Barber, and K. Sartor. 2013. Feedback and Modularization in a Bayesian Meta-analysis of Tree Traits Affecting Forest Dynamics. *Bayesian Analysis* 8:133–168.
- Ogle, K., and S. W. Pacala. 2009. A modeling framework for inferring tree growth and allocation from physiological, morphological and allometric traits. *Tree Physiology* 29:587–605.
- Ogle, K., S. Pathikonda, K. Sartor, J. W. Lichstein, J. L. D. Osnas, and S. W. Pacala. 2014. A model-based meta-analysis for estimating species-specific wood density and identifying potential sources of variation. *Journal of Ecology* 102:194–208.
- Pacala, S. W., C. D. Canham, J. Saponara, J. A. Silander Jr, R. K. Kobe, and E. Ribbens. 1996. Forest models defined by field measurements: estimation, error analysis and dynamics. *Ecological Monographs* 66:1–43.
- Pacala, S. W., C. D. Canham, and J. A. Silander Jr. 1993. Forest models defined by field measurements: I. The design of a northeastern forest simulator. *Canadian Journal of Forest Research* 23:1980–1988.
- Pearl, R., and L. J. Reed. 1920. On the rate of growth of the population of the United States since 1790 and its mathematical representation. *Proceedings of the National Academy of Sciences* 6:275–288.
- Poorter, L., S. J. Wright, H. Paz, D. D. Ackerly, R. Condit, G. Ibarra-Manríquez, K. E. Harms, J. C. Licona, M. Martínez-Ramos, S. J. Mazer, H. C. Muller-Landau, M. Peña-Claros, C. O. Webb, and I. J. Wright. 2008. Are functional traits good predictors of demographic rates? Evidence from five neotropical forests. *Ecology* 89:1908–1920.
- Purves, D. W., J. W. Lichstein, N. Strigul, and S. W. Pacala. 2008. Predicting and understanding forest dynamics using a simple tractable model. *Proceedings of the National Academy of Sciences* 105:17018–22.
- Reich, P. B. 2014. The world-wide “fast-slow” plant economics spectrum: a traits manifesto. *Journal of Ecology* 102:275–301.
- Reich, P. B., D. S. Ellsworth, M. B. Walters, J. M. Vose, C. Gresham, J. C. Volin, and W. D. Bowman. 1999. Generality of Leaf Trait Relationships: A Test Across Six Biomes. *Ecology* 80:1955–1969.
- Ruger, N., C. Wirth, S. J. Wright, and R. Condit. 2012. Functional traits explain light and size response of growth rates in tropical tree species. *Ecology* 93:2626–2636.

- Runkle, J. R. 1985. Disturbance Regimes in Temperate Forests. Pages 17–33 in S. T. A. Pickett and P. S. White, editors. *The Ecology of Natural Disturbance and Patch Dynamics*. United Kin. Academic press, London.
- Runkle, J. R., and T. C. Yetter. 1987. Treefalls Revisited : Gap Dynamics in the Southern Appalachians. *Ecology* 68:417–424.
- Savage, V. M., C. T. Webb, and J. Norberg. 2007. A general multi-trait-based framework for studying the effects of biodiversity on ecosystem functioning. *Journal of Theoretical Biology* 247:213–229.
- Scheiter, S., L. Langan, and S. I. Higgins. 2013. Next-generation dynamic global vegetation models: Learning from community ecology. *New Phytologist* 198:957–969.
- Sinclair, T. R., and T. Horie. 1989. Leaf Nitrogen, Photosynthesis, and Crop Radiation Use Efficiency: A Review. *Crop Science* 29:90.
- Skomarkova, M. V., E. A. Vaganov, M. Mund, A. Knohl, P. Linke, A. Boerner, and E. D. Schulze. 2006. Inter-annual and seasonal variability of radial growth, wood density and carbon isotope ratios in tree rings of beech (*Fagus sylvatica*) growing in Germany and Italy. *Trees* 20:571–586.
- Sperry, J. S., F. R. Adler, G. S. Campbell, and J. P. Comstock. 1998. Limitation of plant water use by rhizosphere and xylem conductance: results from a model. *Plant, Cell & Environment* 21:347–359.
- Stahl, U., J. Kattge, B. Reu, W. Voigt, and K. Ogle. 2013. Whole-plant trait spectra of North American woody plant species reflect fundamental ecological strategies. *Ecosphere* 4:128.
- Strigul, N. I. S., D. Pristinski, D. Purves, J. Dushoff, S. Pacala, D. E. P. Ristinski, D. R. E. W. P. Urves, and J. O. D. Ushoff. 2008. Scaling From Trees To Forests: Tractable Macroscopic Equations for Forest Dynamics. *Ecological Monographs* 78:523–545.
- Stubbs, W. J., and J. B. Wilson. 2004. Evidence for limiting similarity in a sand dune community. *Journal of Ecology* 92:557–567.
- Tilman, D. 1985. The resource-ratio hypothesis of plant succession. *American Naturalist* 125:827–852.
- Tuzet, A., A. Perrier, and R. Leuning. 2003. A coupled model of stomatal conductance, photosynthesis and transpiration. *Plant, Cell & Environment* 26:1097–1116.

- Van der Valk, A. . G. 1981. Succession in Wetlands: A Gleasonian Approach. *Ecology* 62:688–696.
- Valverde, T., and J. Silvertown. 1997. Canopy closure rate and forest structure. *Ecology* 78:1555–1562.
- Violle, C., P. B. Reich, S. W. Pacala, B. J. Enquist, and J. Kattge. 2014. The emergence and promise of functional biogeography. *Proceedings of the National Academy of Sciences* 111:13690–13696.
- Wang, A. Y. P., P. G. Jarvis, and C. M. a Taylor. 1991. PAR Absorption and Its Relation to Above-Ground Dry Matter Production of Sitka Spruce. *Journal of Applied Ecology* 28:547–560.
- Webb, C. T., J. a. Hoeting, G. M. Ames, M. I. Pyne, and N. LeRoy Poff. 2010. A structured and dynamic framework to advance traits-based theory and prediction in ecology. *Ecology Letters* 13:267–283.
- Weiher, E., and P. Keddy. 1999. Introduction: The scope and goals of research on assembly rules. Pages 1–19 *in* W. Evan and K. Paul, editors. *Ecological Assembly Rules: Perspectives, Advances, Retreats*. First. Cambridge University Press, New York.
- Weiher, E., A. van der Werf, K. Thompson, M. Roderick, E. Garnier, and O. Eriksson. 1999. Challenging Theophrastus: a common core list of plant traits for functional ecology. *Journal of Vegetation Science* 10:609–620.
- Westoby, M., and I. J. Wright. 2006. Land-plant ecology on the basis of functional traits. *Trends in Ecology & Evolution* 21:261–8.
- Woodward, F. I., and A. D. Diament. 1991. Functional approaches to predicting the ecological effects of global change. *Functional Ecology* 5:202–212.
- Wright, I. J., P. B. Reich, J. H. C. Cornelissen, D. S. Falster, E. Garnier, K. Hikosaka, B. B. Lamont, W. Lee, J. Oleksyn, N. Osada, H. Poorter, R. Villar, D. I. Warton, and M. Westoby. 2005. Assessing the generality of global leaf trait relationships. *The New phytologist* 166:485–96.
- Wright, I. J., P. B. Reich, M. Westoby, D. D. Ackerly, Z. Baruch, F. Bongers, J. Cavender-Bares, T. Chapin, J. H. C. Cornelissen, M. Diemer, J. Flexas, E. Garnier, P. K. Groom, J. Gulias, K. Hikosaka, B. B. Lamont, T. Lee, W. Lee, C. Lusk, J. J. Midgley, M.-L. Navas, U. Niinemets, J. Oleksyn, N. Osada, H. Poorter, P. Poot, L. Prior, V. I. Pyankov, C. Roumet, S. C. Thomas, M. G. Tjoelker, E. J. Veneklaas, and R. Villar. 2004. The worldwide leaf economics spectrum. *Nature* 428:821–827.

Wright, S. J., K. Kitajima, N. J. B. Kraft, P. B. Reich, I. J. Wright, D. E. Bunker, R. Condit, J. W. Dalling, S. J. Davies, S. Díaz, B. M. J. Engelbrecht, K. E. Harms, S. P. Hubbell, C. O. Marks, M. C. Ruiz-Jaen, C. M. Salvador, and A. E. Zanne. 2010. Functional traits and the growth — mortality trade-off in tropical trees. *Ecology* 91:3664–3674.

## Tables

**Table 4.1:** Descriptions of the 32 parameters ( $\theta_k$ ) in the ACGCA model that represent tree functional traits, including units of the parameters (dashes indicate unitless quantities). Bolded variables are mentioned explicitly in the paper. Table follows from Ogle and Pacala (2009).

<b>Symbol</b>	<b>Unit</b>	<b>Description</b>
$H_{max}$	m	Maximum tree height
$\varphi_H$	-	Slope at $H$ versus $r$ curve at $r = 0$ m
$\eta$	-	Relative height at which trunk transitions from paraboloid to cone
$SW_{max}$	m	Maximum sapwood width
$\lambda_S$	-	Proportionality between $B_T$ and $B_O$ for sapwood
$\lambda_H$	-	Proportionality between $B_T$ and $B_O$ for heartwood
$\rho$	g dw m <sup>-3</sup>	Wood density
$f_1$	-	Fine root area to leaf area ratio
$f_2$	-	Leaf area to xylem conducting area ratio
$\gamma_C$	g gluc m <sup>-3</sup>	Maximum storage capacity of living sapwood cells
$\gamma_W$	m <sup>3</sup> g dw <sup>-1</sup>	(Inverse) density of sapwood structural tissue
$\gamma_X$	-	Xylem conducting area to sapwood area ratio
$C_{GL}$	g gluc g dw <sup>-1</sup>	Construction costs of producing leaves
$C_{GR}$	g gluc g dw <sup>-1</sup>	Construction costs of producing fine roots
$C_{Gw}$	g gluc g dw <sup>-1</sup>	Construction costs of producing sapwood
$\delta_L$	g gluc g dw <sup>-1</sup>	Labile carbon storage capacity of leaves
$\delta_R$	g gluc g dw <sup>-1</sup>	Labile carbon storage capacity of fine roots
$S_L$	year <sup>-1</sup>	Senescence rate of leaves
$SLA$	m <sup>2</sup> g dw <sup>-1</sup>	Specific leaf area
$S_R$	year <sup>-1</sup>	Senescence rate of fine roots
$S_O$	year <sup>-1</sup>	Senescence rate of coarse roots and branches
$r_R$	m	Average fine root radius
$\rho_R$	g dw m <sup>-3</sup>	Tissue density of fine roots
$R_{mL}$	g gluc g dw <sup>-1</sup> year <sup>-1</sup>	Maintenance respiration rate of leaves
$R_{mS}$	g gluc g dw <sup>-1</sup> year <sup>-1</sup>	Maintenance respiration rate of sapwood
$R_{mR}$	g gluc g dw <sup>-1</sup> year <sup>-1</sup>	Maintenance respiration rate of fine roots
$\eta_B$	-	Relative height at which trunk transitions from neiloid to paraboloid
$k$	-	Crown light extinction coefficient
$\varepsilon$	g gluc MJ <sup>-1</sup>	Radiation-use efficiency
$m$	-	Maximum relative crown depth
$\alpha$	-	Crown curvature parameter

<b><math>R_0</math></b>	m	Maximum potential crown radius of a tree with diameter at breast height of 0 m (i.e., for a tree that is exactly 1.37 m tall)
<b><math>R_{40}</math></b>	m	Maximum potential crown radius of a tree with diameter at breast height of 0.4 m (40 cm).

---

**Table 4.2:** Methods of calculating mortality are shown relative to the simulation design. Each entry in the table (one for each trait) represents a single instance of a given vector of 32 traits ( $\theta$ ) being subjected to a given gap dynamics scenario (62 total scenarios); the binary entries indicate tree-level mortality ( $m_{g,p}$ ; 1= died, 0 = survived). The gap scenarios can be thought of as representing different environments, with each denoting an environment for a particular forest stand. Thus, stand-level mortality ( $m_g^S$ ) is found by averaging across all 33,000 columns for each row to obtain the proportion of trees that died in each gap scenario (stand). Each unique vector of  $\theta$ , representing a particular “phenotype,” is subjected to 62 gap scenarios. Thus, phenotype-level mortality ( $m_p^\theta$ ) is found by averaging across all 62 rows within each column, giving the proportion of trees that survived across all 62 gap scenarios, for each unique  $\theta$ .

		$\theta$ (unique traits vector)				
		$\theta_1$	$\theta_2$	...	$\theta_{33,000}$	Simulation (stand-level)
Gap scenarios	1	1	0	...	1	$m_1^S$
	2	0	1	...	0	$m_2^S$
	3	1	1	...	0	$m_3^S$
	⋮	⋮	⋮		⋮	⋮
	⋮	⋮	⋮		⋮	⋮
	⋮	⋮	⋮		⋮	⋮
	61	1	1	...	0	⋮
	62	0	1	...	1	$m_{62}^S$
Phenotype level		$m_1^\theta$	$m_2^\theta$	...	$m_{33,000}^\theta$	

## Figures

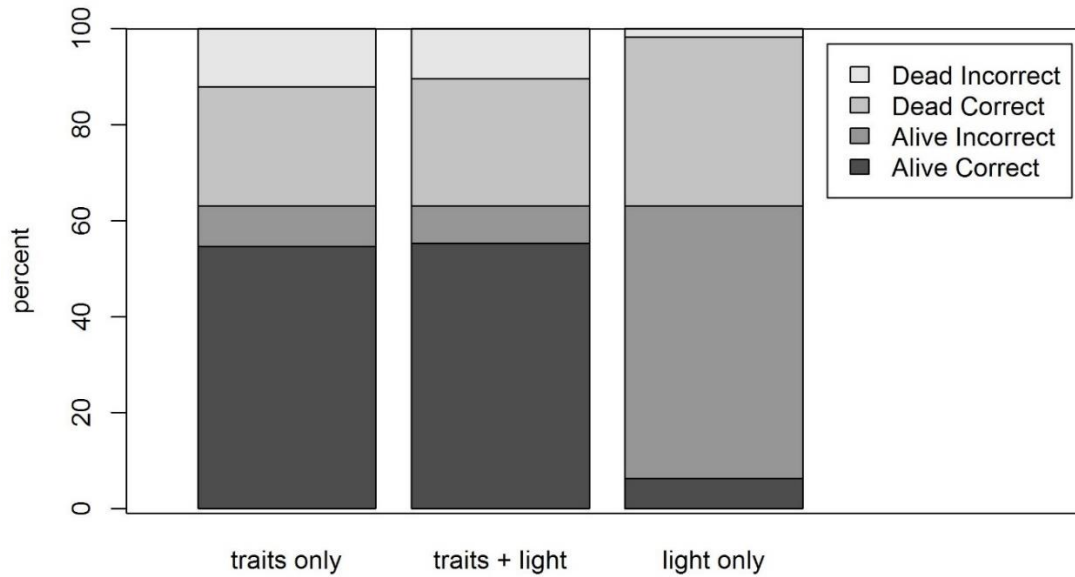


**Figure 4.1.** Percent of trees correctly or incorrectly classified ( $n = 1,023,000$ ) as dead or surviving based on applying each of the three stepwise, logistic models of tree-level mortality ( $m_{g,p}$ ) to a hold-out or test dataset. The traits only model included all 32 ACGCA traits, but excluding light; the traits + light model included the 32 traits, the average light level ( $PAR_{avg}$ ), and all 2-way interactions between  $PAR_{avg}$  and each trait; the light only model only included  $PAR_{avg}$  (not traits). Overall, we found the light only model was best at identifying trees that died, but it did very poorly at identifying trees that survived. The models that included the traits were generally similar and successfully identified living trees far better than when only  $PAR_{avg}$  was considered.

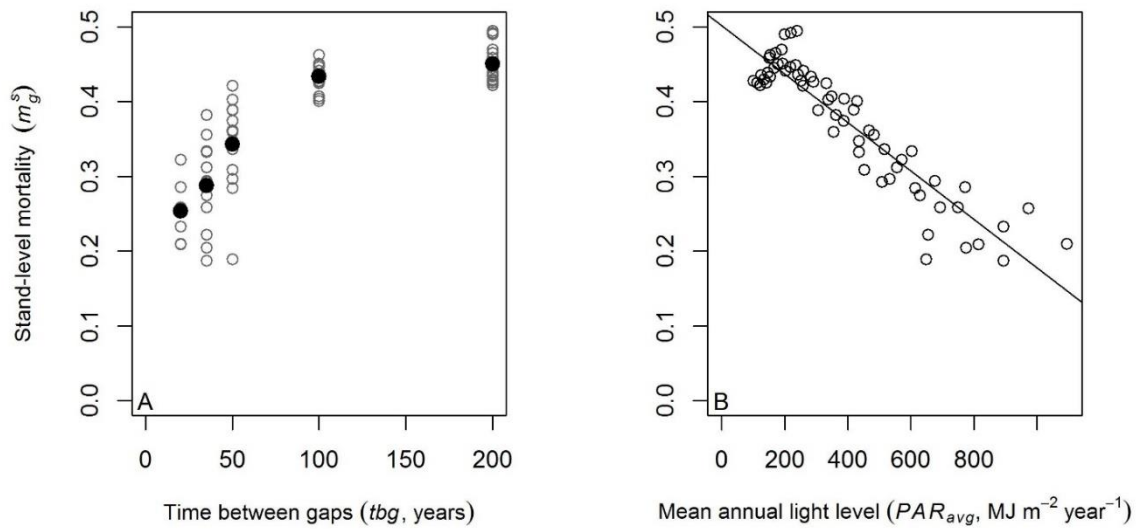


**Figure 4.2.** Regression of stand-level mortality ( $m_g^s$ ) as explained by (A) time between gaps ( $tbg$ ) and (B) mean annual light level at the forest floor ( $PAR_{avg}$ ). In (A), black symbols are the average mortality across all  $gt$  (gap time) and  $ct$  (closure time) levels within each  $tbg$  level; open circles are the mortality values for each simulation. (A) Among the three gap phase variables ( $tbs$ ,  $gt$ ,  $ct$ ),  $tbg$  was the best predictor out of the three gap simulation variables ( $p < 0.05$ ,  $R^2 = 0.74$ ), and (B)  $PAR_{avg}$  was the overall best predictor of  $m_g^s$  ( $p < 0.05$ ,  $R^2=0.85$ ).

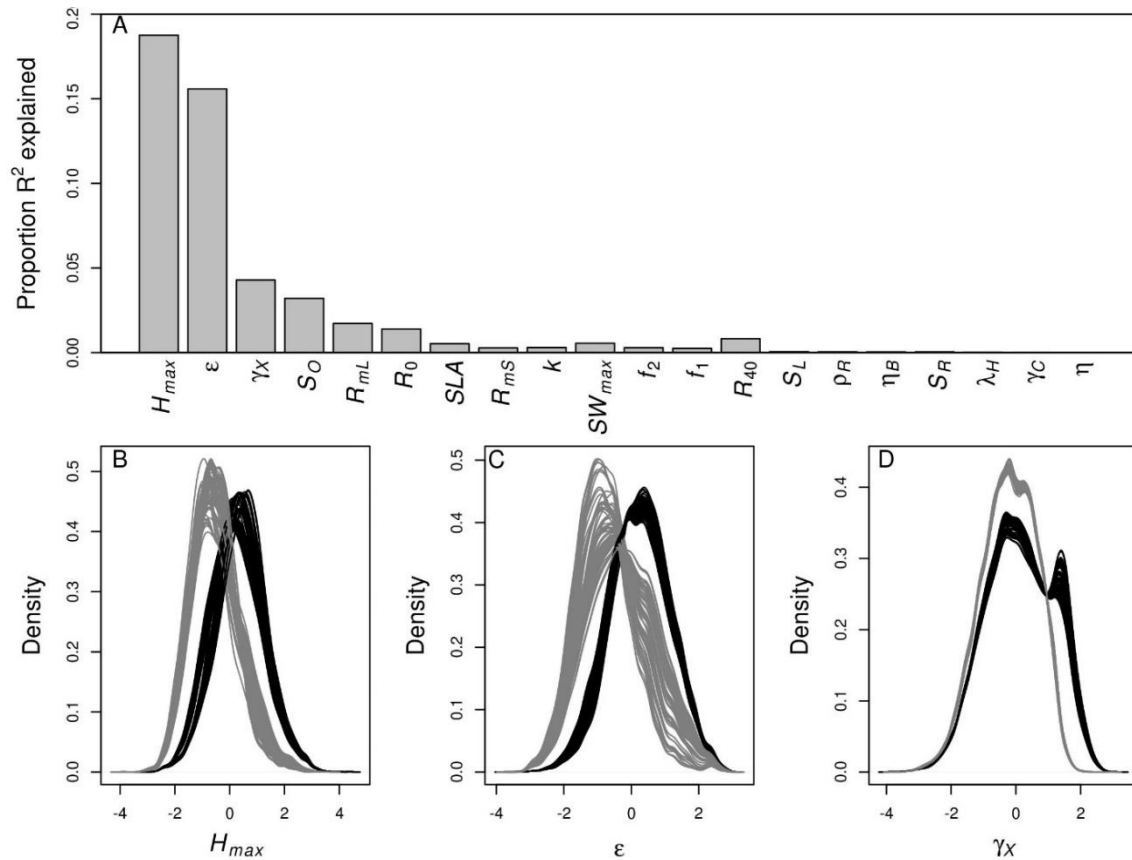


**Figure 4.3.** Stepwise regression relating phenotype-level mortality ( $m_p^\theta$ ) to functional traits. **(A)** Variables on the x-axis are the main effects (traits; see Table 4.1) included through a stepwise regression that only considered main effects, and the bars indicate the relative importance of each trait based on its  $R^2$  contribution. The proportions were found using the “lmg” method in R, which averages over all possible orderings of variables in the model. The sum of the  $R^2$  proportions sums to the overall  $R^2$  of 0.48. For the top three traits in **(A)**, kernel density estimates are shown for normalized **(B)**  $H_{max}$  (maximum tree height), **(C)**  $\epsilon$  (light-use efficiency), and **(D)**  $\gamma_X$  (proportion of xylem conducting area). In **(B)-(D)**, grey lines denote trees that died during the gap simulations, and black lines denote trees that survive; 62 lines are overlaid for each group (dead and live), one for each gap scenario.

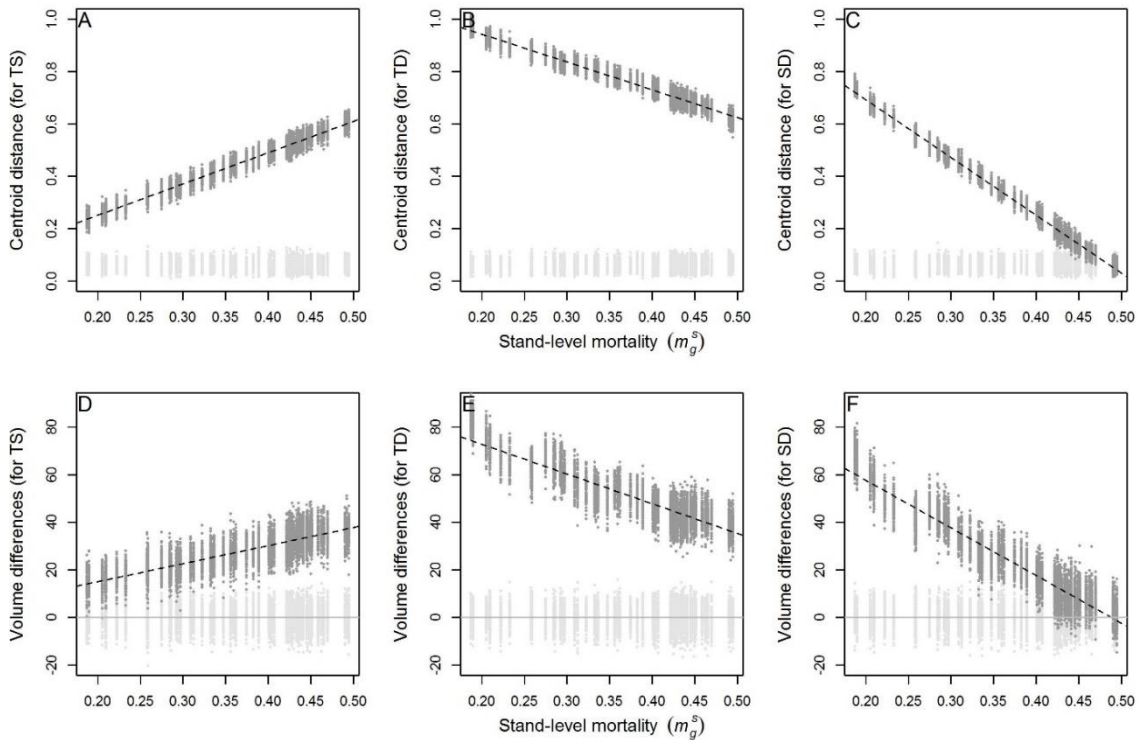


**Figure 4.4.** Hypercube centroid distances and volume differences based on six-dimensional hypercubes constructed from “mortality” traits ( $H_{max}$ ,  $\varepsilon$ ,  $\gamma_X$ ,  $S_O$ ,  $R_{mL}$ , and  $R_0$ ), as a function of stand-level mortality ( $m_g^S$ ). TS compares hypercubes representing the theoretical trait space (TTS) versus surviving trees; TD compares the TTS versus trees that died; SD compares surviving versus dead trees. In particular, centroid differences are shown for (A) TS, (B) TD, and (C) SD, and volume differences for (D) TS (i.e., TTS volume – surviving volume), (E) TD (TTS – dead), and (F) SD (surviving – dead). Dark grey points show estimates for each gap scenario, with the range of values obtained by randomly sampling 3000 points from the TTS, surviving, and dead trait spaces, for each of the 62 gap dynamics scenarios. Dashed black lines show a linear best fit of the distances or volume differences versus  $m_g^S$ . Light grey points show results from performing the same analysis for data sampled at random from the TTS to ensure the resultant patterns were not an artifact of the analysis structure.

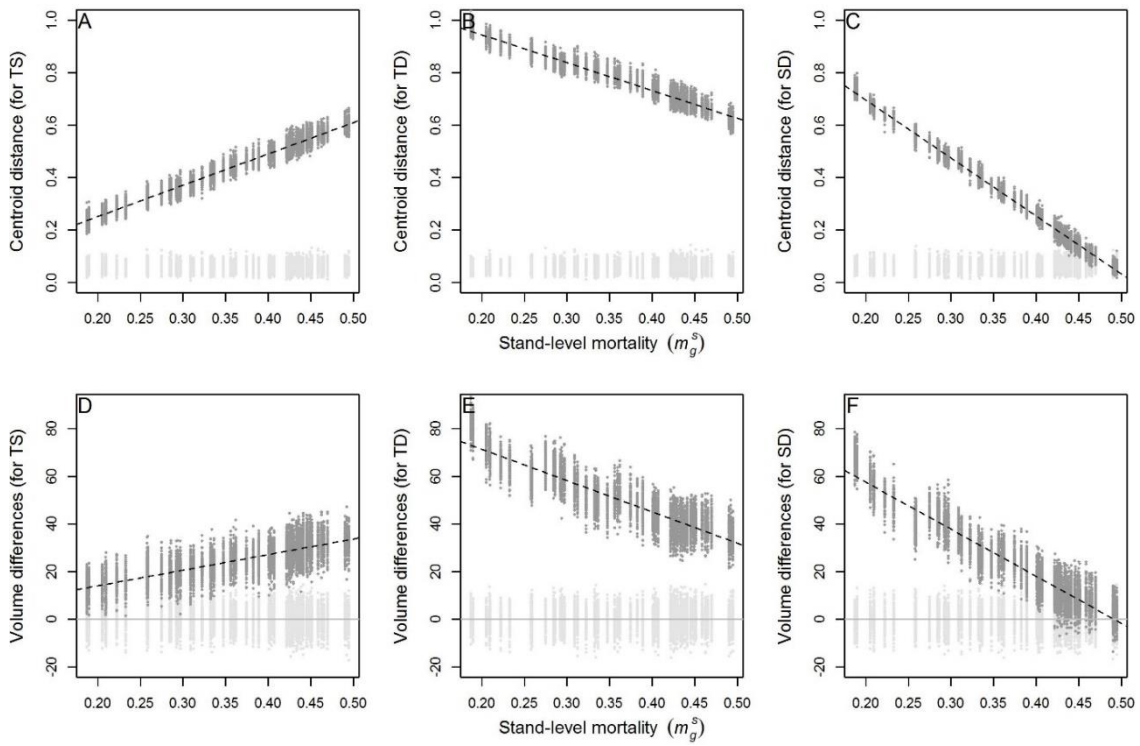


**Figure 4.5.** Hypercube centroid distances and volume differences based on six-dimensional hypercubes constructed with leaf/wood traits related to the LES and WES ( $SLA$ ,  $\varepsilon$ ,  $R_{mL}$ ,  $S_L$ ,  $\gamma_X$ , and  $\rho$ ), as a function of stand-level mortality ( $m_g^S$ ). See Figure 4.4 for details about plots.

## CHAPTER 5 – CONCLUSION

My dissertation work described herein addressed my overall objective: to quantify tree functional traits and their interrelationships. I did this through three studies that assessed functional traits at varying scales, from traits affecting leaf-level physiology (Chapter 2) to traits affecting whole-plant growth and mortality (Chapters 3-4). In particular, Chapter 2 focused on a potentially important leaf-level trait (mesophyll conductance,  $g_m$ ) affecting photosynthesis, while Chapters 3-4 evaluated relationships among 32 traits affecting tree allometries, carbon gain, carbon allocation, growth, and mortality. A few general conclusions can be drawn from my work. First, less commonly studied traits—such as mesophyll conductance, root respiration rates, root:leaf allometries, tissue senescence rates—emerged as being important predictors of tree function under different environmental conditions. Second, the 32-dimensional functional trait space occupied by North American trees is complex, but many potential trade-offs emerge that are governed by other interacting traits and environmental conditions. Third, even though there are many potential traits combinations that could lead to a successful tree, it is likely that only a relatively small subset of traits are strongly predictive of growth and mortality under particular environmental settings. Below I summarize key aspects of my three main research chapters (Chapters 2-4).

Chapter 2 utilized field data that I directly obtained, complemented by artificially generated data, to incorporate new data sources into the Farquhar et al. (1980) (FvCB) model of photosynthesis, while also showing that  $g_m$  varies across an aridity gradient, between species, and possibly growth forms (angiosperms vs. gymnosperms). This addressed my first overall objective (**O1**): Improving the quantification of  $g_m$  by

introducing fluorescence data into a biochemically based model of photosynthesis. By estimating  $g_m$  across an aridity gradient, I found that mean  $g_m$  and its variation decreased with increasing aridity in *Prosopis velutina*. In some cases, estimated mean  $g_m$  for two woody species (*P. velutina* and *Juniperous monosperma*) and was low enough to significantly impact predicted daily assimilation rates, indicating that  $g_m$  must be accounted for to accurately predict photosynthesis under water limitation. These results are relevant to ecological work more broadly because the FvCB model is incorporated into other larger-scale models and used to evaluate data obtained from field studies, at scales ranging from leaf/canopy levels (Crous and Ellsworth 2004, Cano et al. 2013, Peltier and Ibáñez 2014) to the global scale (Shugart and Woodward 2011, Fyllas et al. 2014). My results indicate that for arid parts of the globe, explicitly incorporating variation in  $g_m$  within the FvCB model is important for obtaining accurate estimates of photosynthesis and its underlying biochemical-related parameters.

Chapter 3 addressed my second objective (**O2**) of quantifying the functional trait space occupied by North American trees. This was accomplished by utilizing a Bayesian framework to fit the Allometrically Constrained Growth and Carbon Allocation (ACGCA) model (Ogle and Pacala 2009) to forest inventory and analysis (FIA) data—pooled across species—and literature data (Kattge et al. 2011; Ogle et al. 2013; Ogle et al. 2014). The Bayesian approach produced posterior estimates for 32 functional traits, which I used to describe the theoretical trait space (TTS) for North American trees. That is, the TTS emerges from the relationships inherent in the ACGCA model, as constrained by the different data sources. After accounting for relationships between each trait and the 31 other traits and light, the directions of trait-trait relationships for a subset of traits

were comparable to those in the leaf and wood economics spectra (Wright et al. 2004, Chave et al. 2009). My results suggest that these empirical trait spectra represent a subset of the TTS reflecting filtering mechanisms limiting the combinations of traits realized. Finally, there appears to be many ways of achieving realistic growth despite little refinement in the marginal posterior distributions for most of the 32 traits in the ACGCA model (Figure 3.2). This, along with the strong dependence of realistic tree growth on some traits (Figure 3.3), could be useful in thinking about how coexisting species can respond differently to limitations in the environment (Tilman 1985) or respond to environmental heterogeneity (Hutchinson 1957, Tilman 2004). However, the number of potential combinations will likely be limited by changes in the trait space due to filtering.

Chapter 4 addressed my third objective: **(O3)** assessing the impact of filtering on the TTS utilizing a gap dynamics simulation. There were three key findings from this work. First, non-random mortality led to a refinement of the TTS, as evidenced by decreased volume and increased centroid distance for surviving trees relative to the original TTS (Figures 4.4 and 4.5). Trait-trait relationships were strongest at low stand-level mortality and in trees that died (Figure S4.7 and S4.8). The traits with the greatest effect sizes for tree-level mortality were maximum potential tree height ( $H_{max}$ ) and radiation-use efficiency ( $\epsilon$ ); both of these traits clearly relate to a tree's ability to utilize light, the only environmental variable driving tree growth in the ACGCA model (Ogle and Pacala 2009). Other traits may be important if a different filter (e.g., water stress) was incorporated into the model. For instance, if a representation of plant hydraulics were integrated, such as those described by Sperry et al. (1998) or Tuzet et al. (2003), other traits related to hydraulics and water-use efficiency may be more important. Even

given the limitation of only having one environmental filter or driver, important predictors of mortality, such as  $H_{max}$ , are known to be predictive of mortality as shown by empirical studies in the tropics (Wright et al. 2010, Ruger et al. 2012).

Overall, the most meaningful findings are with respect to the multidimensional nature of the TTS. When filtered by light stress, both surviving and dead trees had a subset of traits significantly correlated with other functional traits, indicating potentially important tradeoffs. For example, stepwise regression models treating  $\varepsilon$  as dependent variable (trait) on the 31 other traits and light, yielded  $R^2$  values of 38% and 63% for surviving and dead trees, respectively (Table S4.7 and S4.8). In the context of coexistence theory, the wide range of trait values in surviving trees could help explain how species with very different traits can both be successful in the same environment. If many axes of variation, differential responses to axes of variation, or some degree of environmental heterogeneity (Hutchinson 1957, Tilman 2004) are needed to explain coexistence (Tilman 1985), then the multidimensional nature of the TTS seems to imply that there are many potential ways for trees or species to respond to a given environment. These findings also relate to evolutionary theory with respect to the tradeoffs found between traits. For example, if a species is characterized by high specific leaf area (SLA; e.g., thinner leaves), this could imply a faster senescence rate and greater leaf respiration per unit leaf area (Wright et al. 2004) (Table 3.5). However, one should not expect to find a tree with both high xylem conducting area ratio and dense wood (Table 3.5) because of potential engineering tradeoffs. Thus, there are many potential combinations of traits that may allow a specific tree, or species to cope with the environment, but each species'

functional traits are constrained by tradeoffs between other traits, similarly to what is seen in the TTS.

Finally, my work could help guide future empirical and modeling studies. For example, several traits emerged as being important predictors of mortality and/or that played important roles in trait-trait tradeoffs. Some of these traits (e.g., related to root function and senescence rates of long-lived tissues) are rarely measured in the field, but perhaps should be considered in combination with other commonly measured traits. Future work aimed at understanding the TTS could provide explicit information at the species level – here, the TTS is representative of a “generic” North American tree – by applying the techniques described in Chapter 3 to data pooled across individuals, within a species (rather than across all species). I anticipate that the TTS will differ among species, especially those with distinctly different life-history characteristics and stress-tolerance strategies.

## References

- Cano, F. J., D. Sánchez-Gómez, J. Rodríguez-Calcerrada, C. R. Warren, L. Gil, and I. Aranda. 2013. Effects of drought on mesophyll conductance and photosynthetic limitations at different tree canopy layers. *Plant, Cell & Environment* 36:1961–1980.
- Chave, J., D. Coomes, S. Jansen, S. L. Lewis, N. G. Swenson, and A. E. Zanne. 2009. Towards a worldwide wood economics spectrum. *Ecology Letters* 12:351–366.
- Crous, K. Y., and D. S. Ellsworth. 2004. Canopy position affects photosynthetic adjustments to long-term elevated CO<sub>2</sub> concentration (FACE) in aging needles in a mature *Pinus taeda* forest. *Tree Physiology* 24:961–970.
- Farquhar, G. D., S. Caemmerer, and J. A. Berry. 1980. A biochemical model of photosynthetic CO<sub>2</sub> assimilation in leaves of C<sub>3</sub> species. *Planta* 149:78–90.
- Fyllas, N. M., E. Gloor, L. M. Mercado, S. Sitch, C. A. Quesada, T. F. Domingues, D. R. Galbraith, A. Torre-Lezama, E. Vilanova, H. Ramírez-Angulo, N. Higuchi, D. A. Neill, M. Silveira, L. Ferreira, G. a. Aymard C., Y. Malhi, O. L. Phillips, and J. Lloyd. 2014. Analysing Amazonian forest productivity using a new individual and trait-based model (TFS v.1). *Geoscientific Model Development* 7:1251–1269.
- Hutchinson, G. E. 1957. Concluding remarks. *Cold Spring Harbor Symposia on Quantitative Biology* 22:415–427.
- Kattge, J., K. Ogle, G. Bönisch, S. Díaz, S. Lavorel, J. Madin, K. Nadrowski, S. Nöllert, K. Sartor, and C. Wirth. 2011. A generic structure for plant trait databases. *Methods in Ecology and Evolution* 2:202–213.
- Ogle, K., J. Barber, and K. Sartor. 2013. Feedback and Modularization in a Bayesian Meta-analysis of Tree Traits Affecting Forest Dynamics. *Bayesian Analysis* 8:133–168.
- Ogle, K., and S. W. Pacala. 2009. A modeling framework for inferring tree growth and allocation from physiological, morphological and allometric traits. *Tree Physiology* 29:587–605.
- Ogle, K., S. Pathikonda, K. Sartor, J. W. Lichstein, J. L. D. Osnas, and S. W. Pacala. 2014. A model-based meta-analysis for estimating species-specific wood density and identifying potential sources of variation. *Journal of Ecology* 102:194–208.
- Peltier, D. M. P., and I. Ibáñez. 2014. Patterns and variability in seedling carbon assimilation: Implications for tree recruitment under climate change. *Tree Physiology* 35:71–85.

- Ruger, N., C. Wirth, S. J. Wright, and R. Condit. 2012. Functional traits explain light and size response of growth rates in tropical tree species. *Ecology* 93:2626–2636.
- Shugart, H. H., and F. I. Woodward. 2011. *Global Change and the Terrestrial Biosphere, Achievements and Challenges*. John Wiley & Sons.
- Sperry, J. S., F. R. Adler, G. S. Campbell, and J. P. Comstock. 1998. Limitation of plant water use by rhizosphere and xylem conductance: results from a model. *Plant, Cell & Environment* 21:347–359.
- Tilman, D. 1985. The resource-ratio hypothesis of plant succession. *American Naturalist* 125:827–852.
- Tilman, D. 2004. Niche tradeoffs, neutrality, and community structure: a stochastic theory of resource competition, invasion, and community assembly. *Proceedings of the National Academy of Sciences of the United States of America* 101:10854–10861.
- Tuzet, A., A. Perrier, and R. Leuning. 2003. A coupled model of stomatal conductance, photosynthesis and transpiration. *Plant, Cell and Environment* 26:1097–1116.
- Wright, I. J., P. B. Reich, M. Westoby, D. D. Ackerly, Z. Baruch, F. Bongers, J. Cavender-Bares, T. Chapin, J. H. C. Cornelissen, M. Diemer, J. Flexas, E. Garnier, P. K. Groom, J. Gulias, K. Hikosaka, B. B. Lamont, T. Lee, W. Lee, C. Lusk, J. J. Midgley, M.-L. Navas, U. Niinemets, J. Oleksyn, N. Osada, H. Poorter, P. Poot, L. Prior, V. I. Pyankov, C. Roumet, S. C. Thomas, M. G. Tjoelker, E. J. Veneklaas, and R. Villar. 2004. The worldwide leaf economics spectrum. *Nature* 428:821–827.
- Wright, S. J., K. Kitajima, N. J. B. Kraft, P. B. Reich, I. J. Wright, D. E. Bunker, R. Condit, J. W. Dalling, S. J. Davies, S. Díaz, B. M. J. Engelbrecht, K. E. Harms, S. P. Hubbell, C. O. Marks, M. C. Ruiz-Jaen, C. M. Salvador, and A. E. Zanne. 2010. Functional traits and the growth — mortality trade-off in tropical trees. *Ecology* 91:3664–3674.

APPENDIX A  
SUPPLEMENTAL TABLES AND FIGURES REGARDING MESOPHYLL  
CONDUCTANCE

**Table S2.1:** Prior distributions specified for model parameters; normal distributions were use for most parameters, with the following prior mean and standard deviations. The exceptions were  $\beta$  and  $\varphi_{max}$  which were given beta distributions.

Parameter	Prior	Type
$\mu g_m$	<i>Normal</i> (0, 10)*	SI
$\mu R_d$	<i>Normal</i> (0, 10)*	SI
$\mu J_{max}$	<i>Normal</i> (0, 100)*	SI
$\mu V_{cmax}$	<i>Normal</i> (0, 100)*	SI
$E_{Rd}$	<i>Normal</i> (63.90, 4.47)	I
$E_{Vcmax}$	<i>Normal</i> (65.48, 4.47)	I
$E_{Jmax}$	<i>Normal</i> (50.13, 4.47)	I
$E_{gm}$	<i>Normal</i> (49.6, 4.47)	I
$E_{\Gamma^*}$	<i>Normal</i> (26.84, 4.47)	I
$E_{Kc}$	<i>Normal</i> (70.37, 4.47)	I
$E_{Ko}$	<i>Normal</i> (29.83, 4.47)	I
$S_v$	<i>Normal</i> (00.650, 0.14)	I
$H_v$	<i>Normal</i> (200, 4.47)	I
$S_j$	<i>Normal</i> (0.643, 0.14)	I
$H_j$	<i>Normal</i> (200, 4.47)	I
$\Gamma_{25}^*$	<i>Normal</i> (3.6, 0.32)	I
$K_{c25}$	<i>Normal</i> (27.238, 1)	I
$K_{o25}$	<i>Normal</i> (16582, 316.23)	I
$\beta$	<i>Beta</i> (10, 10)	I
$\varphi_{max}$	<i>Beta</i> (16, 4)	I

Priors specified with a mean of 0 and a standard deviation of 100 are relatively non-informative; the remaining priors are semi-informative with means and standard deviations derived from the literature based on Patrick *et al.* (2009). \*These prior distributions were truncated at zero such that the parameters were constrained to be

positive values. The two beta distributions used were informative priors based on the literature.

**Table S2.2:** Artificial Data Parameters

Parameter	Acer	Larrea	Tobacco	Source
$\alpha$	0.85	0.85	0.85	von Caemmerer 2000 (von Caemmerer 2000)
$\theta$	0.7	0.7	0.7	von Caemmerer 2000 (von Caemmerer 2000)
$f$	0.15	0.15	0.15	Evans 1987 (Evans 1987)
$g_m$	1.67	6	4.5	Manter and Kerrigan 2004, Patrick <i>et al.</i> 2009, Yamori <i>et al.</i> 2010 (Manter and Kerrigan 2004, Patrick <i>et al.</i> 2009, Yamori <i>et al.</i> 2010) Turnbull <i>et al.</i> 2002, Patrick <i>et al.</i> 2009, Yamori <i>et</i>
$V_{cmax}$	43.8	70	122.9	<i>al.</i> 2010 (Turnbull <i>et al.</i> 2002, Patrick <i>et al.</i> 2009, Yamori <i>et al.</i> 2010) Turnbull <i>et al.</i> 2002, Patrick <i>et al.</i> 2009, Yamori <i>et</i>
$J_{max}$	109	112	159.6	<i>al.</i> 2009 (Turnbull <i>et al.</i> 2002, Patrick <i>et al.</i> 2009, Yamori <i>et al.</i> 2010) Weston and Bauerle 2013, Patrick <i>et al.</i> 2009,
$R_d$	0.45	3.5	3.9	Yamori <i>et al.</i> 2010 (Weston and Bauerle 2007, Patrick <i>et al.</i> 2009, Yamori <i>et al.</i> 2010) von Caemmerer 2000 , Patrick <i>et al.</i> 2009, von
$K_c$	26	30.34	26.34	Caemmerer 2000 (von Caemmerer 2000, Patrick <i>et</i> <i>al.</i> 2009) von Caemmerer 2000, Patrick <i>et al.</i> 2009, von
$K_o$	17900	16590	16582	Caemmerer 2000 (von Caemmerer 2000, Patrick <i>et</i> <i>al.</i> 2009) von Caemmerer 2000, Patrick <i>et al.</i> 2009, von
$\Gamma^*$	3.9	5.76	3.9	Caemmerer 2000 (von Caemmerer 2000, Patrick <i>et</i> <i>al.</i> 2009)
$P$	101.325	101.325	101.325	Sea level (constant)
$\beta$	0.5	0.5	0.5	Commonly Assumed

**Table S2.3:** CI widths for full (including  $\phi PSI$  data) and reduced (excluding  $\phi PSI$  data) models. The values were calculated as the 95% BCI – 2.5% BCI for each of the values shown in Fig 6 (n=7 per variable). The greatest difference in BCI widths is seen in  $g_m$  followed by  $J_{max}$  while there is less of an effect seen in  $V_{cmax}$  where the intervals are only slightly higher for the full model and Rd where the intervals are slightly wider for the full model.

	Mean	Median	1st Qu.	3rd Qu.	Min	Max
<b><math>g_{m25}</math></b>						
Full	9.981	5.265	3.772	14.46	2.458	25.69
reduced	17.96	20.29	15.89	21.11	8.274	23.13
<b><math>R_{d25}</math></b>						
Full	3.1949	2.73	2.258	4.194	1.781	4.631
reduced	2.926	2.714	2.448	3.726	1.241	4.177
<b><math>V_{cmax25}</math></b>						
Full	179.4	173.7	161.1	188.5	148.5	234.4
reduced	199.3	184.9	168.3	238.2	149.4	247.9
<b><math>J_{max25}</math></b>						
full	98.07	102.8	63.06	126	56.96	148.5
reduced	141.4	123.3	115.4	138	98.38	260.4

**Table S2.4:** Posterior estimates for terminal nodes

<b>parameter</b>	<b>species</b>	<b>site</b>	<b>mean</b>	<b>sd</b>	<b>2.5% BCI</b>	<b>97.5% BCI</b>
<i>g<sub>m25</sub></i>	<i>P. velutina</i>	McDowell	3.85	1.36	1.95	7.22
<i>g<sub>m25</sub></i>	<i>P. velutina</i>	Sycamore Lowland	12.56	6.52	4.36	30.05
<i>g<sub>m25</sub></i>	<i>S. gooddingii</i>	Sycamore Lowland	14.08	5.03	6.24	26.51
<i>g<sub>m25</sub></i>	<i>Q. gambelii</i>	Chevelon Lowland	4.30	2.13	1.19	9.83
<i>g<sub>m25</sub></i>	<i>J. monosperma</i>	Chevelon Lowland	1.36	1.07	0.14	4.11
<i>g<sub>m25</sub></i>	<i>J. monosperma</i>	Chevelon Upland	1.46	0.93	0.20	3.78
<i>g<sub>m25</sub></i>	<i>P. velutina</i>	Sycamore Upland	0.75	1.24	0.14	2.60
<i>R<sub>d25</sub></i>	<i>P. velutina</i>	McDowell	2.63	0.53	1.62	3.70
<i>R<sub>d25</sub></i>	<i>P. velutina</i>	Sycamore Lowland	2.66	0.62	1.42	3.86
<i>R<sub>d25</sub></i>	<i>S. gooddingii</i>	Sycamore Lowland	0.74	0.48	0.07	1.86
<i>R<sub>d25</sub></i>	<i>Q. gambelii</i>	Chevelon Lowland	3.97	1.17	1.75	6.38
<i>R<sub>d25</sub></i>	<i>J. monosperma</i>	Chevelon Lowland	4.88	1.11	2.82	7.13
<i>R<sub>d25</sub></i>	<i>J. monosperma</i>	Chevelon Upland	8.43	1.02	6.40	10.48
<i>R<sub>d25</sub></i>	<i>P. velutina</i>	Sycamore Upland	2.68	0.70	1.35	4.08
<i>V<sub>cmax25</sub></i>	<i>P. velutina</i>	McDowell	212.03	48.80	152.65	349.18
<i>V<sub>cmax25</sub></i>	<i>P. velutina</i>	Sycamore Lowland	156.29	46.89	93.83	274.33
<i>V<sub>cmax25</sub></i>	<i>S. gooddingii</i>	Sycamore Lowland	133.71	42.36	81.00	229.50
<i>V<sub>cmax25</sub></i>	<i>Q. gambelii</i>	Chevelon Lowland	225.64	39.38	153.70	307.15
<i>V<sub>cmax25</sub></i>	<i>J. monosperma</i>	Chevelon Lowland	152.37	44.75	78.51	252.20
<i>V<sub>cmax25</sub></i>	<i>J. monosperma</i>	Chevelon Upland	187.07	45.23	121.10	289.95
<i>V<sub>cmax25</sub></i>	<i>P. velutina</i>	Sycamore Upland	176.04	59.12	57.91	292.35
<i>J<sub>max25</sub></i>	<i>P. velutina</i>	McDowell	118.87	16.84	86.65	152.50
<i>J<sub>max25</sub></i>	<i>P. velutina</i>	Sycamore Lowland	124.08	14.93	94.15	154.43
<i>J<sub>max25</sub></i>	<i>S. gooddingii</i>	Sycamore Lowland	113.00	14.45	84.94	141.90

$J_{max25}$	<i>Q. gambelii</i>	Chevelon Lowland	165.94	30.27	108.38	228.45
$J_{max25}$	<i>J. monosperma</i>	Chevelon Lowland	145.06	34.98	79.63	211.60
$J_{max25}$	<i>J. monosperma</i>	Chevelon Upland	167.89	26.66	117.40	220.23
$J_{max25}$	<i>P. velutina</i>	Sycamore Upland	172.11	39.57	101.30	249.80
$E_r$	<i>P. velutina</i>	McDowell	53.98	4.44	45.48	62.38
$E_r$	<i>P. velutina</i>	Sycamore Lowland	64.32	4.50	55.58	73.07
$E_r$	<i>S. gooddingii</i>	Sycamore Lowland	63.91	4.50	55.09	72.59
$E_r$	<i>Q. gambelii</i>	Chevelon Lowland	62.47	4.46	53.89	71.10
$E_r$	<i>J. monosperma</i>	Chevelon Lowland	62.29	4.62	53.19	71.47
$E_r$	<i>J. monosperma</i>	Chevelon Upland	61.22	4.43	52.65	70.01
$E_r$	<i>P. velutina</i>	Sycamore Upland	63.38	4.51	54.35	71.94
$E_v$	<i>P. velutina</i>	McDowell	65.79	3.73	59.02	70.91
$E_v$	<i>P. velutina</i>	Sycamore Lowland	65.75	4.36	57.03	74.22
$E_v$	<i>S. gooddingii</i>	Sycamore Lowland	65.48	4.62	56.78	74.40
$E_v$	<i>Q. gambelii</i>	Chevelon Lowland	71.47	3.28	60.34	73.90
$E_v$	<i>J. monosperma</i>	Chevelon Lowland	66.44	5.13	60.64	74.16
$E_v$	<i>J. monosperma</i>	Chevelon Upland	65.57	4.50	56.63	74.27
$E_v$	<i>P. velutina</i>	Sycamore Upland	65.66	4.49	56.90	74.44
$E_j$	<i>P. velutina</i>	McDowell	52.99	6.36	41.30	60.96
$E_j$	<i>P. velutina</i>	Sycamore Lowland	49.96	4.50	40.98	58.71
$E_j$	<i>S. gooddingii</i>	Sycamore Lowland	49.03	3.98	40.39	56.01
$E_j$	<i>Q. gambelii</i>	Chevelon Lowland	48.98	1.57	45.27	51.59
$E_j$	<i>J. monosperma</i>	Chevelon Lowland	51.90	3.18	47.91	58.80
$E_j$	<i>J. monosperma</i>	Chevelon Upland	50.21	4.55	41.26	59.23
$E_j$	<i>P. velutina</i>	Sycamore Upland	49.87	4.39	41.09	58.42
$E_m$	<i>P. velutina</i>	McDowell	47.89	4.50	39.17	56.39

$E_m$	<i>P. velutina</i>	Sycamore Lowland	49.53	4.51	40.71	58.37
$E_m$	<i>S. gooddingii</i>	Sycamore Lowland	49.67	4.43	40.84	58.40
$E_m$	<i>Q. gambelii</i>	Chevelon Lowland	49.08	4.50	40.32	57.89
$E_m$	<i>J. monosperma</i>	Chevelon Lowland	49.09	4.54	40.10	57.66
$E_m$	<i>J. monosperma</i>	Chevelon Upland	48.90	4.50	39.95	57.68
$E_m$	<i>P. velutina</i>	Sycamore Upland	49.05	4.39	40.28	57.58
$\Gamma^*_{25}$	<i>P. velutina</i>	Species level	3.39	0.15	3.10	3.69
$\Gamma^*_{25}$	<i>S. gooddingii</i>	Species level	2.92	0.27	2.41	3.45
$\Gamma^*_{25}$	<i>Q. gambelii</i>	Species level	3.00	0.27	2.49	3.55
$\Gamma^*_{25}$	<i>J. monosperma</i>	Species level	4.20	0.28	3.66	4.76
$K_{c25}$	<i>P. velutina</i>	Species level	26.98	1.01	25.01	28.96
$K_{c25}$	<i>S. gooddingii</i>	Species level	27.08	1.08	24.86	29.06
$K_{c25}$	<i>Q. gambelii</i>	Species level	26.96	1.05	24.85	28.97
$K_{c25}$	<i>J. monosperma</i>	Species level	27.02	1.01	25.04	29.01
$K_{o25}$	<i>P. velutina</i>	Species level	16859.61	78.90	16730.00	16990.00
$K_{o25}$	<i>S. gooddingii</i>	Species level	16812.26	345.01	16250.00	17512.50
$K_{o25}$	<i>Q. gambelii</i>	Species level	16922.22	198.58	16560.00	17210.00
$K_{o25}$	<i>J. monosperma</i>	Species level	17019.62	403.51	16450.00	17640.00
$E_g$	<i>P. velutina</i>	Species level	28.45	1.39	25.72	31.13
$E_g$	<i>S. gooddingii</i>	Species level	26.68	1.42	23.90	29.44
$E_g$	<i>Q. gambelii</i>	Species level	26.60	1.41	23.88	29.32
$E_g$	<i>J. monosperma</i>	Species level	26.99	1.41	24.21	29.74
$E_{kc}$	<i>P. velutina</i>	Species level	70.38	1.42	67.56	73.14
$E_{kc}$	<i>S. gooddingii</i>	Species level	70.30	1.42	67.51	73.04
$E_{kc}$	<i>Q. gambelii</i>	Species level	70.34	1.42	67.52	73.16
$E_{kc}$	<i>J. monosperma</i>	Species level	70.32	1.44	67.52	73.12

$E_{ko}$	<i>P. velutina</i>	Species level	29.86	1.38	27.10	32.56
$E_{ko}$	<i>S. gooddingii</i>	Species level	29.87	1.41	27.12	32.57
$E_{ko}$	<i>Q. gambelii</i>	Species level	29.83	1.40	27.13	32.52
$E_{ko}$	<i>J. monosperma</i>	Species level	29.88	1.41	27.14	32.57
$S_v$	<i>P. velutina</i>	Species level	0.53	0.09	0.30	0.64
$S_v$	<i>S. gooddingii</i>	Species level	0.60	0.12	0.36	0.86
$S_v$	<i>Q. gambelii</i>	Species level	0.56	0.11	0.34	0.83
$S_v$	<i>J. monosperma</i>	Species level	0.54	0.09	0.33	0.64
$H_v$	<i>P. velutina</i>	Species level	199.31	3.16	193.60	208.20
$H_v$	<i>S. gooddingii</i>	Species level	201.19	4.38	193.60	209.00
$H_v$	<i>Q. gambelii</i>	Species level	192.84	2.27	189.40	199.10
$H_v$	<i>J. monosperma</i>	Species level	198.25	3.06	192.60	206.30
$S_j$	<i>P. velutina</i>	Species level	0.56	0.09	0.35	0.66
$S_j$	<i>S. gooddingii</i>	Species level	0.54	0.09	0.33	0.65
$S_j$	<i>Q. gambelii</i>	Species level	0.65	0.05	0.48	0.68
$S_j$	<i>J. monosperma</i>	Species level	0.63	0.06	0.42	0.67
$H_j$	<i>P. velutina</i>	Species level	202.92	2.79	198.70	209.10
$H_j$	<i>S. gooddingii</i>	Species level	200.40	3.99	193.78	209.50
$H_j$	<i>Q. gambelii</i>	Species level	201.56	4.03	195.40	206.80
$H_j$	<i>J. monosperma</i>	Species level	201.86	2.11	198.50	206.10

---

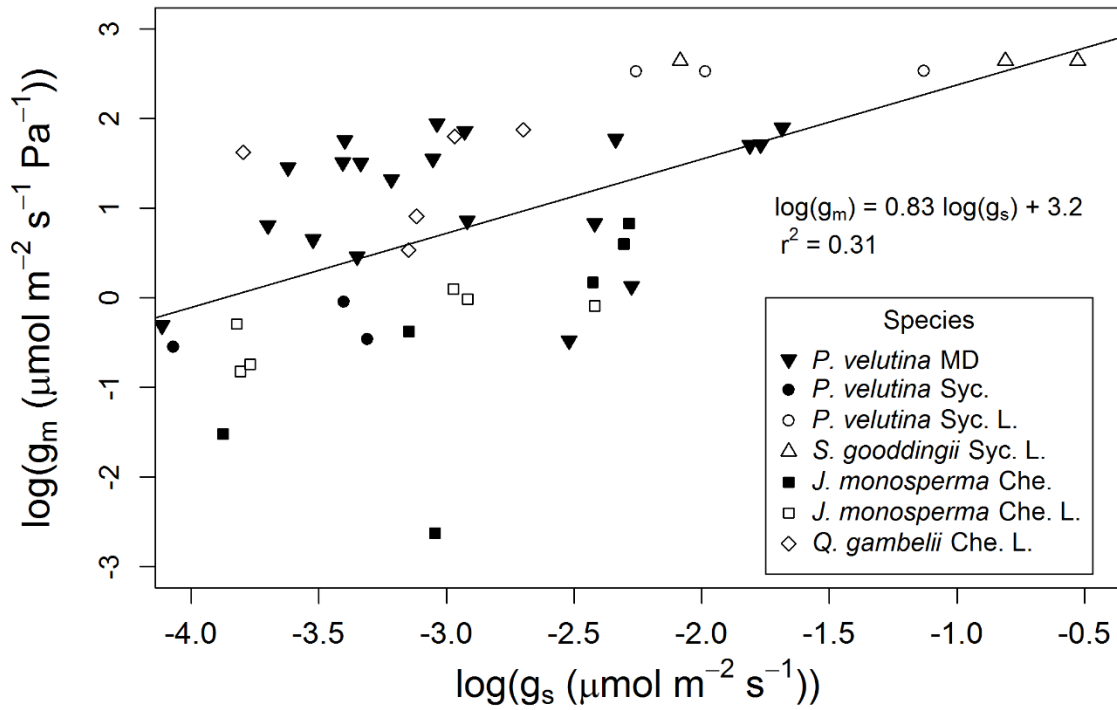


**Figure S2.1:** Log transformed posterior means for curve level predicted  $g_m$  vs log transformed  $g_s$  (measured by the licor) at ambient  $\text{CO}_2$  (400 ppm) and saturating light ( $1500 \mu\text{mol photons m}^{-2} \text{s}^{-1}$ ). The data were log transformed to avoid outliers with high leverage. A weak positive trend ( $r^2 = 0.31$ ) was found between log transformed  $g_s$  and  $g_m$ . Both the intercept and slope parameters were significant with  $P < 0.001$ .

## References

- von Caemmerer, S. 2000. *Biochemical Models of Leaf Photosynthesis*. Brown Prior Anderson, Collingwood.
- Evans, J. 1987. The Dependence of Quantum Yield on Wavelength and Growth Irradiance. *Functional Plant Biology* 14:69–79.
- Manter, D. K., and J. Kerrigan. 2004. A/C(i) curve analysis across a range of woody plant species: influence of regression analysis parameters and mesophyll conductance. *Journal of Experimental Botany* 55:2581–8.
- Patrick, L. D., K. Ogle, and D. T. Tissue. 2009. A hierarchical Bayesian approach for estimation of photosynthetic parameters of C(3) plants. *Plant, Cell & Environment* 32:1695–1709.
- Turnbull, M. H., D. Whitehead, D. T. Tissue, W. S. F. Schuster, K. J. Brown, V. C. Engel, and K. L. Griffin. 2002. Photosynthetic characteristics in canopies of *Quercus rubra*, *Quercus prinus* and *Acer rubrum* differ in response to soil water availability. *Oecologia* 130:515–524.
- Weston, D. J., and W. L. Bauerle. 2007. Inhibition and acclimation of C(3) photosynthesis to moderate heat: a perspective from thermally contrasting genotypes of *Acer rubrum* (red maple). *Tree Physiology* 27:1083–92.
- Yamori, W., J. R. Evans, and S. von Caemmerer. 2010. Effects of growth and measurement light intensities on temperature dependence of CO(2) assimilation rate in tobacco leaves. *Plant, Cell & Environment* 33:332–43.

## APPENDIX B

### ADDITIONAL MODEL DETAILS AND CODE

This appendix aims to provide a simple means of relating the equations in the paper to the code provided for the model. Each equation in the paper and below can be easily linked with the provided code for OpenBUGS.

Eqns. 1-6 in the main text, and eqn. 1-4 in table 3, explain the version of the FvCB model used. Multiple parameters from these equations are modeled hierarchically as indicated in eqn. 9 and 10. Below we explicitly state the equations used for each parameter given by  $Y_{25_c} = R_{d25}, g_{m25}, V_{cmax25}$ , or  $J_{max25}$  given more generally in eqn. 9 where  $c$  indexes the curve ( $c = 1, \dots, 46$ ). These curve-level parameters were assumed to vary around plant-level mean parameters such that for plant  $p$  ( $p = 1, \dots, 23$ ) as discussed in the main text:

$$R_{d25_c} = Normal\left(\mu R_{d25_p}, \sigma_{R_{d25}}^2\right) \quad 1S.$$

$$g_{m25_c} = Normal\left(\mu g_{m25_p}, \sigma_{g_{m25}}^2\right) \quad 2S.$$

$$V_{cmax25_c} = Normal\left(\mu V_{cmax25_p}, \sigma_{V_{cmax25}}^2\right) \quad 3S.$$

$$J_{max25_c} = Normal\left(\mu J_{max25_p}, \sigma_{J_{max25}}^2\right) \quad 4S.$$

Eqn. 10 described generally how each of the above plant level means varied around a species by site level mean parameter where  $st$  ( $st=1, \dots, 7$ ) as discussed in the main text:

$$\mu R_{d25_p} = Normal\left(\mu^* R_{d25_{st}}, \sigma_{R_{d25}}^{2*}\right) \quad 5S.$$

$$\mu g_{m25_p} = Normal\left(\mu^* R_{d25_{st}}, \sigma_{R_{d25}}^{2*}\right) \quad 6S.$$

$$\mu V_{cmax25_p} = Normal\left(\mu^* R_{d25_{st}}, \sigma_{R_{d25}}^{2*}\right) \quad 7S.$$

$$\mu J_{max25_p} = Normal\left(\mu^* R_{d25_{st}}, \sigma_{R_{d25}}^{2*}\right) \quad 8S.$$

Model Code: This code implements the HB model in OpenBUGS. OpenBUGS is free software and can be obtained from [www.openbugs.net](http://www.openbugs.net).

```

# Model begins here
Model {
  for (i in 1:N){

    # Likelihood for observed photosynthesis data (eqn. 7)
    Aobs[i] ~ dnorm(mu.A[i],tau.A)

    # Generate predicted data to calculate posterior predictive loss
    (D)
    Arep[i]~dnorm(mu.A[i],tau.A)
    Dsq[i]<-pow((Aobs[i]-Arep[i]),2)

    # Generate predicted logitPhiPSII
    logitPhiPSIIrep[i]~dnorm(mu.logit.PhiPSII[i], tau.PSII)
    PhiPSIIrep[i]<-
    exp(logitPhiPSIIrep[i])/(1+exp(logitPhiPSIIrep[i]))

    # Convert Ci and O from the Li-6400 into partial pressure using
    ambient #pressure
    CiP[i]<-Ci[i]*(Pressure[i]/1000)
    O[i]<-(21/100)*(Pressure[i]*1000)

    # mu.A is either limited by carboxylation or electron transport
    or the # constraint mentioned in Gu et al 2010. The constraint
    in Gu et al
    # 2010 makes sure the correct limitation state is chosen at low
    [CO2]. # (eqn. 1 top)
    mu.Atemp[i] <- min(Wc[i],Wj[i])

    # Cc is needed for the below step and is temporary in that it is
    not
    # useful for analysis and does not need to be monitored. (eqn. 1
    # bottom)
    Cc.temp[i] <- CiP[i]-mu.Atemp[i]/gi2[i]

    # When step(Gstar2[i]-Cc.temp[i]) is < 0) the expression
    evaluates to
    # 0. This takes care of the case where Cc < Gstar2. (eqn. 1
    bottom)
    mu.A[i] <- step(Gstar2[i]-Cc.temp[i])*Wc[i]+step(Cc.temp[i]-
    Gstar2[i])*mu.Atemp[i]

    # if limited by carboxylation (quadratic incorporating mesophyll
    # conductance) (eqn. 2 and Table 3 eqn. 1)
    Wc[i]<- (-b1[i]+sqrt(max(b24ac1[i],0)))/(2*a1[i])
    b24ac1[i]<-pow(b1[i],2)-(4*a1[i]*c1[i])
    a1[i]<-(-1/gi2[i])
    b1[i]<-(Vcmax2[i]-Rday[i])/gi2[i]+CiP[i]+Kc2[i]*(1+O[i]/Ko2[i])
    c1[i]<-Rday[i]*(CiP[i]+Kc2[i]*(1+O[i]/Ko2[i]))-Vcmax2[i]*(CiP[i]-
    Gstar2[i])
  }
}

```

```

# if limited by electron transport (quadratic incorporating
mesophyll
# conductance) (eqn. 3 and Table 3 eqn. 2)
Wj[i]<- (-b2[i]+sqrt(max(b24ac2[i],0)))/(2*a2[i])
b24ac2[i]<-pow(b2[i],2)-(4*a2[i]*c2[i])
a2[i]<-(-1/gi2[i])
b2[i]<-((J[i]/4)-Rday[i])/gi2[i]+CiP[i]+2*Gstar2[i]
c2[i]<-Rday[i]*(CiP[i]+2*Gstar2[i])-(J[i]/4)*(CiP[i]-Gstar2[i])

# Mean model to incorporate Fluorescence data as well as the
logit
# transformation used.
logit.PhiPSII[i] <- log((PhiPSII[i])/(1-PhiPSII[i]))
logit.PhiPSII[i] ~ dnorm(mu.logit.PhiPSII[i], tau.PSII)
mu.logit.PhiPSII[i] <- log((mu.PhiPSII[i])/(1-mu.PhiPSII[i])) #
convert to PhiPSII scale from logit scale
# This line comes from the function for ETR where ETR =
J*alpha*beta*Q # (eqn. 6)
mu.PhiPSII[i] <-
J[i]/(Q[i]*alpha[i]*Beta[stind[Plant[Curve[i]]]]+(equals(Q[i],0)))+(equ
als(Q[i],0)*Phimax)

# Calculate J (rate of electron transport) (eqn. 4 and Table 3
eqn. 3)
J[i]<-(Q2[i]+Jmax2[i]-(sqrt(max(F[i],0))))/(2*Qtheta)
F[i]<-pow(Q2[i]+Jmax2[i],2)-4*Qtheta*Q2[i]*Jmax2[i]
Q2[i]<-Q[i]*alpha[i]*(1-f)*Beta[stind[Plant[Curve[i]]]]

# Specify which parameters to use from the A-Ci curve if
including A-Q
# curve data; i.e., cut function propagates uncertainty in
parameters, # informed by A-Ci data, to A-Q model equations.
eqAQ0[i] <- equals(AQ[i],0)
eqAQ1[i] <- equals(AQ[i],1)

Vcmax2[i] <- eqAQ0[i]*Vcmax[i] + eqAQ1[i]*cut.Vcmax[i]
cut.Vcmax[i]<-cut(Vcmax[i])

Jmax2[i] <- equals(AQ[i],0)*Jmax[i] + equals(AQ[i],1)*cut.Jmax[i]
cut.Jmax[i]<-cut(Jmax[i])

# Rday was used above so Rday2 is used here in the function.
# correct. The light response data alone informs Rday
Rday[i] <- equals(AQ[i],1)*Rday2[i] +
equals(AQ[i],0)*cut.Rday2[i]
cut.Rday2[i]<-cut(Rday2[i])

# Compute the common temperature "part" of the temperature
function
# once (Table 3, eqn. 4 for all temperature corrections other
than
# Vcmax and Jmax):
CTpart[i] <- exp((KTemp[i]-KTref)/(KTref*R*KTemp[i]))

#Temp correct gi (mesophyll conductance - gm in paper text)
gi2[i]<-gi25[Curve[i]]*exp((KTemp[i]-
KTref)*E7[stind[Plant[Curve[i]]]]/(KTref*R*KTemp[i]))

```

```

    # Temp correct Gstar (CO2 compensation point with
photorespiration)
    Gstar2[i]<-
Gstar25[species[Plant[Curve[i]]]]*pow(CTpart[i],E1[species[Plant[Curve[
i]]]])

    #Temp correct Rday (mitochondrial respiration rate in light)
    Rday2[i]<-
Rday25[Curve[i]]*pow(CTpart[i],E2[stind[Plant[Curve[i]]]])

    #Temp correct Kc and Ko (Michaelis constants for CO2 and O2)
    Kc2[i]<-
Kc25[species[Plant[Curve[i]]]]*pow(CTpart[i],E3[species[Plant[Curve[i]]
]])

    Ko2[i]<-Ko25[species[Plant[Curve[i]]]]*pow(CTpart[i],
E4[species[Plant[Curve[i]]]])

    # Temp correct Vcmax (maximum RuBP saturated rate of
carboxylation)
    # (Table 3, eqn. 5 for Vcmax and Jmax)
    Vcmax[i]<-
Vcmax25[Curve[i]]*firstexpv[i]*(topexpv[species[Plant[Curve[i]]]]/botto
mexpv[i])
    firstexpv[i]<- pow(CTpart[i], E5[stind[Plant[Curve[i]]]])
    bottomexpv[i]<-(1+exp((Sv[species[Plant[Curve[i]]]]*KTemp[i]-
Hv[species[Plant[Curve[i]]]])/(R*KTemp[i])))

    # Temp correct Jmax (maximum rate of electron transport)
    Jmax[i]<-
Jmax25[Curve[i]]*firstexp[i]*(topexp[species[Plant[Curve[i]]]]/bottomex
p[i])
    firstexp[i]<- pow(CTpart[i], E6[stind[Plant[Curve[i]]]])
    bottomexp[i]<-(1+exp((Sj[species[Plant[Curve[i]]]]*KTemp[i]-
Hj[species[Plant[Curve[i]]]])/(R*KTemp[i])))

} # End of the i loop

# To calculate the posterior predictive loss for model comparison
# uncomment the term below.
# D <- sum(Dsq[])

#topexpv and topexp only vary by species, so compute in species
loop
# (Table 3 Eqn 5):
for (s in 1:Nspecies){
    topexpv[s]<-(1+exp((KTref*Sv[s]-Hv[s])/(KTref*R)))
    topexp[s]<-(1+exp((KTref*Sj[s]-Hj[s])/(KTref*R)))
}

# Hierarchical priors for photosynthesis parameters
# Curve level parameters vary around plant-level parameters
# Eqn. 2S, 1S, 3S, 4S in descending order below.
for (c in 1:Ncurve){
    gi25Temp[c]~dnorm(mu.gi25[Plant[c]],tau.gi25)I(0,)

```

```

Rday25Temp[c]~dnorm(mu.Rday25[Plant[c]],tau.Rday25)I(0,)

Vcmax25Temp[c]~dnorm(mu.Vcmax25[Plant[c]],tau.Vcmax25)I(0,)

Jmax25Temp[c]~dnorm(mu.Jmax25[Plant[c]],tau.Jmax25)I(0,)

# Determine if there is only one curve per plant
eqcurve1[c] <- equals(onlycurve[c],1)
eqcurve0[c] <- equals(onlycurve[c],0)

# If only one curve for plant, use curve as plant-level mean
gi25[c] <- eqcurve1[c]*gi25Temp[c] +
eqcurve0[c]*mu.gi25[Plant[c]]

Rday25[c] <- eqcurve1[c]*Rday25Temp[c] +
eqcurve0[c]*mu.Rday25[Plant[c]]

Vcmax25[c] <- eqcurve1[c]*Vcmax25Temp[c] +
eqcurve0[c]*mu.Vcmax25[Plant[c]]

Jmax25[c] <- eqcurve1[c]*Jmax25Temp[c] +
eqcurve0[c]*mu.Jmax25[Plant[c]]

# Hierarchical priors for photosynthesis parameters.
# Plant level parameters vary around species-level parameters
# Eqn. 6S, 5S, 7S, 8S in descending order below.
for (p in 1:Nplant){
  mu.gi25[p]~dnorm(mu.gis[stind[p]],tau.gip)I(0,)

  mu.Rday25[p]~dnorm(mu.Rdayp[stind[p]],tau.Rdayp)I(0,)

  mu.Vcmax25[p]~dnorm(mu.Vcmaxp[stind[p]],tau.Vcmaxp)I(0,)

  mu.Jmax25[p]~dnorm(mu.Jmaxp[stind[p]],tau.Jmaxp)I(0,)
}

# Species and treatment-level parameters vary around population
# parameters. In this case the treatment is the region.
# All normal and beta priors are in Table S1.
for (s in 1:Nst){
  mu.gis[s]~dnorm(0,0.01)I(0,)
  mu.Rdayp[s]~dnorm(0,0.01)I(0,)
  mu.Vcmaxp[s]~dnorm(0,0.0001)I(0,)
  mu.Jmaxp[s]~dnorm(0,0.00001)I(0,)

  # Slightly informative, non-hierarchical priors for energy
  # of activation and kinetic constant parameters
  E2[s]~dnorm(63.90,0.05)
  E5[s]~dnorm(65.48,0.05)
  E6[s]~dnorm(50.13,0.05)
  E7[s]~dnorm(49.6,0.05)

  # Informative BETA prior for Beta
  Beta[s] ~ dbeta(10,10)
}

```

```

# prior with mean of 0.8 strongly informative
# This sets an upper bound on PhiPSII as light decreases
otherwise
# there is the potential to have the code fail if Q drops too
low.
Phimax ~ dbeta(16,4)

for(s in 1:Nspecies){
  E1[s]~dnorm(26.84,0.5)
  E3[s]~dnorm(70.37,0.5)
  E4[s]~dnorm(29.83,0.5)

  Sv[s]~dnorm(0.650,50)
  Hv[s]~dnorm(200,0.05)
  Sj[s]~dnorm(0.643,50)
  Hj[s]~dnorm(200,0.05)

  Gstar25[s]~dnorm(3.6,10)
  Kc25[s]~dnorm(27.238,1)
  Ko25[s]~dnorm(16582,0.00001)
}

KTref<-Tref+273.15

# Prior for "observation" variance
sig.A~dunif(0,5)
tau.A<-1/(sig.A*sig.A)
# Prior for PSII "observation" variance
sig.PSII~dunif(0,10)
tau.PSII<-1/(sig.PSII*sig.PSII)

# Priors for precisions (folded Cauchy)
for (k in 1:Nsig){
  sig[k]<-abs(w[k])/sqrt(t[k])
  w[k]~dnorm(0,1)
  t[k]~dgamma(0.5, beta[k])
  beta[k]<-A[k]*A[k]/2
}

# Set standard deviations and computes associated precisions
sig.gip<-sig[1]
tau.gip<-1/(sig.gip*sig.gip)

sig.Rdayp<-sig[2]
tau.Rdayp<-1/(sig.Rdayp*sig.Rdayp)

sig.Vcmaxp<-sig[3]
tau.Vcmaxp<-1/(sig.Vcmaxp*sig.Vcmaxp)

sig.Jmaxp<-sig[4]
tau.Jmaxp<-1/(sig.Jmaxp*sig.Jmaxp)

sig.gi25<-sig[5]
tau.gi25<-1/(sig.gi25*sig.gi25)

sig.Rday25<-sig[6]
tau.Rday25<-1/(sig.Rday25*sig.Rday25)

```

```

sig.Vcmax25<-sig[7]
tau.Vcmax25<-1/(sig.Vcmax25*sig.Vcmax25)

sig.Jmax25<-sig[8]
tau.Jmax25<-1/(sig.Jmax25*sig.Jmax25)

# Below is not necessary, but is provided for ease of monitoring
unknown
# parameters. Create "dummy" arrays to hold parameters of interest.
Monitor
# dummy arrays instead of each individual parameter.

for (p in 1:Ncurve){
  mu.c[1,p]<-gi25[p]
  mu.c[2,p]<-Rday25[p]
  mu.c[3,p]<-Vcmax25[p]
  mu.c[4,p]<-Jmax25[p]
}

for (p in 1:Nplant){
  mu.p[1,p]<-mu.gi25[p]
  mu.p[2,p]<-mu.Rday25[p]
  mu.p[3,p]<-mu.Vcmax25[p]
  mu.p[4,p]<-mu.Jmax25[p]
}

for (s in 1:Nst){
  mu.s[1,s]<-mu.gis[s]
  mu.s[2,s]<-mu.Rdayp[s]
  mu.s[3,s]<-mu.Vcmaxp[s]
  mu.s[4,s]<-mu.Jmaxp[s]
  mu.s[5,s]<-E2[s]
  mu.s[6,s]<-E5[s]
  mu.s[7,s]<-E6[s]
  mu.s[8,s]<-E7[s]
}

for (s in 1:Nspecies){
  mu.st[1,s]<-Gstar25[s]
  mu.st[2,s]<-Kc25[s]
  mu.st[3,s]<-Ko25[s]
  mu.st[4,s]<-E1[s]
  mu.st[5,s]<-E3[s]
  mu.st[6,s]<-E4[s]
  mu.st[7,s]<-Sv[s]
  mu.st[8,s]<-Hv[s]
  mu.st[9,s]<-Sj[s]
  mu.st[10,s]<-Hj[s]
}

sig.all[1]<-sig.gip
sig.all[2]<-sig.Rdayp
sig.all[3]<-sig.Vcmaxp
sig.all[4]<-sig.Jmaxp
sig.all[5]<-sig.A

```

```
sig.all[6]<-sig.PSII
```

```
} # END model
```

**DATA**

```
# Input the following data or constraints in addition to rectangular
array
# data below.
```

```
list(N=905, Nspecies=4, Ncurve=46, Nplant=23, R=0.008314, Qtheta=0.7,
Tref=25, f=0.15, Nsig=8, A=c(5,5,5,5,5,5,5,5,5), Nst=7)
```

```
# Rectangular array (may be read-in as a separate text file) with a
subset of # observational data from Li-cor 6400 used in paper. KTemp
is Leaf temp in
# Kelvin. AQ column designates the curve type, where AQ=0 are data
from an
# A-Ci curve and AQ=1 are data from an A-Q curve. PhiPSII comes from
the LI-
# 6400 with the fluorometer attachment.
```

Curve[]	AQ[]	Aobs[]	Ci[]	Temp[]	Q[]	Pressure[]	KTemp[]	ETR[]	alpha[]	PhiPSII[]
1	0	7.70	88.0	26.3	1502.3	94.93	299.47	160.6828	0.8499	0.2517
1	0	4.48	91.4	26.3	1500.7	94.93	299.47	145.9178	0.8499	0.2288
1	0	-0.08	79.0	26.3	1499.7	94.93	299.40	140.3830	0.8499	0.2203
1	0	5.09	102.6	26.3	1497.8	94.92	299.47	149.8853	0.8499	0.2355
1	0	11.18	172.6	26.7	1501.0	94.92	299.83	165.2896	0.8499	0.2591
1	0	13.65	302.7	26.8	1499.9	94.92	299.97	163.2264	0.8499	0.2561
1	0	13.91	430.3	27.2	1499.5	94.91	300.33	156.8055	0.8499	0.2461
1	0	13.50	786.4	27.2	1499.9	94.91	300.32	143.7504	0.8499	0.2255
1	0	13.72	972.8	27.6	1498.4	94.90	300.73	139.3076	0.8499	0.2188
1	0	14.52	1261.1	27.7	1497.6	94.91	300.87	150.2152	0.8499	0.2360
1	1	5.38	144.8	27.8	1499.3	94.92	300.98	158.2335	0.8499	0.2484
1	1	5.79	161.6	27.4	997.6	94.91	300.59	148.3602	0.8500	0.3499
1	1	5.98	187.9	27.2	801.3	94.91	300.33	140.0862	0.8501	0.4113
1	1	5.32	216.4	26.9	498.3	94.91	300.03	101.8373	0.8502	0.4808
1	1	2.71	289.5	26.4	201.6	94.91	299.58	47.5089	0.8504	0.5543
1	1	0.83	347.4	26.3	99.3	94.92	299.43	24.8919	0.8500	0.5900
1	1	-0.39	412.4	26.2	50.7	94.92	299.34	13.1055	0.8510	0.6069
1	1	-2.02	579.0	26.1	0.3	94.92	299.24	0.0735	0.8553	0.6516

...(more data)

END

Along with the above rectangular array and list, a few additional files are needed to relate each row in the rectangular array with the correct plant and treatments for the hierarchical structure to be used. The below

```
# This rectangular array relates each curve to the appropriate plant.  
Each  
# row corresponds to a specific curve so there is one row per curve  
# indicating which plant the curve went with and if it was the only  
curve for  
# that plant.
```

```
Plant[]      onlycurve[]  
1      1  
2      1  
3      1  
4      0  
5      0  
6      0  
7      0  
8      0  
9      0  
10     1  
... More rows  
END
```

```
# This vector relates each plant to the right species by site  
combination.  
# The values went from 1-7 for the data in the paper. The rows in this  
list  
# correspond to plants, so there is one row per plant.
```

```
species[]  
1  
1  
1  
1  
1  
1  
1  
2  
2  
2  
1  
... More rows  
END
```

APPENDIX C

SUPPLEMENTAL TABLES AND FIGURES REGARDING THE ACGCA TRAIT

SPACE

**Table S3.1:** Prior distributions used for each  $\theta_k$  in the Bayesian model. All priors are based on normal or truncated normal distributions. Prior means (mean and transmean) are based on a meta-analysis of the TreeTraits database. The standard deviation terms (sd and transsd) are the maximum of either the meta-analysis standard deviations or an inflated value that guaranteed that the parameter values used in Ogle and Pacala (2009) fell within the prior interquartile range defined by the 25<sup>th</sup> and 75<sup>th</sup> percentiles for each parameter’s prior. Mean and sd are on the untransformed scale (units as in Table 3.1); transmean and transsd are on the transformed scale indicated by “transform” (log is natural log).

Parameter	mean	sd	transsd	transmean	transform	truncated
$H_{\max}^\dagger$	29.412	7.543	0.313	3.339	log	yes
$\phi_H$	248.620	20.320	0.084	5.512	log	no
H	0.619	0.059	0.252	0.492	logit	yes
$SW_{\max}^\dagger$	0.050	0.004	0.080	-3.001	log	no
$\lambda_s^*$	0.950	0.000	0.200	-0.051	log	no
$\lambda_h^*$	0.950	0.000	0.200	-0.051	log	no
P	546599.611	10891.573	0.208	13.191	log	yes
$f_{1\ddagger}$	4151.002	872.144	0.231	8.306	log	no
$f_2^*$	4.000	0.000	1.028	1.386	log	no
$\Upsilon_C$	130211.284	77937.409	0.546	11.626	log	no
$\Upsilon_X^\dagger$	0.361	0.044	0.190	-0.575	logit	no
$C_{GL}$	1.456	0.062	0.044	0.375	log	no
$C_{GR}^\ddagger$	1.201	0.015	0.013	0.183	log	no
$C_{GW}$	1.418	0.026	0.019	0.349	log	no
$\delta_{L\ddagger}$	0.087	0.009	0.119	-2.360	logit	no
$\delta_{R^\dagger}$	0.059	0.005	0.094	-2.765	logit	no
$S_L$	1.264	0.819	0.979	-0.122	log	no
SLA	0.012	0.006	0.512	-4.512	log	no
$S_{R\ddagger}$	1.590	0.330	0.180	0.446	log	no
$S_O$	1.846	0.055	0.030	0.612	log	no
$r_{R^\dagger}$	3.29E-04	3.68E-05	0.108	-8.026	log	no
$\rho_R$	146460.965	45063.024	0.362	11.836	log	no
$R_{mL\ddagger}$	12.392	4.987	0.350	2.452	log	no
$R_{mS^\dagger\ddagger}$	1.447	0.380	0.283	0.331	log	no
$R_{mR^\dagger\ddagger}$	24.842	1.413	0.058	3.211	log	no
$\eta_B^*$	0.045	0.000	1.272	-3.055	logit	yes
$k^\dagger$	0.495	0.085	0.177	-0.719	log	no
$\varepsilon^\ddagger$	37.815	28.771	0.389	3.522	log	no
$m^*$	0.950	0.000	1.108	2.944	logit	no
$\alpha$	0.343	0.058	0.262	-0.661	logit	no
$R_0$	1.727	0.487	0.302	0.504	log	no
$R_{40}$	4.932	1.763	0.426	1.520	log	no

\* No data to inform *SD* value; † *SD* based on *Acer rubrum* or ‡ *SD* based on *Pinus taeda* (Ogle and Pacala 2009).

**Table S3.2:** Posterior estimates for all parameters ( $\theta_k$ ) in the ACGCA model, including posterior mean, median, standard deviation (sd), and the 95% credible interval defined by the 2.5<sup>th</sup> and 97.5<sup>th</sup> percentiles. Values are provided on the untransformed scale, with units corresponding to those given in Table 3.1.

<b>Parameter</b>	<b>mean</b>	<b>median</b>	<b>sd</b>	<b>2.50%</b>	<b>97.50%</b>
$H_{\max}$	32.90	31.40	9.07	19.65	54.66
$\phi_H$	248.91	248.00	20.68	210.78	292.12
$\eta$	0.64	0.63	0.07	0.54	0.92
$SW_{\max}$	0.04	0.04	0.01	0.02	0.08
$\lambda_s$	0.98	0.96	0.20	0.64	1.43
$\lambda_h$	0.96	0.95	0.19	0.64	1.40
$\rho$	494085.95	493300.00	69359.19	359527.01	630085.82
$f_1$	3730.19	3516.00	1284.64	1862.00	6796.27
$f_2$	4.61	2.72	7.01	0.41	19.59
$\gamma_C$	131754.86	113100.00	79168.49	38935.50	334706.36
$\gamma_X$	0.44	0.42	0.18	0.13	0.76
$C_{GL}$	1.46	1.45	0.06	1.34	1.58
$C_{GR}$	1.20	1.20	0.05	1.11	1.30
$C_{GW}$	1.42	1.42	0.03	1.37	1.47
$\delta_L$	0.09	0.09	0.01	0.07	0.11
$\delta_R$	0.07	0.06	0.03	0.02	0.15
$S_L$	1.30	0.84	1.57	0.12	5.26
$SLA$	0.01	0.01	0.01	0.00	0.03
$S_R$	1.80	1.53	1.13	0.49	4.81
$S_O$	0.14	0.10	0.14	0.01	0.50
$r_R$	0.00	0.00	0.00	0.00	0.00
$\rho_R$	140264.52	132100.00	51937.56	64121.23	264767.65
$R_{mL}$	11.86	7.07	14.55	0.71	51.24
$R_{mS}$	0.73	0.19	3.72	0.01	4.58
$R_{mR}$	23.33	9.01	47.16	0.44	137.77
$\eta_B$	0.06	0.03	0.07	0.00	0.25
$k$	0.49	0.48	0.09	0.33	0.68
$\epsilon$	25.43	18.63	20.40	4.60	81.70
$m$	0.92	0.95	0.08	0.69	0.99
$\alpha$	0.34	0.34	0.06	0.24	0.46
$R_0$	1.47	1.41	0.45	0.80	2.55
$R_{40}$	6.77	6.36	2.48	3.12	12.72

**Table S3.3:** Model fits (i.e., coefficient of determination,  $R^2$ ) obtained from the best subsets and stepwise regressions that included main effects and all two-way interactions (“w/ int”) or only main effects (“w/o int”). Within each regression approach, “Diff in  $R^2$ ” is the difference in the  $R^2$  between the model with and without interactions. Each best subsets regression approach only included 10 effects, while the stepwise regressions contain various numbers of parameters indicated by “#  $\theta$ s” in the table. Adjusted  $R^2$  values were approximately the same as the  $R^2$  values, and thus the simple (non-adjusted)  $R^2$  values are provide.

$\theta$	Best Subsets			Stepwise				
	w/ int $R^2$	w/o int $R^2$	Diff in $R^2$	w/ int $R^2$	# $\theta$ s	w/o int $R^2$	# $\theta$ s	Diff in $R^2$
$H_{\max}$	0.01	0.01	0.00	0.01	14	0.01	15	0.00
$\phi_H$	0.00	0.00	0.00	-	-	0.00	7	-
$\eta$	0.02	0.02	0.00	0.04	52	0.02	17	0.02
$SW_{\max}$	0.12	0.10	-0.02	0.15	44	0.11	21	0.04
$\lambda_s$	0.01	0.01	0.00	0.01	11	0.01	11	0.00
$\lambda_h$	0.01	0.01	0.00	0.01	6	0.01	5	0.00
$\rho$	0.07	0.07	-0.01	0.07	16	0.07	15	0.01
$f_2$	0.08	0.08	0.00	0.12	56	0.09	15	0.03
$f_1$	0.35	0.34	-0.01	0.51	117	0.38	23	0.13
$\gamma_C$	0.00	0.00	0.00	-	-	-	-	-
$\gamma_X$	0.28	0.27	0.00	0.31	63	0.28	22	0.02
$C_{GL}$	0.00	0.00	0.00	-	-	-	-	-
$C_{GR}$	0.00	0.00	0.00	-	-	-	-	-
$C_{gw}$	0.00	0.00	0.00	-	-	-	-	-
$\delta_L$	0.00	0.00	0.00	-	-	-	-	-
$\delta_R$	0.00	0.00	0.00	0.00	1	0.00	1	0.00
$S_L$	0.02	0.02	0.00	0.04	51	0.02	14	0.02
$SLA$	0.12	0.12	-0.01	0.28	116	0.14	23	0.14
$S_R$	0.01	0.01	0.00	0.01	22	0.01	13	0.00
$S_O$	0.18	0.15	-0.03	0.28	98	0.15	15	0.13
$r_R$	0.08	0.07	-0.01	0.17	87	0.08	19	0.08
$\rho_R$	0.07	0.07	0.00	0.15	88	0.08	19	0.07
$R_{mL}$	0.31	0.29	-0.02	0.48	108	0.33	23	0.15
$R_{mS}$	0.24	0.20	-0.04	0.30	87	0.20	12	0.10
$R_{mR}$	0.38	0.38	0.00	0.53	102	0.42	22	0.12
$\eta_B$	0.01	0.01	0.00	0.01	10	0.01	9	0.00
$k$	0.04	0.04	0.00	0.11	83	0.05	19	0.06
$\epsilon$	0.71	0.71	0.00	0.82	117	0.74	26	0.08
$m$	0.00	0.00	0.00	-	-	0.00	11	-
$\alpha$	0.02	0.02	0.00	0.05	62	0.02	14	0.03
$R_0$	0.21	0.18	-0.02	0.27	83	0.20	24	0.07
$R_{40}$	0.27	0.26	-0.01	0.53	114	0.32	21	0.21

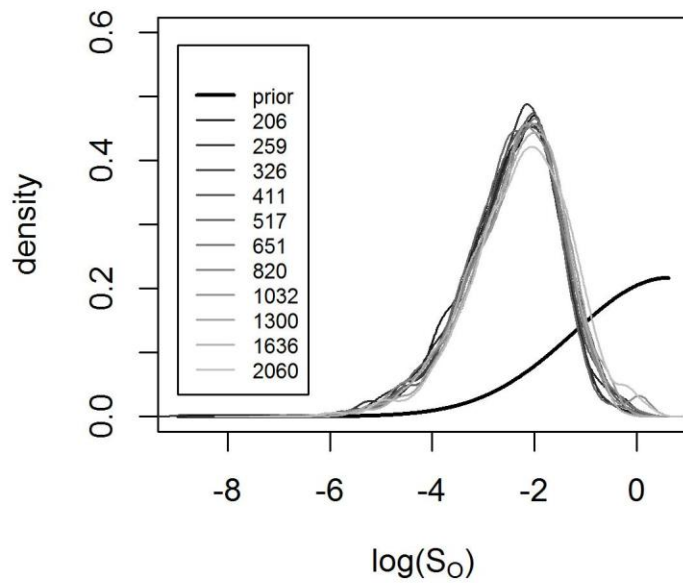


**Figure S3.1:** The marginal posterior densities for the senescence rate of other (non-trunk) woody tissue ( $S_O$ ) shown for each light level (thin gray lines;  $\text{MJ m}^{-2} \text{ year}^{-1}$ ) versus the prior distribution (thick black line). The posteriors are shifted to the left for all light levels, indicating a lower value for  $S_O$  (i.e., slow senescence or longer life-span) than expected based on the prior. The distributions are for log-transformed  $S_O$ , where  $S_O$  has units of  $\text{year}^{-1}$ .

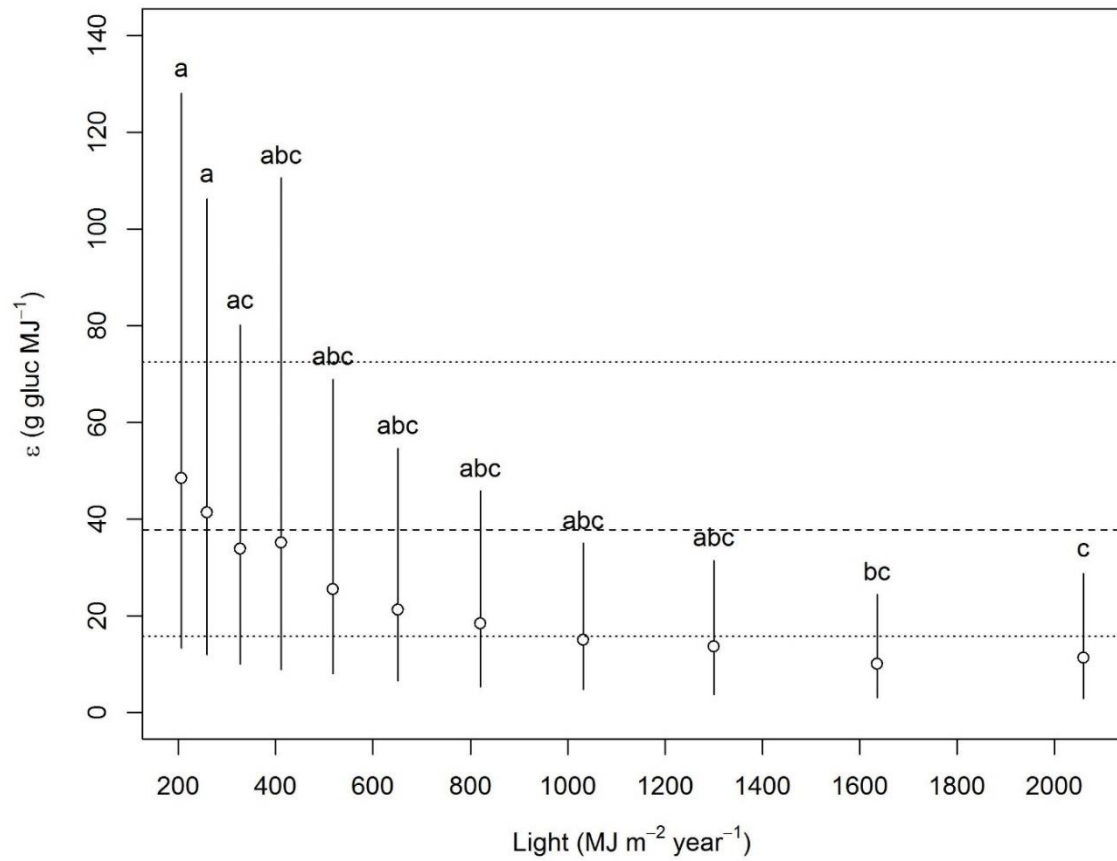


**Figure S3.2:** Posterior means (open symbols) and 95% credible intervals (CIs, whiskers) for radiation-use efficiency ( $\epsilon$ ) by light level ( $PAR_{max}$ ). Posterior means for the highest three light levels are significantly different (lower) from the prior, and the two highest light levels resulted in  $\epsilon$  values that are significantly different from the lowest two light levels (letters above each CI indicate differences among light levels). The horizontal dotted lines (top and bottom) and dashed line (middle) indicate the prior 95% CI and prior mean, respectively.

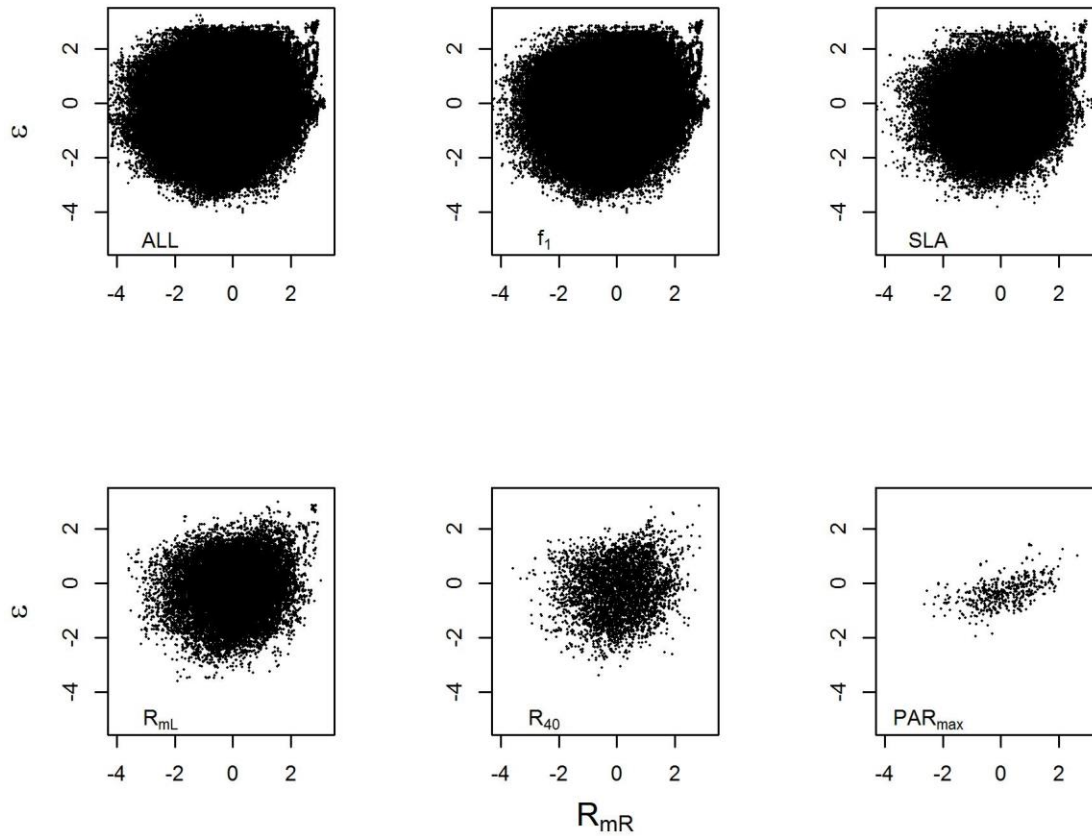


**Figure S3.3:** An example of how filtering the posterior samples generated from the MH algorithm by values of other traits can reveal correlations among pairs of traits. For example, the top left (“All”) figure shows the bivariate posterior distribution for samples of  $\varepsilon$  and  $R_{mR}$  (see Table 3.1 for definitions) prior to filtering by other traits ( $n = 1.6$  million points from unthinned MH output). Each subsequent plot from the top left (all data) to bottom right (filtered by all five variables) shows the addition of a filter based on the middle 20% quantile of the variable indicated by text in the lower left corner of each plot (see Table 3.1). This shows that as these filters are applied, a bivariate relationship can emerge among a pair of traits.

APPENDIX D

SUPPLEMENTAL CODE USED TO GENERATE THE THEORETICAL TRAIT

SPACE FOR NORTH AMERICAN TREES

This appendix contains some of the more novel code written to allow me to generate the Theoretical Trait Space for North American Tress. Not all of the code necessary to run the model is provided. Only the code that I felt was unique or that allowed me to deal with a number of challenges that came up while trying to implement the MCMC used. The first section of code sets up the computing environment for funning the MCMC chains, the second contains the code used to call the function containing the MCMC, and the third section is the MCMC code used.

The first section of code was used for managing the computational load required for running 55 MCMC chains. It starts and monitors a number of running R sessions input by the user. When one R sessission (chain) completed another automatically started until all 55 were complete. The code also had limited built in error control to prevent crashes from being an issue and the ability to start at the next chain needing to be processed if the computer reset unexpectedly or a power outage occurred.

```
#####  
#####  
#  
# This function will open each file created in initialization and then  
run  
# each set of parameters in an R session.  
#  
# threads: the number of threads to run  
# its: the number of iterations to run each thread for  
# r0: a vector of starting radii  
# par: a vector of light values as a percent of max par (2060)  
#  
# Initial values should be generated prior to running this function and  
saved  
# to files that contain ALL OF THE VALUES needed to run the ACGCA  
model. If  
# any of the variables are missing this code will fail.  
#  
# Written by Michael K. Fell on June 3, 2014. This code is based on my  
code  
# for running the filtered version of the model. This can be seen in  
the  
# Master MVN code which is a functioning version of the filter and  
sampling
```

```

# code based on parameter generation using a Latin-hypercube followed
by a
# multivariate normal sampling method.
#####
#####
par_MCMC_ACGCA <- function(
  threads, filestring, extern=0
){
  #library(fork)
  #Replace fork with Sys.getpid() from the base package
  source("Source/FileFunctions.r")
  source("Source/ACGCA_call_met.r")
  source("Source/generatesamples.r")
  source("Source/R_error_func.r")
  source("Source/FilterFunctions_2014_05_09.r")
  source("FIAdata/FIA_functions_master2015_v2.r")
  source("Source/MiscFunctions.r")
  source("Source/MCMC9.r")
  source("Source/initial_values.r")
  # Set up files for each R session to run when it starts. The names
  # should correspond to the process number.
  # filestring="parACGCA.Rdata"
  # there will be one file per PAE (light) and initial radius
combination
  #filenumber <- length(r0values) * length(lightper)

  # Open a file connection and that opens the above inputs and then
  # passes them to parbugs_2 in the WOPR.r source file (this file)
  fileConn<-file("multi_chain.r")
  writeLines(c(
    "",
    "source(\"Source/MCMC9.r\")",
    "",
    "MCMC_ACGCA_file()",
    "",
    ""
  ), #end of file text
  fileConn)
  # Close the connection
  close(fileConn)

  # get the number of files
  files <- getfiles(filestring=filestring)
  filenumber <- as.numeric(length(files))
  # set a progressBarup
  # pb <- txtProgressBar(min = 0, max = filenumber, style=3)

  # files needs to be a number here so I set it to 0 its starting value
  files <- 0
  started <- 0
  death.count <- 0
  PIDlist <- matrix(data=NA, nrow=filenumber, ncol=2)
  PIDlist[,1] <- PIDlist[,1]<-1:filenumber
  running <- numeric(filenumber)

  # Run from where the model left off. This works by checking for
output files

```

```

# using the known naming pattern. It then fills in the running
vector with
# 3's where the files that ran should be. This way if an early run
was not
# done it will still run it since the runs are not always sequential.
# added on 8/11/2014
for(i in 1:filenumber){
  if(i < 10){
    filecheck <- paste("PAR_ACGCA_out_file_0", i,
"_of_",filenumber,".Rdata", sep="")
  }else{
    filecheck <- paste("PAR_ACGCA_out_file_", i,
"_of_",filenumber,".Rdata", sep="")
  }
  filetest <- length(getfiles(filestring=filecheck))
  if(sum(filetest) > 0){
    running[i] <- 3 # 3 indicates that the run is done
  }
}

while(filenumber > sum(running==3)){
  files <- length(getfiles(filestring="PAR_ACGCA_out_file_"))
  if(length(files)==0){files<-0}

# Find PIDs for running R sessions spawned by this code
PIDcheck <- getfiles(filestring="PIDinfo_")
if(length(PIDcheck>0)){
  for(i in 1:length(PIDcheck)){
    PIDmodnum <- scan(file=PIDcheck[i], nlines=1)
    PIDlist[PIDmodnum,1] <- scan(file=PIDcheck[i], nlines=1)
    PIDlist[PIDmodnum,2] <- scan(file=PIDcheck[i], nlines=1,
skip=1)
    running[PIDmodnum] <- 1
    # remove files after data is read
    system(paste("rm ", PIDcheck[i], sep=""))
  } # end of for
}# end of if
# check that each PID is associated with a running R session
for(i in 1:filenumber){
  if(running[i]!=0 & running[i]!=3 & running[i] !=2){
    testPID <- paste("ps -p " ,PIDlist[i,2], " -o comm=", sep="")
    PID_out <- system(testPID, intern=T)
    if(length(PID_out)==0){PID_out<-0}
    if(PID_out != "R"){
      # Here it is necessary to check if the process stopped due to
      # completion or because of an error. To do this check for
      # the output file.

      if(PIDlist[i,1] <= 9){
        filecheck <- paste("PAR_ACGCA_out_file_0", PIDlist[i,1],
"_of_",filenumber,".Rdata", sep="")
        filetest <- length(getfiles(filestring=filecheck))
      } else if(PIDlist[i,1] > 9){
        filecheck <- paste("PAR_ACGCA_out_file_", PIDlist[i,1],
"_of_",filenumber,".Rdata", sep="")
        filetest <- length(getfiles(filestring=filecheck))
      }
    }
  }
}

```

```

    # Check if the file is present.  If not run it again
    if(filetest != 1){
        running[i] <- 2 # 2 indicates to run again
        death.count <- death.count+1
    }else if(filetest == 1){
        running[i] <- 3 # 3 indicates that the run is done
    }
    }else{
        running[i] <- 1 # 1 indicates that the run is still going
    }
}}# end of for and if

#running <- started-files

print(running)
print(started)
#print(files)
#print(threads)
#print(filename)

if(sum(running==2)>0){
    sel <- running==2
    # Make sure the Modelcomm file exists
    #if(length(getfiles(filestring="Modelcomm.txt"))!=1){
    # write(paste(""), file="Modelcomm.txt", append=F)
    #}
    # What number should be used for this model?
    # This must execute before this code is executes
    # a second time.
    modnum <- PIDlist[sel,1][1]
    write(paste(modnum), file="Modelcomm.txt", append=F)
    running[sel][1] <- 1
    # run the model
    system("R --no-save < multi_chain.r", wait=F, ignore.stdout=T,
ignore.stderr=T)
}else if(sum(running==1)<threads){
    started <- started + 1

    sel <- running==0
    modnum <- PIDlist[sel,1][1]
    running[sel][1] <- 1

    # Write Modelcomm.txt with modnum which sets the file to use
    write(paste(modnum), file="Modelcomm.txt", append=F)

    system("R --no-save < multi_chain.r", wait=F, ignore.stdout=T,
ignore.stderr=T)
}

# this command gets pid information ps -p 4857 -o comm=
# update progress bar
#setTxtProgressBar(pb, files)

Sys.sleep(1.0) #Stop execution for 1.0s

```

```

    # Keep the loop from running at full speed which is far faster
    # than what is required here.
  }

  # Clean up files
  # system("rm inputs_*_parACGCA.Rdata")
  system("rm Modelcomm.txt")
  system("rm multi_chain.r")
  model.stats <- list(death.count)
  return(model.stats)
}

```

The next block of code was responsible for setting up the ACGCA model to run with each set of initial values and was used by the automation code above when it started each R session.

```

#####
#####
# This function is a wrapper for the MCMC_ACGCA function that allows it
# to be
# called by simply providing an Rdata file that has the starting
# parameters.
# This method is useful when starting the file from a list of input
# files for
# instance as part of a batch processing routine.
#
# Code set up as a function on May 28, 2014 by Michael Fell
#####
#####
MCMC_ACGCA_file <- function(){
  rm(list=ls())
  source("Source/FileFunctions.r")
  source("Source/ACGCA_call_met.r")
  source("Source/generatesamples.r")
  source("Source/R_error_func.r")
  source("Source/FilterFunctions_2014_05_09.r")
  source("FIAdata/FIA_functions_master2015_v2.r")
  source("Source/MiscFunctions.r")
  source("Source/MCMC9.r")
  #require("truncnorm") # This is needed for a truncated normal for
# parameters 3 and 28
  library("truncnorm")
  #require("fork")
  #library("fork")
  #require("ks")
  #library("ks")
  #detach("package:ks", unload=TRUE, character.only = TRUE)
  #detach("package:msm", unload=TRUE, character.only=TRUE)
  #detach("package:mvtnorm", unload=TRUE, character.only = TRUE)
  #library("mvtnorm")
  #library("msm")

  modnum <- 3

```

```

# NOTE: the file loaded here MUST contain all of the variables needed
for the
# MCMC_ACGCA call. These should be generated elsewhere and saved to
an
# Rdata file. Once loaded they will be available for the MCMC_ACGCA
call.
# The variable names in the file loaded must exactly match those
below or the
# function will fail.

# Make sure the Modelcomm file exists
if(length(getfiles(filestring="Modelcomm.txt"))!=1){
  #write(paste(""), file="Modelcomm.txt", append=F)
  stop()
}

# What number should be used for this model?
# This must execute before this code is executes
# a second time.
fileexist <- getfiles(filestring="Modelcomm.txt")
if(length(fileexist) != 0){
  modnum <- scan(file="Modelcomm.txt", nlines=1)
  if(length(modnum)==0){
    stop()
  }
}

# Append the modelcomm file so the next run knows which run it is.
# write(paste(modnum+1), file="Modelcomm.txt", append=F)

# start R with a script to run don't wait for it to finish

# Set the model to run by getting the files and opening the correct
file
files <- getfiles(filestring="parACGCA.Rdata")
filenumber <- length(files)

# Load the files that are needed
load(files[modnum])

# Get the PID and write it to a new textfile for the master process
PID <- Sys.getpid()

filecom <- paste("PIDinfo_", modnum, ".txt", sep="")
fileConn<-file(filecom)
writeLines(c(
paste(modnum, sep=""),
paste(PID, sep="")
), #end of file text
fileConn)
# Close the connection
close(fileConn)

# sigma small
#sigma.start <- sigma.start*0+0.005

```

```

#sigma.start <- sigma.start*0+0.01
load("FIAdata/FIA_prob_array_nomort_2015_09_15.R")

ACGCA_out <- MCMC_ACGCA(numparms, eparms, iterations, its.past,
sigma, names.thetaj, theta.j, transform, disttype, trunca, truncb,
truncmean, truncprior, gparm, r0, years, minmax, trans.statsmean,
finalsd, sigma.start, prob.array, min.alive, prob.j, maxwhile,
tune.start, tune.end, prob.array2, l.prob.array)

# Save the model output
if(modnum <= 9){
  save(ACGCA_out, file=paste("PAR_ACGCA_out_file_0", modnum,
"_of_",filename, ".Rdata", sep=""))
} else if(modnum > 9){
  save(ACGCA_out, file=paste("PAR_ACGCA_out_file_", modnum,
"_of_",filename, ".Rdata", sep=""))
}
} # End of function

```

The Final block of code in the primary script for running the ACGCA model is the MCMC routine which is started by the MCMC\_ACGCA(...) function call above.

```

#####
#####
# This is the break between the initialization and MCMC part of the
code
#
# I moved this to its own function so it can be called once initial
values
# are generated. This can then be used as part of a script for running
the
# code as part of a group of R instances.
#
# numparms: the number of parameters to sample
# eparms: extra parameters not sampled (2 for the ACGCA)
# iterations: how many samples are desired
# its.past: how many iterations back to look for tuning. This does not
# correspond directly to iterations above but to the while loop in
the MCMC
# routine.
# sigma: starting step size (modified for tuning)
# sigma.start: starting step size (not-modified)
# names.thetaj: variable names
# theta.j: starting parameter values (initial values)
# transform: a vector giving the transforms using codes 1-3. 1:log,
2:logit,
# 3:none, 0:none.
# gparm: model variables that are not in theta.j (sparms in ACGCA)
# r0: starting radius
# years: how many years to run ACGCA (100 most of the time)
# minmax: a matrix of min and max values from FIA data

```

```

# trans.statsmean: transformed means from kparms generated from
TreeTraits
#   database output
# finals: standard deviation to use in the prior.  These must be on
the
#   transformed scale
#
#####
#####
MCMC_ACGCA <- function(numparms, eparms, iterations, its.past, sigma,
names.theta.j, theta.j, transform, disttype, trunca, truncb, truncmean,
truncprior, gparm, r0, years, minmax, trans.statsmean, finals,
sigma.start, prob.array, min.alive, prob.j, maxwhile, tune.start,
tune.end, prob.array2, l.prob.array){
  #library("truncnorm")

  # Tracks sigma values associated with rate
  sigma.rate <- matrix(NA, nrow=numparms, ncol=((tune.end-
tune.start)/(tune.start/2)+2)
)

  Jtop.theta <- 1
  Jbottom.j <- 1

  VwVc <- 0.5
  LCmax <- 7.3861*10^5
  LT <- 4*10^(-4)
  beta <- 0.05127

  # Calculate gxmax and set its transformed values as the maximum value
for
  # p.gammax which is variable 13.
  gxmax <- min(min(VwVc/(VwVc+beta), 1/(beta+1)), 1)
  truncb[13]<-transformvar(gxmax, transform[13])

  # Set the truncation for gammax - xylem conducting area to sapwood
area ratio
  # truncb[13] <- gxmax

  rate.save <- sigma.rate
  sigma.rate[,1]<-sigma.start
  sigma.its <- 0
  rate.v <- matrix(NA, nrow=numparms, ncol=2)
  sigma.value <- matrix(sigma, nrow=numparms, ncol=2)
  accept.rate <- matrix(NA, nrow=numparms, ncol=(its.past+1))
  accept.rate[, (its.past+1)] <- 1
  theta.out <- matrix(NA, nrow=iterations, ncol=(numparms+eparms))
  colnames(theta.out) <- names.theta.j
  theta.star <- theta.j
  prior.j <- numeric(numparms)
  prior.theta <- numeric(numparms)
  skip.track <- matrix(NA, nrow=iterations, ncol=(numparms+eparms))
  MCMC.track <- array(NA, dim=c(34,11,iterations)) # track alpha,
alpha.l dunif, accept

  theta.jsave <- theta.j
  prob.jsave <- prob.j

```

```

###
# Constants used to specify constraints on a few "free" growth
parameters
#
###
# volume ratio of structural tissue to internal cell for living cells
in
# sapwood (e.g., rays, etc.), also called "alpha"
VwVc <- 0.5
# Maximum amount of labile carbon that can

# This was taken from ACGCA_call2.r the values can just be appended
for each
# run and then the vectors can be split in the prod.files.MCMC code.
output2 <- list(h=numeric(0), r=numeric(0), rBH=numeric(0),
status=numeric(0), errorind=as.integer(numeric(0)), cs=numeric(0),
clr=numeric(0), growth_st=as.integer(numeric(0)))
# stores the last good output
output3 <- list(h=numeric(0), r=numeric(0), rBH=numeric(0),
status=numeric(0), errorind=as.integer(numeric(0)), cs=numeric(0),
clr=numeric(0), growth_st=as.integer(numeric(0)))
output <- numeric(0)

# Output variables these should include ACGCA output needed so that
the model
# does not need to be ran again. This can then be processed in the
same way
# as the output for multiple files was in the filter model.
theta.out <- matrix(NA, nrow=iterations, ncol=(numparms+eparms))

sigma<-sigma.start # set the starting step size
sigma.value[,1] <- sigma
start <- proc.time() # save the current time

# theta.j must be defined before this loop is started
for(i in 1:(iterations)){
  for(k in 1:(numparms)){
    accept <- 0 # accept new parm in vector
    accept.index <- i #accept.rate[k, (its.past+1)]
    skip <- 0 #reset skip variable

    print(paste(rep(i,10), " ", rep(k,10))) # for testing
    #thetastar2 <- function(parmin, trans=0, sigma)
    # theta.j[k] is the mean until a value is accepted

    # This is not needed because of the outer if statement
    if(k != 12 & k != 8 & k != 3 & k != 28){ # don't include gammaw
or rhomin
    theta.star[k] <- thetastar2(theta.j[k], trans=transform[k],
sigma[k])
    theta.star[k] <- as.numeric(unlist(theta.star[k]))
  }else if(k == 12 | k == 8){
    skip <- 1
    accept <- 0
  }
}

```

```

# These must be generated relative to each other. The
truncated normal
# distribution is used to prevent overlap. theta.star28 <=
theta.star3.
  if(k == 3){
    theta.star[k] <- tstartruncnorm(theta.j[k],
trans=transform[k], sigma=sigma[k], a=theta.star[28], b=Inf)
    trunca[k] <- theta.star[28]
  }
  if(k == 28){
    theta.star[k] <- tstartruncnorm(theta.j[k],
trans=transform[k], sigma=sigma[k], a=-Inf, b=theta.star[3])
    truncb[k] <- theta.star[3]
  }
  if(k == 7){ #this is for rhomax it is between rlo and rhi
    # This is based on gammax which in my code is theta.j[13].
This is
    # from the SA code provided by K. Ogle.
    p.gammax <- exp(theta.j[13])/(1+exp(theta.j[13]))
    rlo <- (VwVc-p.gammax*(VwVc-beta))/((1+VwVc)*theta.j[12])
    rhi <- (1-p.gammax)/theta.j[12]

    # The values for trunca and truncb must be transformed to the
correct
    # scale. The third lines runs the truncated normal code whree
theta.j
    # is not transformed. It is transformed in tstartruncnorm.
This
    # function is in generatesamples.r.
    trunca[k]<-transformvar(rlo, transform[k])
    truncb[k]<-transformvar(rhi, transform[k])
    theta.star[k] <- tstartruncnorm(theta.j[k],
trans=transform[k], sigma=sigma[k], a=trunca[k], b=truncb[k])
  }
  if(k == 13){ # This is for gxmax. gxmax < p.gammax
    # the truncb points is transformed above when gxmax is
calculated.
    theta.star[k] <- tstartruncnorm(theta.j[k],
trans=transform[k], sigma=sigma[k], a=-Inf, b=truncb[k])
  }

  # Stop ACGCA from running if inf/-inf/NA or the code will crash
also
  # stop if the generated parameter is 0 don't accept.
  if(!is.finite(theta.star[k])){
    skip <- 2
    accept <- 0
    #exp.prob.theta <- 0
    #stop("inf or -inf or na value detected")
  }else if(theta.star[k]< 0){
    skip <- 3
    accept <- 0
    #exp.prob.theta <- 0
    #stop("theta.star is less than 0")
  }
}

```

```

    if(skip==0){ #only run if no inf/-inf NA values are present
      # Run the ACGCA model
      output <- growthloopR(sparms2 = theta.star, gparms2=gparm,
r0=r0, dim=c(1,1),lenvars2=1)

      # don't accept if there was an error in the ACGCA model
      if(sum(output$errorind) > 0){
        skip <- 6
        accept <- 0
        #exp.prob.theta <- 0
      }
    }

    # Filter the output at this point so there is only one value
per year.
    #if(skip==0){
    output <- proc.output(output, years, gparm)
    #}

    # don't accept if the tree was dead at year 100
    if(skip == 0){
      if(output$status[years+1]==0){
        skip <- 5
        accept <- 0
        #exp.prob.theta <- 0
      }
    }

    if(skip==0){
      # calculate dh and dr without using a for loop!
      dh <- output$h[2:length(output$h)] -
output$h[1:(length(output$h)-1)]
      dr <- output$r[2:length(output$r)] -
output$r[1:(length(output$r)-1)]
      if(output$status[years+1]==0){ #remove values lescd s than 0
        sel <- dh < 0
        dh[sel] <- 0
        sel <- dr < 0
        dr[sel] <- 0
      }

      # I found that these should be in a skip statement on 4/22/2015
      vars <- matrix(data=c(dr,dh,output$r[2:length(output$r)]),
output$h[2:length(output$h)]), ncol=4, byrow=F)
      boxarray <- as.matrix(vars)
      #apply(X=as.matrix(vars), MARGIN=c(1,2), FUN=logbin)

      if(output$status[min.alive]==0){
        skip <- 7
        accept <- 0
        #exp.prob.theta <- 0
      } #stop if the tree never lived
    } # end of skip above dh, dr, calculations.

    boxarray <- log(boxarray)
    if(sum(!is.finite(boxarray))>0){
      skip <- 12
    }
  }

```

```

# Check for values outside of minmax (these result in
probability 0
  if(skip == 0){ #don't do this if the tree is dead
  for(j in 1:4){
    # sum(boxarray[,j] < minmax[j,1])+ # removed this because it
is not needed anymore
    if((sum(boxarray[,j] > minmax[j,2]))>0){
      #exp.prob.theta <- 0
      skip <- 8
      accept <- 0 #Added on 10/1/2014
    }
    # This prevents the values from being too small.
    if((sum(boxarray[,j] < minmax[j,1]))>0){
      #exp.prob.theta <- 0
      skip <- 8
      accept <- 0 #Added on 11/19/2014
    }
  }} # end of minmax for

if(skip == 0){

  # create a matrix for output
  binout <- matrix(data = NA, nrow = length(dh), ncol = 4)

  ## This finds which bins each number is in
  for(j in 1:dim(boxarray)[2]){
    binout[,j] <- apply(X=as.matrix(boxarray[,j]), MARGIN=1,
FUN=findbin, min.interval=minmax[j,])
  }

  # find probout using a multivariate normal distribution
  # probout <- mvtnorm::dmvnorm(x=boxarray,
mean=prob.array2$log.mean, sigma=prob.array2$cov.matrix, log=TRUE)
  probout <- numeric(dim(binout)[1])

  # I had an error when I did not do this with a loop so I put
this back in
  for(j in 1:length(probout)){
    probout[j] <-
1.prob.array[binout[j,1],binout[j,2],binout[j,3],binout[j,4]]
  }

  # check that no value in probout is NA if they are theta.j=0
and the
# parameter set is rejected. This leads to
theta.star=theta.j.
  if(sum(!is.finite(probout))>0){
    #exp.prob.theta <- 0
    skip <- 9
  }
  if(skip == 0){
    # find prop.j
    prob.theta <- (1/years)*sum(probout)
    #exp.prob.theta <- exp(prob.theta)
  }
#bracket # end of second if

```

```

        if(is.finite(prob.theta) & skip == 0){ # don't accept if
prob.theta is 0
        # calculate the prior values for theta and j. The calc for J
is not
        # needed if it is saved from when teh set is accepted.
        if(i == 1 | i==(tune.end+1)){ # only calculate this for the
first iteration save values after that
            if(disttype[k] == 1){
                if(!is.finite(trunca[k])){
                    trunca.use <- -Inf
                }else{trunca.use<-transformvar(trunca[k], transform[k])}
                if(!is.finite(truncb[k])){
                    truncb.use <- Inf
                }else{truncb.use<-transformvar(truncb[k], transform[k])}
                prior.j[k] <-
log(truncnorm::dtruncnorm(x=transformvar(theta.j[k], transform[k]),
a=trunca.use, b=truncb.use, mean=trans.statsmean[k], sd=finalsd[k]))
                }else if(disttype[k] == 0){
                    prior.j[k] <-
log(dnorm(x=transformvar(theta.j[k],transform[k]),
mean=trans.statsmean[k], sd=finalsd[k]))
                }
            }

            if(disttype[k] == 1){
                if(!is.finite(trunca[k])){
                    trunca.use <- -Inf
                }else{trunca.use<-transformvar(trunca[k], transform[k])}
                if(!is.finite(truncb[k])){
                    truncb.use <- Inf
                }else{truncb.use<-transformvar(truncb[k], transform[k])}

                # height is truncated to 127
                if(truncprior[k]==1){
                    prior.theta[k] <-
log(truncnorm::dtruncnorm(x=transformvar(theta.star[k], transform[k]),
a=trunca.use, b=truncb.use, mean=trans.statsmean[k], sd=finalsd[k]))
                }
                # Domec 2008 suggest max h is no more than 127m.
                if(truncmean[k] != 0){
                    # mean is theta.j with sd = the previous iterations
step size.
                    Jtop.theta <-
log(truncnorm::dtruncnorm(x=transformvar(theta.star[k],transform[k]),
a=trunca.use, b=truncb.use, mean=transformvar(theta.j[k],transform[k]),
sd=sigma.value[k,2]))
                    # mean is theta.star with sd = the current step size.
                    Jbottom.j <-
log(truncnorm::dtruncnorm(x=transformvar(theta.j[k],transform[k]),
a=trunca.use, b=truncb.use,
mean=transformvar(theta.star[k],transform[k]), sd=sigma.value[k,1]))
                }
            } # the below can't be else because it needs to be
evaluated
            if(disttype[k] == 0 | truncprior[k]==0){

```

```

        # if truncprior==1 then the prior is truncated not the
likelihood so the correction is not needed.
        prior.theta[k] <-
log(dnorm(x=transformvar(theta.star[k],transform[k]),
mean=trans.statsmean[k], sd=finalsd[k]))
        # These will just cancel so set them to 1
        Jtop.theta <- 1
        Jbottom.j <- 1
    }

    # I added the following two lines following p279 in Gelman
2014
        # Jtop.theta <-
log(dnorm(x=transformvar(theta.star[k],transform[k]),
mean=transformvar(theta.j[k],transform[k]), sd=finalsd[k]))
        # Jbottom.j <-
log(dnorm(x=transformvar(theta.j[k],transform[k]),
mean=transformvar(theta.star[k],transform[k]), sd=finalsd[k]))

    if(!is.finite(prior.theta[k])){ # Stop if the value is not
finite
        skip <- 10
        accept <- 0
    } else{
        # save the values going into alpha.l
        MCMC.track[k,5,i] <- prob.theta
        MCMC.track[k,6,i] <- prob.j
        MCMC.track[k,7,i] <- prior.theta[k]
        MCMC.track[k,8,i] <- prior.j[k]
        MCMC.track[k,9,i] <- Jtop.theta
        MCMC.track[k,10,i] <- Jbottom.j
        MCMC.track[k,11,i] <- -2*prob.theta

        alpha.l <- prob.theta - prob.j + prior.theta[k] -
prior.j[k] + Jtop.theta - Jbottom.j
        alpha <- -alpha.l

        # Test for acceptance
        rexp.track <- rexp(1)
        MCMC.track[k,1,i] <- alpha # track alpha, alpha.l dunif,
accept
        MCMC.track[k,2,i] <- alpha.l
        MCMC.track[k,3,i] <- rexp.track

        print(rexp.track)
        print(alpha)

        if(rexp.track > alpha){
            accept <- 1 # accept the new value
            accept.rate[k,counter(i, its.past)] <- 1
            accept.rate[k,(its.past+1)] <-
accept.rate[k,(its.past+1)] + 1
            theta.j[k] <- theta.star[k] # Set theta.j to equal
theta.star
            prior.j[k] <- prior.theta[k]
            prob.j <- prob.theta

```

```

        # append the output vectors for saving and processing
        output3$h <- output$h
        output3$r <- output$r
        output3$rBH <- output$rBH
        output3$status <- output$status
        output3$errorind <- output$errorind
        output3$cs <- output$cs
        output3$clr <- output$clr
        output3$growth_st <- output$growth_st

        }else{accept <- 0}
    } # end of else
}}else{
    accept <- 0

    } # end of if

    # If the parameter was not accepted a zero goes in accept.rate
    if(accept == 0){
        accept.rate[k,counter(i, its.past)] <- 0
        accept.rate[k,(its.past+1)] <- accept.rate[k,(its.past+1)] +
1
    }

    # Tune the sigma vector with a target rate of 0.44
    # Changed to i on 10/6/2014
    if(i%(its.past)==0 & i > tune.start & i < tune.end){
        rate.v[k,1] <- mean(accept.rate[k,1:(its.past)], na.rm=T)
        #sigma[k]<-tuneit(accept=rate.v[k,1], target=0.44,
tpar=sigma[k])
        sigma[k]<-tuneit(accept=accept.rate[k,1:(its.past)],
target=0.44, tpar=sigma[k])
        rate.v[k,2] <- rate.v[k,1] # not really needed
        if(k == 1){sigma.its <- sigma.its+1} # this must be done
first so it is 1
        sigma.rate[k,(sigma.its+1)] <- sigma[k] # Save the new sigma
value

        rate.save[k,sigma.its] <- rate.v[k,1]
        # This saves sigma values for use in the correction function
        sigma.value[k,2] <- sigma.value[k,1]
        sigma.value[k,1] <- sigma[k]
    }

    if(i == tune.end){
        # tunewin(rate=rate.save[1,1:50], sigma=sigma.rate[1,1:50],
winsize=3)
        tunerate <- numeric(34)*NA
        tunesigma <-numeric(34)*NA
        tune.it <- numeric(34)*NA
        for(j in 1:34){
            tuneout <- tunewin(rate=rate.save[j,1:((tune.end-
tune.start)/its.past)], sigma=sigma.rate[j,1:((tune.end-
tune.start)/its.past)], winsize=3, target=0.44)
            tunerate[j] <- tuneout$best[1]
            tunesigma[j] <- tuneout$best[2]
            tune.it[j] <- tuneout$best[3]
        }
    }

```

```

# Reset the parameters to their
# Make sure all theta.j and prob.j values are the starting points.
The
# prior will be recalculated above when the next iteration runs.
theta.j <- theta.jsave
prob.j <- prob.jsave
theta.star <- theta.jsave
prob.theta <- prob.jsave
}

# print the iteration the loop is on for testing. This is not
visible
# when running the code using the batch MCMC routine.
print(paste("inner for iteration: ", k, ".", sep=""))

# reset all theta.star values to theta.j if accept == 1
if(accept == 0){
  theta.star[k] <- theta.j[k]
  prior.theta[k] <- prior.j[k]
  prob.theta <- prob.j
  MCMC.track[k,11,i] <- -2*prob.j

  # append the output vectors for saving and processing
  output$h <- output3$h
  output$r <- output3$r
  output$rBH <- output3$rBH
  output$status <- output3$status
  output$errorind <- output3$errorind
  output$cs <- output3$cs
  output$clr <- output3$clr
  output$growth_st <- output3$growth_st
}

skip.track[i, k] <- skip

#Save the value of accept
MCMC.track[k,4,i] <- accept
} # End inner for loop
# Store the new theta vector
theta.out[i,]<-theta.j # Store theta.j
# prior.j does not change on a k basis since it does not depend on
other
# parameters so it is updated in the i loop.
prior.j <- prior.theta # Store new prior.j values so they don't
need to be
# calculated again
theta.j <- theta.star # Set theta.j to equal theta.star
prob.j <- prob.theta # Set a new prob for j
#print(paste("Iteration: ", i , " of ", iterations, sep=""))
#print(paste(rep(i,100)))

# append the output vectors for saving and processing
output2$h <- c(output2$h, output$h)
output2$r <- c(output2$r, output$r)
output2$rBH <-c(output2$rBH, output$rBH)
output2$status <-c(output2$status, output$status)
output2$errorind <- c(output2$errorind, output$errorind)

```

```

output2$cs <- c(output2$cs, output$cs) # Added 7/21/2014
output2$clr <- c(output2$clr, output$clr) # Added 7/21/2014
output2$growth_st <- c(output2$growth_st, output$growth_st) # Added
9/23/14

  if(i%100==0){
    plot(x=1:i, y=theta.out[1:i,1], ylab="height", xlab="iteration",
type="l")
  }
} # End outer for loop

end <- proc.time()
time <- end-start
print(end-start)

# final.rate <- mean(accept.rate[, (its.past+1)])
# final.rate=final.rate,

return(list(output=output2, theta.out=theta.out, rate = rate.v,
accept.rate=accept.rate, r0=r0, gparm=gparm, skip.track=skip.track,
sigma.rate=sigma.rate, time=time, MCMC.track=MCMC.track,
rate.save=rate.save, sigma=sigma))
} # End of function MCMC_ACGCA

```

APPENDIX E

SUPPLEMENTAL TABLES AND FIGURES REGARDING THE FILTERING THE  
THEORETICAL TRAIT SPACE FOR NORTH AMERICAN TREES

**Table S4.1.** Coefficient estimates (effect sizes) and p-values for a logistic regression of tree-level mortality ( $m_{g,p}$ ) versus annual average light level at the forest floor ( $PAR_{avg}$ ; light only model).

<b>Coefficient/term</b>	<b>Estimate</b>	<b>p-value</b>
Intercept	-0.55	< 0.01
$PAR_{avg}$	-0.36	< 0.01

**Table S4.2.** Coefficient estimates (effect sizes) and p-values from a stepwise logistic regression of tree-level mortality ( $m_{g,p}$ ) versus 32 functional traits (see Table 4.1 for a description of the traits) that only considered the main effects of the traits, and did not consider light (traits only model). The traits are ordered from highest to lowest effect size.

<b>Coefficient/term</b>	<b>Estimate</b>	<b>p-value</b>
Intercept	-0.89	<0.01
$H_{max}$	-1.24	<0.01
$\varepsilon$	-1.26	<0.01
$\gamma_X$	-0.71	<0.01
$S_O$	0.56	<0.01
$R_{mL}$	0.43	<0.01
$R_0$	-0.34	<0.01
$SLA$	-0.25	<0.01
$R_{mS}$	0.23	<0.01
$K$	-0.22	<0.01
$SW_{max}$	-0.24	<0.01
$f_2$	-0.22	<0.01
$f_1$	0.16	<0.01
$R_{40}$	0.13	<0.01
$\rho_R$	0.08	<0.01
$S_L$	0.08	<0.01
$\eta_B$	-0.07	<0.01
$S_R$	0.06	<0.01
$\lambda_h$	0.05	<0.01
$\gamma_C$	0.05	<0.01
$\alpha$	0.03	<0.01
$\eta$	0.03	<0.01
$\lambda_s$	0.03	<0.01
$r_R$	0.03	<0.01
$\varphi_H$	-0.03	<0.01
$Cg_w$	0.02	<0.01
$R_{mR}$	-0.03	<0.01
$\delta_L$	0.01	<0.01
$\delta_R$	0.01	<0.01
$Cg_L$	0.01	<0.01

**Table S4.3.** Coefficient estimates (effect sizes) and p-values from a stepwise logistic regression of tree-level mortality ( $m_{g,p}$ ) versus 32 functional traits (see Table 4.1 for a description of the traits), annual average light level at the forest floor ( $PAR_{avg}$ ), and all 2-way interactions between  $PAR_{avg}$  and each trait (traits + light model). Within the main effects, the traits are ordered from highest to lowest effect size; within the two-way interactions, interactions are ordered from highest to lowest effect size.

<b>Coefficient/term</b>	<b>Estimate</b>	<b>p-value</b>
Intercept	-1.00	<0.01
$\varepsilon$	-1.41	<0.01
$H_{max}$	-1.33	<0.01
$\gamma_X$	-0.77	<0.01
$PAR_{avg}$	-0.67	<0.01
$S_O$	0.59	<0.01
$R_{mL}$	0.5	<0.01
$R_0$	-0.38	<0.01
$SLA$	-0.29	<0.01
$R_{mS}$	0.26	<0.01
$SW_{max}$	-0.26	<0.01
$k$	-0.24	<0.01
$f_2$	-0.23	<0.01
$f_1$	0.18	<0.01
$R_{40}$	0.12	<0.01
$\rho_R$	0.09	<0.01
$S_L$	0.09	<0.01
$\eta_B$	-0.08	<0.01
$S_R$	0.07	<0.01
$\lambda_h$	0.05	<0.01
$\gamma_C$	0.05	<0.01
$\eta$	0.04	<0.01
$\lambda_s$	0.04	<0.01
$\alpha$	0.04	<0.01
$\varphi_H$	-0.03	<0.01
$r_R$	0.03	<0.01
$C_{g_w}$	0.03	<0.01
$R_{mR}$	-0.03	<0.01

$C_{gL}$	0.01	<0.01
$\delta_L$	0.01	<0.01
$\delta_R$	0.01	<0.01
$PAR_{avg} \times \varepsilon$	-0.32	<0.01
$PAR_{avg} \times R_{mL}$	0.19	<0.01
$PAR_{avg} \times S_O$	-0.19	<0.01
$PAR_{avg} \times H_{max}$	0.16	<0.01
$PAR_{avg} \times R_{40}$	-0.12	<0.01
$PAR_{avg} \times R_{mS}$	0.11	<0.01
$PAR_{avg} \times SLA$	-0.08	<0.01
$PAR_{avg} \times f_1$	0.07	<0.01
$PAR_{avg} \times SW_{max}$	0.04	<0.01
$PAR_{avg} \times \eta$	0.04	<0.01
$PAR_{avg} \times k$	-0.03	<0.01
$PAR_{avg} \times \alpha$	0.03	<0.01
$PAR_{avg} \times S_L$	0.03	<0.01
$PAR_{avg} \times R_0$	-0.03	<0.01
$PAR_{avg} \times \gamma_X$	0.03	<0.01
$PAR_{avg} \times \rho_R$	0.02	<0.01
$PAR_{avg} \times S_R$	0.02	<0.01
$PAR_{avg} \times r_R$	0.02	<0.01
$PAR_{avg} \times f_2$	0.02	<0.01
$PAR_{avg} \times \lambda_s$	0.02	<0.01
$PAR_{avg} \times \lambda_h$	-0.01	<0.01
$PAR_{avg} \times C_{gL}$	0.01	<0.01

---

**Table S4.4.** Coefficient estimates (effect sizes) and p-values from a regression of stand-level mortality ( $m_g^S$ ) versus time between gaps ( $tbg$ , years), where  $tbg$  is treated as a categorical variable (factor);  $p < 0.01$  and  $R^2 = 0.74$ . Models were also conducted that separately regressed  $m_g^S$  on gap time ( $gt$ ) and closure time ( $ct$ ), with both treated as factors; both models had far lower  $R^2$  values (0.002 and 0.052).

<b>Level (<math>tbg</math>)</b>	<b>Estimate</b>	<b>p-value</b>
Intercept	0.254	< 0.01
35	0.034	0.113
50	0.089	< 0.01
100	0.179	< 0.01
200	0.196	< 0.01

**Table S4.5.** Coefficient estimates (effect sizes) and p-values from a stepwise regression of phenotype-level mortality ( $m_p^\theta$ ) versus 32 functional traits (see Table 4.1 for a description of the traits) that only considered the main effects of the traits (main effects model). The traits are ordered from highest to lowest effect size.

<b>Coefficient/term</b>	<b>Estimate</b>	<b>p-value</b>
Intercept	0.37	<0.01
$\varepsilon$	-0.184	<0.01
$H_{max}$	-0.174	<0.01
$\gamma_X$	-0.102	<0.01
$S_O$	0.078	<0.01
$R_{mL}$	0.063	<0.01
$R_0$	-0.052	<0.01
$SLA$	-0.037	<0.01
$SW_{max}$	-0.033	<0.01
$R_{mS}$	0.031	<0.01
$k$	-0.031	<0.01
$f_2$	-0.03	<0.01
$f_1$	0.024	<0.01
$R_{40}$	0.017	<0.01
$S_L$	0.011	<0.01
$\rho_R$	0.011	<0.01
$\eta_B$	-0.011	<0.01
$S_R$	0.009	<0.01
$\lambda_h$	0.008	<0.01
$\gamma_C$	0.006	<0.01
$\eta$	0.005	<0.01

**Table S4.6.** Coefficient estimates (effect sizes) and p-values from a stepwise regression of phenotype-level mortality ( $m_p^\theta$ ) versus 32 functional traits (see Table 4.1 for a description of the traits), for the model that considered the main effects of the traits and all 2-way interactions among traits. The traits are ordered from highest to lowest effect size.

<b>Coefficient/term</b>	<b>Estimate</b>	<b>p-value</b>
Intercept	0.389	<0.01
$\varepsilon$	-0.195	<0.01
$H_{max}$	-0.171	<0.01
$S_O$	0.103	<0.01
$\gamma_X$	-0.100	<0.01
$R_{mS}$	0.076	<0.01
$R_{mL}$	0.068	<0.01
$SLA$	-0.039	<0.01
$k$	-0.035	<0.01
$R_0$	-0.031	<0.01
$f_2$	-0.031	<0.01
$f_1$	0.021	<0.01
$SW_{max}$	-0.015	<0.01
$S_L$	0.013	<0.01
$\rho_R$	0.011	<0.01
$\eta_B$	-0.011	<0.01
$R_{40}$	-0.011	<0.01
$\lambda_h$	0.010	<0.01
$S_R$	0.010	<0.01
$\lambda_s$	0.006	<0.01
$\eta$	0.006	<0.01
$\varphi_H$	-0.006	<0.01
$\alpha$	0.005	<0.01
$\gamma_X \times R_{mS}$	-0.063	<0.01
$\varepsilon \times S_O$	0.049	<0.01
$\varepsilon \times \gamma_X$	0.042	<0.01
$S_O \times R_{40}$	0.041	<0.01
$H_{max} \times R_{40}$	-0.033	<0.01
$H_{max} \times \gamma_X$	0.032	<0.01
$H_{max} \times S_O$	-0.029	<0.01
$\gamma_X \times S_O$	-0.024	<0.01

$S_O \times R_{mS}$	-0.023	<0.01
$S_O \times R_{mL}$	-0.018	<0.01
$R_{mL} \times R_{mS}$	-0.017	<0.01
$\gamma_X \times R_{40}$	0.017	<0.01
$\varepsilon \times f_2$	0.014	<0.01
$R_0 \times R_{40}$	0.014	<0.01
$\varepsilon \times R_{40}$	0.014	<0.01
$S_O \times R_0$	-0.013	<0.01
$\gamma_X \times f_2$	0.012	<0.01
$H_{max} \times SW_{max}$	0.012	<0.01
$H_{max} \times R_0$	0.012	<0.01
$R_{mS} \times R_{40}$	0.012	<0.01
$\varepsilon \times f_1$	0.010	<0.01
$R_{mS} \times R_0$	-0.009	<0.01
$\gamma_X \times k$	0.009	<0.01
$R_{mS} \times SW_{max}$	-0.009	<0.01
$R_{mS} \times SLA$	0.009	<0.01
$S_O \times SLA$	0.009	<0.01
$\varepsilon \times k$	0.008	<0.01
$R_{mL} \times S_L$	-0.008	<0.01
$\varepsilon \times R_{mL}$	-0.008	<0.01
$R_{mL} \times f_1$	-0.008	<0.01
$S_O \times k$	0.008	<0.01
$\varepsilon \times SW_{max}$	0.007	<0.01
$R_{mL} \times SLA$	-0.007	<0.01
$R_{mL} \times R_{40}$	0.006	<0.01
$R_{40} \times \eta$	-0.006	<0.01
$H_{max} \times \varphi_H$	-0.006	<0.01
$\gamma_X \times f_1$	-0.006	<0.01
$R_0 \times f_2$	-0.006	<0.01
$R_{mS} \times f_2$	-0.006	<0.01
$S_O \times \alpha$	-0.006	<0.01
$f_1 \times \rho_R$	0.005	<0.01
$S_O \times \lambda_h$	-0.005	<0.01
$H_{max} \times f_2$	0.005	<0.01
$\varepsilon \times \eta_B$	0.005	<0.01
$\gamma_X \times \lambda_s$	-0.005	<0.01

$R_{mS} \times S_R$	-0.005	<0.01
$\gamma_X \times \alpha$	-0.005	<0.01
$H_{max} \times \lambda_s$	0.005	<0.01
$\varepsilon \times R_{mS}$	0.005	<0.01
$\varepsilon \times \varphi_H$	0.005	<0.01

---

**Table S4.7.** Summary of the trait-trait regressions for surviving trees, where each trait was regressed on the remaining 31 traits, phenotype-level mortality (mort =  $m_p^g$ ), and all 2-way interactions. Important main effects and interactions were identified with forward and backward stepwise regression using the Bayesian Information Criteria (BIC) for model selection. Each column represents the “dependent trait” that was regressed on the “predictor” variables (rows) using a randomly selected subset of 3000 parameter sets for surviving trees under the gap dynamics scenario that resulted in the lowest mortality rate (i.e.,  $gt = 8$  years,  $ct = 25$  years,  $tbg = 35$  years, for scenario  $g = 57$ , giving  $m_{57}^g = 19\%$ ). Within each cell, + or – represents the direction of the regression coefficient (or correlation between the dependent and independent traits); the number under each diagonal line represents the number of interaction terms the variable (e.g., dependent trait) was included in (if blank, it was not included in any interactions); blank cells indicate variables that were not included in the final model. Cells shaded gray were statistically significant ( $p < 0.05$ , most at  $p \ll 0.05$ ). The three non-significant main effects (e.g., associated with the  $R_{40}$  and  $H_{max}$  models) were included in at least one significant interaction. The bottom row contains the overall, adjusted  $R^2$  from each regression.

	$\epsilon$	$R_{40}$	$R_{mR}$	$R_{mL}$	$f_1$	SLA	$R_{mS}$	$r_R$	$\rho_R$	$S_O$	$f_2$	$k$	$SW_{max}$	$\gamma_X$	$R_0$	$\alpha$	$\eta$	$S_L$	$\rho$	$S_R$	$m$	$\lambda_S$	$H_{max}$	$\eta_B$	$\phi_H$	$\lambda_H$	$CgW$	$CgR$	$CgL$	$\delta_R$	$\delta_L$	$\gamma_C$		
$\epsilon$	█																																	
$R_{40}$		█																																
$R_{mR}$			█																															
$R_{mL}$				█																														
$f_1$					█																													
SLA						█																												
$R_{mS}$							█																											
$r_R$								█																										
$\rho_R$									█																									
$S_O$										█																								
$f_2$											█																							
$k$												█																						
$SW_{max}$													█																					
$\gamma_X$														█																				
$R_0$															█																			
$\alpha$																█																		
$\eta$																	█																	
$S_L$																		█																
$\rho$																			█															
$S_R$																				█														
$m$																					█													
$\lambda_S$																						█												
$H_{max}$																							█											
$\eta_B$																								█										
$\phi_H$																									█									
$\lambda_H$																										█								
$CgW$																											█							
$CgR$																													█					
$CgL$																														█				
$\delta_R$																															█			
$\delta_L$																																█		
$\gamma_C$																																	█	
mort																																		█
$r^2$	0.38	0.3	0.21	0.13	0.15	0.06	0.2	0.03	0.03	0.33	0.09	0.02	0.12	0.35	0.16	0	0	0.01	0.07	0	0	0	0.3	0.01	0	0.01	0	0	0	0	0	0	0	

**Table S4.8.** Summary of the trait-trait regressions for tree that died, where each trait was regressed on the remaining 31 traits, phenotype-level mortality (mort =  $m_p^\theta$ ), and all 2-way interactions. See Table S4.7 for details about the analysis. The stepwise regression was applied to a randomly selected subset of 3000 parameter sets for trees that died under the gap dynamics scenario that resulted in the lowest mortality rate. Similar to the model for surviving trees (Table S4.7), the two non-significant main effects (e.g., associated with the  $R_{mR}$  model) were included in at least one significant interaction.

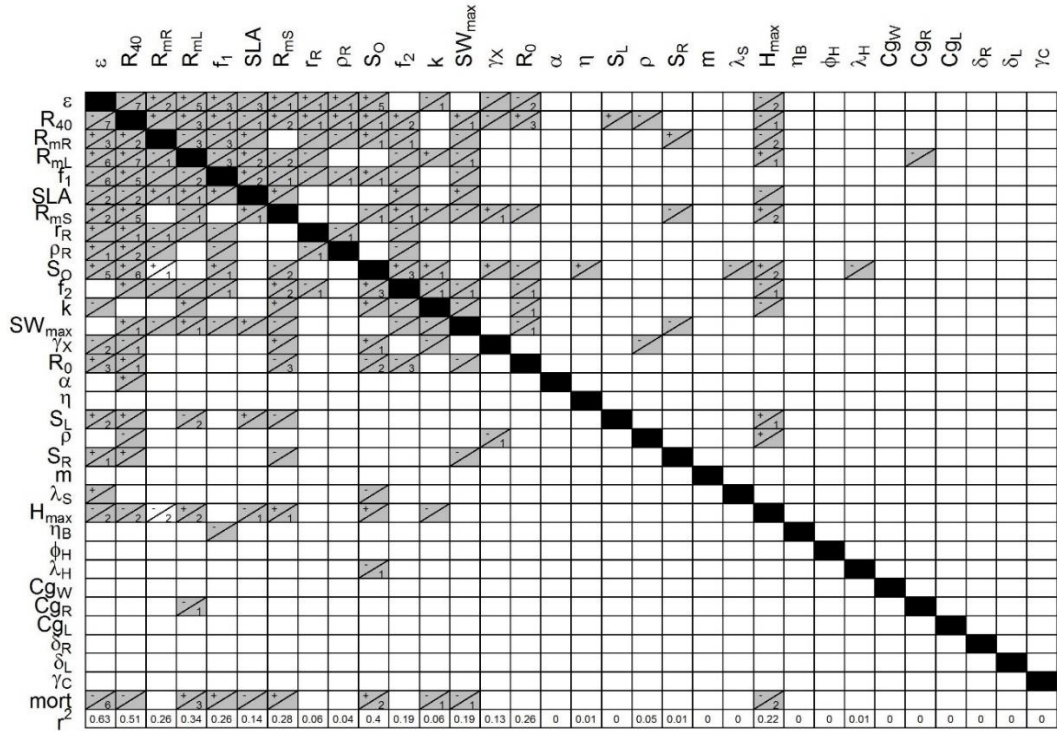


**Table S4.9.** Similarities and differences between the trait-trait stepwise regressions for surviving (Table S4.7) versus dead trees (Table S4.8). As in Tables S4.7 and S4.8, the column headers denote the dependent traits, and the row headers denote the predictor variables or traits. Within each cell, + indicates that the regression coefficients from both models had the same sign (+ or -), while a – indicates they had opposite signs. A dark grey shaded cell indicates a predictor trait that was only included in the model for surviving trees, while light grey cells indicate traits that were only included in models for dead trees (white cells indicate consistencies between models; either a trait was or was not included in both models). The original sign of the coefficients for each model are given in Tables S4.7 and S4.8. The difference in  $R^2$  (diff  $R^2$ ) between the two models is indicated in the second-to-last row, and the difference in the total number of variables (diff var) included in each model is given in the last row; differences are calculated as the result for surviving trees minus the result for dead trees.

	$\varepsilon$	$R_{40}$	$R_{mR}$	$R_{mL}$	$f_1$	SLA	$R_{mS}$	$f_R$	$p_R$	$S_O$	$f_2$	k	$SW_{max}$	$\gamma_X$	$R_0$	$\alpha$	$\eta$	$S_L$	$\rho$	$S_R$	m	$\lambda_S$	$H_{max}$	$\eta_B$	$\phi_H$	$\lambda_H$	$C_{gw}$	$C_{gR}$	$C_{gL}$	$\delta_R$	$\delta_L$	$\gamma_C$			
$\varepsilon$	+	-	+	+	+	+	+	+	+	+	+	+	+	+	+	+	+	+	+	+	+	+	+	+	+	+	+	+	+	+	+	+	+		
$R_{40}$	+	+	+	+	+	+	+	+	+	+	+	+	+	+	+	+	+	+	+	+	+	+	+	+	+	+	+	+	+	+	+	+	+	+	
$R_{mR}$	+	+	+	+	+	+	+	+	+	+	+	+	+	+	+	+	+	+	+	+	+	+	+	+	+	+	+	+	+	+	+	+	+	+	
$R_{mL}$	+	+	+	+	+	+	+	+	+	+	+	+	+	+	+	+	+	+	+	+	+	+	+	+	+	+	+	+	+	+	+	+	+	+	
$f_1$	+	+	+	+	+	+	+	+	+	+	+	+	+	+	+	+	+	+	+	+	+	+	+	+	+	+	+	+	+	+	+	+	+	+	
SLA	+	+	+	+	+	+	+	+	+	+	+	+	+	+	+	+	+	+	+	+	+	+	+	+	+	+	+	+	+	+	+	+	+	+	
$R_{mS}$	+	+	+	+	+	+	+	+	+	+	+	+	+	+	+	+	+	+	+	+	+	+	+	+	+	+	+	+	+	+	+	+	+	+	
$f_R$	+	+	+	+	+	+	+	+	+	+	+	+	+	+	+	+	+	+	+	+	+	+	+	+	+	+	+	+	+	+	+	+	+	+	
$p_R$	+	+	+	+	+	+	+	+	+	+	+	+	+	+	+	+	+	+	+	+	+	+	+	+	+	+	+	+	+	+	+	+	+	+	+
$S_O$	+	+	+	+	+	+	+	+	+	+	+	+	+	+	+	+	+	+	+	+	+	+	+	+	+	+	+	+	+	+	+	+	+	+	+
$f_2$	+	+	+	+	+	+	+	+	+	+	+	+	+	+	+	+	+	+	+	+	+	+	+	+	+	+	+	+	+	+	+	+	+	+	+
k	+	+	+	+	+	+	+	+	+	+	+	+	+	+	+	+	+	+	+	+	+	+	+	+	+	+	+	+	+	+	+	+	+	+	+
$SW_{max}$	+	+	+	+	+	+	+	+	+	+	+	+	+	+	+	+	+	+	+	+	+	+	+	+	+	+	+	+	+	+	+	+	+	+	+
$\gamma_X$	+	+	+	+	+	+	+	+	+	+	+	+	+	+	+	+	+	+	+	+	+	+	+	+	+	+	+	+	+	+	+	+	+	+	+
$R_0$	+	+	+	+	+	+	+	+	+	+	+	+	+	+	+	+	+	+	+	+	+	+	+	+	+	+	+	+	+	+	+	+	+	+	+
$\alpha$	+	+	+	+	+	+	+	+	+	+	+	+	+	+	+	+	+	+	+	+	+	+	+	+	+	+	+	+	+	+	+	+	+	+	+
$\eta$	+	+	+	+	+	+	+	+	+	+	+	+	+	+	+	+	+	+	+	+	+	+	+	+	+	+	+	+	+	+	+	+	+	+	+
$S_L$	+	+	+	+	+	+	+	+	+	+	+	+	+	+	+	+	+	+	+	+	+	+	+	+	+	+	+	+	+	+	+	+	+	+	+
$\rho$	+	+	+	+	+	+	+	+	+	+	+	+	+	+	+	+	+	+	+	+	+	+	+	+	+	+	+	+	+	+	+	+	+	+	+
$S_R$	+	+	+	+	+	+	+	+	+	+	+	+	+	+	+	+	+	+	+	+	+	+	+	+	+	+	+	+	+	+	+	+	+	+	+
m	+	+	+	+	+	+	+	+	+	+	+	+	+	+	+	+	+	+	+	+	+	+	+	+	+	+	+	+	+	+	+	+	+	+	+
$\lambda_S$	+	+	+	+	+	+	+	+	+	+	+	+	+	+	+	+	+	+	+	+	+	+	+	+	+	+	+	+	+	+	+	+	+	+	+
$H_{max}$	+	+	+	+	+	+	+	+	+	+	+	+	+	+	+	+	+	+	+	+	+	+	+	+	+	+	+	+	+	+	+	+	+	+	+
$\eta_B$	+	+	+	+	+	+	+	+	+	+	+	+	+	+	+	+	+	+	+	+	+	+	+	+	+	+	+	+	+	+	+	+	+	+	+
$\phi_H$	+	+	+	+	+	+	+	+	+	+	+	+	+	+	+	+	+	+	+	+	+	+	+	+	+	+	+	+	+	+	+	+	+	+	+
$\lambda_H$	+	+	+	+	+	+	+	+	+	+	+	+	+	+	+	+	+	+	+	+	+	+	+	+	+	+	+	+	+	+	+	+	+	+	+
$C_{gw}$	+	+	+	+	+	+	+	+	+	+	+	+	+	+	+	+	+	+	+	+	+	+	+	+	+	+	+	+	+	+	+	+	+	+	+
$C_{gR}$	+	+	+	+	+	+	+	+	+	+	+	+	+	+	+	+	+	+	+	+	+	+	+	+	+	+	+	+	+	+	+	+	+	+	+
$C_{gL}$	+	+	+	+	+	+	+	+	+	+	+	+	+	+	+	+	+	+	+	+	+	+	+	+	+	+	+	+	+	+	+	+	+	+	+
$\delta_R$	+	+	+	+	+	+	+	+	+	+	+	+	+	+	+	+	+	+	+	+	+	+	+	+	+	+	+	+	+	+	+	+	+	+	+
$\delta_L$	+	+	+	+	+	+	+	+	+	+	+	+	+	+	+	+	+	+	+	+	+	+	+	+	+	+	+	+	+	+	+	+	+	+	+
$\gamma_C$	+	+	+	+	+	+	+	+	+	+	+	+	+	+	+	+	+	+	+	+	+	+	+	+	+	+	+	+	+	+	+	+	+	+	+
mort	+	+	+	+	+	+	+	+	+	+	+	+	+	+	+	+	+	+	+	+	+	+	+	+	+	+	+	+	+	+	+	+	+	+	+
diff $R^2$	-0.25	-0.21	-0.06	-0.21	-0.11	-0.07	-0.07	-0.03	-0.02	-0.07	-0.1	-0.04	-0.07	0.22	-0.1	0	-0.01	0	0.02	-0.01	0	0	0.07	0.01	0	-0.01	0	0	0	0	0	0	0		
diff var	-9	-13	-4	-17	-10	-10	-18	-5	-2	1	-8	-7	2	9	5	1	-1	1	3	-3	1	-1	2	1	1	0	1	-1	0	1	0	0	0		

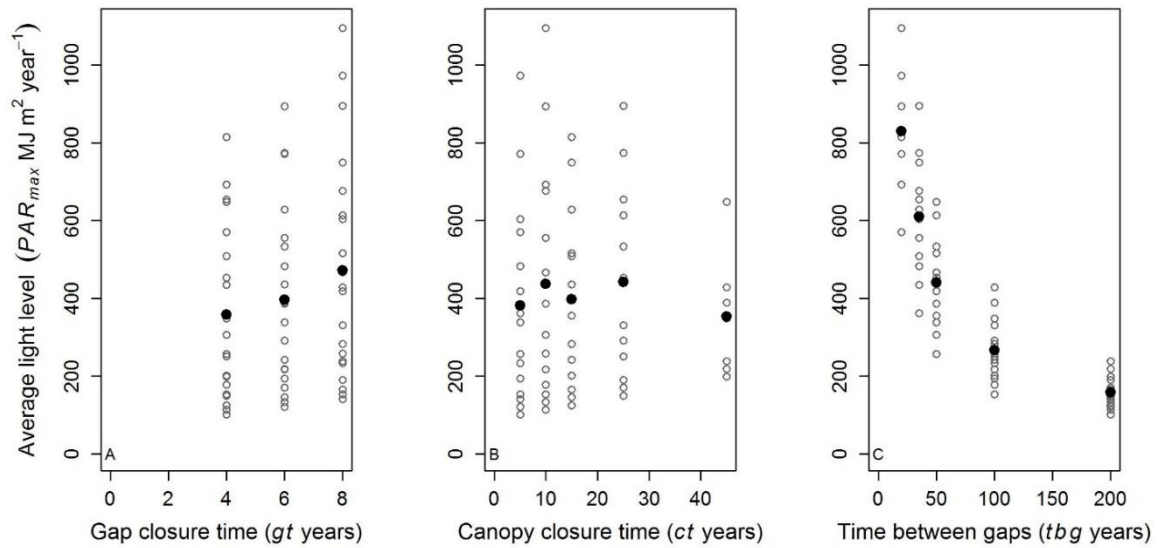


**Figure S4.1.** Relationship between the simulated average annual light level at the forest floor ( $PAR_{avg}$ ) versus **(A)** gap closure time ( $gt$ , years), **(B)** canopy closure time ( $ct$ , years), and **(C)** time between gaps ( $tbg$ , years). In all panels, black symbols are the average  $PAR_{avg}$  across the other gap phase levels with the level indicated by the gap phase variable on the x-axes; open circles are the  $PAR_{avg}$  values for each gap scenario simulation. In general, **(A)** and **(B)** do not show any relationships between  $PAR_{avg}$  and  $gt$  or  $ct$ , such that linear regressions associated with each were non-significant (with  $p = 0.32$  and  $p = 0.91$ , respectively); **(C)** shows that  $PAR_{avg}$  is well predicted by  $tbg$  ( $p < 0.01$ ,  $R^2 = 0.79$ ).

APPENDIX F

STATEMENT OF CO-AUTHOR PERMISSION

## STATEMENT OF CO-AUTHOR PERMISSION

The information in Chapter 2-4 of my dissertation has been or will be submitted for review in peer-reviewed journals. Each journal submission is co-authored by Dr. Kiona Ogle, Chapter 2 is additionally co-authored by Dr. Lisa Patrick, Chapter 3 is additionally co-authored by Dr. Jarrett Barber and Dr. Jeremy Lichstein.